# SUSTAINABLE PAVEMENT APPLICATIONS UTILIZING QUARRY BY-PRODUCTS AND RECYCLED/NONTRADITIONAL AGGREGATE MATERIALS

BY

ISSAM I. A. QAMHIA

DISSERTATION

Submitted in partial fulfillment of the requirements
for the degree of Doctor of Philosophy in Civil Engineering
in the Graduate College of the
University of Illinois at Urbana-Champaign, 2019

Urbana, Illinois

Doctoral Committee:

Professor Erol Tutumluer, Chair
Professor Imad L. Al-Qadi
Professor Emeritus Marshall Thompson
Research Assistant Professor Hasan Ozer
Professor Anand Puppala, University of Texas at Arlington

# ABSTRACT

Quarry By-products (QB), usually less than 0.25 in. (6 mm) in size, are the residual deposits from the production of required grades of aggregates and are often stockpiled in excess quantities at the quarries. More than 175 million US tons of QB are produced every year from the 3,000 operating quarries around the US. QB pose environmental and economic challenges as they accumulate in large quantities in landfills or interfere with quarry operations. With recent focus on sustainable construction practices and the scarcity of natural resources, more common and sustainable uses of by-product materials such as QB are becoming imperative.

This dissertation focuses on the introduction and evaluation of new sustainable applications of QB and/or QB mixed with other marginal, virgin or recycled aggregate materials in pavements. The selected QB applications were evaluated through the construction of full-scale pavement test sections utilizing QB in targeted sustainable applications, and testing them with heavy wheel loads through Accelerated Pavement Testing (APT).

The QB applications studied included both unbound and bound (chemically stabilized) pavement subsurface/foundation layers. The studied QB pavement applications were in five categories: (1) Using QB for filling voids between large stones as aggregate subgrade on soft subgrades; (2) increased fines content (e.g. 15% QB fines passing No. 200 sieve) in dense-graded aggregate subbase over soft subgrade soils; (3) using QB as a cement or fly ash-treated subbase (e.g., in inverted pavements); (4) using QB as a cement-treated base material; and (5) for base course applications, blending QB with coarse aggregate fractions of recycled materials and stabilizing the blends with 3% cement or 10% class C fly ash.

In preparation for the field evaluations, several laboratory studies were conducted to finalize the designs of intended QB applications. The main laboratory studies were: (1) A packing study of QB with recycled coarse aggregates to determine the optimum blending ratio; (2) a packing study to aid the construction of large aggregate subgrade with QB materials filling the inherent voids; and, (3) Unconfined Compressive Strength (UCS) tests for chemically stabilized QB samples.

Fifteen full-scale pavement test sections utilizing QB applications and one conventional flexible section were constructed in three ‘Test Cells.’ Cell 1 had four paved and four unpaved test sections to study construction platforms and low volume road applications of QB. Cells 2 and 3 studied chemically stabilized QB applications for base and subbase layers. Construction activities included engineering the top 305 mm (12 in.) of existing subgrade to a California Bearing Ratio (CBR) = 1% for Cell 1 test sections and to a CBR = 6% for all the pavement test sections in Cells 2 and 3. Subgrade modification was achieved through moisture adjustment and compaction. The construction of the QB layers were successfully achieved and extensively monitored. The data for nuclear density measurements and moisture contents indicated that nearly all the test sections were constructed at or near the targeted optimum moisture contents and achieved proper densities.

A Lightweight Deflectometer (LWD) was used to assess the stiffness of the constructed layers after the construction of each lift. It was also used to monitor the increase in stiffness of the chemically stabilized layers. The

increase in stiffness of the chemically stabilized layers was the highest for cement-stabilized test sections and usually lower for fly ash-stabilized sections. Following the paving of test sections with Hot Mix Asphalt (HMA), Falling Weight Deflectometer (FWD) tests were conducted on all finished surfaces. Significantly low deflection values were measured for the sections with cement-stabilized QB and QB blends with recycled aggregates.

APT was conducted using the Advanced Transportation Loading Assembly (ATLAS). A constant unidirectional wheel load of 10 kips (44.5 kN), a tire pressure of 110 psi (760 kPa), and a constant speed of 5 mph (8 km/h) were assigned. The exceptionally good performance of some of the stabilized QB applications in Cells 2 and 3 necessitated trafficking in excess of 100,000 passes; an increased wheel load/tire pressure combination of 14 kip (62.3 kN)/ 125 psi (862 kPa) was adopted for the additional 35,000 passes. Four of the test sections in Cells 2 and 3 were instrumented with soil pressure cells on top of the engineered CBR = 6% subgrade. Data collected from these pressure cells showed that significantly low vertical pressures were transmitted to the subgrade for sections with stabilized bases/subbases.

Measurements for rutting progression for the construction platform and HMA-paved test sections in Cell 1 showed good performance for the sections constructed with 15% nonplastic fines and with blends of large aggregate subgrade rocks with QB. Measurements of rutting progression in Cells 2 and 3 indicated exceptionally good performance of sections with blends of QB and recycled coarse aggregates stabilized with cement. Generally, sections stabilized with cement accumulated lower rutting than those stabilized with fly ash. No significant differences in rutting performance were detected for sections with QB from two different aggregate sources. For the inverted section with a cement-stabilized QB subbase, measured rut amounts were significantly lower than those in the test section with the fly ash-stabilized QB subbase. None of the stabilized sections showed any signs of cracks.

Additional testing and forensic analyses were conducted after the APT study to better assess the performance of the constructed sections. These tests included: (1) FWD testing before and after APT; (2) HMA coring; (3) Dynamic Cone Penetrometer (DCP) testing for the aggregate subbase/base layers; (4) flooded tests for the aggregate subgrade/QB test sections; and (5) trenching to assess uniformity of construction and determine as-constructed layer thicknesses. Results from these forensic tests further supported the conclusions from the APT study indicating the overall quite satisfactory performance for the studied sustainable QB applications.

Mechanistic analysis was conducted using GT-PAVE axisymmetric finite-element program to analyze the FWD results, and to calculate response benefits based on resilient FWD deflection for various design thicknesses and material properties. Life Cycle Assessment (LCA) and Life Cycle Cost Analysis (LCCA) studies were conducted to assess the environmental impacts and cost benefits for the studied QB applications. LCA and LCCA results for three scenarios, i.e. as-constructed and as-designed pavement thicknesses studied though APT and newly proposed pavement sections for low volume pavement alternatives, indicated that chemically stabilized QB and QB blended with recycled coarse aggregates could be successfully used to construct sustainable, resilient, and low cost pavements. Particularly, pavement structures with a low 3% cement-stabilized QB applications created high stiffness base/subbase layers in this study; they exhibited significant response benefits due to low FWD measured and predicted surface deflections and can withstand higher traffic volumes over pavement life.

# ACKNOWLEDGEMENTS

First, I would like to offer my sincere gratitude to my mentor and advisor, Dr. Erol Tutumluer, who contributed to every step in preparing this dissertation. Without his contribution, patience and encouragement, this dissertation could not have been possible. I could not ask for a more knowledgeable, understanding and humble advisor than Dr. Tutumluer, and I am very pleased and proud that I had the opportunity to work under his supervision. I am especially thankful for the confidence that Dr. Tutumluer had in my potential, and for his unconditional support and eagerness to steer me in the right direction. His kind words and trust have given me confidence and were always a great motivation to keep me going throughout my Ph.D. years.

Secondly, I would like to offer my deepest gratitude to Dr. Hasan Ozer, who was the co-Principal Investigator on the Illinois Center of Transportation R27-168 project that led to a significant part of the results shown in this dissertation. Dr. Ozer has given me countless ideas related to the work presented in this dissertation, and countless advice in life. Dr. Ozer has been a great role model for me, and I learnt a lot from his selfless character, passion, and eagerness to work and succeed.

I would also like to offer my sincere gratitude to my other PhD Committee members: Dr. Imad Al-Qadi, Dr. Anand Puppala, and Dr. Marshall Thompson, for their valuable time, and their jointly contribution and precious insights towards improving the quality of my Ph.D. research. I am especially thankful to ICT Director Dr. Imad Al-Qadi for the countless conversations and advice, and for sharing many inspirational stories with me; those related to work, career goals and life experience. Dr. Al-Qadi has inspired me with his positive attitude, hard work, well-rounded knowledge, and leadership skills. I am highly thankful to Dr. Al-Qadi for his contribution to the R27-168 project, particularly for his help and guidance with the instrumentation of the soil pressure cells in the full-scale test sections.

The research reported in my dissertation was primarily sponsored by the Illinois Department of Transportation (IDOT). I wholeheartedly appreciate the contribution of the Technical Review Panel for the R27-168 project: James Trepanier, Sheila Beshears, Heather Z. Shoup, Sean Stutler, Ryan Culton, Joshua Smith, Michael Short, Dennis Bachman, Dan Eichholz, Brian Rice, James S. Sergent, Lehigh-Hanson, Ed Bartholomew, Lehigh Hanson, Dan Barnstable, Mike Boyda, Will Pyatt, Doug Roehrs, and Bill Sheftick. Their comments and guidance throughout the R27-168 project had a great impact on shaping up this dissertation.

Sincere acknowledgments are also due to ICT research engineers Greg Renshaw, Michael Johnson, James Meister, and Shenghua Wu for their support throughout the various stages of the R27-168 project. This dissertation would not have been possible without their contribution and guidance on numerous occasions. Thanks are extended to the staff of ICT: Kristi Anderson, Todd Kato, Noelle Arbulu, Patty Altstetter, Audrey Welborn, and Peggy Currid for their contribution to ICT project management. Also, many thanks go to Kimberly Howard with ICT for her help with filming and documenting testing activities.

I am particularly grateful for the help with material procurement and technical support given by Timothy Prunkard, Marc Killion, Donald Marrow, and Darold Marrow from the machine shop at the Civil Engineering Department - University of Illinois. I also thank John Hart with the Beckman Institute for his help with aggregate imaging. Many sincere thanks go to Dr. Pranshoo Solanki with Illinois State University for his help with data analysis of FWD results. The help of Chad Arkenberg and Ronald Wagoner from IDOT District 5 in field density measurements is highly appreciated.

My great appreciation is extended to Open Road Paving Company, LLC for their dedication to constructing all engineered subgrade layers and aggregate layers during field construction, and to Cross Construction Corporation for paving all constructed test sections with hot mix asphalt. The help of all aggregate producers who provided and/or facilitated the delivery of the materials used for the field construction is highly appreciated.

I would also like to express my sincere gratitude to my fellow lab mates and colleagues at the University of Illinois and ICT, who helped on countless occasions during the various stages that led to the production of this dissertation. Thanks go to Dr. Hasan Kazmee, Dr. Yong-Hoon Byun, Jose Rivera Perez, Dr. Maziar Moaveni, Bin Feng, Maximilian Orihuela, Haohang Huang, Seunggu Kang, Huseyin Boler, Yue Gong, Edoardo Barber, Arturo Espinoza Luque, João Crucho, Izak Said, Dr. Shan Zhao, Siqi Wang, Dr. Jaime Hernandez, Angeli Gamez, Priyanka Sarker, Hyung Suk Chae, Punit Singhvi, Dr. Mojtaba Ziyadi, Wenting Hou, Scott Schmidt, Sagar Shah, Dr. Saleh Yousefi, Jiyai Luo, Omar Jadallah, Jeff LaHucik, Qingwen Zhou, Sushobhan Sen, and Yumo Chi.

With gratitude, I would also like to acknowledge my former advisor at the University of Wisconsin – Milwaukee (UWM), Dr. Rani Elhajjar, for offering me the first opportunity to pursue my graduate studies in the U.S., for being a great advisor, and for continuously being a great support after I left UWM. My deepest appreciation goes to Dr. Hani Titi with UWM for his great advice and support during and after my studies at UWM. My thanks also go to all my Professors and teachers at my undergraduate university (Birzeit University) and Al-Mustaqbal school, whom I am grateful for every single one of them for the influence they had on my character and education.

Finally, I would like to humbly thank my parents and my brother for their encouragement and support throughout my graduate studies. I could not ask for a more loving and caring family. I dedicate this dissertation to them as an appreciation for their countless support and endless love.

*Dedication*

*To my parents, Imad and Ikram, and my brother Ahmad for their infinite love and endless support*

*To all my loving friends, caring family members, and inspiring teachers and mentors*

# TABLE OF CONTENTS

# LIST OF ACRONYMS

| Acronym | Description |
|---|---|
| AASHTO | American Association of State Highways and Transportation Officials |
| ABC | Aggregate Base Course |
| AC | Asphalt Concrete |
| AI | Asphalt Institute |
| ANN | Artificial Neural Networks |
| APT | Accelerated Pavement Testing |
| AREA | American Railway Engineering Association |
| ATLAS | Advanced Transportation Loading Assembly |
| ATREL | Advanced Transportation Research and Engineering Laboratory |
| AUPP | Area Under Pavement Profile |
| BCI | Base Curvature Index |
| BDI | Base Damage Index |
| BLRS | Bureau of Local Roads and Streets |
| CBR | California Bearing Ratio |
| COV | Coefficient of Variation |
| CRCP | Continuously Reinforced Concrete Pavements |
| C#S# | Cell # - Section # (Number of Cell and Section) |
| DCP | Dynamic Cone Penetrometer |
| DGABC | Dense-Graded Aggregate Base Course |
| DOT | Department of Transportation |
| EOL | End of Life |
| EPA | Environmental Protection Agency |
| EPD | Environmental Product Declarations |
| ESALs | Equivalent Single Axle Loads |
| FE | Finite Element |
| FEM | Finite Element Modeling / Finite Element Method |
| FHWA | Federal Highway Administration |
| FRAP | Fractionated Reclaimed Asphalt Pavements |
| FRCA | Fractionated Recycled Concrete Aggregate |
| FWD | Falling Weight Deflectometer |
| GA | Genetic Algorithms |
| $G_{mm}$ | Theoretical maximum specific gravity for HMA |

| | |
|---|---|
| $G_{mb}$ | Bulk specific gravity for HMA |
| GWP | Global Warming Potential |
| HMA | Hot Mix Asphalt |
| IBV | Immediate Bearing Value |
| ICT | Illinois Center for Transportation |
| IDOT | Illinois Department of Transportation |
| in. | Inch |
| IRI | International Roughness Index |
| ISO | International Organization for Standardization |
| kg | Kilogram |
| kg $CO_2e$ | Carbon Dioxide Equivalence |
| kN | Kilo Newtons |
| Lb. | Pounds |
| LCA | Life Cycle Assessment |
| LCCA | Life Cycle Cost Analysis |
| LCI | Life Cycle Inventory |
| LCIA | Life Cycle Impact Assessment |
| LL | Liquid Limit |
| LWD | Lightweight Deflectometer |
| MDD | Maximum Dry Density |
| m | Meter |
| M-E | Mechanistic-Empirical |
| MET | Method of Equivalent Thickness |
| MEPDG | Mechanistic-Empirical Pavement Design Guide |
| mm | Millimeter |
| MJ | Mega Joule |
| NCHRP | National Cooperative Highway Research Program |
| NCSA | National Crushed Stone Association |
| NMAS | Nominal Maximum Aggregate Size |
| OMC | Optimum Moisture Content |
| PCA | Portland Cement Association |
| pcf | Pounds per Cubic Foot |
| PI | Plasticity Index |
| PSI | Present Serviceability Index |
| psi | Pounds per Square Inch |
| QA | Quality Assurance |

| | |
|---|---|
| QB | Quarry By-products |
| QC | Quality Control |
| $Q_u$ | Unconfined Compressive Strength |
| RCWMs | Recycled, Coproduct, and Waste Materials |
| RAP | Reclaimed Asphalt Pavements |
| RCA | Recycled Concrete Aggregates |
| RCM | Recycled Concrete Materials |
| sh. Ton | Short Tons (U.S. Tons) |
| SCI | Surface Curvature Index |
| SI | Système international: The international system of units |
| SSR | Subgrade Stress Ratio |
| TED | Total Energy Demand |
| TRACI | Tool for the Reduction and Assessment of Chemical and Other Environmental Impacts |
| UCS | Unconfined Compressive Strength |
| XRD | X-Ray Diffraction |
| XRF | X-Ray Fluorescence |
| $yd^2$ | Square Yards |
| $Yd^3$ | Cubic Yards |

# CHAPTER 1: INTRODUCTION

## 1.1 BACKGROUND AND MOTIVATION

Quarry by-products (QB), usually less than 0.25 in. (6 mm) in size, are produced during quarry operations such as blasting, crushing, screening, and washing operations. QB are mostly coarse-, medium-, and fine-grained sand particles with a small fraction of silts and clays. QB can exist in aggregate production sites in three distinct types: screenings, pond fines, and baghouse fines (Chesner et al., 1998). During the crushing stages, QB are generally carried out in three stages, i.e. primary, secondary, and tertiary crushing (Petavratzi and Wilson, 2008).

The importance of utilizing aggregate quarry by-products in pavement applications stems from the vast quantities that are produced and remain excessive within many quarries each year. QB stockpiling and disposal is a serious issue facing the aggregate industry as they accumulate in stockpiles and interfere with quarry operations (Hudson et al, 1997). A report by the Federal Highway Administration estimated the quantity of quarry by-products generated in the United States each year to exceed 175 million US tons (159 million metric tons), little of which is being put into use for pavement applications (Chesner et al., 1998). The same report also estimated that aggregate QB accumulation in the US alone exceeded 4.0 billion US tons (3.6 billion metric tons) from the 3,000 operating quarries. In the state of Illinois, where this research was conducted, the annual production of crushed stone QB was estimated though a survey conducted among aggregate producers in the state, and was found to be as high as 855,000 tons (950,000 US short tons) (Tutumluer et al., 2015). Research conducted by Kumar and Hudson (1992) showed that stockpiled fines comprised an average of approximately 12% of the total annual aggregate production. More recently, NCHRP Synthesis 435 (volume 4) reported that, depending on the type of rock quarried, QB could make up to 25% of the total aggregates produced (Stroup-Gardiner and Wattenberg-Komas, 2013).

Given these massive quantities, and the negative environmental/economic consequences that result from QB accumulation at the quarries, the investigation of successful applications of QB as a sustainable and inexpensive construction alternative for pavements has become imperative. However, only few research studies have been conducted to date to evaluate the use of QB as a geotechnical pavement material in subgrade, subbase or base applications. Especially, the use of QB as an unbound material was found to be scarce in literature. Additionally, only few field evaluation studies investigated the performance trends of chemically stabilized layers of QB.

Most of the previous work documented to date has focused on laboratory characterization and evaluation of QB materials and proposing field applications based on laboratory performance. Further, most of the literature collected for the evaluation of QB as a sustainable or cost-effective material for pavements merely proposed the future use of sustainability frameworks or guidelines. NCHRP synthesis 435 (volume 4), being a main source of information on the use of QB, summarized the different QB applications in pavements by the different states in the U.S. and worldwide (Stroup-Gardiner and Wattenberg-Komas, 2013).

Since little work has been done to quantify the environmental and economic benefits that can result from using QB as a sustainable pavement material, the focus of this Ph.D. dissertation is on the design and evaluation of potential promising sustainable applications of QB materials in subsurface pavement layers. A detailed quantification of the economic and environmental benefits resulting from QB use is targeted to provide examples within the sustainability framework.

Some recent projects conducted at the Illinois Center for Transportation (ATREL) characterized and tested in the laboratory the properties of QB materials collected from several quarries in the state. In the recent ICT R27-125 project, entitled, "Sustainable Aggregates Production – Green Applications for Aggregate By-Products," QB production in Illinois was evaluated through questionnaires distributed to the aggregate producers. The amount of QB accumulated in the quarries, the annual production rate, excess QB generated, and the current application areas of QB were among the survey questions. Ninety percent of the survey respondents indicated that they were producing QB. Among the quarries that produced quarry fines in Illinois, 55% of them produced in excess of 100,000 tons of QB in a year (Tutumluer et al., 2015).

As part of the ICT R27-125 project, a detailed laboratory study was also conducted to characterize the engineering properties of QB materials produced in the primary, secondary, and tertiary aggregate production stages from four different major quarries operating in the State of Illinois. Property tests were conducted for determining aggregate gradation, particle shape characteristics, and mineralogical analyses of the QB samples. Differences in shape and gradation properties of QB materials produced in each crushing stage were observed. Because the unconfined compressive strength for QB materials is typically low (less than 11 psi [76 kPa]), two chemical admixture stabilizers (Portland cement and Class C fly ash) were used to improve the strength properties of QB materials. In general, the 2% cement or 10% Class C fly ash treated QB materials were 10 to 30 times stronger than the virgin QB samples (Tutumluer et al., 2015). Such significant increases observed in the strength of stabilized QB materials have indicated the suitability of QB for sustainable pavement applications, which established the need for the research efforts undertaken in this Ph.D. dissertation.

Another recent ICT project R27-124, titled, "Evaluation of Aggregate Subgrade Materials Used as Pavement Subgrade/Granular Subbase," had the objective of evaluating and validating the existing Illinois Department of Transportation (IDOT) 'Aggregate Subgrade' gradation bands through full-scale field testing (Kazmee and Tutumluer, 2015). Aggregate subgrades are large-sized rocks used in the IDOT Standard Specifications for Road and Bridge Construction linked to furnishing, transporting, and placing granular materials for subgrade improvement and subbase.

As part of the findings of the ICT R27-124 project, some of the penetration of aggregate subgrade materials into a very soft subgrade was demonstrated to be effective in improving the weak subgrade and preparing a fairly stable working platform layer in pavement construction (Kazmee and Tutumluer, 2015). Nevertheless, the uniformly graded materials, such as the railway ballast size or large primary crusher run aggregates with 6-8 in. (150-200 mm) top size, exhibited a wider variation in rutting performance trends because of the presence of large inherent voids

(Kazmee and Tutumluer, 2015). Therefore, one of the recommendations of the ICT R27-124 project was to consider the inclusion of smaller sized aggregate materials to fill voids, improve aggregate interlock, and improve the performance of the uniformly graded large size aggregate subgrade materials. Low cost QB or nonplastic fines were especially recommended for such beneficial and sustainable pavement applications. The challenge was to ensure uniformity by avoiding segregation among different blended aggregate sizes. The inclusion of QB for subgrade remediation activities with 'aggregate subgrade' is another aspect investigated in this Ph.D. dissertation.

Lastly, a study by LaHucik et al. (2016) investigated various proportions of cement-treated mixes of QB and Fractionated Reclaimed Asphalt Pavement (FRAP) or virgin coarse aggregates, and reported improvement in lab-measured unconfined strength properties for cement-stabilized mixes of 70% QB and 30% FRAP. The field performance and sustainability evaluations for such applications of chemically-stabilized QB blends with recycled coarse aggregates are further investigated in this Ph.D. dissertation.

In summary, various pavement applications can provide opportunities to utilize mass quantities of QB (Tutumluer et al., 2018). This Ph.D. dissertation therefore aims to evaluate sustainable pavement applications to incorporate QB materials by adequately evaluating their field performance, environmental impacts, and cost benefits. To assess the field performances of these QB applications, both unsurfaced and Hot Mix Asphalt (HMA) surfaced pavements were constructed as test sections at the Advanced Transportation Research and Engineering Laboratory (ATREL) and tested to failure using the Advanced Transportation Loading Assembly (ATLAS) equipment. Following Accelerated Pavement Testing (APT), forensic analysis tests (such as Falling Weight Deflectometer or FWD testing, HMA coring, Dynamic Cone Penetration or DCP testing, and trenching) were conducted to further evaluate the constructed test section performances. The results of APT and forensic analyses, followed by mechanistic analysis of FWD results, modeling, and sustainability/cost quantifications are reported in this dissertation to recommend the most successful and sustainable QB applications for proper utilization and construction practices.

## 1.2 STUDIED APPLICATIONS FOR QUARRY BY-PRODUCTS

In total, sixteen bound and unbound applications of aggregate quarry by-products were selected for performance evaluation. These applications were selected based on successful previous studies that provided initial evaluations of these applications through laboratory testing (Tutumluer et al., 2015; LaHucik et al., 2016; LaHucik et al., 2016a) and field evaluation recommendations (Kazmee and Tutumluer, 2015). In light of the outcomes of these previous research projects, the following applications were selected for studying QB usage as unbound aggregate materials and as chemically-stabilized materials:

1. Using QB for filling voids/gaps between large stones known as 'aggregate subgrade' on soft subgrades;
2. Increased fines content (e.g. 15% passing the No. 200 sieve) in dense-graded aggregate base layer over soft subgrade soils with CBR 1% or less;

3. Using QB as a cement or fly ash-treated subbase (e.g., in inverted pavements);
4. Using QB as a cement-treated base material; and
5. For base course applications, blending QB with coarse aggregate fractions of recycled materials [Fractionated Reclaimed Asphalt Pavements (FRAP) or Fractionated Recycled Concrete Aggregates (FRCA)] and stabilizing the blends with 3% cement or 10% class C fly ash by weight.

These selected QB applications were investigated by constructing 16 full-scale test sections, i.e. four construction working platforms and 12 flexible pavement test sections, evaluating their performances through APT as well as other nondestructive and destructive testing techniques during construction, and forensic analyses after APT. Following the field investigation, the flexible pavement applications were evaluated through mechanistic analysis using an axisymmetric finite element modeling approach. The environmental impacts and economic feasibility of using the chemically stabilized flexible pavement applications were further evaluated for field implementation.

## 1.3 OBJECTIVE AND SCOPE

The primary objective of this Ph.D. dissertation is to investigate, and document potential uses of aggregate quarry by-products as successful road subsurface/foundation layer applications. An application is considered successful when it shows satisfactory or good field performance, and is environmentally sustainable and economically feasible. The following specific scope items were considered to achieve the overall study objective:

- Develop and evaluate laboratory characterization techniques to select and investigate the proper construction of blended aggregate subgrade and QB layers, and the proper mix-proportioning of QB with and without recycled coarse aggregates and chemical admixtures, i.e., cement and fly ash.
- Evaluate the field performances of unstabilized and chemically stabilized QB applications for weak subgrade replacement, subbase and base layers through the accelerated testing of full-scale test sections: both unsurfaced working platform applications and asphalt-surfaced low to medium volume pavements are considered.
- Use the findings of the field performance evaluations and laboratory studies to properly model the studied applications, backcalculate layer modulus parameters, and calculate the response benefits for different pavement structures and scenarios. The response benefit is calculated as the ratio of the resilient surface deflections of a structure to those of a conventional flexible pavement with the same layer thicknesses and subgrade conditions.
- Evaluate the environmental footprint and the cost benefits of using chemically stabilized QB materials and mixes of QB and other recycled materials in selected subbase and base applications. The environmental and

economic feasibility of the evaluated QB applications are evaluated by conducting a Life Cycle Assessment (LCA) and Life Cycle Cost Analysis (LCCA) by considering impacts of materials acquisition, transportation, and construction of pavement test sections with selected QB applications.

## 1.4 RESEARCH METHODOLOGY

To fulfill the above stated research objective and scope, the following tasks and methodologies are considered in this Ph.D. dissertation:

- Characterize properties and engineering behavior of the selected construction materials by collecting and testing adequate amounts of the selected QB and other construction materials to determine their engineering properties. Properties such as grain size distribution, morphological shape properties, moisture-density relationships, packing of QB with other recycled/marginal materials, and unconfined compressive strength tests were conducted.
- Construct, instrument, and test full-scale pavement test sections designed to incorporate the selected sustainable applications of QB materials. Sixteen test sections were constructed in three test 'Cells' to evaluate a unique set of QB applications. Soil pressure cells were used to collect pressure values on top of the subgrade under some of the stabilized QB test sections and the conventional flexible section.
- Conduct accelerated pavement testing and performance monitoring of the constructed test sections through frequent measurements of rutting progression, subgrade pressures, and visual inspection of the test sections.
- Test and monitor the full-scale pavement layers during construction, performance testing, and after trafficking. The quality and strength of the constructed test sections were investigated by collecting data for the achieved nuclear gauge densities, DCP testing, LWD modulus measurements, FWD deflection measurements, HMA coring, and trenching.
- Analyze field section performances and make recommendations for implementation of research findings. The recommendations were documented based on the construction and accelerated testing stages, and the interpretation of the study results in comparison with results from previously conducted field studies.
- Conduct mechanistic analyses of the FWD deflections using GT-PAVE finite element analysis program, and use the backcalculated layer modulus properties to model pavement structures, with different layer thicknesses, utilizing chemically stabilized QB materials in base or subbase layers.
- Conduct LCA and LCCA studies considering three different scenarios for all evaluated chemically stabilized QB applications. The three scenarios consider the as-constructed layer thicknesses (i.e. accounting for thickness variations during construction), targeted layer thicknesses in design (a thicker

pavement structure for higher anticipated traffic volumes), and thinner proposed pavement structures with the different chemically stabilized QB mixes, targeting low volume road applications.

## 1.5 DISSERTATION OUTLINE

This Ph.D. dissertation consists of nine chapters, including this introduction chapter. The outline of the dissertation chapters, and the topics covered in each chapter are illustrated in Figure 1.1. The detailed contents of the chapters are as follows:

**Chapter 2** Titled 'Literature Review,' provides a comprehensive literature of the previous studies associated with using QB, recycled materials, and marginal aggregates in pavement applications. Quarry operations and the impact of crusher types on QB production are discussed. This chapter also discusses common methods used to design and analyze construction working platforms and flexible pavements, nondestructive and destructive methods used to evaluate pavement quality, as well as an overview of the cost/ benefits of using QB in pavements and other sustainability and performance aspects.

**Chapter 3** Titled 'Materials Selection and Laboratory Studies,' provides a discussion of the materials selection criteria and the laboratory component of this dissertation. Laboratory tests such as grain size distribution, moisture-density tests, packing studies of QB with recycled coarse aggregates and with large aggregate subgrade rocks, and unconfined compressive strength testing of chemically stabilized QB applications are discussed in this chapter.

**Chapter 4** Titled 'Design, Construction and Quality Assurance of Field Experiment,' provides layouts of the field pavement test sections, and detailed descriptions of construction activities such as subgrade strength modification, various construction phases of the full-scale test sections, pavement instrumentation with subgrade soil pressure cells, and associated quality control tests.

**Chapter 5** Titled 'Full-Scale Testing and Performance Monitoring,' provides a summary of the performance records of the constructed working platform and flexible pavement test sections. This includes the rutting progression in all test sections and the measured top of subgrade wheel load stresses for sections instrumented with soil pressure cells.

**Chapter 6** Titled 'Full-Scale Study Results and Interpretations,' provides a summary of the tests conducted after the APT, and an interpretation of the performance of the test sections in light of the different datasets collected during the stages of construction, trafficking, and forensic analysis.

**Chapter 7** Titled 'Mechanistic Analyses of Pavement Test Sections,' provides an examination of the FWD deflection basin parameters to identify trends in the load-deformation behavior of the constructed pavement layers evaluating QB applications. A Finite-Element (FE) analysis and pavement modeling scheme using GT-PAVE FE program is presented to backcalculate the modulus properties from FWD deflections. Critical pavement responses for various pavement structures and thicknesses are evaluated based on the backcalculated moduli values, and resilient response benefits are computed for each pavement structure as the ratio of the FWD measured/predicted maximum surface deflection to that of a conventional flexible pavement with the same layer thicknesses and similar subgrade and loading conditions.

**Chapter 8** Titled 'Environmental and Economic Impacts for QB Usage,' provides detailed discussion for the LCA and LCCA studies that were conducted for the stabilized QB applications. The three design scenarios considered for pavements with as-constructed and as-designed layer thicknesses and new proposed pavement sections and the LCAs and LCCAs conducted for each scenario are discussed in detail. The sustainability study goal and scope, system boundary, functional unit, impact categories, and the quality of collected data are all defined in this chapter. The interpretation of LCA results are then presented and discussed for all studied scenarios and pavement sections. Finally, the total cost of each pavement test section is presented based on the quantities and the activities involved for each bid item.

**Chapter 9** Titled 'Summary and Conclusions,' provides a summary of the test results, and the main recommendations and conclusions from the field evaluations of QB applications. The main conclusions from the mechanistic analyses of the pavement test sections, as well as the recommendations for materials selection and pavement design based on the results of the LCA and LCCA are outlined in this chapter. Finally, this chapter discusses recommended implementation practices considering performance, cost, and environmental aspects, and outlines the limitations considered in this dissertation and the areas for future research needs.

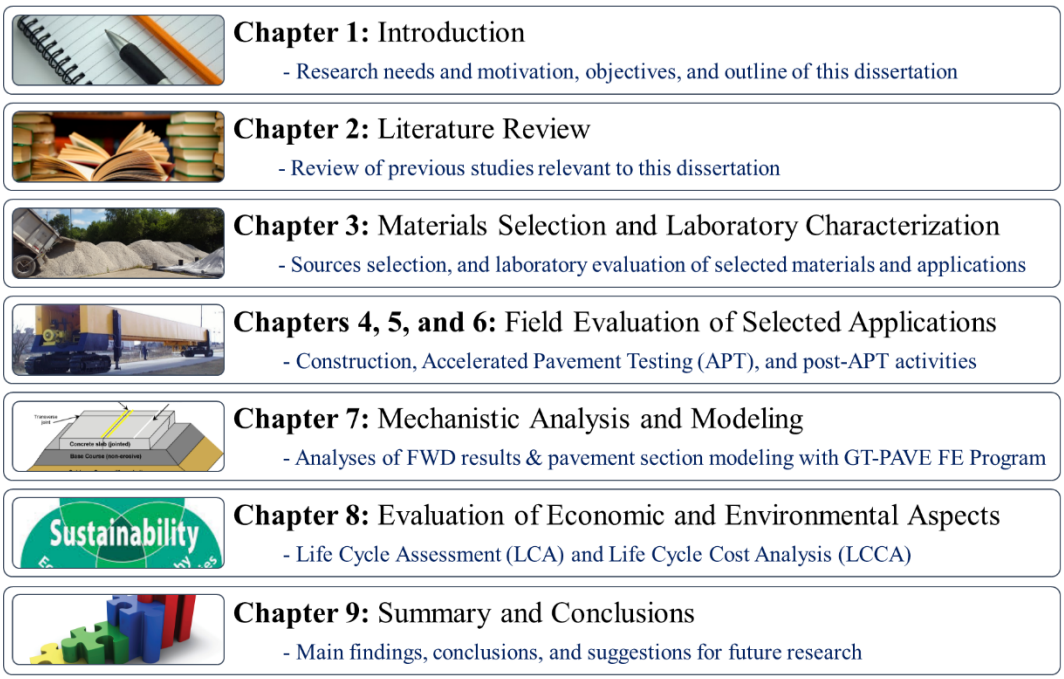


Figure 1.1 Outline of dissertation chapters and topics

# CHAPTER 2: LITERATURE REVIEW

## 2.1 INTRODUCTION

This chapter presents a brief summary of research related to the topics presented in this dissertation. Studies related to the use and characterization of Quarry By-Products (QB) in pavement applications are first presented. A comprehensive literature review is presented for the laboratory characterization of QB, and their utilization in pavement applications. The use of other recycled/nontraditional aggregates, an overview of quarry operations and fines productions, and a brief review of the current design practices for low volume roads/construction platforms are also described in this chapter. Quality assurance methods are reviewed for constructed pavement applications. Finally, a discussion for the cost benefits of QB use, and previous efforts to evaluate QB as a sustainable and economic material through Life Cycle Assessment (LCA) and Life Cycle Cost Analysis (LCCA) are presented.

## 2.2 BY-PRODUCT FINES GENERATED AT QUARRIES

Quarry by-products are found abundantly all over the United States as an entailment to the vast network of crushed rock extraction facilities. Quarry by-products are generated during blasting, crushing, and washing operations. The processes involved in QB generation, and the types of QB generated from each process are detailed in Figure 2.1. These QB materials are produced during the extraction and processing phases as scalpings and quarry fines (Petavratzi and Wilson 2008). QB can exist in three types during these quarry operations: screenings, settling pond fines, and baghouse fines (Chesner et al., 1998; Stroup-Gardiner and Wattenberg-Komas, 2013). NCHRP Synthesis 435 (volume 4) defines screenings as materials finer than No. 4 sieve (4.75 mm) that accumulates after primary and secondary crushing. Settling pond fines are minus No. 30 sieve (minus 0.60 mm) materials collected by gravity from settling ponds after washing aggregates and recovery. Baghouse fines, on the other hand, are collected by dry processing plant dust collection systems (Stroup-Gardiner and Wattenberg-Komas, 2013).

During the crushing stages, QB are generally carried out in three stages: primary crushing, secondary crushing, and tertiary crushing (Petavratzi and Wilson 2008). Research conducted in the early 1990s showed that stockpiled fines comprised an average of approximately 12% of the total annual aggregate production of the surveyed companies (Kumar and Hudson, 1992). The more recent NCHRP Synthesis 435 (volume 4), reports that, depending on the type of rock quarried, QB can make up to 25% or more of the total aggregates produced (Stroup-Gardiner and Wattenberg-Komas, 2013). Due to the high accumulation of QB that exceeds four billion tons (3.6 billion metric tons) of QB from 3,000 quarries in the U.S. (Chesner et al., 1998) and the high quantities of QB produced yearly, which can be as high as 950,000 tons in Illinois alone (Tutumluer et al., 2015), the use of QB as a sustainable pavement construction material becomes imperative.

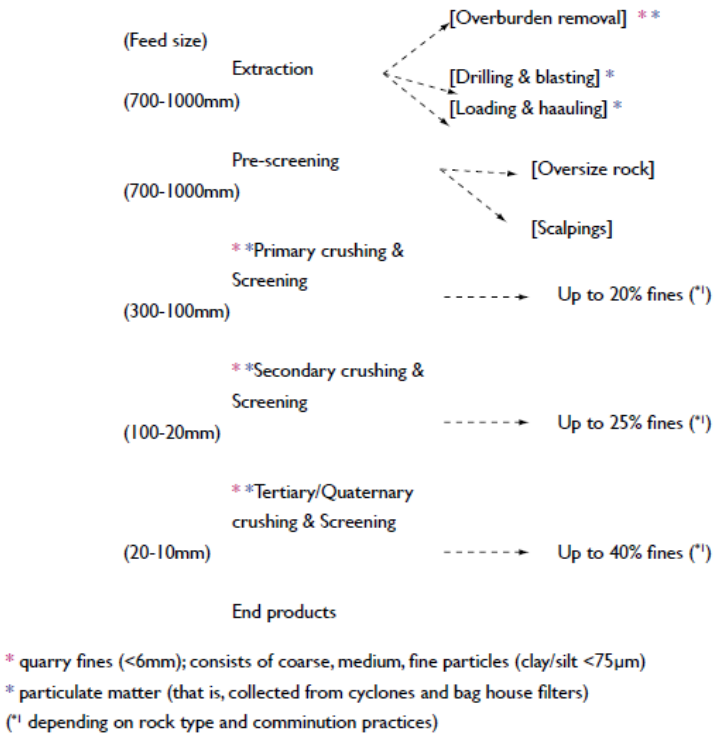


Figure 2.1 Processes involved in QB generation during crushed aggregates production (Source: Petavratzi and Wilson 2008)

Petavratzi and Wilson (2008) reported more detailed percentages for QB generation based on the rock type quarried. These percentages, along with other details are summarized in Table 2.1, which indicates that the use of hammer mill impact crushers generate higher fines content than other types of crushers, while jaw crushers generally produce the lowest fine materials. Additionally, the crushing of limestone rocks generally produces higher quantities of fines when compared to igneous, metamorphic and sandstone rocks. Common type of crushers used for the production of crushed aggregate materials at the quarries are presented in Figure 2.2. These crusher types are jaw crushers, cone crushers, gyratory crushers, and impact crushers. Jaw crushers are normally utilized for the primary crushing. The cone crusher is widely used by crushed rock producers due to its relatively lower operational costs and low fines (QB) generation. The gyratory crusher is quite similar in operation to the jaw crusher, and the main difference is that a gyratory crusher has a conical head and a concave plate. Finally, impact rushers are divided into two types: vertical shaft impact crushers and horizontal shaft impact crushers. The horizontal shaft impact crushers are more commonly used for processing softer materials such as limestone, while the vertical shaft impact crushers have more capability of producing cubical aggregates needed for concrete production. Additionally, with vertical impact crushers, the quantities of fines generated during aggregates production can be limited to acceptable levels if the right operation techniques are implemented (Tarmac Ltd and Partners, 2011).

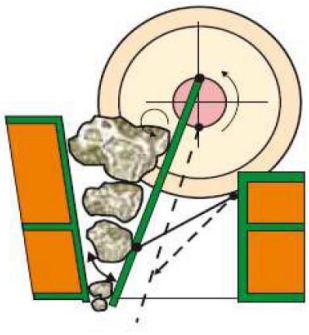

Jaw Crusher [1]

Cone Crusher [2]

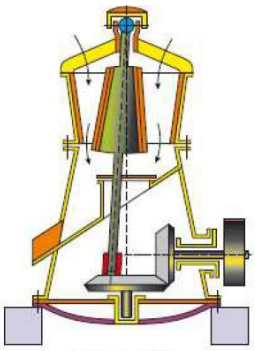

Gyratory Crusher [1]

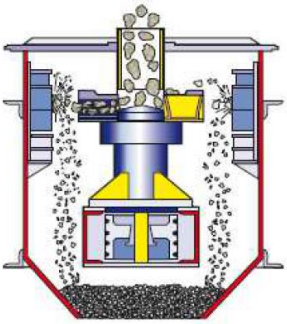

Vertical Shaft Impact Crusher [1]

Horizontal Shaft Impact Crusher [3]

Figure 2.2 Common types of crushers used for crushed aggregates production [Adapted from (1) Tarmac Ltd and Partners, 2011; (2) Stedman ™, 2019; (3) Blue group, 2019]

Table 2.1 Estimation of quarry fines produced during crushing (After Petavratzi and Wilson, 2008)

| **Crushing stage** | **Rock type** | **Proportion of fines in the crusher product (% by weight)** | **Good practice** |
|---|---|---|---|
| Primary Crushing | Igneous and metamorphic | 3 - 6% (j) to 10 - 15% (g) | Changes at the closed side setting (CSS) of jaw crushers (optimizing the CSS) or the feed system (such as replace choke system with non-choke system) may reduce fines. |
| | Limestone | 6 - 7% (j) to 20% (hm) | |
| | Sandstone | 1 - 2% (j) to 15 - 20% (j, g) | Overall, small quantities are produced (<5%) and any changes may have little effect on the total arisings of quarry fines. |
| Secondary Crushing | Igneous and metamorphic | 0 - 23% (c) | |
| | Limestone | 15 - 25% (c) to 30% (hm) | During secondary and tertiary crushing higher quantities of quarry fines are produced and minimization of them will have an effect on overall fines production. |
| | Sandstone | 10 - 15% (c) | |
| Tertiary Crushing | Igneous and metamorphic | 5 - 30% (c) to 40% (hm) | Pre-screening of the feed can remove a substantial proportion of fines, avoid packing of material in the chamber and introduce a more uniform feed distribution to the crusher. |
| | Limestone | < 20% to 40% (hm) | |
| | Sandstone | ~15% (c) to 40% (hm) | Optimization of the closed side settings of crushers may reduce fine material.<br>The rotor speed of impact crushers is directly proportional to the production of fines. Slower rotor speeds may reduce the amount of fines produced. |

Key: (j) refers to jaw crushers, (g) refers to gyratory crushers, (c) refers to cone crushers, (hm) refers to hammer mill crushers

## 2.3 LABORATORY CHARACTERIZATION OF QUARRY BY-PRODUCTS

Due to the high production and accumulation rates of QB, potential application areas in the construction and rehabilitation of the transportation infrastructure have been reported in the literature (Kumar and Hudson, 1992; Puppala et al., 2008; Lohani et al., 2012; Stroup-Gardiner and Wattenberg-Komas, 2013; Tutumluer et al., 2015). Several past research studies focused on laboratory property testing and evaluating potential field applications of QB: Kalcheff and Machemehl (1980) conducted particle size distribution tests for different types of QB. It was reported that screenings generally contain freshly fractured faces, have fairly uniform gradation, and contain few plastic fines. The particle distributions of the tested QB materials followed a similar gradation trend, with particles smaller than sieve No. 200 (0.075 mm) ranging from 6% to 12%. The particle distributions of different QB aggregate sources are presented in Figure 2.3(a). Similarly, Tutumluer et al. (2015) investigated the grain size distributions of freshly-produced QB screenings collected from several quarry locations and crushing stages - primary, secondary, and tertiary - in the state of Illinois. These grain size distributions are shown in Figure 2.3(b). The different QB materials generally had a nominal maximum size of 0.19 in. (4.75 mm or No. 4 sieve), and a fines content passing the No. 200 sieve (0.076 mm) ranging from 7% to 15%.

It is generally agreed upon that the properties of QB can vary largely depending on the parent rock and the employed crushing technologies. Thus, the properties of QB materials may not be easily generalized or predicted (Stroup-Gardiner and Wattenberg-Komas, 2013; Wood and Marek, 1995; Manning, 2004). Dumitru et al. (2001), proposed conducting mineralogical tests, such as X-ray diffraction analysis, to determine the compositions of QB materials and quantify secondary minerals or other harmful content that can impact the performance of QB materials used for certain applications. The chemical and mineralogical composition of QB material can vary based on the parental material and handling. Stokowski (1992) concluded that quarry fines have higher contents of calcium carbonate ($CaCO_3$), silicon oxide ($SiO_2$), aluminum oxide ($Al_2O_3$), and ferrous oxide ($Fe_2O_3$) relative to magnesium carbonate ($MgCO_3$), and thus have lower specific gravity due to their chemical and mineralogical properties. He also concluded that the presence of calcite ($CaCO_3$) and clay minerals ($SiO_2$, $Al_2O_3$, and $Fe_2O_3$) make QB materials relatively soft. Petavratzi and Wilson (2008) reported that QB materials were generally non-hazardous and composed of the same minerals as the parent rock/soil, but exposure to atmospheric conditions could detrimentally alternate some of their physical and chemical properties (Petavratzi and Wilson, 2008).

Several research studies conducted laboratory investigations for untreated (virgin) QB materials. Puppala et al. (2008) reported that the liquid limit and plastic limit of a QB material in Texas were found to be 21.5% and 11.7%, respectively, while the specific gravity was 2.65. Similarly, several QB materials collected from different crushing stages from four quarries in Illinois were tested for Atterberg limits, in accordance with ASTM D4318 method, and were found to have relatively low liquid limits. All these QB materials had essentially nonplastic fines passing the No. 40 (0.42 mm) sieve. (Tutumluer et al., 2015). Studies also reported that the compressive strength properties of untreated QB could be relatively low, and recommended stabilizing QB materials for pavement applications (Puppala et al., 2008; Tutumluer et al., 2015; Mwumvaneza et al., 2015).

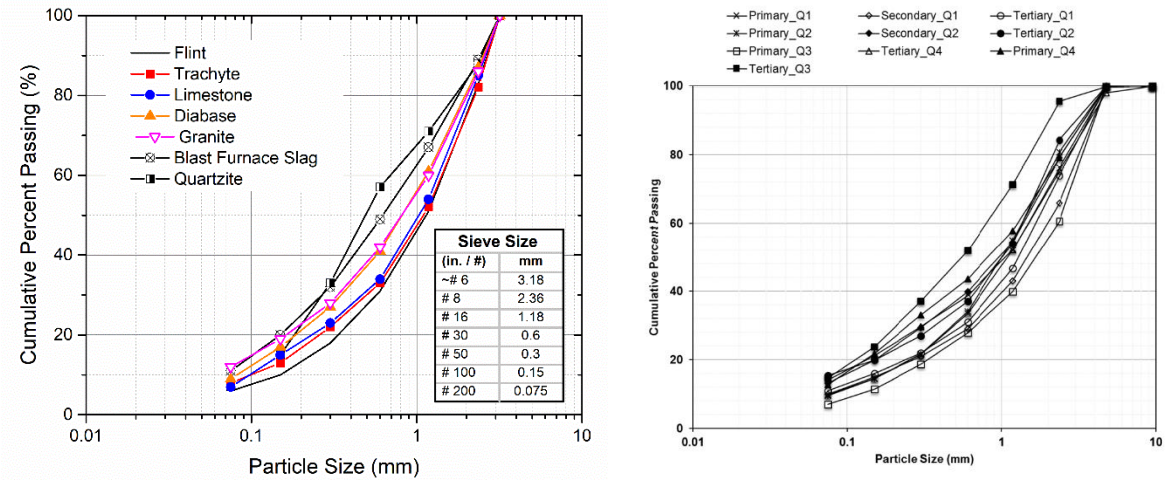


(a) (b)

Figure 2.3 Average particle size distributions of (a) QB materials from different rock types [Adapted from Kalcheff and Machemehl, 1980], and (b) QB materials from different quarries/ crushing stages in IL [Source: Tutumluer et al., 2015]

Additional tests conducted on untreated QB materials, and reported in literature, include free-swelling tests in accordance to ASTM D698, modified Methylene blue test to investigate the content of harmful clay, and direct shear tests to determine the shear strength properties of QB materials. Puppala et al. (2012) conducted one-dimensional vertical free-swelling tests for QB and found the QB samples used in the study had moderate swelling potential. Tutumluer et al. (2015) concluded that the harmful clay content of QB materials was generally less than 3% for different sources and crushing stages. The same study reported that QB from primary crushing stages generally comprised higher contents of harmful clay. Direct shear tests were performed in accordance with ASTM D3080 on QB materials selected from different crushing stages in the same quarry. The friction angles obtained for primary, secondary, and tertiary crusher QB samples were rather high around 59º (Tutumluer et al., 2015). The results from the direct shear study are summarized in Figure 2.4.

Based on laboratory testing results, some researchers have utilized chemical stabilization and accordingly recommended specific field applications for QB. According to Kalcheff and Machemehl (1980), the stabilization of QB with cement developed relatively high rigidity with a small amount of Portland cement compared with granular soil-cement stabilization. The use of low-cement content has the advantage of decreasing the shrinkage cracking. Kumar and Hudson (1992) examined the unconfined compressive strength, tensile modulus of elasticity, and Poisson's ratio of cement-treated QB materials. They concluded that stabilizing QB with cement could produce the adequate compressive strength, modulus of elasticity, and tensile strength required for subbase materials. They proposed a base course material additive, flowable fill, under slab granular fill, and cement-stabilized subbase/base layers as possible pavement applications of QB.

Stabilized QB mixes were also evaluated for applications such as flowable fills, soil modification and Self-Consolidating Concrete (SCC). According to the results presented in the study by Wood and Marek (1995), using 3% cement, 8% fly ash, and 89% QB resulted in a flowable fill with adequate performance. Naik et al. (2005) examined the use of QB in SCC and reported that the addition of QB minimized the needed quantity of admixtures without reducing the strength of the SCC. Koganti and Chappidi (2012) reported that using up to 40% QB by weight proved to be beneficial in improving the strength of black cotton expansive soil.

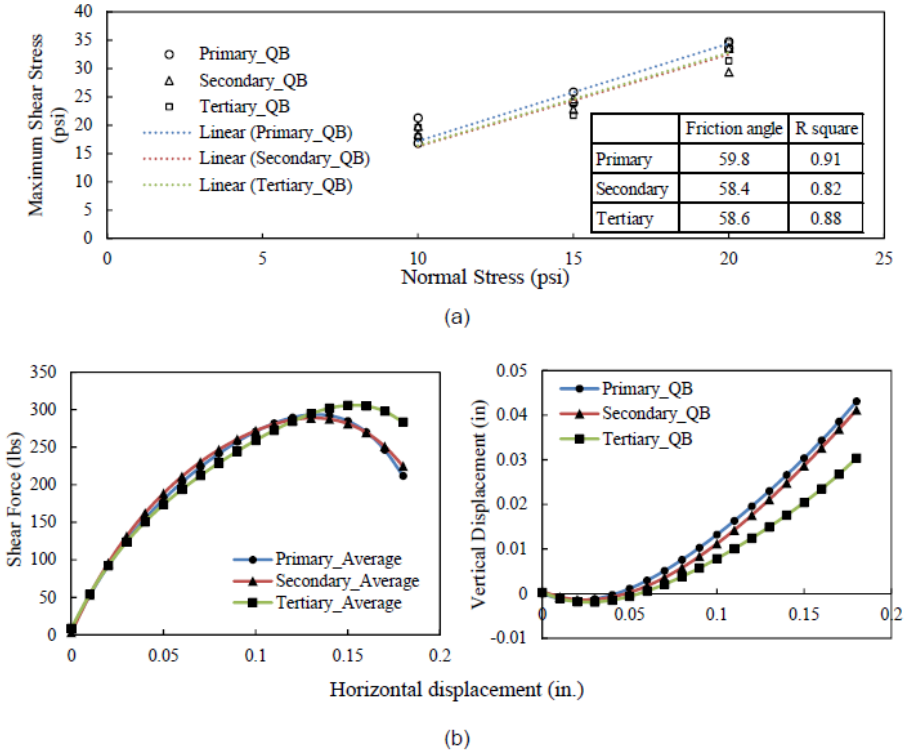


Figure 2.4 Direct shear test results for (a) the different normal stresses studied, and (b) at the 10-psi normal stress (Source: Tutumluer et al., 2015)

Recent laboratory studies investigated the use of QB (or quarry fines) for pavement applications. Abdullah et al. (2018) conducted workability tests, flexural strength tests, and compressive strength tests on concrete samples with 100% quarry dust used for sand replacement in concrete. The study concluded that concrete samples with 100% QB as fine aggregates produced more sustainable concrete samples with better durability, compressive strength and furnishing properties. The same study reported that concrete samples with QB had higher water absorption and workability at lower water cement ratios. Schankoski et al. (2017) evaluated the rheological properties of fresh cement paste with QB (diabase or gneiss quarry rock powders). They concluded that cement pastes containing QB had lower yield stress and lower viscosity than samples with cement pastes only.

Puppala et al. (2008) reported that the addition of 2.3% cement increased the unconfined compressive strength of QB materials to 174 psi (1,200 kPa). They concluded that the strength and resilient modulus of the cement-treated QB were similar to those of sandy materials with very few fines. Mwumvaneza et al. (2015) conducted Unconfined Compressive Strength (UCS) tests on 10% Class 'C' fly ash and 2% Portland cement-stabilized QB samples, and they examined that the chemically stabilized QB specimens exhibited up to 30 times strength improvement when compared with untreated QB materials (Mwumvaneza et al., 2015; Tutumluer et al., 2015). The results of the study are presented in Figure 2.5.

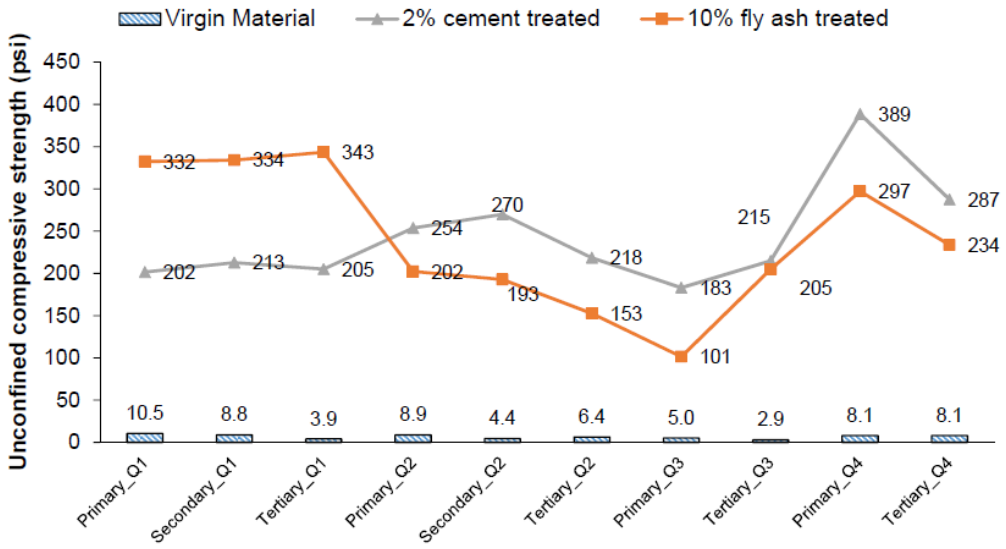


Figure 2.5 Average UCS for virgin, 2% cement-, and 10% Class C fly ash–treated QB materials. 1 psi = 6.9 kPa. (Source: Tutumluer et al., 2015)

Finally, in a laboratory study conducted by LaHucik et al. (2016; 2016a), various proportions of cement-treated mixes of QB and Fractionated Reclaimed Asphalt Pavement (FRAP) or virgin coarse aggregates were evaluated. Based on aggregate packing tests conducted with different proportions of QB and FRAP by weight, an optimal blending ratio of 70% QB with 30% FRAP was found to maximize density/minimize void content. LaHucik et al. (2016) also evaluated mix design performances through strength tests (compression/split tension) and modulus tests. Higher cement content increased both the strength and elastic modulus properties of all the tested mixes. Mixtures containing virgin aggregates with QB yielded statistically greater elastic moduli than mixtures with FRAP and QB. Fibers were used as additives in some of the mixtures. From statistical analysis, the fibers did not have a considerable influence on strength or elastic modulus but did provide residual shear capacity across cracks. The QB and FRAP or QB and virgin aggregate mixtures with 3% to 4% cement content exceeded the strength of typical cement-stabilized base materials reported in the literature (LaHucik et al., 2016; LaHucik et al., 2016a). The mix designs used in their study are presented in Table 2.2, while the test results for UCS, split tensile strength, and resilient modulus are detailed in Figure 2.6.

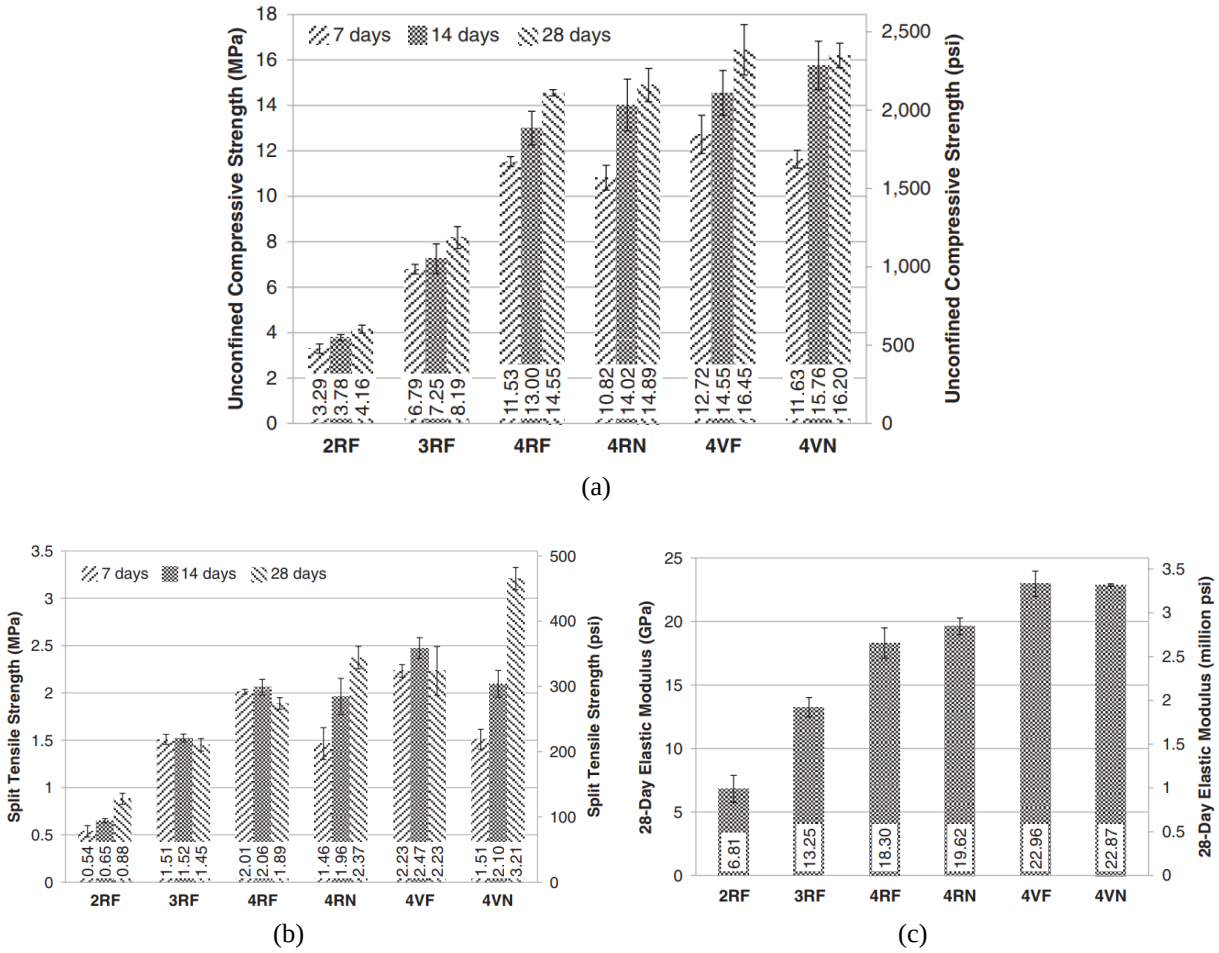


Figure 2.6 Results for (a) UCS, (b) Split tensile strength, and (c) elastic modulus for QB samples blended with FRAP or virgin aggregates. 1 MPa = 145 psi. (Source: LaHucik et al., 2016a)

Table 2.2 Mix proportions by weight. 1 pcf = 16 kg/m$^3$ (Adapted from LaHucik et al., 2016a)

| **Mixture** | **2RF** | **3RF** | **4RF** | **4RN** | **4VF** | **4VN** |
|---|---|---|---|---|---|---|
| Fibers (kg/m$^3$) | 3.64 | 3.64 | 3.64 | NA | 3.64 | NA |
| Cement (kg/m$^3$) | 62.9 | 94.3 | 125.8 | 125.8 | 125.8 | 125.8 |
| FRAP (kg/m$^3$) | 647.9 | 648.5 | 638.4 | 647.3 | NA | NA |
| Coarse (kg/m$^3$) | NA | NA | NA | NA | 471.7 | 474 |
| Intermediate dolomite (kg/m$^3$) | NA | NA | NA | NA | 202.3 | 203.5 |
| QB (kg/m$^3$) | 1,577.00 | 1,578.20 | 1,554.40 | 1,575.20 | 1,565.10 | 1,574.00 |
| Water (kg/m$^3$) | 151.9 | 148.3 | 152.5 | 147.1 | 154.9 | 148.3 |

R = FRAP, V = Virgin aggregates, F = Fibers added, N = No fibers added, NA = Not Available, 2/3/4 = % of cement by volume

## 2.4 QUARRY BY-PRODUCT APPLICATIONS IN PAVEMENTS

Various field applications to utilize QB materials were proposed by researchers to date based on their mechanical and physical properties and laboratory test results. McClellan et al. (2002) sampled QB from several quarries in Florida and reported on the engineering backfill use, and the direct addition to concrete mixes as a filler or fine aggregates for potential sustainable applications of QB. These applications required the usage of mass quantities of QB. Other potential applications for QB included self-consolidating concrete (Wood and Marek, 1995; Naik et al., 2005), and the replacement of sand in concrete to enhance pozzolanic reactions and durability (Lohani, 2012).

NCHRP synthesis 435 (volume 4) summarized the different uses of QB in pavement applications from a limited number of research projects and highway applications, and evaluated usage of QB and mineral by-products, most of which focused on bound layer applications (Stroup-Gardiner and Wattenberg-Komas, 2013). The following QB applications were listed for bound pavement layers: (1) Portland cement substitution, (2) Portland cement concrete, (3) self-consolidating concrete, (4) hot mix asphalt, and (4) stabilized base materials. On the other hand, the unbound applications of QB were mostly limited to base and subbase applications. Whereas other applications may include QB usage in embankments as fill materials, chip seals, flowable fill, and fine aggregate in HMA overlays. Table 2.3 and Table 2.4 list the usage data for QB materials in pavement applications in the United States, as reported by Stroup-Gardiner and Wattenberg-Komas (2013).

A comprehensive survey for QB usage was sent to aggregate producers in the state of Illinois (Tutumluer et al., 2015). The results of the survey, as shown in Figure 2.7, identified the following as the main QB applications in Illinois: Aglime (highest usage category), trench backfill, earth fill applications, fine aggregates replacement for concrete, and other uses such as HMA mixes, limestone cement, and aggregate subgrade (Tutumluer et al., 2015).

Table 2.3 States using QB in highway applications (After Stroup-Gardiner and Wattenberg-Komas, 2013)

| Number of applications | Baghouse fines | Pond fines | Screenings | Unknown types |
|---|---|---|---|---|
| 9 | - | - | - | ID |
| 6 | - | - | - | GA |
| 5 | - | - | ND | |
| 4 | - | - | SC, VA | |
| 3 | - | SC | CO, KY, MS, NY, VT, WA, WI | |
| 2 | VA, WI | - | CT, FL, GA, IL, IN, IA, NC, NE, PA | NY |
| 1 | AL, CT, DC, FL, GA, KY, MN, MS, NJ, NM, NV, NY, OK, TX, VT, WA, WV | CT, IL, IN, MD, OH, WI | AL, AR, DC, DE, LA, MD, ME, MO, OH, OR, TX | CT, IL, NM |

Table 2.4 Number of States using QB in various applications (After Stroup-Gardiner and Wattenberg-Komas, 2013)

| Byproduct | Asphalt Cements or Emulsions | Crack Sealants | Drainage Materials | Embankments | Flowable Fill | HMA | Pavement Surface Treatment (non-structural) | PCC | Soil Stability |
|---|---|---|---|---|---|---|---|---|---|
| Baghouse Fines (aggregate production) | 1 | 0 | 0 | 0 | 0 | 17 | 2 | 1 | 0 |
| Pond Fines | 0 | 0 | 0 | 1 | 1 | 4 | 2 | 1 | 0 |
| Screenings | 0 | 0 | 6 | 5 | 8 | 25 | 11 | 7 | 1 |
| Mineral or Quarry Byproduct, Unknown Type | 1 | 1 | 2 | 3 | 3 | 5 | 1 | 2 | 2 |

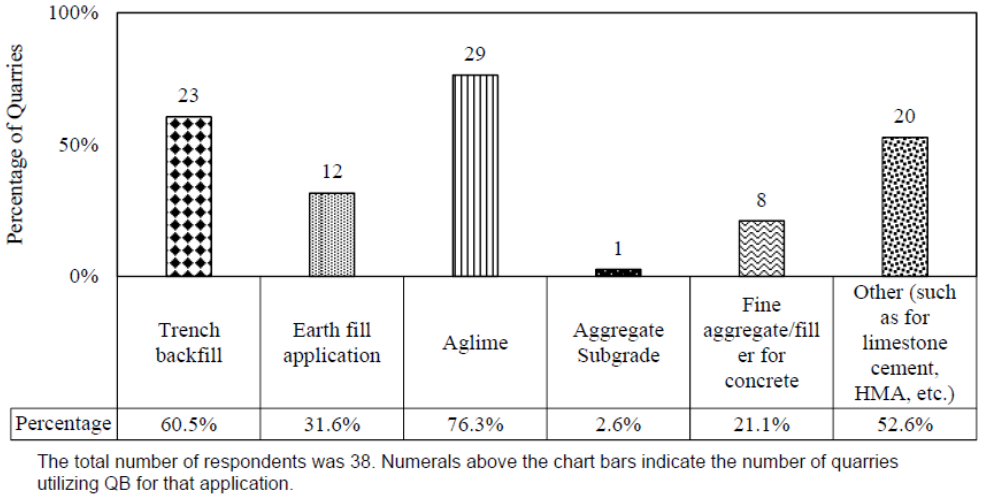


Figure 2.7 QB utilization in the State of Illinois (Source: Tutumluer et al., 2015)

In Europe, on the other hand, the following bound and unbound applications were proposed and applied for QB materials. Unbound applications included: (1) soil re-mineralization, (2) compost, (3) artificial soils, (4) remediation site restoration, (5) landscaping road pavements, (6) embankment construction, (7) landfill capping, (8) filler applications, (9) manufactured sand, (10) cement making, (11) green roofs, and (12) straw and clay blocks. Bound applications, on the other hand, included: (1) concrete, (2) hydraulically bound mixtures, (3) manufactured aggregates, (4) ceramic products, (5) asphalt pavement, (6) bituminous blocks, (7) synthetic rock, (8) kerbs (curbs), (9) fiber reinforced pre-cast units, and (10) grout products (Petavratzi and Wilson, 2008). Note that these listed applications also include other applications in addition to the pavement-related ones.

The use of QB as a subsurface material, in a base or a subbase layer, was evaluated through field studies. The QB was used as a 8-in. (203-mm) thick base layer, topped with 1.2 in. (30 mm) of surface treatment for a low traffic volume roadway in Brazil (de Rezende and de Carvalho, 2003). No significant structural damages were observed for more than three years of service. However, the QB that was used had around 45% of material passing the No. 4 sieve (4.75 mm) and had a relatively high percentage of silt- and clay-sized materials (22%). Lab-measured resilient modulus values ranged from 28.5 to 68.4 ksi (196.6 to 471.6 MPa).

Researchers have investigated the use of QB in a stabilized base layer. In a study in Lynn County, Iowa, the use of emulsion-stabilized limestone screening was investigated as a base material (Nelson et al., 1994). Several test sections with base thicknesses of 4 to 6 in. (100 to 150 mm) and asphalt-cement contents of 2.5%, 3.5%, and 4.5% were inspected. The 4-in. (100-mm) thick base did not produce a satisfactory low cost maintenance roadway, based on periodic crack survey data and structural adequacy assessment using a Road Rater equipment. Thus, the researchers recommended a 6-in. (150-mm) thick emulsion-stabilized QB base with more than 3.5% asphalt cement, topped with 2 in. (50 mm) HMA surface, which could provide a low maintenance roadway (Nelson et al., 1994).

In a study in Arlington, Texas, the use of limestone QB was evaluated as a base material for sections of State Highway 360 (Puppala et al., 2008). A 36-in. (914-mm) thick layer of quarry fines stabilized with 2.3% cement was used as the base overlain by a 4-in. (102-mm) thick HMA and 8-in. (203-mm) thick Continuously Reinforced Concrete Pavement (CRCP) surface. The cross section of the constructed highway is presented in Figure 2.8. Field monitoring using horizontal inclinometers showed that the sections experienced low permanent deformation during service. Additionally, the International Roughness Index (IRI) values were measured to be within 32-158 in./mile (0.5-2.5 m/km) after 30 months of service, which is lower than the threshold value of 200 in./mile (3.15 m/km), thus indicating good performance (Puppala et al., 2012).

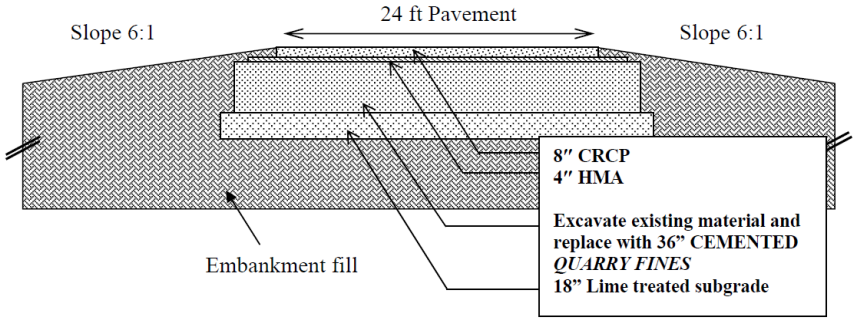


Figure 2.8 Typical cross section of Texas highway 360 with cement-stabilized QB base (Source: Puppala et al., 2008)

## 2.5 RECYCLED / MARGINAL AGGREGATE APPLICATIONS IN PAVEMENTS

Large quantities of construction and demolition wastes are produced each year in the United States and the world. The U.S. Environmental Protection Agency (EPA) estimated that 534 million tons of construction and demolition waste was generated in the United States in 2014 from demolition, rehabilitation and renovation activities for buildings, roads and bridges. The composition of these 534 million tons is shown in Figure 2.9. Of the total waste before recycling, 70% was concrete and 14% was asphalt concrete (EPA, 2016). Another recent study in Illinois by Lippert et al. (2014) reported that a total of 1.7 million tons of materials was recycled in 2013, which indicated a 43% increase in recycled tonnage from 2012 in Illinois (Lippert et al., 2014). To this end, several researchers have reported that Reclaimed Asphalt Pavement (RAP) and Recycled Concrete Aggregates (RCA) account for the highest percentages of recycled tonnage. A Federal Highway Administration (FHWA) report estimated that around 80% of the recovered old asphalt pavements were recycled, and two-thirds of the recycled quantity ended up being used as aggregates for road base (Bloomquist et al., 1993; Horvath, 2003).

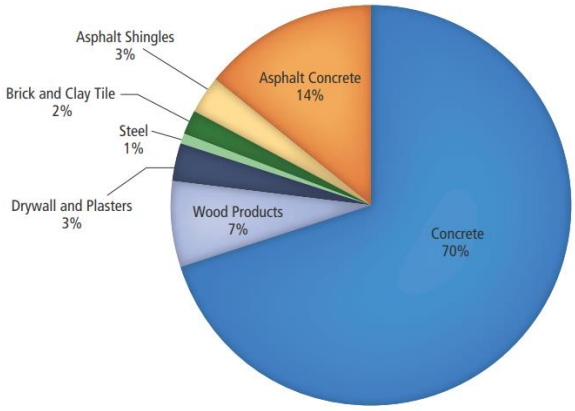


Figure 2.9 Composition of construction and demolition waste in the United States in 2014 before recycling (Source: Environmental Protection Agency, 2016).

Due to the wide use of recycled materials in pavement foundation and subsurface (base/subbase/subgrade) applications, researchers have focused on the evaluation of the engineering properties and field performance of recycled materials in unbound and bound pavement layers. Bennert et al. (2000) evaluated recycled concrete aggregates and recycled asphalt pavement aggregates for resilient modulus and permanent deformation trends and compared their performance with virgin Dense-Graded Aggregate Base Course (DGABC) materials in New Jersey. Mixes of various percentages of RCA and RAP with virgin DGABC were prepared to investigate optimum blending ratios that could enhance performance. The researchers reported that the blends of RAP, RCA, and DGABC materials obtained higher resilient modulus values than the currently used virgin aggregates, while the blends containing RCA accumulated the lowest amount of permanent deformation.

Arulrajah et al. (2012) reported that RCA and waste rock used as subbase materials have geotechnical engineering properties equivalent or superior to those of conventional granular quarry materials. Similar research

findings were reported on the use of RAP, RCA, or blends with virgin aggregates for unbound pavement applications (Arulrajah et al., 2013) and for cement-treated pavement applications (Mohammadinia et al., 2014).

Illinois Department of Transportation (IDOT) has recently introduced gradation bands allowing the inclusion of large rocks having a maximum dimension in the range of 6 to 8 in. (152 to 203 mm). These large rocks can originate from both the primary crushing stage at quarries and recycled sources, and are often referred to as "aggregate subgrade" materials for highway pavement applications in Illinois. In a recent full scale accelerated pavement testing study, such application of large rocks was proven to be beneficial in terms of improved pavement rutting performance for pavements and construction platforms constructed over very weak subgrade soil (Kazmee and Tutumluer, 2015). However, the researchers also concluded that uniformly graded large rocks could exhibit variable performance trends in terms of quality assurance, strength, and deformation characteristics due to potential particle reorientation in the presence of large voids in the granular matrix (Kazmee and Tutumluer, 2015). For this, the researchers argued that sufficient amount of fine materials is necessary for a stable unbound aggregate layer to occupy voids and fill gaps of uniformly graded large rocks; and QB materials has the potential as a readily available by-product material for this application.

More widespread usage of recycled, artificial and nontraditional aggregate sources is gaining momentum in the United States and worldwide. In a recent NCHRP study, Tutumluer et al. (2018) collected responses from the transportation agencies of 45 U.S. states and eight Canadian provinces about their uses of nontraditional and recycled aggregate materials in pavement applications. The responses indicated that 94% of the agencies utilized RAP in pavement projects, while 70% utilized blended virgin aggregate sources. Additionally, 15% of the agencies reported the use of marginal aggregates, 21% indicated the use of nontraditional large size aggregates, while 55% reported that they used RCA in pavement applications. Additionally, 45% of the surveyed agencies indicated that they used artificial/by-product and manufactured aggregates (Tutumluer at al., 2018). The results of the survey are summarized in Figure 2.10.

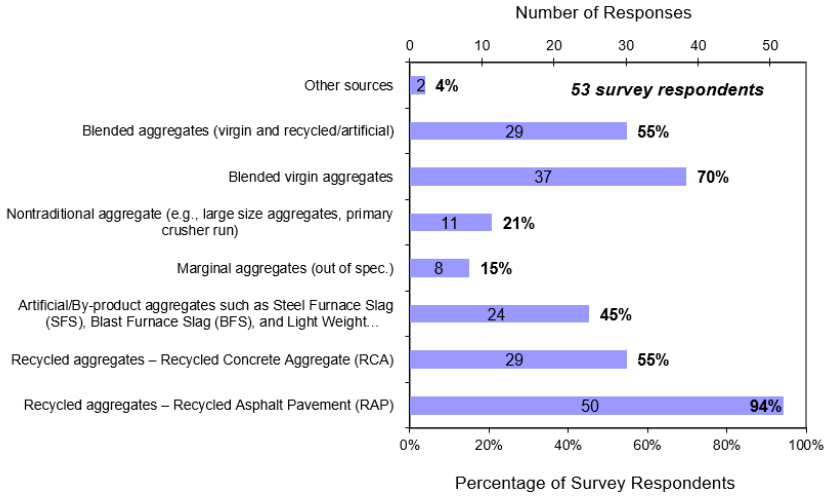


Figure 2.10 Aggregate types and sources used in pavement layer construction in the U.S. and Canada (Source: Tutumluer et al., 2018)

## 2.6 DESIGN APPROACHES FOR PAVEMENT CONSTRUCTION PLATFORMS

The design methodology adopted by the Illinois Department of Transportation (IDOT) for construction working platforms is based on subgrade strength. The method is outlined in the Subgrade Stability Manual (SSM), and requires some remedial actions to be carried for in situ subgrade soils having an Immediate Bearing Value (IBV) or a California Bearing Ratio (CBR) of 6% or lower, and optional remediation for subgrade IBV ranging from 6% to 8%. The design philosophy limits tire sinkage of construction equipment to 0.5 in. (12.5 m) or less and provides an adequate platform to compact the overlaying aggregate layers (Illinois DOT, 1982; 2005). The SSM provides a chart and table for minimum required thicknesses of aggregate covers to be compacted on top of the weak subgrade (see Figure 2.11).

The early development of the SSM design methodology for construction working platforms was based on the work of Thompson et al. (1977). The methodology was developed based on nonlinear finite element analyses of pavement sections constructed over very soft, soft, medium and stiff subgrades soils. The aggregate cover used was railway ballast size conforming to the American Railway Engineering Association (AREA) No. 4 gradation requirements. The standardized traffic loading considered was 500 coverages of a 32 kip (142 kN) tandem axle, which is equivalent to a 12 kip (53 kN) single wheel load. The deviator stress on top of subgrade was considered as the critical pavement response of interest, and the aggregate cover thickness required to limit surface rutting to 0.5 in. (12.5 m) was chosen by setting the threshold value for the Subgrade Stress Ratio (SSR) to 0.75. SSR is defined as the ratio of the applied deviator stress on top of subgrade to the subgrade unconfined compressive strength ($Q_u$). The final equation that was developed (and adopted by IDOT SSM) to determine the required aggregate cover thickness was a modification of the CBR-based design approach of the U.S. Army Corps of Engineers (Ahlvin, 1962). The equation is given as (Thompson et al. 1977; Illinois DOT, 1982):

$$t = F\sqrt{P\left(\frac{1}{8.1 * IBV} - \frac{1}{\pi p}\right)} \qquad \text{(Equation 2.1)}$$

where

‘t’ is the aggregate cover thickness (in.);

‘P’ is equivalent single axle load (lbs.);

‘IBV’ is the immediate bearing value (%);

‘p’ is the tire contact pressure (psi);

F = 0.23logC + 0.15; and

‘C’ is the number of wheel passes.

The procedure adopted by the IDOT SSM in the 1982 manual (IDOT, 1982), i.e. the design thicknesses of the aggregate covers at different subgrade strength levels, was further validated in 2005 using ILLI-PAVE finite element program, using different load configurations. Load was approximated as uniform pressure applied on a circular contact area in the axisymmetric finite element analysis. A load magnitude and pressure of 10 kip (45 kN) and 115 psi (794 kPa), respectively, were applied. The aggregate cover used had a friction angle (Ø) of 40°. The analyses conducted at various subgrade strengths concluded that the aggregate covers recommended in the original SSM resulted in subgrade stress ratios that did not exceed 0.75, indicating adequate thicknesses (Tutumluer et al., 2005).

The design chart adopted in the most recent 2005 IDOT SSM is shown in Figure 2.11. Additional considerations on the use of geogrids and geotextiles resulting in smaller aggregate cover thicknesses were further added to the IDOT design procedure (Kwon et al., 2006). Nonetheless, one of the drawbacks of using the IDOT design methodology is that the procedure does not account for the quality of the materials being used in the aggregate cover. No considerations are given for shear strength, morphological shape properties, or percentage of fines, i.e. materials passing the No. 200 sieve size, which can ultimately lead to overdesigning or under-designing these aggregate covers.

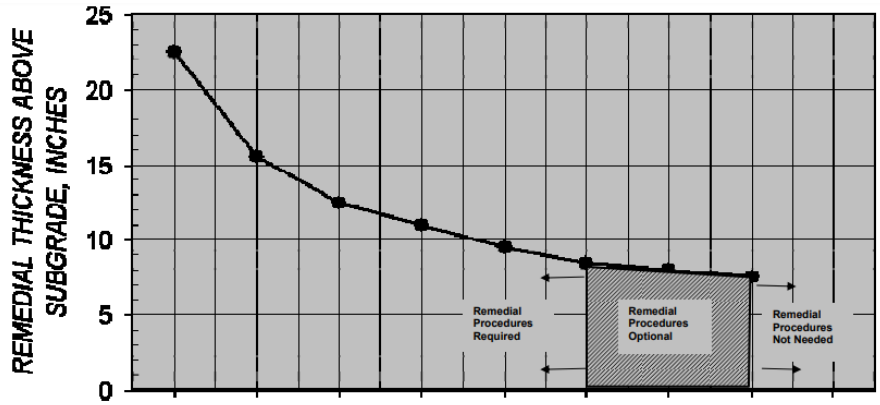


| IBV | 1 | 2 | 3 | 4 | 5 | 6 | 7 | 8 | 9 |
|---|---|---|---|---|---|---|---|---|---|
| Cone Index(CI) | 40 | 80 | 120 | 160 | 200 | 240 | 280 | 320 | 360 |
| Shear Strength (psi) | 2.25 | 4.50 | 6.75 | 9.00 | 11.25 | 13.50 | 15.75 | 18.00 | 20.25 |
| Qu (tsf) | 0.32 | 0.64 | 1.00 | 1.28 | 1.60 | 1.94 | 2.24 | 2.56 | 2.88 |
| Rate (in./Blow) | 4.6 | 2.6 | 2.0 | 1.5 | 1.3 | 1.1 | 1.0 | 0.9 | 0.8 |
| Rate (Blows/6") | 1.3 | 2.3 | 3.0 | 4.0 | 4.6 | 5.5 | 6.0 | 6.7 | 7.5 |
| Treatment Thickness | 22.5 | 15.5 | 12.5 | 11 | 9.5 | 8.5 | 8 | 7.5 | 0 |

Figure 2.11 Thickness design for granular fill or modified soil as a function of IBV and subgrade properties (Source: IDOT Subgrade Stability Manual, 2005)

A commonly used procedure for aggregate cover design in Europe is the Dutch procedure, which accounts for the change of in situ subgrade strength with the height of water table, the undrained shear strength of the

subgrade soil, and the magnitude and number of load repetitions. The procedure allows for rut depths ranging from ¾ in. to 2 in. (19 to 50 mm) using the following equation (van Gurp and Van Leest, 2003):

$$h_d = \frac{125.7\log(N)+496.52\log(P)-294.14RD_{constr}-2412.42}{f_{undr}^{0.63}} \quad \text{(Equation 2.2)}$$

where

'N is the number of axle loads;

'P is the average load (N);

'$RD_{constr}$' is the allowable rut depth at surface (m);

'f' is the undrained shear strength of subgrade (Pa);

'$f_{undr}$'= 20 × CBR x 1000 for shallow ground water table; and

f = 30 × CBR x 1000 for deep ground water table.

Another design approach for aggregate cover is the United Kingdom empirical design method (UK Highways Agency, 1994). The method requires using a 6 in. (150 mm) thick subbase material on a varying thickness of capping material depending on the strength (i.e. CBR value) of the subgrade soil. The pavement foundation thickness can thus vary from 6 in. (150 mm) to 24 in. (600 mm) based on the CBR of the underlying subgrade soil. This approach requires minimum CBR values of 30% and 15% for the subbase and capping materials, respectively. Alternatively, for subgrade soils having CBR values ranging from 2.5% to 15%, the method allows using a varying thickness of subbase materials without a capping layer; where the thickness of the subbase increases for lower subgrade soil strengths. The design chart of the UK empirical method is given in Figure 2.12. More recently, in 2009, a new development was adopted for the design approach for construction platforms in the United Kingdom. The new approach is performance-based, and accounts for the in situ stiffness of the used aggregate cover layer. Thus, considerable reduction in granular layer thicknesses can be achieved with the use of better quality aggregate materials having higher modulus properties (UK Highways Agency, 2009).

The aforementioned design philosophies for IDOT, UK and Dutch approaches mostly rely on designing the thickness of the aggregate cover based on subgrade strength. Other design methods, particularly earlier developments, were based on the bearing capacity equations and also certain empirical sinkage predictions developed over the years by Army Corps of Engineers and Air Force in the U.S. Such methods using the theory of bearing capacity include the developments by Broms and McLeod (McLeod, 1953; McLeod, 1954; Broms, 1963; and Broms; 1964). The method proposed by Broms assumes the shear failure to occur primarily in the subgrade, and does not account for the contribution of the overlying aggregate layers to shear resistance (Broms, 1963; Broms; 1964; Mishra, 2012).

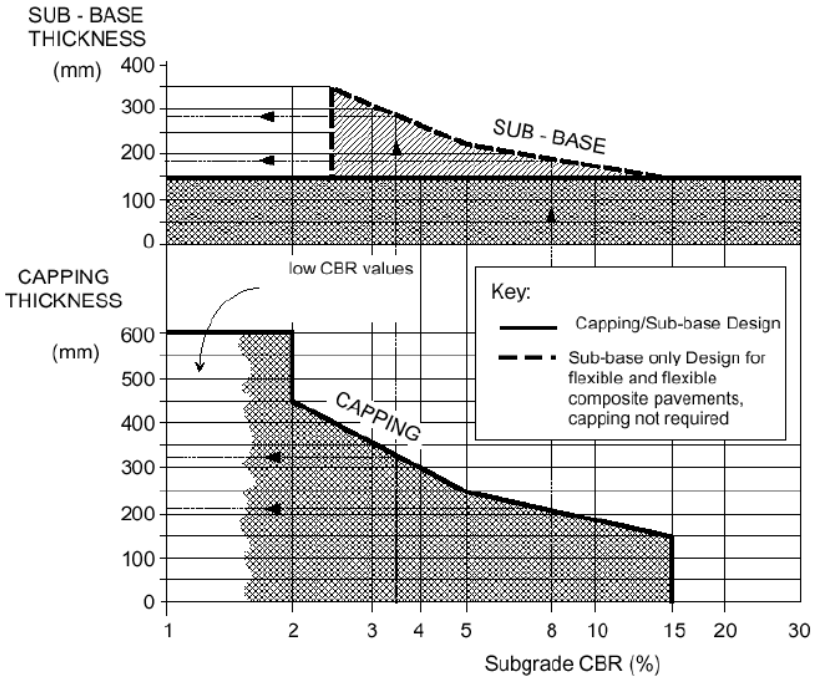


Figure 2.12 Thickness design for subbase and capping using the UK empirical method (adapted from UK Highways Agency, 1994)

## 2.7 DESIGN PHILOSOPHIES FOR FLEXIBLE PAVEMENTS

For the designs of low volume flexible pavements, several design methods have been developed and used all around the world. A doctoral dissertation from the University of Nottingham summarized the most commonly used procedures worldwide for the design of surfaced and unsurfaced low volume roads (Brito, 2011). Similarly, a doctoral dissertation by Kazmee (2018) summarized some of the existing design methods for low volume roads (Kazmee, 2018). These design methods are presented in Table 2.5, along with their respective design considerations and approaches. Design methods for low volume roads can be divided into empirical and mechanistic-empirical methods.

Empirical methods are based on experience and observed performance trends of existing pavements. Most of the empirical methods are based on subgrade soil strength, commonly represented with a CBR value, and a failure criterion (e.g. number of axle passes to generate a certain surface rut depth). Such empirical methods include design methods developed by Ahlvin (1959), and Hammitt and Aspinall (1970) as a function of CBR. Giroud and Noiray (1981) method considers the CBR of the subgrade and aggregate layers, and rut depth as a failure criterion. The empirical method by Verveka (1979) considers unbound granular materials to be linear elastic, assigns the values of their elastic moduli on the basis of empirical rules, and use a design criterion that limits the maximum vertical elastic strain at the top of the unbound layers and/or the top of the subgrade (Verveka, 1979). Similarly, the design method adopted by the National Crushed Stone Association (NCSA) considers the cumulative gravel equivalence

for design (NCSA, 1972; Kazmee, 2018). Minnesota DOT (MnDOT) also uses a similar procedure involving gravel equivalency factor in the design of low volume roads. This method is less conservative than their preceding procedure that was based on soil classification and an estimate of the R-value (MnDOT, 2017).

A more commonly used empirical design procedure in the U.S. and worldwide is the American Association of State Highway and Transportation Officials (AASHTO) design guide (AASHTO, 1993), which is principally based on the results of the AASHO Road Test, which took place from 1958 to 1960 in Ottawa, Illinois. This procedure is often supplemented by existing design procedures by many state transportation agencies in the United States. A survey by Hall and Bettis (2000) for design methods for low volume roads indicated that 37 States in the U.S. used the AASHTO design methodology. The AASHTO-1993 design procedure predicts pavement condition as a function of distresses translated into one single index, the Present Serviceability Index (PSI), and provides empirical design monographs/equations that are used to determine the structural number and the required pavement layer thicknesses (AASHTO, 1993).

Table 2.5 Low volume road design approaches (Adapted from Kazmee, 2018)

| **Design Procedure** | **Approach** | **Material Properties** | **Subgrade Properties** | **Environment** | **Traffic** | **Failure Criteria** |
|---|---|---|---|---|---|---|
| 1972 AASHTO | Structural Number[1] | Layer Coefficient | Soil Support Value | Regional Factors | ESAL | Terminal Service |
| 1986 AASHTO* | Structural Number[1] | Layer Coefficient | Resilient Modulus | Climatic Regions | ESAL | Terminal Service |
| National Crushed Stone Association | Gravel Equivalency[1] | Gravel Equivalency | CBR | Frost Susceptibility Class | Group Index | - |
| Asphalt Institute | Layered Elastic[2] | Resilient Modulus | Resilient Modulus | Mean Annual Air Temp. | ESAL | Strain Values |
| Shell Oil | Layered Elastic[2] | Resilient Modulus | Resilient Modulus | Mean Annual Air Temp. | 80 kN Single Axle | Strain Values |
| Australia | Layered Elastic[2] | Resilient Modulus | Resilient Modulus | Moisture/ Temperature | 80 kN Single Axle | Strain Values |
| New Zealand Supplement | Layered Elastic[2] | Resilient Modulus | CBR/ Resilient Modulus | Moisture/ Temperature | 80 kN Single Axle | Strain Values |
| AASHTOWare+ | Layered Elastic[2] | Resilient Modulus[3] | Resilient Modulus[3] | Enhanced Integrated Climatic Model | FHWA Vehicle Classifications | IRI (Overall)[4] |

* AASHTO 1993 design procedure is similar to AASHTO 1986 for flexible pavements design

'1' indicates an empirical design procedure

'2' indicates a mechanistic-empirical design procedure

+ Not mentioned in the original source

'3' AASHTOWare has three levels of inputs. Materials/subgrade properties can vary depending on the input level

'4' Overall performance indicator for AASHTOWare in the International Roughness Index (IRI). AASHTOWare also consider failure due to distresses based on material performance: fatigue (top-down and bottom-up), rutting, and thermal cracking

Mechanistic-empirical design procedures calculate the critical pavement responses using mechanistic layered system analysis and relate them to the failure criteria through empirical transfer functions. More recently, the U.S. Mechanistic-Empirical Pavement Design Guide (MEPDG) was introduced through the National Cooperative Highway Research Program, NCHRP 1-37A (Hicks, 2002). The design guide adopts Mechanistic-Empirical (M-E) design of new and rehabilitated pavement structures and allows complex modeling of asphalt behavior by considering several inputs for binder and mix properties, and predicting several distress modes. The design software (AASHTOWare) has a powerful integrated climatic tool as part of the database provided by the guide, and is thus considered highly relevant for the design procedures. AASHTOWare predicts the permanent deformation of unbound materials using a model by El-Basyouny and Witczak (NCHRP 2004), which was modified after Ayres and Witczak (1998) based on the original Tseng and Lytton's model (Tseng & Lytton 1989). The AASHTOWare pavement design offers an iterative procedure, where the design thicknesses are checked against the failure criteria, and layer thicknesses are adjusted accordingly. The features of AASHTOWare and its comparison with the original AASHTO 1993 are presented in Table 2.5.

Mechanistic-empirical methods used in Australia include the Austroads Pavement Design Guide (1992). According to their method, the subgrade strength is initially evaluated by its CBR value, elastic parameters and/or modulus of subgrade reaction (k). The thickness of the unbound granular material is then chosen to limit the deviator strain on top of the subgrade to a tolerable level throughout the life of the pavement based on the allowable number of load repetitions (N) and design traffic. This method also accounts for stress dependency in the granular layer stiffness through sublayering the granular base layer, calculating a modular ratio (R) for vertical moduli of the adjoining sublayers, and assigning a modulus to each sublayer based on the modular ratio which accounts for the ratio of the stiffness of the base layer to that of the underlying subgrade. The design approach for low volume roads requires choosing a pavement composition from a set of layouts offered by the guide. The four layouts that are offered are (1) asphalt and granular base, (2) asphalt and cemented-stabilized base, (3) inverted pavement with asphalt, granular base and cemented-stabilized subbase material, and (4) full depth HMA on top of subgrade (Brito, 2011).

Another mechanistic-empirical method is New Zealand supplement to the Australian pavement design guide, which covers some of the aspects that were overlooked by Austroads. In this design guide, granular material performance is accounted for by considering their stiffness. Nonlinearity and cross-anisotropy are also available as options to include in the analysis and design by this method (Brito 2011). Other mechanistic-empirical pavement design procedures for low volume roads include the Asphalt Institute (AI) procedure, as well as the design method by Shell Oil. Details for the latter two procedures are presented in Table 2.5.

Specifically for the State of Illinois, the IDOT low volume road design is outlined in the Bureau of Local Roads and Streets Manual (BLRS Manual). The design method was developed in 1995 and updated over time. The final available version was originally issued in 2005 and intermittently revised last in December 2018. Several research studies at the University of Illinois contributed to the development of the pavement design procedure for

low volume roads (e.g. Thompson et al., 1977; Thompson and LaGrow, 2003). The manual considers four procedures for pavement design for local agencies: (1) Rigid pavement design, (2) conventional flexible pavement design, (3) composite pavement design, and (4) full-depth HMA pavement design. No special pavement design procedures are outlined for inverted pavements or pavements with stabilized base materials. For conventional pavement designs, the IDOT BLRS manual considers low volume roads as Class IV highway, and requires a minimum of 3 in. (76 mm) HMA and 8 in. (203 mm) base course. Class IV highways typically have an Annual Daily Traffic (ADT) of less than 400, and a 64,000 or 85,000 Equivalent Single Axle Loads (ESALs) for a 15 and 20 years design, respectively (Illinois Department of Transportation, 2005).

In addition, several analysis and design programs have been developed for pavements including layered elastic programs and two-dimensional and three-dimensional Finite Elements (FE) programs. A layered elastic model requires a minimum number of inputs including material properties of each layer such as modulus of elasticity/Poisson's ratio, pavement layer thicknesses, and loading conditions (magnitude, geometry, repetitions). Different loading patterns are calculated based on the principle of superposition. Based on these assumptions, public domain software programs such as ELSYM5, WESLEA, JULEA, KENLAYER have been developed, and programs such as MnLayer and ERAPAVE improved the convergence and accuracy of the responses (Huang, 2004; Khazanovich and Wang, 2007; Erlingsson and Ahmed, 2013). The major concern in layered elastic analysis is that the nonlinear resilient behavior of aggregate layers is not well addressed in these programs. A summary of a partial list of available programs based on layer elastic approach is presented in Table 2.6.

For model simplicity and computing efficiency, two-dimensional axisymmetric finite element analysis has been extensively investigated and many improved implementations have been proposed. Dehlen (1969) considered the nonlinearity of both modulus and Poisson's ratio with stress level for evaluating pavements with finite element techniques. Zeevaert (1980) and Barksdale et al. (1982) developed a comprehensive finite element program, GAPPS7, for the analysis of flexible pavements and generalized soil-fabric systems. Finite element SENOL program by Brown and Pappin (1981) accounts for nonlinear bulk and shear moduli in the granular material. ILLI-PAVE (Raad and Figueroa, 1980; Thompson and Garg, 1999) and MICH-PAVE (Harichandran, et al., 1989) were two commonly used finite element programs developed for the analysis of flexible pavements. Both programs modeled the pavement as an axisymmetric solid of revolution and used the K-θ model for granular materials, and used the bilinear approximation for fine-grained subgrade soils.

Further, Crockford et al. (1990) developed an unconventional type of nonlinear resilient response model for characterization of granular layers and pavement evaluation in conjunction with the use of a Falling Weight Deflectometer (FWD). GT-PAVE finite element program (Tutumluer, 1995) considers nonlinear material characterizations of granular materials and subgrade soils. This program has been further extended to a mechanistic model for the response analysis of geogrid-reinforced flexible pavements (Kwon, et al., 2005). GT-PAVE was used for conducting mechanistic analyses for the QB applications studied in this dissertation, and more details about GT-PAVE are presented in Chapter 7. DSC2D finite element program developed by Desai and Schwartz (2000) and

modified by AASHTO's MEPDG (2004) follows the axisymmetric nonlinear analysis formulation and provides comprehensive pre-processing and post-processing modules. A summary of a partial list of available programs based on finite element analysis approach is presented in Table 2.8.

To overcome the inherent discrepancy between two-dimensional finite element analysis and the reality, comprehensive studies of pavement responses have been conducted via three-dimensional finite element analysis, implementing more sophisticated structural models and well-formulated dynamic loading responses. The leading academic or commercial finite element programs using three-dimensional analysis are EVERFLEX, ABAQUS™, ADINA™, etc. (Kim, 2007).

Table 2.6 Multi-layered elastic programs for pavement analysis and design

| **Name** | **Programming Language** | **Features** | **Limitations** |
|---|---|---|---|
| KENLAYER | Visual Basic | Used for single, dual, dual-tandem, or dual-tridem wheels; Used for linear elastic, nonlinear elastic, or viscoelastic layer; Up to 19 layers | Works on 32-bit computers |
| WESLEA | Fortran | Use a forward calculation scheme; Enable the analysis of multiple loading conditions; Considers variable interface conditions | Up to five pavement layers |
| WINJULEA | Visual Basic | Use an evaluation scheme to get the final stress, strain and displacement; Consider variable loading conditions at different location; Interface conditions between layers are considered | Material nonlinearity is not addressed |
| MNLAYER | WESLEA-based | Input includes climate, structure and traffic; Output contains fatigue and rutting evaluation; Batch mode allows the user to specify a range of layer thickness values and have all results tabulated | Must have two to five layers; Layer 5 cannot be analyzed for rutting. |
| ELSYM5 | Pascal | Use axisymmetric geometry in the structural analysis; Determine pavement responses along with principal values in a three-dimensional ideal elastic layered system; Perfect adherence between two consecutive layer interface. | Material nonlinearity is not addressed; Only uniform circular loads are applied; Errors with greater than 5 layers; Less user friendly |
| EVERSTRESS | WESLEA-based | Consider stress sensitive characteristics of unbound pavement materials | Up to five layers, 20 loads and 50 evaluation points; Cannot work on latest laptop |

Table 2.7 Multi-layered elastic programs for pavement analysis and design

| Program Name | Stress-strain Nonlinearity | | Element Type | Modulus Approximation | Boundary Type | Other Features** |
|---|---|---|---|---|---|---|
| Dehlen, 1969 | Granular | - | Four-node | Tangent modulus | Rigid Boundary | Consider Poisson's ratio nonlinearity |
| | Subgrade | - | | | | |
| GAPPS7 | Granular | K-θ model | Eight-node | Tangent modulus | Rigid Boundary | Interface conditions; large displacement conditions; no-tension conditions; plasticity yielding |
| | Subgrade | Bilinear model | | | | |
| SENOL | Granular | Contour model | Four-node | Secant modulus | Rigid Boundary | Nonlinearity in both bulk modulus and shear modulus |
| | Subgrade | Contour model | | | | |
| ILLI-PAVE<br>MICH-PAVE | Granular | K-θ model | Four-node | Secant modulus | Rigid Boundary<br>Flexible Boundary | Mohr-Coulomb failure theory |
| | Subgrade | Bilinear model | | | | |
| TTIPAVE | Granular | K-θ model & Uzan model | Four-node | Secant modulus | Rigid Boundary | Interface conditions; residual stress conditions; cross-anisotropic conditions |
| | Subgrade | Bilinear model | | | | |
| GT-PAVE | Granular | Uzan model & UT-Austin model | Hybrid* | Secant modulus | Rigid Boundary | Cross-anisotropic conditions; residual stress conditions; elimination of horizontal tension; reinforced geogrid interface condition |
| | Subgrade | Bilinear model & Loach's model | | | | |
| DSC2D | Granular | General model | Four-node | Tangent modulus | Infinite Boundary | Interface conditions; no-tension conditions; pre- and post-processing user interface |

* Hybrid elements refer to eight-node layer element, three-node geogrid element, and six-node interface elements

** All programs in the table adopt incremental loading and iterative procedure for nonlinearity

## 2.8 IN-PLACE MONITORING OF PAVEMENT LAYER RESPONSE AND PERFORMANCE

Both transportation agencies and researchers in the past have implemented several measures to approve and check the anticipated performance of constructed pavement layers. Such methods include density-based and strength/stiffness-based methods (Nazzal, 2003; Abu-Farsakh et al., 2004; Mishra, 2012; Khosravifar et al., 2013; White et al., 2013; Nazzal, 2014; Qamhia et al., 2017b; Qamhia et al., 2018a; Kazmee, 2018). Furthermore, trends for assessment of the constructed layer properties, responses, and performance are shifting from density-based techniques to stiffness- or strength-based techniques (Abu-Farsakh et al., 2004; White et al., 2013; Nazzal 2014). Among these methods, the Dynamic Cone Penetrometer (DCP), GeoGauge, and Lightweight Deflectometer (LWD) are the most evaluated techniques by DOTs (Nazzal, 2014). The depth of influence for these techniques, along with the depth of influence of a vibratory roller compacter, nuclear density gauge, and Falling Weight Deflectometer (FWD) are shown in Figure 2.13.

The aforementioned methods have been applied in previous research projects at the Illinois Center for Transportation to evaluate the performance of constructed subsurface pavement layers (Mishra, 2012; Kazmee, 2018). The results of using the various property and response evaluation techniques were interpreted in light with the limitations and depth of influence of each technique. For projects in the state of Illinois, IDOT implements density-based specifications to check the quality of the constructed pavement layers. IDOT requires a relative density exceeding 95% of the standard compactive effort laboratory density for subgrade, subbase, and base materials; including soil-cement base and subbase materials. IDOT also requires that the in-place dry density be determined by AASHTO T191, or Illinois Modified AASHTO T310 for direct transmission density and backscatter moisture (Illinois DOT, 2016). For hot mix asphalt layers, the standard IDOT practice requires that the density of extracted cores or placed thin HMA lifts conform with the density limits shown in Table 2.8. Different densities are targeted depending on the mix design and the design number of gyrations ($N_{design}$).

Table 2.8 IDOT's Density requirements for HMA lifts (Adapted from: IDOT, 2016)

| **Mixture Composition** | **Parameter** | **Individual Test** |
|---|---|---|
| IL-4.75 | $N_{design} = 50$ | 93.0 – 97.4 % |
| IL-9.5 | $N_{design} = 90$ | 92.0 – 96.0 % |
| IL-9.5, IL-9.5L | $N_{design} < 90$ | 92.5 – 97.4 % |
| IL-19.0 | $N_{design} = 90$ | 93.0 – 96.0 % |
| IL-19.0, IL-19.0L | $N_{design} < 90$ | 93.0 – 97.4 % |
| SMA | $N_{design} = 50$ and 80 | 93.5 – 97.4 % |

Nazzal (2014) also reported that only five states in the U.S. have implemented specifications for stiffness- or strength-based compaction control for unbound materials. Indiana is one of the states leading with specifications on the use of LWD for evaluating unbound aggregates compaction: Indiana Test Method (ITM) No. 508-12T require

additional compaction or aeration if two consecutive drops of an LWD exhibits a change in deflection of 10% or greater. Further, ITM No. 514-15T assumes that the compaction of soil/unbound materials has peaked if the difference between the average of ten LWD readings from four and five roller passes is equal to or less than 0.79 mils (0.02 mm).

Studies have also been conducted with using LWD to evaluate the time-dependent stiffness of stabilized and bound base layers. Khosravifar et al. (2013) evaluated the change of stiffness of foamed asphalt stabilized base and granular aggregate base in consecutive days after placement using a Humboldt GeoGauge 4140 and a Zorn ZFG 3000 LWD, and reported high relative errors in LWD measurements that underestimated the stiffness back-calculated from FWD (Khosravifar et al., 2013). Similarly, Isola et al. (2013) used LWD to evaluate the surface moduli of different cement-treated mixtures with high percentage of RAP prior to the placement of the overlaying pavement layers and found the surface modulus to correlate well to the curing of the bases (Isola et al., 2013).

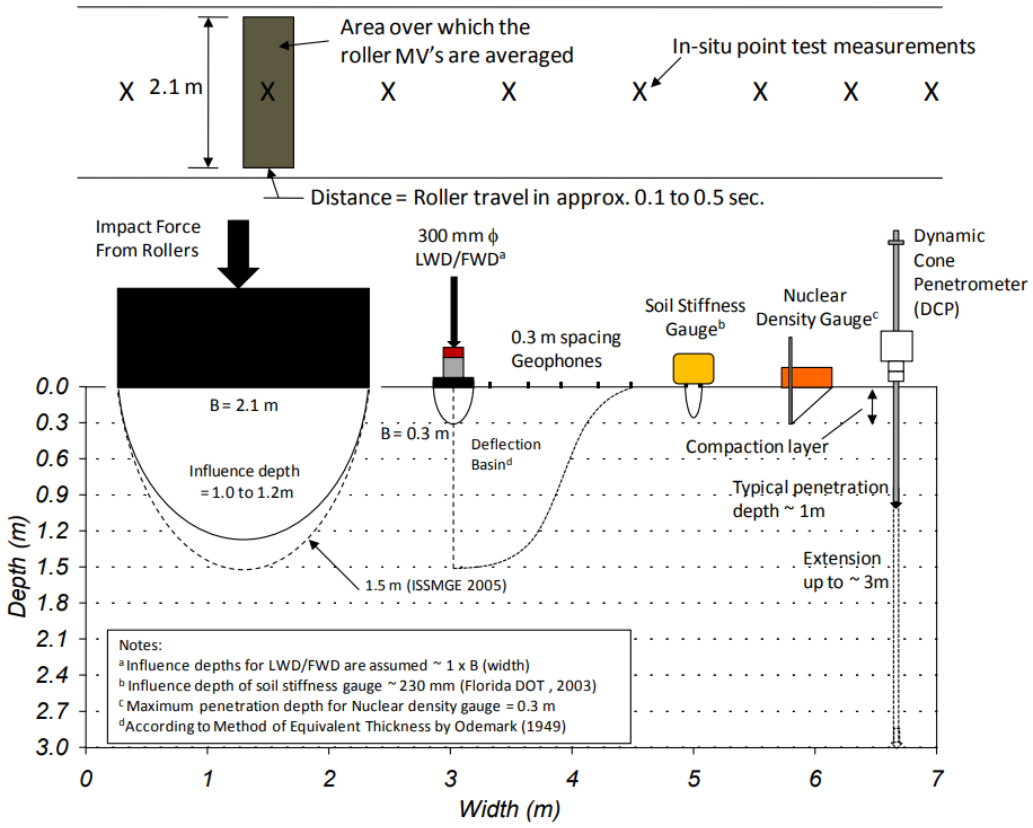


Figure 2.13 Depth of influence for different in situ pavement evaluation techniques (Source: Chang et al., 2014)

For the purposes of the field evaluation of the studied QB applications, in-place monitoring methods for the constructed pavement layers will be employed. Methods such as density measurements using a nuclear density gauge, LWD and FWD for constructed layer moduli evaluation, and DCP for strength evaluations will be used to evaluate the field performance and structural capacity of the constructed test sections.

## 2.9 COSTS, BENEFITS, AND SUSTAINABLE EVALUATIONS OF QB USAGE

A recent NCHRP synthesis on the practices of unbound aggregate layers for pavement layers stated that pavement projects using granular layers needed to be sustainable and cost-effective by: (1) making more effective use of locally available materials through beneficiation and use of marginal aggregate materials, (2) increasing effective use of recycled aggregate products such as RCA and RAP, and (3) targeting long life and improvement in pavement performance (Tutumluer, 2013). The use of aggregate QB as a marginal material can pose a challenge to achieving all three goals due to the high fines content. However, a research study by Ashtiani et al. (2007) showed that aggregate systems with higher fines benefited considerably from low percentages of cement stabilizer (Ashtiani, et al., 2007). In their study, fines were considered as materials passing the No. 40 sieve (425 µm). The reference gradation had 15% fines (Passing No. 40 sieve), and samples with fines content of 20%, 30%, and 40% were evaluated. The study found that with the proper selection of fines content, cement content, and moisture content, the performance of the stabilized systems with high fines content can perform equivalent to or even better than systems with standard fines content, as demonstrated by enhancing the resilient and permanent deformation properties (Ashtiani et al., 2007).

Very little research was conducted in the U.S. to evaluate the cost, cost-benefit ratio, and sustainability aspects of QB utilization. This dissertation aims to fill some of the knowledge gaps by evaluating the environmental and economic impacts of QB utilization in sustainable pavement applications. To this end, NCHRP synthesis 435 (volume 4) reported some cost considerations for QB usage by transportation agencies in the United States. These considerations include: (1) Hauling costs associated with long transportation distances, (2) projected additional cost for QB byproduct preparation (e.g. overburden and removal and plastic fines), and (3) testing requirements to adhere to the requirements of the Environmental Protection Agency (EPA). The study also indicated that no detailed cost or sustainable studies were noted in the literature, but merely some conceptual flow charts and product evaluations were only considered (Stroup-Gardiner and Wattenberg-Komas, 2013)

More detailed research efforts were conducted on the evaluation of the cost and environmental benefits of using aggregate by-product materials in pavement applications by Petavratzi and Wilson (2008), who indicated that the quantities of excess quarry fines stockpiled, produced and marketed had to be determined in order to promote sustainable utilization. The researchers reported that this would require enforcing mineral planning policies and legislations on sustainable construction and waste management; particularly because the focus on sustainable utilization of quarry fines was relatively recent, and no statistical data were readily available to assess quantities used, successful applications, possible substitution of primary materials, and sales data.

Petavratzi and Wilson (2008) and WRAP (2006) reported a feasibility case study in West Midlands in the UK to develop an economic model for the sustainable resourcing of aggregate supply relative to demand, market price and resource availability. Variables studied included: supply, costs, market price, and demand. The feasibility study predicted a shift in resource use between 2004 and 2016. The shifts included more demand and use of recycled aggregates, meaning that crushed rock selling price would decrease, which would potentially increase the production

of aggregate fines above market demand. Thus, some investment in washing plants was essential to process crushed rock fines. Additionally, this would necessitate the development of processes to minimize QB and dust production. Such development that minimizes the production of QB materials achieved by thoughtfully designing the quarrying process is shown in Figure 2.14. The development proposes the replacement of a Horizontal Shaft Impact (HIS) crusher with a cone crusher to reduce the fines production by 21%, from 38% to 30%. However, Petavratzi and Wilson (2008) recommended that such quarry optimization efforts must be followed by pilot or full-scale trials to assess feasibility and profitability.

Stroup-Gardiner and Wattenberg-Komas (2013) and McClellan et al. (2008) reported/proposed a sustainability assessment tool flow chart to assess the sustainability of QB usage. The model was originally developed for bauxite, which is a by-product with storage and disposal issues. The framework, shown in Figure 2.15, considers environmental and socio-economical sustainability aspects, and can thus be applied to other aggregate quarry by-products. This framework proposed three hierarchical levels: headline performance indicators, 23 key performance indicators, and case-dependent performance measures. Such broad tool will be partially utilized and built upon in this dissertation to evaluate the environmental impacts of the evaluated QB applications.

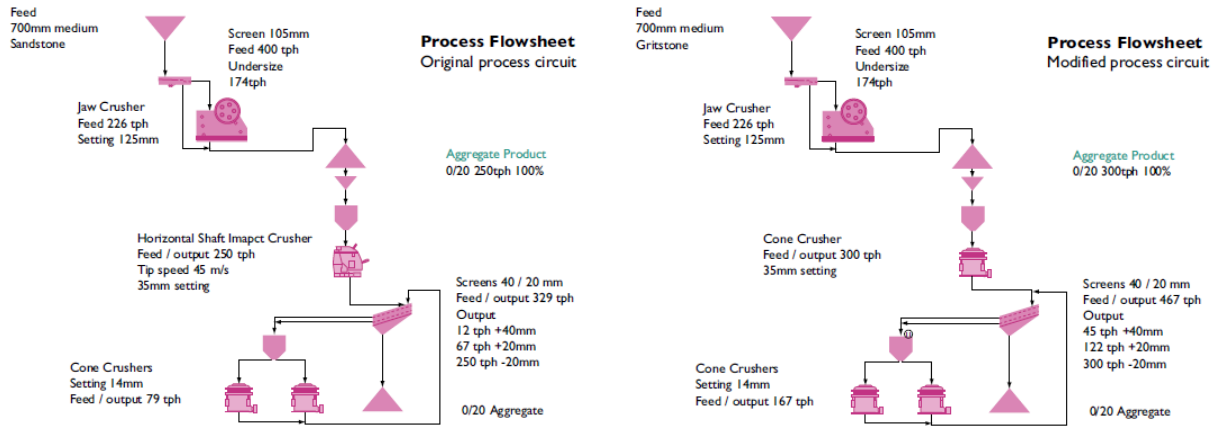


Figure 2.14 A simulated case study to optimize quarry operations (Source: Mitchell and Benn, 2007; The University of Leeds, 2007b; Metso minerals, 2007)

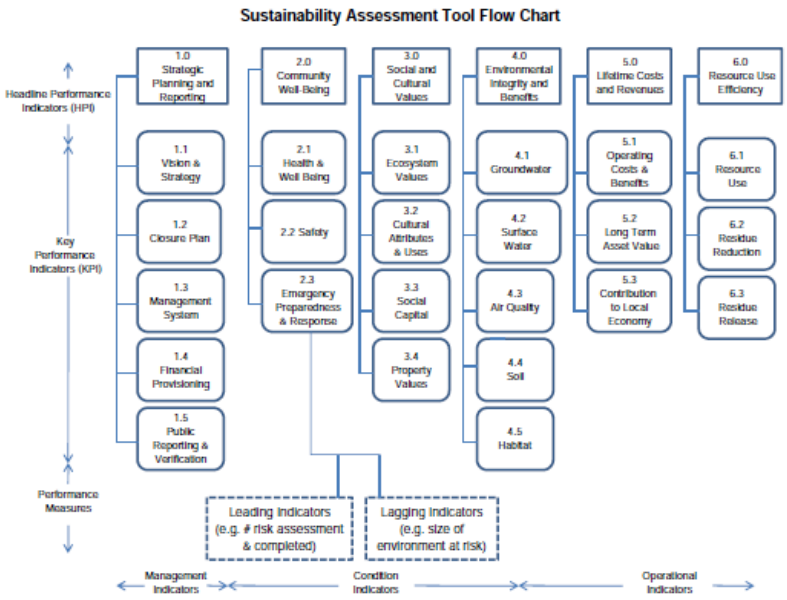


Figure 2.15 A sustainability assessment tool flow chart (Source: Stroup-Gardiner and Wattenberg-Komas, 2013 – adapted from McClellan et al., 2008)

## 2.10 SUMMARY

This chapter provided a literature review of the past studies associated with using QB, recycled materials, and marginal aggregates in pavement applications. Since the 1980s, several research studies focused on the quantification of QB production rates, and the characterization of their mechanical and physical properties in the laboratory. Many researchers have proposed applications for QB in pavements based on the laboratory characteristics. The proposed applications were mainly in concrete mixes or as chemically stabilized subsurface layers. Such applications included cement-stabilized base/subbase QB layers, flowable fills, replacement of sand in concrete, and engineering backfill.

Despite proposing many applications for QB, most of the research studies to date have only focused on the laboratory characterization of QB materials. Only few research efforts and full-scale/field studies were conducted to incorporate QB in pavement design, or to evaluate the field performance of QB materials under heavy wheel loading. Very limited research has also been conducted to evaluate the environmental and economic impacts of using QB materials in pavement applications. The current field effort described in this dissertation serves as a continuity of recent research efforts to evaluate more sustainable pavement designs, primarily focusing on studying QB applications that demonstrated through laboratory testing to be potentially beneficial to use for improved pavement foundation. The modeling and sustainability efforts proposed in this dissertation solve to better understand the performance of QB materials in subsurface pavement layers, and their environmental and economic impacts though life cycle assessment and life cycle cost analysis.

# CHAPTER 3: MATERIALS SELECTION AND LABORATORY STUDIES

## 3.1 INTRODUCTION

This chapter presents a discussion of the criteria for materials selection for the field accelerated pavement testing study, and the laboratory testing and characterization results for the selected materials. The materials were selected to cover different geographical regions and sources in the state of Illinois. The laboratory tests performed were deemed necessary for characterizing the collected materials and ensuring good quality construction. Laboratory testing included grain size distribution, compaction characteristics (moisture-density relationships), unconfined compressive strength tests for the stabilized QB samples, a packing study for blending a primary crusher run aggregate subgrade material and QB, and a packing study of QB with coarse recycled aggregates (FRAP and FRCA). The results and conclusions from these laboratory tests are summarized in this chapter.

## 3.2 SELECTION OF MATERIALS

In total, nine aggregate materials were selected from across the state of Illinois to construct the full-scale pavement test sections. Out of the nine materials, three are QB materials obtained from three different quarries that have excess quantities of QB stored on-site. Three materials are conventional aggregate base course materials, referred to here as CA06_R, CA06_15NPF, and CA06_15PF. The CA06_R (R stands for regular) material falls in the IDOT CA06 gradation band for coarse aggregates (see Table 3.1). The other two aggregate materials (CA06_15NPF, and CA06_15PF) conform to the IDOT CA06 gradation, except that they have 15% nominal nonplastic and plastic fines content, respectively, passing the No. 200 sieve, or finer than 0.075 mm. The plastic fines had a plasticity index (PI) of 8%, and a liquid limit (LL) of 21%. The current IDOT specification permits a maximum of 12% fines passing No. 200 sieve.

A Primary Crusher Run (PCR) virgin aggregate conforming to IDOT CS02 gradation for aggregate subgrade materials (see Table 3.2) was obtained to study an application of using QB as a filler material for the voids in these large aggregates for increased stability. In addition, two recycled materials (FRAP and FRCA) were obtained to study chemically stabilized applications of QB mixed with these recycled materials and stabilized with cement or class ‘C’ fly ash. A summary of the nine aggregate materials and their source locations in the state of Illinois is presented in Table 3.3.

In addition to the nine aggregate materials, Type I Portland cement, and self-cementitious Class ‘C’ fly ash materials were obtained from local vendors in Urbana, IL to be used as stabilizing agents or chemical admixtures in the pavement test sections for studying chemically stabilized applications of QB. The hot mix asphalt (HMA) used to pave the test sections comprised an asphalt binder with a Superpave performance grade of PG 64-22, and a 0.375-in. (9.5-mm) nominal aggregate size. The mix design properties of the asphalt mix are given in Table 3.4.

Table 3.1 IDOT gradation band for CA06 coarse aggregate material

| **Sieve Size** | **1 ½"** | **1"** | **1/2"** | **# 4** | **# 16** | **# 200** |
|---|---|---|---|---|---|---|
| **Sieve Size (mm)** | 38 mm | 25 mm | 12.7 mm | 4.75 mm | 1.19 mm | 0.075 mm |
| **Percent Passing (%)** | 100 | 95 ± 5 | 75 ± 15 | 43 ± 14 | 25 ± 15 | 8 ± 4 |

Table 3.2 IDOT gradation band for CS02 aggregate subgrade material

| **Sieve Size** | **6”** | **4”** | **3”** | **2”** | **#4** | **# 200** |
|---|---|---|---|---|---|---|
| **Sieve Size (mm)** | 152 mm | 102 mm | 76 m | 51 mm | 4.75 mm | 0.075 mm |
| **Percent Passing (%)** | 100 | 80 ± 10 | | 25 ± 15 | | |

Table 3.3 Selected aggregate materials and quarry locations

| **Material ID** | **Quarry Location** | **Materials Collected** | **Quarry Locations (Illinois)** |
|---|---|---|---|
| QB1 | (A) Bolingbrook | Quarry By-product |  |
| QB2 | (B) Thornton | Quarry By-product | |
| QB3 | (C) Dupo | Quarry By-product | |
| CA06_R | (D) Fairmont | Aggregate material, conforming to CA06 Gradations | |
| CA06_15 NPF | (E) Aurora | Aggregate material, conforming to IDOT CA06 gradations, 15% nonplastic fines Passing No. 200 sieve | |
| CA06_15 PF | (F) Milan | Aggregate material, conforming to IDOT CA06 gradations, 15% plastic fines Passing No. 200 sieve | |
| PCR (CS02) | (G) Lisbon | Primary Crusher Run aggregates, conforming to IDOT CS02 gradations | |
| FRAP | (H) Urbana | Fractionated RAP | |
| FRCA | (H) Urbana | Fractionated RCA | |

Table 3.4 HMA mix design for the surface course mix

| Material | Source city in Illinois | Weight of total mix (%) |
|---|---|---|
| Crushed coarse aggregates | Manteno | 50.7 |
| Crushed fine aggregates | Manteno | 11.4 |
| Natural sand | Paxton | 16.1 |
| Mineral filler (fly Ash class F) | Decatur | 2.4 |
| RAP (5% binder content) | Rantoul | 14.2 |
| Asphalt binder (PG 64-22) * | Urbana | 5.2 |
| | **Sum** | **100.0 %** |

* Total binder content (by weight of aggregate) = 5.9%, and the theoretical maximum specific gravity ($G_{mm}$) = 2.484 g/cm$^3$

## 3.3 LABORATORY CHARACTERIZATIONS OF SELECTED MATERIALS AND APPLICATIONS

Several laboratory tests were conducted to characterize the physical and engineering properties of the construction materials selected to build the full-scale test sections for studying unbound and chemically stabilized applications of QB aggregates. These laboratory tests were deemed necessary to ensure high quality material preparations and construction for field testing. The conducted laboratory tests discussed in this section include: (1) Grain size distribution; (2) packing study of QB2 with recycled coarse FRAP and FRCA aggregates; (3) compaction characteristics, i.e. moisture-density relationships; (4) X-ray Fluorescence (XRF) to determine the chemical composition of the selected QB materials; (5) Unconfined Compressive Strength (UCS) tests for the chemically stabilized material combinations; (6) packing study of PCR with QB1 shaken from the surface to fill the voids between the large rocks for increased stability; and (7) gradation optimization study to determine the effect of grain size distribution on the UCS of chemically stabilized QB materials.

### 3.3.1 Particle Size Distributions

The particle size distributions of four aggregate materials (QB1, QB2, QB3, and FRAP) were determined by dry sieve analyses in accordance with the ASTM C136/C136M Standard (ASTM, 2014). For the other four materials that conform to IDOT's CA06 aggregate gradation specifications, namely FRCA, CA06_15NPF, CA06_15PF, and CA06_R, the gradations were determined with washed sieve analyses using a mechanical apparatus as per ASTM C117 Standard (ASTM, 2017). For the primary crusher run aggregate material having a nominal maximum aggregate particle size of 6 in. (152 mm), representative samples were separated on the 3 in. (76 mm) sieve, and the gradation of aggregate particles passing the 3 in. (76 mm) sieve was determined with conventional dry sieve analysis. For particles retained on the 3 in. (76 mm) sieve, the field imaging technique previously used by Kazmee and Tutumluer (2015), was used to determine the particle sizes and aggregate morphological shape properties. Figure 3.1 shows the particle size distributions of the nine selected aggregate materials, and the corresponding IDOT aggregate gradation bands.

Figure 3.1(a) presents the particle size distributions for the three QB materials. All three materials have similar grain size distribution curves and are relatively well-graded. All QB aggregates are smaller than 3/8 in. (9.5 mm). The fines, passing sieve No. 200 (0.075 mm), ranges between 12% and 13% for all QB materials. Overall, QB1 exhibited the finest gradation among all three materials, which can be advantageous for the field application to facilitate the percolation of QB1 to fill up the voids between the large PCR stones. Additionally, QB2 has a relatively coarser gradation when compared to QB1 and QB3.

Figure 3.1(b) shows the gradations of the CA06_15NPF, CA06_15PF, and CA06_R materials. The particle size distribution for CA06_R conforms with IDOT's CA06 gradation band limits, while the gradations of CA06_15NPF and CA06_15PF have higher fines content than the currently accepted limit for CA06 (i.e. 12%). The fines content passing sieve No. 200 (0.075 mm) for CA06_R is 8.8%, as determined by washed sieving. The fines contents for CA06_15NPF and CA06_15PF were 14.2% and 16.2%, respectively, slightly lower/higher than the target fines content of 15%. The CA06_15NPF material has the finest gradation curve, while the CA06_15PF material has a higher percentage of coarser aggregates. Additionally, both CA06_15NPF and CA06_15PF aggregate materials have aggregate particles up to 1.5 in. (38.1 mm) in size, while CA06_R material has a smaller nominal maximum aggregate size of 1.0 in. (25.4 mm).

The particle size distribution of the PCR stones is shown in Figure 3.1(c). The gradation falls within the CS02 gradation band specified by IDOT. These aggregates have a nominal maximum aggregate size of 6 in. (152 mm) and are mostly larger than 0.5 in. (12.5 mm) in size. The grain size distribution curves for QB1 and CA06_R materials are also shown superimposed for comparison. QB1 was used to fill the voids between the PCR aggregates, while the CA06_R aggregates were used for the capping layer.

Finally, Figure 3.1(d) shows the gradation curves of the FRCA and FRAP materials that are used as the coarse aggregates and blended with QB2 in the construction of three chemically stabilized base pavement test sections. The FRAP material has a relatively coarser gradation with very little fines, and a smaller nominal aggregate size (0.75 in. or 19 mm). The FRCA material, on the other hand, has a grain size distribution that complies with IDOT's CA06 gradation bands, larger top size particles up to 1.5 in. (38.1 mm), and a higher fines content of 9.1%, determined from washed sieve analysis. Additionally, the FRCA is relatively well-graded while the FRAP material is more uniformly graded.

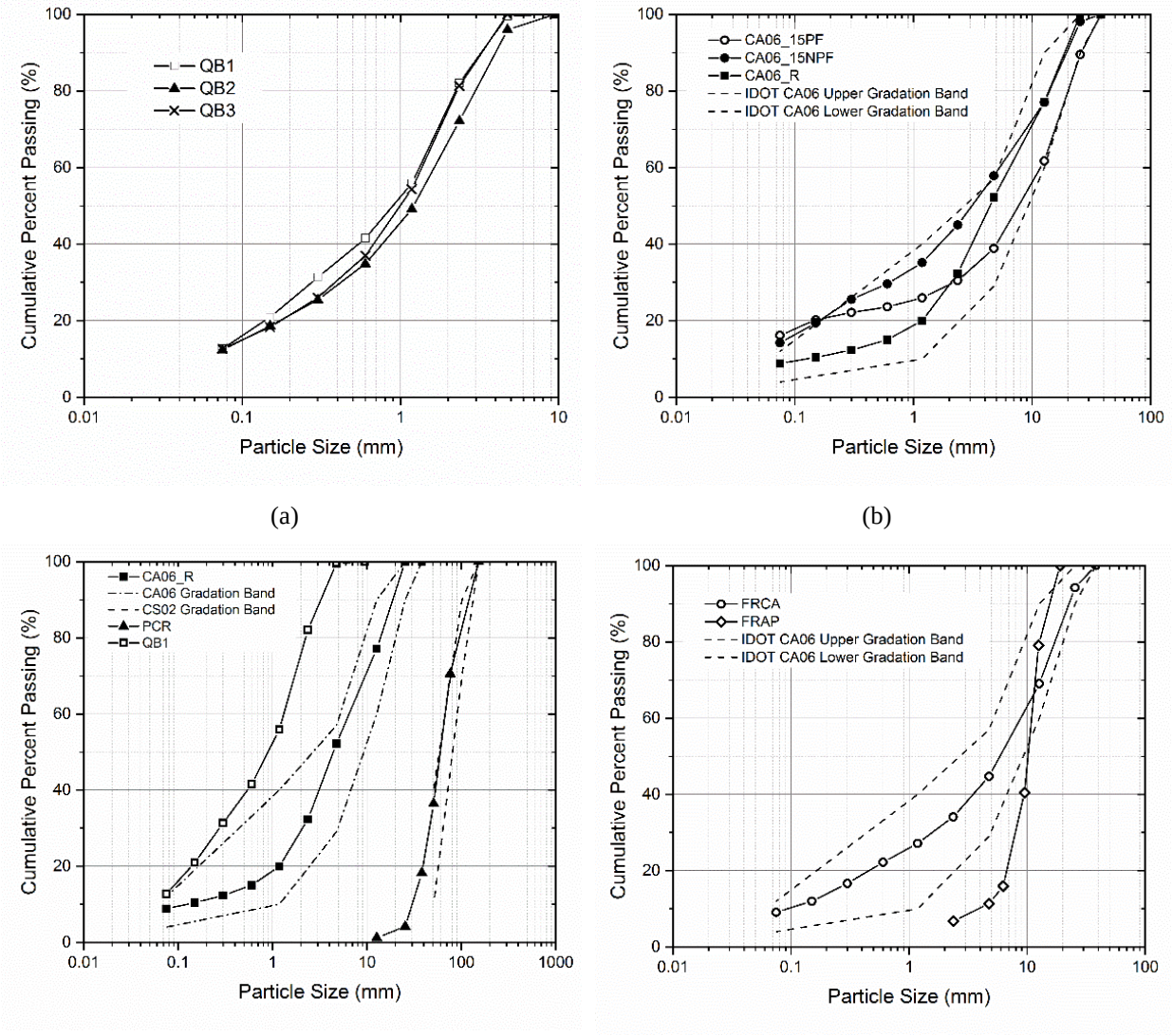


Figure 3.1 Grain size distribution curves for the construction materials: (a) QB materials; (b) CA06 materials; (c) Cell '1' materials, including PCR, QB1 and CA06_R; and (d) FRCA and FRAP

### 3.3.2 Packing Study of QB2 with Coarse Recycled Materials (FRAP & FRCA)

As part of the chemically stabilized applications that utilize large quantities of QB, some of the constructed applications utilize QB mixed with coarse recycled aggregates (FRAP or FRCA). A study was performed to determine a suitable mix ratio that maximizes the packing density (minimizes voids content) and utilizes high quantities of QB in the mix. The tests were performed by dry-mixing QB2 in different percentages by weight with FRAP or FRCA, and compacting the mixes using the modified compactive effort in a standard CBR mold in five equal lifts. The quantity of QB was varied from 30% to 100% by the weight of the total mix, in increments of 10%.

The results are given in Figure 3.2(a), which shows that the density starts to stabilize/maximize at 70% QB and 30% FRAP mix, while the density continues to increase linearly as the amount of QB2 was increased for the case of QB blended with FRCA. A similar laboratory study performed by LaHucik et al. (2016) to determine the optimum blending ratio of QB and FRAP as per ASTM C29 Standard (ASTM, 2017a) concluded that 70% QB by weight maximizes the packing density. However, the trend with changing the QB content was quite different from the one obtained in this study, which was expected due to differences in the gradation of the used FRAP material. For this study, it was decided to use a 70% QB and 30% FRAP or FRCA mixes for the field construction. The mix design provides an opportunity to utilize high quantities of QB within a skeleton of coarse aggregates to achieve higher strength. Figure 3.2(b) shows the combined gradations of 70% QB2 and 30% FRAP/FRCA mixes. It is shown that the QB2/FRAP blend is relatively coarser and has lower fines content compared to the QB2/FRCA blend. The difference is due to the gradations of FRAP and FRCA employed in the respective mix designs.

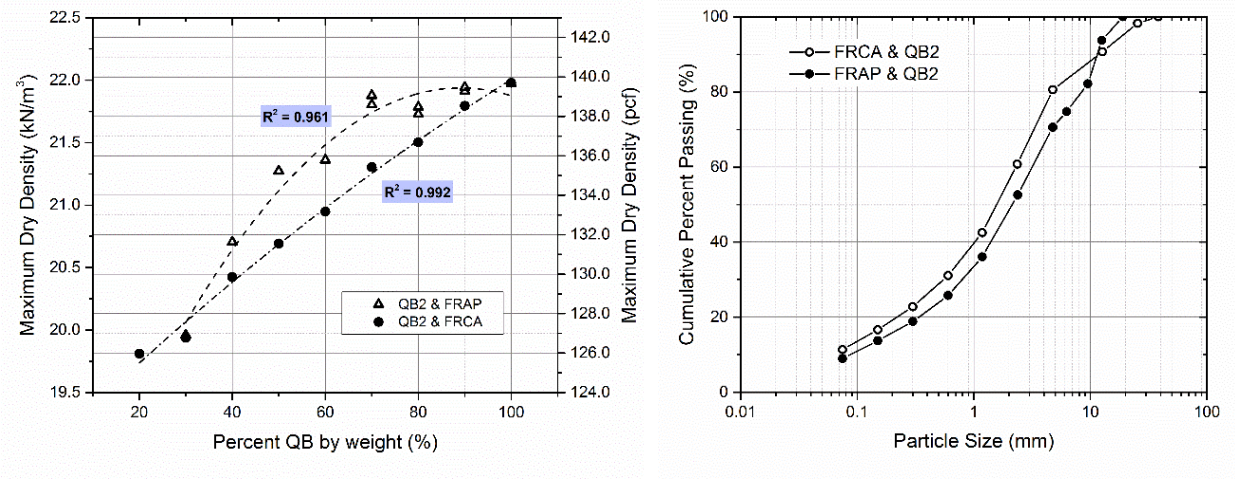


(a) (b)

Figure 3.2 Packing study results: (a) Achieved maximum dry density at different blending ratios; and (b) Grain size distribution for QB2 with FRAP or FRCA with a 70% QB and 30% FRAP or FRCA mixes

## 3.3.3 Moisture-Density Relationships

The Maximum Dry Densities (MDD) and corresponding Optimum Moisture Contents (OMC) were obtained for all materials using the standard compactive effort test procedure as per ASTM D698 Standard (ASTM, 2012). The determination of the moisture-density relationships is deemed critical for the construction stage because the constructed test sections were compacted at the optimum moisture content, and the field densities were checked for the relative compaction, which had to exceed 95% of the MDD as specified by IDOT standards for a passing field density. The compaction characteristics of all the materials that were used in the construction of field test sections are shown in Figure 3.3, grouped by similarity in material or application.

Figure 3.3(a) shows the compaction curves for the three CA06 materials (CA06_R, CA06_15NPF, CA06_15PF). Material CA06_15NPF has the highest MDD and OMC of 138.4 pcf (21.7 kN/m$^3$) and 6.8%, respectively. Material CA06_15PF exhibited a lower MDD of 134.7 pcf (21.2 kN/m$^3$) and a slightly lower OMC of 6.5%, which can be attributed to the significantly coarser gradation and the clumping of fines, resulting in less particle exposure and lowering the OMC. The CA06_R material had the lowest MDD and OMC of 132 pcf (20.75 kN/m$^3$) and 5.4%, respectively. The lower moisture content can be attributed to the lower fines content.

Figure 3.3(b) and Figure 3.3(c) present the moisture-density relationships for the QB2 and QB3 materials, respectively, both for the stabilized and unstabilized QB applications. From Figure 3.3(b), the highest MDD and OMC were for QB2 stabilized with 3% cement, followed by QB2 stabilized by 10% class 'C' fly ash. The MDDs achieved were 137.9, 137.2, and 136 pcf (21.7, 21.6, and 21.4 kN/m$^3$) for the cement-stabilized, fly ash-stabilized, and unstabilized QB2, respectively; while the OMC values were 9.1%, 8.0%, and 7.9%, respectively. The order of decreasing OMC values is comparable to the one presented in a recent study by Tutumluer et al. (2015); while the orders of MDD are different and the researchers reported the highest MDD for the fly ash-stabilized materials. For QB3 material, the QB3 stabilized with 3% cement had a higher OMC than the unstabilized QB3 (8.4% vs. 7.8%), while the MDD values achieved showed an opposite trend (130 pcf [20.4 kN/m$^3$] vs. 132 pcf [20.7 kN/m$^3$]).

Figure 3.3(d) shows the moisture-density curves of the QB2 samples, blended with FRAP or FRCA in a 70% QB and 30% FRAP/FRCA mixes, and stabilized with 3% cement or 10% fly ash. These materials showed similar trends to that seen for stabilized QB2 material, where the fly ash-stabilized QB2/FRAP had a lower OMC compared to the 3% cement-stabilized QB2/FRAP (7.5% vs. 8.0% respectively). However, the fly ash-stabilized QB2/FRAP showed a higher MDD than the cement-stabilized QB2/FRAP (136 pcf or 21.4 kN/m$^3$ vs. 134.8 pcf or 21.2 kN/m$^3$), which is more consistent with the previous research findings (Tutumluer et al., 2015). For the 3% cement-stabilized QB2/FRCA material, the OMC of 9.8% is significantly higher than the cement-stabilized QB2/FRAP material, while the MDD of 129 pcf (20.3 kN/m$^3$) is significantly lower. One possible explanation is the higher fines content, and the finer grain size distribution of the QB2/FRCA blends. The lower OMC for samples containing FRAP is consistent with other study findings in the literature reported by several other researchers (Bennert and Maher, 2005; MacGregor et al., 1999; Sayed et al., 1993).

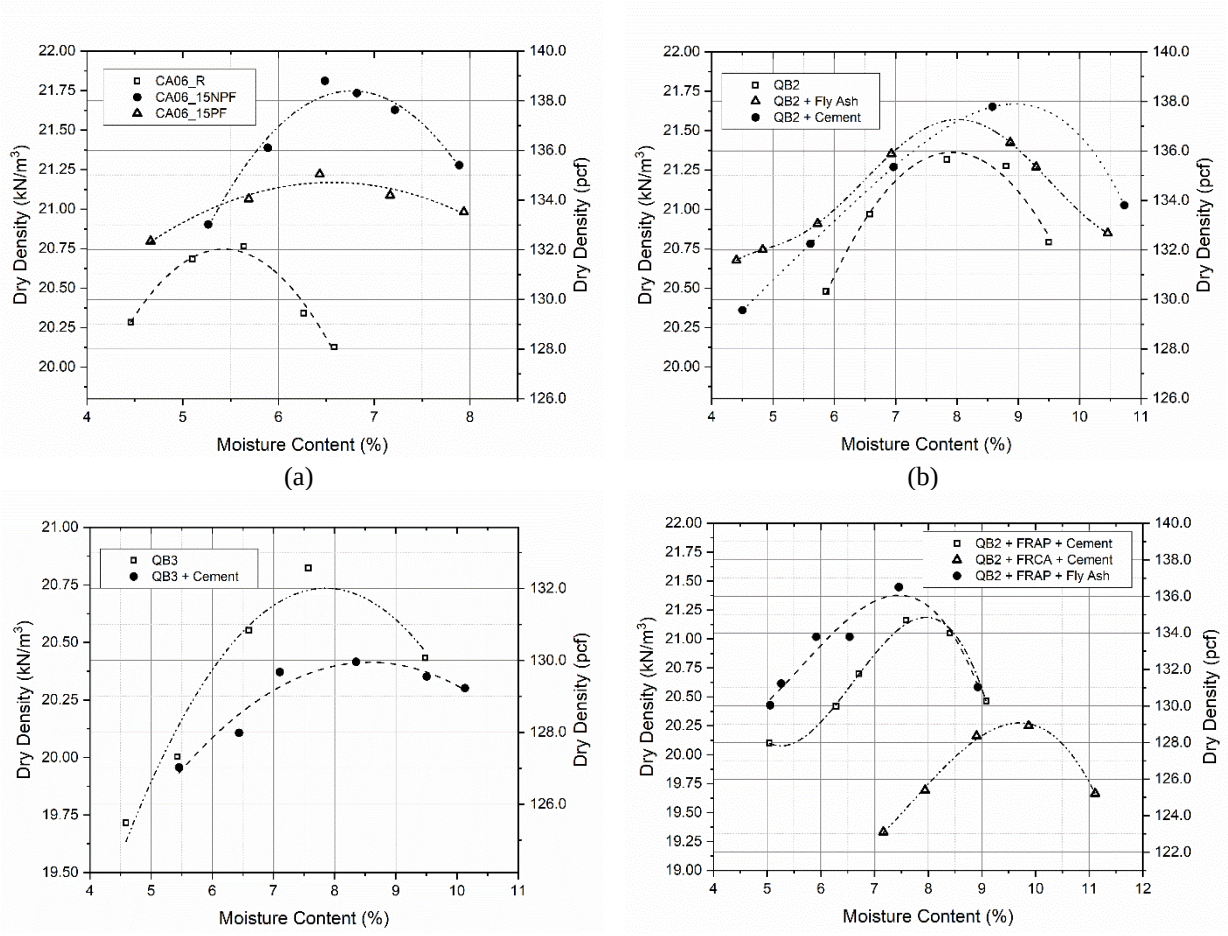


Figure 3.3 Moisture-density curves for the materials used in the construction of field test sections

### 3.3.4 Chemical Compositions of QB Materials

The chemical compositions of the three QB materials used in the field study were characterized using an X-Ray Fluorescence (XRF) technique. XRF spectroscopy has been previously used to determine the elemental composition of aggregate powders and quarry by-products (Chen et al., 2011; Galetakis et al.; 2012). The results for the chemical composition of QB1, QB2, and QB3 are summarized in Table 3.5. For QB2 and QB3 materials, XRF results are given separately for QB materials collected from primary, secondary, and tertiary crushing stages. These two QB materials collected from various crushing stages were characterized extensively by Tutumluer et al. (2015). The chemical composition of QB is a dominant factor that controls the effectiveness of stabilization, and strength increase due to cementitious/pozzolanic reactions.

QB samples from different crushing stages in the same quarry mostly had similar chemical compositions; likely indicating that they are derived from the same parent aggregate material. For all three sources, Calcium Oxide

(CaO) is the major component, followed by Magnesium Oxide (MgO), Silicon dioxide ($SiO_2$), and traces of other oxides. When comparing the percentage of MgO and $SiO_2$, it can be seen that QB2 material had higher MgO content, while QB3 has higher $SiO_2$ content. QB1 was selected to be used for an unbound application to fill the voids of the large PCR aggregates, while QB2 and QB3 were used for chemically stabilized base/subbase applications. Thus, the chemical composition of QB2 and QB3 can indicate the effectiveness of stabilization, field performance, and the potential for long-term strength gain. Long-term pozzolanic reactions are driven by the content of active silica and alumina (i.e. pozzolan materials); where higher contents of active pozzolans tend to indicate higher strength gain potentials with pozzolanic reaction (Massazza, 1998; Walker and Pavia, 2010). QB3 has higher amounts of $SiO_2$ and $Al2O_3$ and is thus expected to have more long-term strength gain.

Table 3.5 Chemical composition of the utilized QB materials

| **Material** | **Crushing Stage** | **Measurement by Weight (%)** | | | | | | |
|---|---|---|---|---|---|---|---|---|
| | | CaO | $SiO_2$ | MgO | $Al_2O_3$ | $Fe_2O_3$ | $K_2O$ | Others |
| QB1 | - | 81.1 | 5.6 | 11.3 | - | 0.8 | 0.5 | 0.7 |
| QB2 | Primary | 54.7 | 6.2 | 36.7 | 0.8 | 0.8 | 0.4 | 0.4 |
| | Secondary | 48.5 | 14.1 | 33.4 | 1.6 | 0.9 | 0.8 | 0.7 |
| | Tertiary | 50.4 | 11.8 | 34.2 | 1.1 | 0.9 | 0.7 | 0.9 |
| QB3 | Primary | 58.7 | 23.2 | 11.0 | 4.4 | 1.1 | 0.8 | 0.8 |
| | Secondary | 71.4 | 14.3 | 10.1 | 2.0 | 1.0 | 0.6 | 0.6 |
| | Tertiary | 71.4 | 14.8 | 9.5 | 2.2 | 0.8 | 0.6 | 0.7 |

### 3.3.5 Unconfined Compressive Strength Tests for Stabilized QB Applications

Due to the significantly low strength of untreated QB (Tutumluer et al., 2015), the stabilization of QB and QB-FRAP/FRCA blends were necessary for achieving sufficient strength for pavement applications (Qamhia et al., 2016). Accordingly, the QB samples were stabilized with either 3% Type I Portland cement or 10% class 'C' fly ash and tested for their 7-day unconfined compressive strength (UCS). Sample preparations for the QB2 and QB3 materials were carried out according to the procedure outlined in ASTM D1632 Standard (ASTM, 2007). The samples were compacted into a 2.8 in. (71 mm) diameter and 5.6 in (142 mm) tall cylinder in three equal lifts using the standard Proctor hammer. Additionally, cylinders for UCS testing for the QB2/FRAP and QB2/FRCA blends were compacted as per ASTM C1435/C1435M Standard (ASTM, 2014), with a small change; 4 in. x 8 in. (102 mm x 203 mm) cylinders were made instead of 6 in. x 12 in. (152 mm x 305 mm) cylinders due to the smaller size of QB. All samples were then cured unsealed in a moisture-controlled room at 100% relative humidity and at room temperature for seven days.

Stabilized samples were tested for the 7-day UCS using the recommendations and procedure outlined in ASTM D1633 standard (ASTM, 2007a). Prior to testing, the samples were completely soaked in water for four hours, surface-dried and capped at the ends using a sulfuric compound, then tested for compressive strength on a Forney

loading frame at a rate of 4,000-11,000 lb./minute (18-49 kN/minute). Figure 3.4 compares the seven-day achieved unconfined compressive strength properties of the stabilized samples. Note that the 28-day compressive strength values were also determined several months after the acquisition of the materials. These results are not shown since the fly ash samples showed a lower 28-day strength than the 7-day strength due to the shelf life of fly ash and degradation in its cementitious properties. For the cement-stabilized samples, the 28-day compressive strengths were consistently 9% to 16% higher for the various combinations. Shown also in Figure 3.4 are the standard deviation and the Coefficient of Variation (COV) for each material combination based on testing five cylinders for UCS.

Excluding the samples for [FRCA + QB2 + 3% Cement], which had a coefficient of variation of 22.3%, all the other samples had a coefficient of variation lower than 13.5%. Additionally, samples for [FRAP + QB2 + 3% Cement] achieved the highest 7-day UCS, and their strength was statistically different from all other combinations except [FRCA + QB2 + 3% Cement]. This was determined using a two-sided t-test with a 95% confidence interval. The mean UCS for [FRAP + QB2 + 10% Fly ash] and [FRCA + QB2 + 3% Cement] are also statistically different from all stabilized QB2 and QB3 samples, while the strengths of the stabilized QB2 and QB3 samples are not statistically different. The UCS values of [FRAP + QB2 + 10% Fly ash] and [FRCA + QB2 + 3% Cement] are not statistically different, partly due to the high variability in the achieved strengths of the [FRCA + QB2 + 3% Cement] samples.

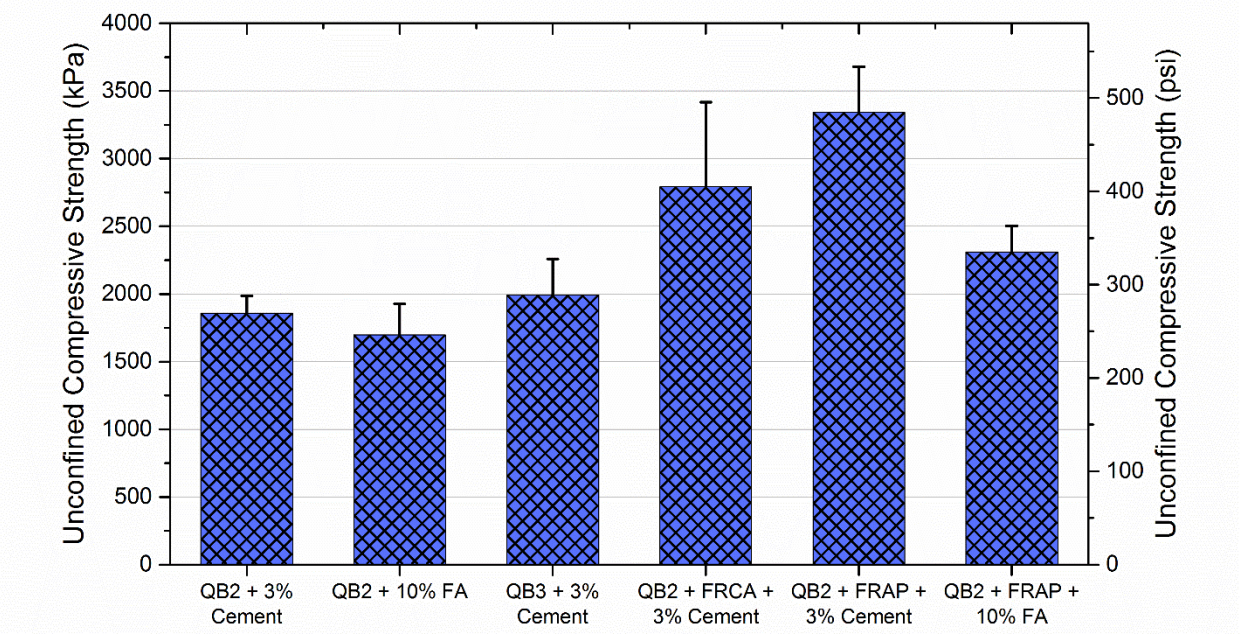


| COV (%) | 6.8 | 13.5 | 13.4 | 22.3 | 10.0 | 8.3 |
|---|---|---|---|---|---|---|

Figure 3.4 Average 7-day UCS values of the different chemical admixture stabilized material combinations used in constructing field test sections

### 3.3.6 Packing Study of the Aggregate Subgrade and QB

Prior to the construction of test sections utilizing PCR rocks and QB, a laboratory investigation was conducted to ascertain the optimized blend of the large PCR rocks and QB1, constructed in a single lift and in two lifts. A customized compaction steel box (called the UIUC packing box) was built according to the ASTM size specifications to investigate the packing efficiency of the two materials. The steel box, shown in Figure 3.5(a), is 24 in. (610 mm) x 24 in. x 21 in. (530 mm) in height. One side of the box has a removable steel door, which can be pulled up to expose the cross-section to a Plexiglass side after compaction. A high-resolution image of the cross-section was taken to further study the packing and percolation of QB1 through the large rocks. The goal was to obtain a consistent and meaningful qualitative assessment of QB1 blends to select the optimized QB1 percentage for field applications.

The test matrix studied in the laboratory consisted of conducting 14 different tests using the UIUC packing box. Several variables were studied to examine factors that might affect the packing of the QB with the large rocks in the field, and the maximum quantity of QB that could be intermixed by shaking from the top of the lift. Table 3.6 presents a summary of the variables studied using the test matrix. More details about the study are presented in Appendix A and elsewhere (Qamhia et al., 2017a). Vibration was achieved using a laboratory-sized vibratory roller (VIBCO US-1600 model), at a vibration frequency of 9000 rpm, to simulate the field construction procedure.

As a first step, tests for the compaction of the large PCR rocks (as the aggregate subgrade) in a single lift and in two lifts were conducted to measure the void ratios or porosities. The bulk specific gravity of the CS02 PCR aggregate material was measured as per ASTM C127 Standard (ASTM, 2015) to be 2.67. Using this specific gravity and based on the packing arrangement of the large rocks in the box (with no particle crushing or breakage), void ratios of 77.5% and 83.1% were calculated ($e = V_v/V_s$) for the large rocks compacted in two lifts and in one lift, respectively. These corresponded to porosity values ($n = V_v/V_T$) of 43.6% and 45.4% for the two- and one-lift arrangements, respectively. Based on these calculations, the maximum possible QB quantity to be used was determined to be approximately 40% of the weight of the large aggregate subgrade rocks.

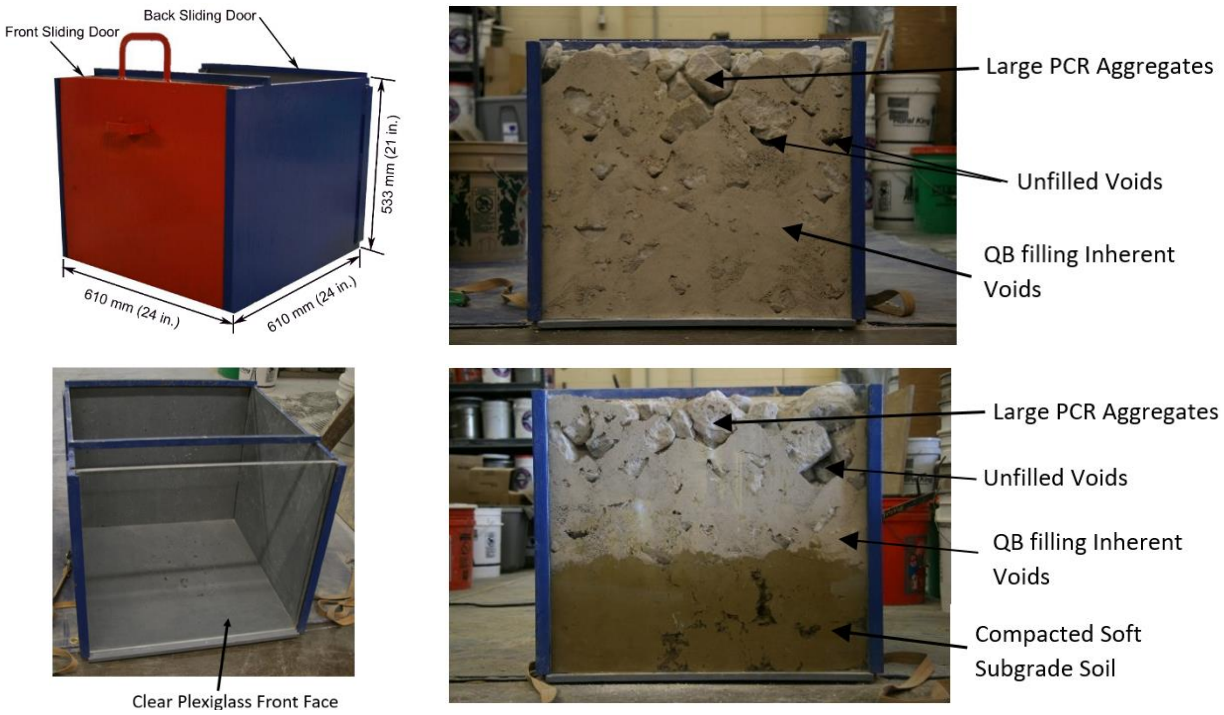


(a) (b)

Figure 3.5 (a) UIUC packing box; and (b) Cross-section of the tests with 25% of wet QB (w% = 2.5-2.6%) constructed in two lifts (top) and in a single lift on top of soft compacted subgrade (bottom)

Following the determination of the void ratios, the effects of the following four study variables on the packing arrangements of QB were mainly investigated in the laboratory. These tests and the variables studied are also summarized in Table 3.6:

1. Number of lifts: A single 21-in. (530-mm) lift and two approximately equal 10.5-in. (265-mm) lifts with the QB1 were used. Appropriate amounts of QB1 were dropped and vibrated on top of each lift (either single lift or two-lift application) of the PCR rocks.
2. The quantity of the QB1: The quantity was varied from 20% all the way up to 40% of the dry weight of the large rocks.
3. The moisture content (w %) of the QB1: Moisture content represents the dryness or wetness variability of the natural state of QBs obtained from a quarry source and used during pavement construction application. It varied from oven-dried QB1 (0%) to the as-received moisture content of the QB1 material from the source quarry (2.5±0.2%).
4. Reaction support in the experimental setup: The support conditions or foundation rigidity on top of which the samples are compacted need to address varying degrees of subgrade support. The support condition was

varied from a rigid steel bottom to a very soft subgrade soil placed at the bottom of the packing box and engineered to a CBR of less than 1% through moisture adjustment.

Table 3.6 Summary of the Test Matrix for Tests Conducted Using the UIUC Packing Box

| Test No. | Percentage of QB (%) | No. of lifts | Moisture Content of QB (%) | Support Condition | Achieved Density pcf (kN/m$^3$) |
|---|---|---|---|---|---|
| 1 | 0 (PCR Only) | 2 | 0 (oven-dried) | Steel Bottom | 93.8 (14.73) |
| 2 | 0 | 2 | 0 | Steel Bottom | 93.9 (14.75) |
| 3 | 0 | 1 | 0 | Steel Bottom | 90.1 (14.15) |
| 4 | 0 | 1 | 0 | Steel Bottom | 91.9 (14.43) |
| 5 | 20 | 2 | 0 | Steel Bottom | 113.3 (17.80) |
| 6 | 40 | 2 | 0 | Steel Bottom | 124.6 (19.57) |
| 7 | 30 | 2 | 0 | Steel Bottom | 120.6 (18.95) |
| 8 | 30 | 1 | 0 | Steel Bottom | 119.0 (18.69) |
| 9 | 30 | 2 | 0 | Steel Bottom | 121.4 (19.07) |
| 10 | 40 | 2 | 0 | Steel Bottom | 129.1 (20.28) |
| 11 | 35 | 1 | 0 | Soft Loose Subgrade | 118.3 (18.58) |
| 12 | 30 | 2 | 2.6 | Steel Bottom | 120.4 (18.91) |
| 13 | 25 | 2 | 2.5 | Steel Bottom | 116.6 (18.32) |
| 14 | 25 | 1 | 2.6 | Soft Compacted Subgrade | 118.3 (18.58) |

The heights of the loose large rocks, loose large rocks and QB1 placed on the surface, and the compacted mix were measured at nine locations (center, midpoint of each face, and each corner), and averaged for density calculations. To minimize variability, the same large aggregates were used for all tests. The rocks were handled with care to eliminate breakage that might results in changing how they pack together and with the QB aggregates.

Laboratory experiments did not show significant differences in densities and characteristic trends of percolation between the single-lift and two-lift experiments with dry QB1. However, the results are expected to differ for wet QB as higher moisture contents reduce the ability of the QB1 to percolate and fill the voids at shallower depths with a single lift arrangement. For tests conducted with varying QB1 content, 30% was found to be the optimum quantity of QB1 to be mixed with the PCR in the case of dry QB1. However, this same quantity was found to result in a relatively large amount of QB1 left on the surface for wet QB1 with a moisture content of 2.5%. Over the CBR=1% engineered subgrade, the optimum quantity of QB1 that could be packed was found to be 25% by dry weight of the large rocks for single lift arrangement. Moisture content was thus found to be the most dominant factor governing the selection of the maximum allowable percentage of QB1 and optimum packing of inherent voids in PCR aggregates**.** Figure 3.5**(**b) showed the cross-section of the compacted large rocks with 25% of QB by dry weight of the PCR aggregates, at a moisture content of 2.5-2.6%, and (1) compacted in two lifts on top of a rigid steel foundation, and (2) compacted in one lift on top of compacted soft subgrade having a CBR of 1%.

### 3.3.7 Effect of Gradation on the Strength of Chemically-Stabilized QB

Particle size distribution and packing were reported to have a significant impact on the mechanical properties of soils, such as shear strength (Cunningham et al. 2013; Ghabchi et al 2013; Qamhia et al., 2016; Qamhia et al., 2017). Studies on the effect of packing and gradation on the engineering properties of QB and quarry fines were rare in literature. Galetakis et al. (2012) used an optimization packing density model to maximize the density of mixtures of stone sludge, lime stone dust and quarry sand, and found that mixtures with 52% limestone dust and 48% quarry sand had slightly higher compressive strength and density compared to other sample proportions. A uniform particle distribution is usually desired to optimize packing and minimize excessive deformation. Fuller and Thompson originally proposed the Fuller curve equation in 1906 with an exponent of 0.5 for proportioning concrete (Fuller and Thompson, 1906). The exponent was then modified to 0.45 by the Federal Highway Administration (FHWA) in 1962, following the work of Nijboer in Netherlands (Traxler, 1949) that showed the 0.45 exponent would result in the minimum voids and the maximum packing for the aggregates in asphalt mixtures (Goode and Lufsey, 1962).

A complementary study was conducted to study the effect of QB gradations on packing, and ultimately on the strength of chemically stabilized QB samples. QB samples were engineered to follow several specified grain size distributions, stabilized with 2% Type I Portland cement or 10% class 'C' fly ash, and tested for their seven-day unconfined compressive strength. The grain size distribution of one QB material (referred to by QB4, hereafter) was engineered to fit five different gradation curves; generated by varying the shape factor (n) value in the Talbot gradation equation (Talbot and Richart, 1923):

$$p_i = \left(\frac{D_i}{D_{max}}\right)^n \qquad \text{(Equation 3.1)}$$

where $p_i$ is the percentage passing the 'i'th sieve, $D_i$ is the 'i'th sieve size in in. (mm), $D_{max}$ is the maximum sieve size (No. 4 or 4.75 mm sieve for the case of QB4), and 'n' is the power exponent of the curve; also known as the shape factor. The shape factor (n) values were varied between 0.3, 0.4, 0.45, 0.5, and 0.6 to obtain five different gradation curves. The 0.45 exponent was found to result in the minimum voids and the maximum packing for the aggregates in asphalt mixtures (Goode and Lufsey, 1962). The gradation curves used for this study are shown in Figure 3.6(a). The results for the 7-day UCS cement and fly ash-stabilized QB4 samples for the different engineered gradations are summarized in Figure 3.6(b and c).

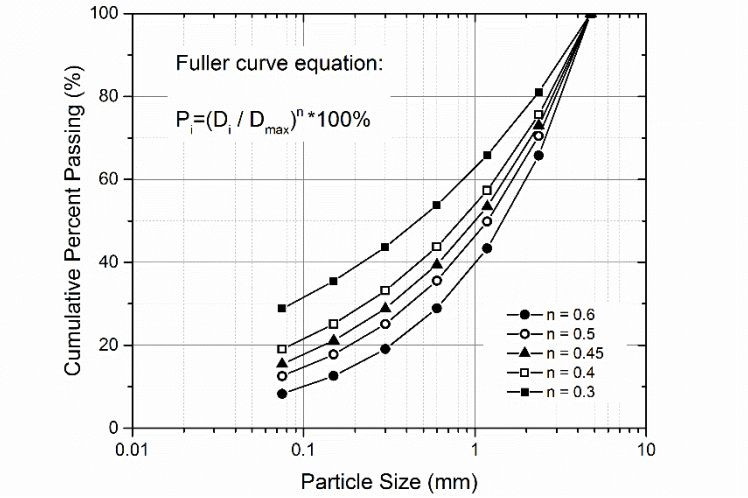


(a)

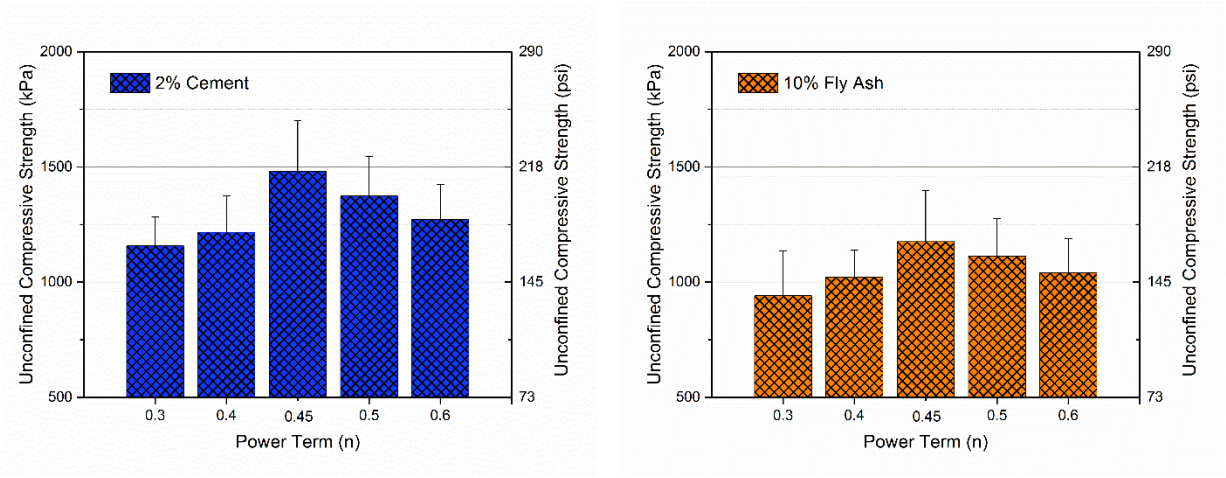


**(b)** (c)

Figure 3.6 (a) Fuller (or Talbot) power curve gradations for different power terms (n), and the average UCS for (b) 2% cement-treated and (c) 10% class 'C' fly ash-treated QB4 materials

As seen in Figure 3.6, for both cement- and fly ash-stabilized QB4 materials, the UCS was the lowest for the 0.3 power curve (highest fines content), and increased steadily up to the 0.45 power curve. The UCS values decreased from n = 0.45 to n = 0.6. Accordingly, the strength was the highest for the 0.45 power curve due to optimum packing that maximizes the solid density for this gradation, leading to the best aggregate interlock and shear strength properties. Note that, the strength drops for the higher 'n' values of 0.5 and 0.6 was not as significant as that for the finer gradations (n = 0.3 and 0.4). For the cement-stabilized QB materials, the Coefficient of Variation (COV) ranged between 10.8% and 14.8%. For the fly ash-stabilized QB4 materials, COV ranged between 11.2% and 20.6%.

The coarser gradations (i.e. n = 0.5 and 0.6) having more of the larger-sized particles had a higher load capacity due to having a greater amount of larger particles acting as the primary structure, and taking a larger percentage of the load, compared to samples with finer gradations. Samples with finer gradations (i.e. n = 0.3 and 0.4), on the other hand, had higher percentages of the secondary structure with smaller-sized particles and lower percentages of interconnected larger primary-sized particles. Note that despite the clear trend seen for the average values, the USC values obtained for the different gradation curves were not found to be statistically different using a two-sided t-test with a 95% confidence interval.

## 3.4 SUMMARY

This chapter provided a discussion of the materials selection criteria and the laboratory research components of this dissertation. Laboratory tests described included grain size distibution, moisture-density tests, packing studies of QB with recycled coarse aggregates and with large aggregate subgrade rocks, and unconfined compressive strength testing of chemically stabilized QB applications.

The laboratory tests indicated that an optimum mixing ratio of QB with recycled coarse materials was 70% QB and 30% FRAP or FRCA by weight. Either 3% cement or 10% class C fly ash was found to provide appropriate compressive strength levels for chemically stabilized QB and QB blends; with QB/FRAP and cement achieving the highest strength, which was statistically different from chemically stabilized QB blends without coarse aggregates. The packing tests of QB into the voids of large aggregate subgrades indicated that 25% QB by the dry weight of the large rocks was approximately an optimum QB quantity to be used considering moist or wet conditions of QB delivery in the field. The next chapter will discuss the field designs and construction of the full-scale test sections based on the information from the laboratory studies.

# CHAPTER 4: DESIGN, CONSTRUCTION AND QUALITY ASSURANCE OF FIELD EXPERIMENT

## 4.1 INTRODUCTION

This chapter presents details for the design and layout of the constructed test sections, the step-by-step construction procedures, and the associated quality assurance procedures that were followed to assess/ensure the quality of the constructed test sections. In total, sixteen different full-scale test sections encompassing four construction platforms and twelve flexible pavements were constructed over weak subgrades of controlled (engineered) strength. Seven of the constructed flexible pavements were aimed at studying chemically stabilized applications of QB in base and subbase pavement layers. Four of the flexible pavement test sections were aimed to study applications that use bulk quantities of QB in unbound aggregate subgrade applications. Quality assurance tests included nuclear gauge densities and Light Weight Deflectometer (LWD) testing of the constructed layers.

## 4.2 LAYOUT OF CONSTRUCTED TEST SECTIONS

The construction of the pavement test sections took place at the Illinois Center for Transportation's (ICT) accelerated pavement testing facility. The Google satellite image of the construction site showing the plan view of the constructed pavements is shown in Figure 4.1 A detailed plan view of the test sections is also given in Figure 4.2 of this report. In total, 16 test sections were constructed. The constructed roads were divided into four test blocks (Cells) designated by: Cell 1 (Cell 1S and Cell 1N), Cell 2, and Cell 3. Each Cell marks one testing zone or location with ATLAS, and is further subdivided into four test sections, each studying a different QB application.

Cell 1 was constructed on top of a subgrade soil with an engineered CBR of 1%. Figure 4.2 and Table 4.1 present Cell 1, which was constructed 119 ft. (35.6 m) long and 18 ft. (5.4 m) wide. Four test sections, each approximately 20 ft. (6.1 m) long and 9 ft. (2.7 m) wide were constructed to study the 'subgrade remediation' applications of QB; namely: (1) Aggregate subgrade introduced previously as the Primary Crusher Run (PCR) mixed with QB1 by shaking and compacting the QB on top of large rocks in a single lift and in two lifts, and (2) dense-graded aggregate subgrade layers with 15% plastic and nonplastic fines passing the No. 200 sieve. For each section, a 21-in. (530-mm) thick aggregate cover and a 3-in. (76-mm) of dense-graded CA06_R capping material were constructed. The 9-ft. (2.7-m) wide north test sections were topped with an additional 4-in. (100-mm) thick HMA layer to evaluate low volume road applications, and are denoted as Cell '1N'. The 9-ft. (2.7-m) south test sections were built to evaluate construction platform applications and was called Cell '1S'.

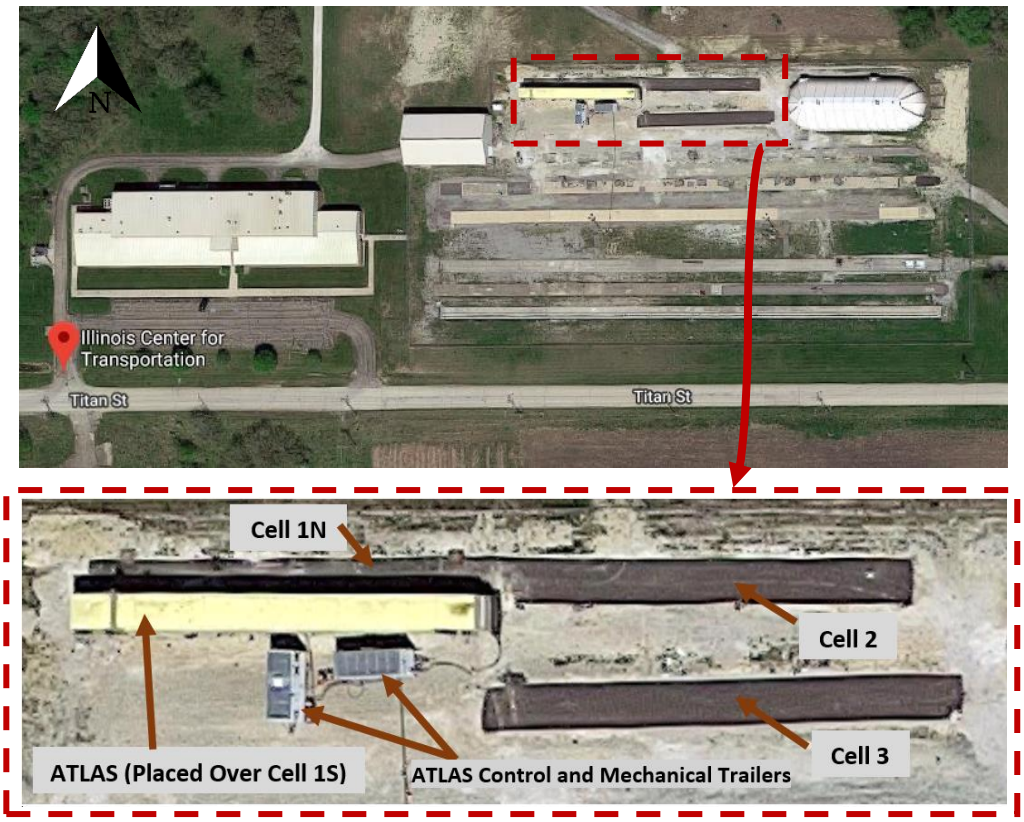


Figure 4.1 Google satellite view of the construction site, showing the constructed test Cells

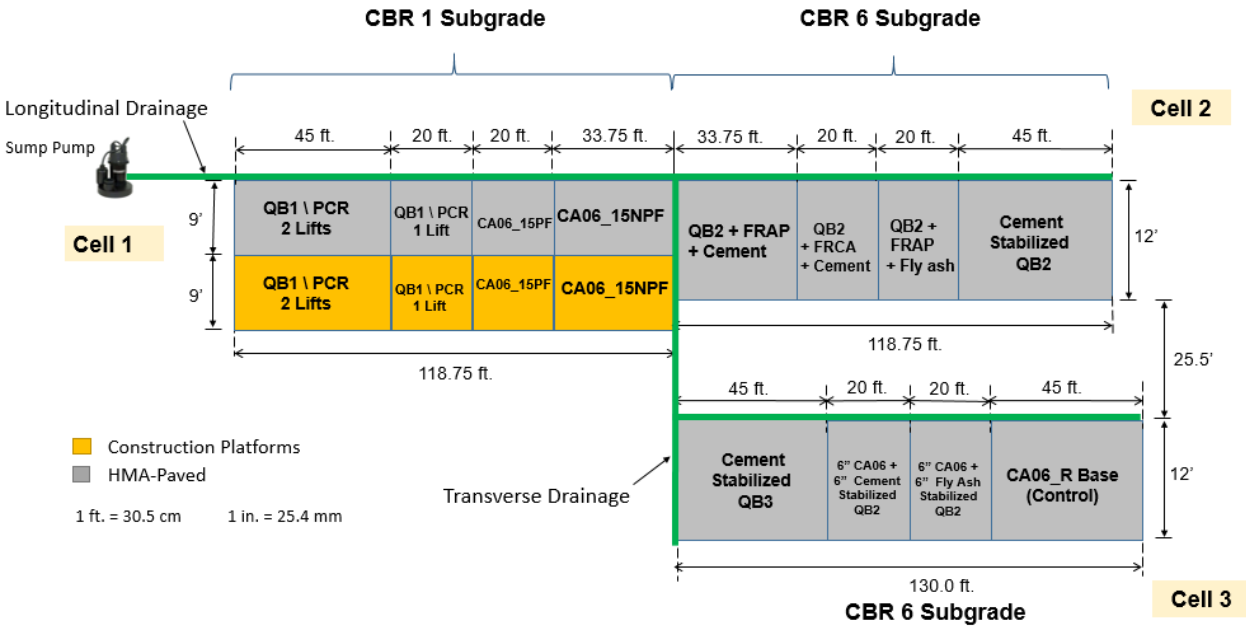


Figure 4.2 Plan view of the constructed test sections encompassing different QB applications

Table 4.1 Constructed test sections for Cell 1 utilizing unstabilized QB applications

| Section | Description and Construction Details* | Typical Cross Sections |
|---|---|---|
| **C1S1** | Primary Crusher Run (PCR) rocks with 25% QB1 by weight, constructed in **two** equal lifts using a vibratory roller compactor. QB1 is placed into the voids of the PCR from the top of **each** lift. | 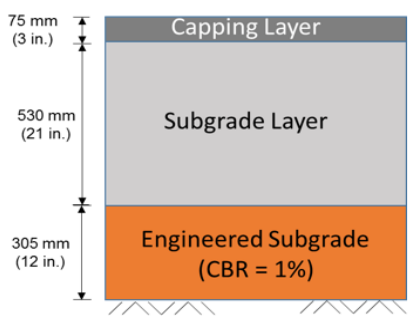 **Cell 1S** |
| **C1S2** | PCR with 16.7% QB1 by weight, constructed in **one** single lift in a similar manner as C1S1. | |
| **C1S3** | CA06_15PF: Dense-graded CA06 aggregates with 15% plastic fines content (passing No. 200 sieve) with a plasticity index (PI) of 8 constructed in **three** equal lifts. | 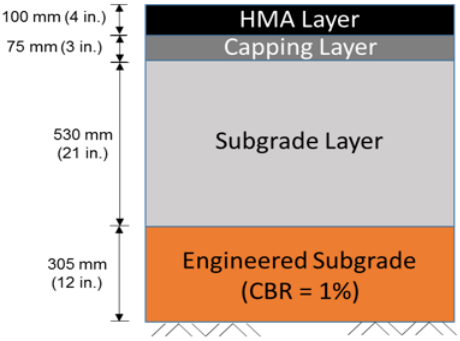 **Cell 1N** |
| **C1S4** | CA06_15NPF: Dense-graded CA06 aggregates with 15% nonplastic fines content (passing No. 200 sieve) constructed in **three** equal lifts. | |
| * All test sections in Cell 1 were overlain by a 3-in. (76-mm) thick dolomite capping (CA06_R material). For Cell 1N, a 4 in. (100-mm) thick HMA layer was paved on top of the capping layer. | | |

Cell 2 was constructed on top of a subgrade soil with an engineered CBR of 6%. Figure 4.2 and Table 4.2 present Cell 2, which was constructed 119 ft. (35.6 m) long and 12 ft. (3.6 m) wide. Four test sections, each approximately 20 ft. (6.1 m) long, were constructed to study the 'base' applications of QB; namely, [70% QB2 + 30% FRAP] + 3% Cement of the total weight, [70% QB2 + 30% FRCA] + 3% Cement base, [70% QB2 + 30% FRAP] + 10% Fly ash, and [100% QB2] + 3% Cement base. The base layers were 12 in. (305 mm) thick and were overlain by 4-in. (100-mm) of HMA.

Cell 3 was constructed on top of a subgrade soil with an engineered CBR of 6%. Figure 4.2 and Table 4.2 present Cell 3, which was constructed 130 ft. (39.0 m) long and 12 ft. (3.6 m) wide. Four test sections, each approximately 20 ft. (6.1 m) long, were constructed to study the base and subbase applications of QB. The first test section was constructed with [100% QB3] + 3% Cement base to evaluate the effect of the QB type and source (QB2 vs. QB3). The next two sections evaluated inverted pavement applications of QB and were constructed with a 6-in. (152-mm) thick QB2 subbase layer stabilized with 3% cement and 10% fly ash, respectively, and topped with 6-in. (152-mm) of conventional dense-graded CA06_R aggregate base. The last section was a conventional flexible

pavement section, constructed with a 12 in. (305 mm) of dense-graded aggregate (CA06_R) base course material. All four sections were overlain by 4 in. (100 mm) of HMA.

Table 4.2 Constructed test sections for Cells 2 and 3 with admixture-stabilized QB applications

| | Section | Description and Construction Details | Typical Cross Sections |
|---|---|---|---|
| Cell 2 | C2S1 | A blend of 70% QB2 and 30% FRAP by weight, mixed with 3% Type I cement by weight. | 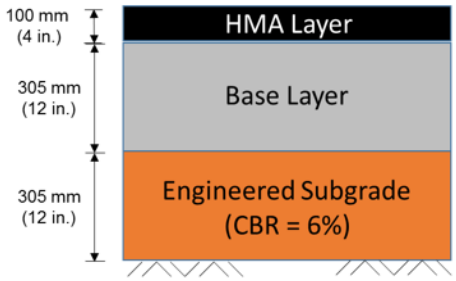 **Cells 2 and 3** |
| | C2S2 | A blend of 70% QB2 and 30% FRCA by weight, mixed with 3% Type I cement by weight. | |
| | C2S3 | A blend of 70% QB2 and 30% FRAP by weight, mixed with 10% Class 'C' fly ash by weight. | |
| | C2S4 | A Blend of QB2 and 3% Type I cement by weight. | |
| Cell 3 | C3S1 | A Blend of QB3 and 3% Type I cement by weight. | 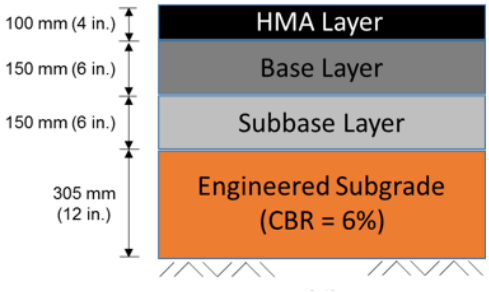 **Cell 3 (C3S2 and C3S3)** |
| | C3S2 | Subbase layer: A Blend of QB2 and 3% Type I cement by weight.<br>Base layer: CA06_R (A dense-graded unbound dolomite aggregate layer) | |
| | C3S3 | Subbase layer: A Blend of QB2 and 10% Class 'C' fly ash by weight.<br>Base layer: CA06_R | |
| | C3S4 | CA06_R dense-graded dolomite base | |

Longitudinal and transverse drainage lines were installed to drain water efficiently from the test sections (Figure 4.2). Longitudinal drainage lines ran along the north side of each cell, and a transverse drainage line ran from south to north along the west side of Cell 3 and connected to the longitudinal drainage line. Perforated, plastic drainage pipes were covered with fabric geotextile and an open-graded granular material that follows IDOT CA07 gradation band for grain size distribution. A storage basin and a sump pump were utilized to store and divert the water from the test sections (see Figure 4.2). Additionally, the beginning and end parts of each cell were designed to

have 22.5 ft. (6.8 m) long crawler zones (where the crawlers of the Accelerated Testing and Loading ASsembly (ATLAS) were placed). The innermost 7.5 ft. (2.3 m) in each crawler area was the speed stabilization zones for the acceleration/deceleration of the wheel to ensure that all test sections were tested at a constant speed of 5 mph (8 km/h). A 10 ft. (3 m) long transition zone was also added at the middle of each cell to minimize any possible influence of changing materials on the APT results. Figure 4.3 shows the details of the transition and buffer zones for each cell, as well as the 'transverse measurement lines.' These lines, indicated in each test section at one third lengths, are used to measure the transverse rut profile at two locations in each section, and were marked in the field to ensure that all surface rut measurements were consistently taken at the same locations.

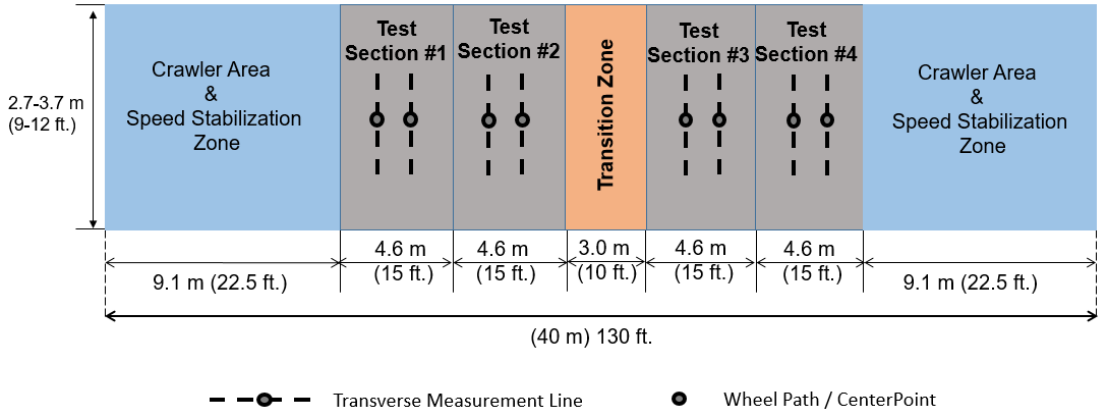


Figure 4.3 Plan view of a typical test cell showing the transition zones, buffer zones and the measurement lines

## 4.3 CONSTRUCTION OF FULL-SCALE TEST SECTIONS

Prior to starting construction activities, existing unsurfaced pavement test sections at the construction site were milled to a depth of 24 in. (60 cm). Further, to prevent any possible contamination from the previous test sections onsite, the existing subgrade soil was scraped off an additional 9 in. (0.2 m) below the existing grade and replaced with fill materials. The drainage lines were repaired and installed next. Following that, the three test cells were constructed. First, the subgrade soil was engineered to a subgrade strength of CBR = 1% for Cell 1, and a CBR = 6% for Cells 2 and 3. Then, the base/subbase layers were constructed and the HMA surface was placed in two equal lifts over test sections in Cells 1N, 2 and 3. The detailed construction activities, including Quality Assurance (QA)/ Quality Control (QC) measures to ensure high quality construction, are discussed in this section.

### 4.3.1 Engineering Subgrade Strength and Subgrade Preparation

The process of engineering subgrade strength and modifying the existing in situ soil to a CBR less than or equal to 1% for Cell 1 and a CBR of 6% for Cells 2 and 3 was achieved through a moisture adjustment procedure

adopted similarly in earlier studies of ICT projects R27-81 and R27-124 (Mishra and Tutumluer, 2013; Kazmee and Tutumluer, 2015). The process is iterative (Qamhia et al, 2017b; Qamhia et al., 2018), and each time an iteration/trial is performed, the achieved CBR profile was tested using Dynamic Cone Penetrometer (DCP) tests to a depth of 12 in. (305 mm) to assess subgrade strength and uniformity.

The subgrade soil at the ATREL site is typically classified as low plasticity clayey silt (CL – ML) by the Unified Soil Classification System or an A-4 soil by the AASHTO classification. The in situ subgrade soil has a Plasticity Index (PI) of 6% (range: 5%-7%). The relationship between CBR and moisture content for this subgrade was adequately established in the laboratory in a previous research study (Mishra, 2012). Accordingly, a moisture content of 15% and a dry density of 115.2 pcf (18.1 kN/m$^3$) corresponds to a CBR of 1%, while a moisture content of 12% and a dry density of 121.6 pcf (19.1 kN/m$^3$) corresponds to a CBR of 6%.

The following procedure was employed for subgrade strength modification:

1. First, the top 14 in. (355 mm) of the existing subgrade soil was tilled with a tiller to achieve better homogeneity. Each cell was then divided into four zones (four zones each for Cells 1N and 1S), and representative soil samples were then collected from at least two spots in each zone and tested for the in situ moisture contents using a microwave test method, as outlined in ASTM D4643 Standard (ASTM, 2008).

2. The amounts of water required to increase the moisture contents to obtain a CBR of 1% for Cell 1 and a CBR of 6% for Cells 2 and 3 were estimated from the volume of earthwork and the in situ moisture content of the soil in each zone separately (see Figure 4.2 for plan view dimensions. A 14 in. (356 mm) depth was considered). The subgrade soil layer was again tilled and compacted to the desired laboratory density level (approximately) using a sheepsfoot roller compactor; for water retention in the sheepsfoot marks. Knowing the flow rate, the estimated additional amount of water was sprayed uniformly over each zone using a fire hose connected to a water truck.

3. The soil was then uniformly mixed, and re-compacted with a sheepsfoot roller compactor (see Figure 4.4). More soil samples were collected and tested for moisture content to ensure uniformity and check that the target moisture content was achieved. Note that for Cells 2 and 3, the mixing was done using a tiller, while for Cell 1 it was done with the bucket of an excavator due to the sinking of the tiller in the soft CBR = 1 subgrade soil. Additionally, for Cell 2, both the existing subgrade and part of the borrow soil were wetter than desired, so the soil was tilled and sun-dried several times to engineer the soil moisture content. Ultimately, the CBR = 6% subgrade strength was successfully achieved.

4. Following subgrade soil compaction using a sheepsfoot roller compactor, DCP tests were carried out on the compacted soil to a depth of 12 in. (305 mm) to assess subgrade strength and uniformity in terms of the CBR profile (see Figure 4.4). This was accomplished by relating the Penetration Rate (PR) of the DCP in mm/blow to the CBR profile by using the original South African Kleyn equation (Kleyn, 1975):

$$\mathrm{Log}_{10}\,(\mathrm{CBR}) = 2.61 - 1.26\log_{10}(\mathrm{PR})$$ (Equation 4.1)

The steps outlined above were repeated until a uniform subgrade foundation with a CBR of less than or equal to 1% for Cell 1 and a CBR of 6% for Cells 2 and 3 to a depth exceeding 12 in. (305 mm) was achieved.

Subgrade soil tilling and mixing

Subgrade compaction


Moisture adjustment

DCP profiling for top 305 mm (12 in.)

Figure 4.4 Construction activities for engineering subgrade strength and subgrade preparation

5. Finally, the surface of the subgrade was sprayed with a prime coat at a rate of 3.6 lb./yd$^2$ (1.95 kg/m$^2$) for Cell 1 and a rate of 3.2 lb./yd$^2$ (1.73 kg/m$^2$) for Cells 2 and 3 in order to minimize any moisture loss and thus maintain the desired subgrade strength levels. For the same reason, the test Cells were further covered with plastic sheets until the subsurface layers were constructed (see Figure 4.5).

Subgrade surface after application of tack coat

Test Cells covered with plastic sheets

Figure 4.5 Subgrade protection and moisture loss prevention

The achieved average DCP values at each measuring point in Cells 1N, 1S, 2 and 3 are shown in Figure 4.6. An average CBR of less than 1% was achieved for all points in Cell 1, while the achieved CBR values for Cell 2 and 3 varied between 5% and 8%. Cell 3 had slightly higher CBR values than Cell 2 at many measurement points. Figure 4.6 shows the average CBR (backcalculated using the Kleyn equation) obtained at each measuring point. This average was computed by considering the top 12 in. (305 mm) subgrade profile, and the iterative subgrade engineering process ensured that the depth profile had a uniform subgrade at each measuring point, which was achieved by multiple rounds of tilling and compaction. Also note that the results are only shown for the last trial (i.e. final CBR profile), on top of which the pavements were constructed. For the earlier and intermediate trials, the DCP profile varied significantly across the cells, and varied from the desired target values.

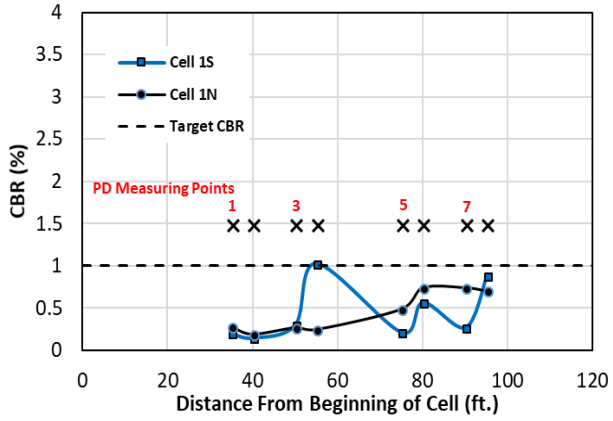


(a)

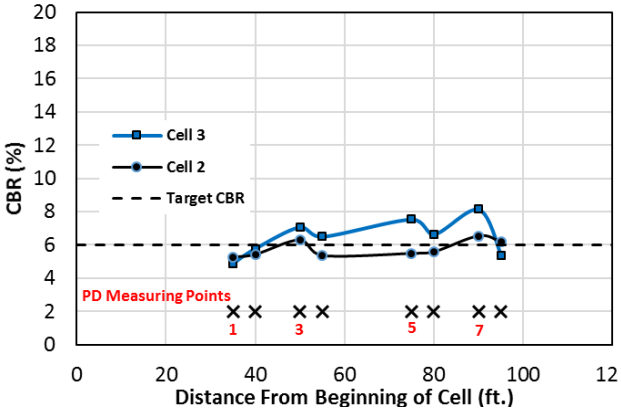


(b)

Figure 4.6 Average CBR values for the top 12 in. (30.5 cm) subgrade for (a) Cells 1N and 1S, showing the final trial with CBR values < 1%, and (b) Cells 2 and 3 showing final achieved CBR of ~6%

Following the final trial, the achieved subgrade densities for Cells 2 and 3 were measured using a nuclear gauge. At least one density measurement was taken for each section at one of the measuring points. The results for the achieved dry densities, moisture contents, and relative compaction values are shown in Figure 4.7, which indicates 100% laboratory density of 121.6 pcf (19.1 kN/m$^3$) as the target density. IDOT considers 95% of the target density as satisfactory; thus, all dry densities exceeding 115.5 pcf (18.1 kN/m$^3$) were considered satisfactory, which was the case for all test sections. The lowest measured subgrade density was for section 1 in Cell 3, which was also satisfactory (i.e. exceeding 95% of target density). Subgrade density measurements were conducted for Cells 2 and 3 only. For Cell 1, density measurements were not possible due to the very soft nature of the engineered subgrade.

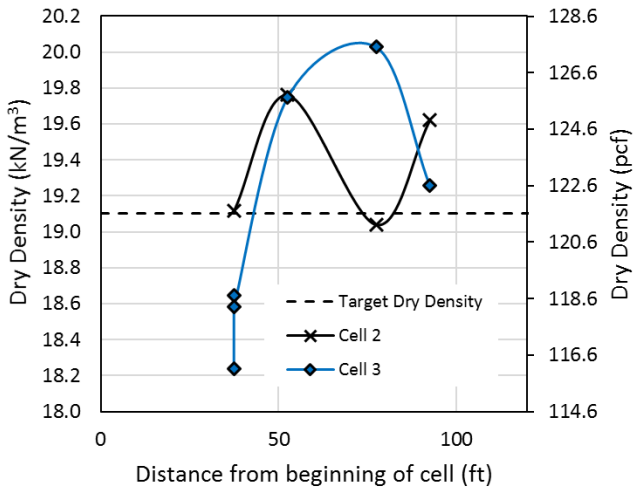


| Cell / Section | Achieved Density Pcf (kN/m$^3$) | Achieved Moisture Content (%) | Relative Field Compaction* (%) |
|---|---|---|---|
| C2S1 | 121.6 (19.1) | 11.9 | 100.1 |
| C2S2 | 126.0 (19.8) | 10.4 | 103.5 |
| C2S3 | 121.0 (19.0) | 11.1 | 99.7 |
| C2S4 | 124.8 (19.6) | 10.8 | 102.7 |
| C3S1 | 117.8 (18.5) | 10.8 | 96.8 |
| C3S2 | 125.4 (19.7) | 10.3 | 103.4 |
| C3S3 | 127.3 (20.0) | 9.3 | 104.9 |
| C3S4 | 122.9 (19.3) | 10.4 | 100.8 |

*Based on ASTM D698

Figure 4.7 Average nuclear gauge densities on top of the subgrade for Cells 2 and 3

## 4.3.2 Construction of the Unbound Aggregate Test Sections

This section covers the construction of the test sections in Cell 1 and Cell 3 with unbound aggregate materials. These sections are mainly the aggregate subgrade sections in Cell 1 (PCR/QB test sections and test sections with 15% fines content) as well as the CA06_R layers in Cell 3 used as base layers in C3S2, C3S3, and the control section (C3S4). The details for these test sections were previously given in Figure 4.2, Table 4.1, and Table 4.2.

### 4.3.2.1 Construction of PCR/QB1 Test Sections (C1S1 and C1S2)

Two test sections were constructed in Cell 1 to study the use of QB to fill the voids of primary crusher run aggregates for increased stability and lower settlement potential. Such rockfill applications of PCR aggregates are common on top of very soft subgrades (e.g. CBR = 1%). They are built in thick lifts to act as construction working

platforms on top of which the pavement sections are constructed. However, these open-graded aggregate layers contain large voids and are prone to variable settlement profiles due to the high porosities. The goal of the constructed test sections was to study the incorporation of QB1 into the voids between PCR stones to provide increased density and stability. They were placed by adding the QB from the surface in one single 21 in.- (530 mm) thick lift or in two 10.5 in.- (265 mm) thick lifts, and then using a vibratory action from a vibratory compactor to drive the QB by gravity into the voids between the large aggregates.

From the UIUC packing box study of PCR/QB1 discussed in Chapter 3, the target QB1 quantity to be added was 25% by weight of the large rocks. This recommendation was based on a single 10.5 in. (265 mm) lift compacted on top of the subgrade with CBR = 1%, and with a QB1 moisture content of 2.5%. Similarly in the field, representative samples of QB1 were first collected and tested for their field moisture contents, and the average moisture content was found to be 3.2%. The field moisture content was higher than the moisture content obtained during the laboratory tests.

During the construction of the first lift in the two-lift test section (C1S1), the large rocks were placed first and then the full amount of QB1 (25% QB materials by the dry weight of the PCR lift) were evenly distributed on the surface using a skid-steer loader. A vibratory compactor was used to shake the QB into the inherent voids in the PCR skeleton. This resulted in the formation of a densely-packed layer of QB on the surface, which slowed down QB percolation, and prevented any further filling of the voids in the PCR skeleton. This is assumed to be a result of the compactive effort, which was considerably higher than that applied in the laboratory box study. To overcome this issue in the first constructed layer in the two-lift test section, the QB were uniformly intermixed with the large rocks using the teeth of an excavator bucket (see Figure 4.8).

To prevent the formation of a densely-packed thin QB lift on the surface of subsequent lifts, the QB were slowly and incrementally spread using shovels on the surface of the large rocks, in smaller increments. The construction procedure is illustrated in Figure 4.8. The QB were then vibrated into the voids of the PCR using a larger (and heavier) standard size vibratory roller, and the process was repeated several times until the full quantity of QB was added (25% by dry weight of the PCR). However, for section C1S2 constructed in a single lift, the maximum possible amount of QB that could be packed was 16.7% by the dry weight of the PCR using this approach described. A possible reason for this can be the higher moisture content of the QB used in the field construction or the more challenging single-lift percolation goal, which might have prevented the QB from percolating the full depth of the 21 in. (530 mm) single-lift layer.

The successful construction demonstrated when the QB was added in smaller increments, followed by a vibratory action, suggests that the future field practice of vibrating QB from the surface into the inherent voids of the PCR skeleton may require developing an automated technique to spread the QB uniformly and more slowly on the surface, accompanied with continuous and strong vibration.

The construction for the PCR/QB1 test sections for Cell 1 were done simultaneously for Cell 1N and Cell 1S (i.e. both paved sections and construction working platform sections). Following the construction of the

PCR/QB1 aggregate layers, these sections were capped with a 3 in. (76 mm) dense-graded CA06_R, mixed and compacted at the optimum moisture content. The capping layers were constructed last for all Cell 1 test sections at the same time. Nuclear gauge dry densities measured with a back-scatter technique for the capping layer ranged between 126.0–138.0 pcf (19.8–21.7 kN/m$^3$), which translates to a satisfactory 97.8%–107.1% relative field compaction.

Construction of the first lift in the two-lift PCR/QB1 test section (C1S1)

QB1 placed on top of PCR (before compaction)

PCR/QB1 blends (after compaction)

Uniform spreading and incremental placement of QB1 on top of PCR lift

Final compacted surface of C1S1

Figure 4.8 Construction of PCR/QB1 sections in Cell 1

To evaluate the quality of the constructed test sections, the stiffness of the PCR/QB1 test sections were measured using a Dynatest Model 3031 Light Weight Deflectometer (LWD). A minimum of nine LWD drops, including three seating drops, were carried out at the two measuring points in each section; both before and after the placement of the capping layer. All LWD tests were conducted in accordance with ASTM E2583 standard (ASTM, 2015a). To ensure the uniformity of the surface, a layer of sand was placed at the locations of LWD drops. This was especially necessary on top of the PCR/QB1 layers, where the surface elevation could vary widely. The results from LWD testing on top of the measuring points for the construction platform and low volume road test sections (i.e. Cell 1S and Cell 1N, respectively) are presented in Figure 4.9.

All test sections indicated a significant increase in stiffness upon the addition of the capping layer. Before the placement of the capping layer, the sections constructed in two lifts had lower moduli compared to the sections constructed in one lift. C1S1 constructed in two lifts in Cell 1N had the lowest back-calculated modulus. As it will be discussed later, trenching results for Cell 1N indicate that this lowest modulus is largely due to the lower layer thickness for the second measuring point in this section, which resulted in a noticeably lower average modulus for this section. The Coefficient of Variation (COV) for the construction platforms sections in Cell 1S ranged between 6.6% and 15.5%, while the COV for the flexible pavement sections in Cell 1N ranged between 6.4% and 19.1%.

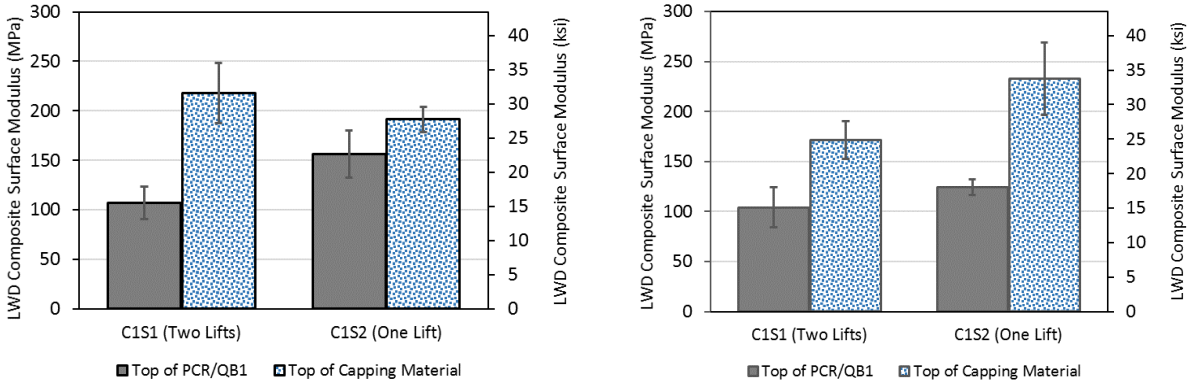


Figure 4.9 Average composite surface moduli measured by LWD for C1S1 and C1S2 for (a) Cell 1S construction platform and (b) Cell 1N flexible pavements sections

#### 4.3.2.2 Construction of CA06_15NPF and CA06_15PF Aggregate Layers

For the other two test sections constructed in Cell 1 with dense-graded aggregate materials (C1S3 with CA06_15PF and C1S4 with CA06_15NPF), the layers were compacted in three equal 7 in. (178 mm) lifts. Representative samples of each material were first collected and tested for their field moisture contents. Both materials had moisture contents lower than the OMC values, and more water was added in order to compact the materials at the OMC. The stockpiles were thoroughly mixed to achieve uniform moisture distributions. These sections were further overlaid by a 3 in. (76 mm) dense-graded CA06_R aggregate capping layer compacted at the

optimum moisture content. Figure 4.10 shows the placement of the CA06_15NPF layer and the compaction of the CA06_R capping material on top of Cell 1.

Construction of C1S4 unbound layers

Placement of CA06_R capping layer for Cell 1

Figure 4.10 Field construction activities for Cell 1 sections

The achieved relative compaction and field moisture contents for the unbound aggregate layers in Cell 1 are given in Table 4.3. The maximum dry density was determined by laboratory testing with the standard compactive effort, and the field moisture content was calculated from the field using the nuclear density gauge measurements. As seen in Table 4.3, the relative compaction for all the test sections except for Section 3 in Cell 1N exceeded the 95% level, indicating satisfactory compaction as required by IDOT construction standards. Section 3 in Cell 1N had a relative compaction of 93.1%, and an achieved moisture content of 2.3% below the optimum.

The capping layer on top of all the test sections had relatively similar compaction levels and similar achieved moisture contents, which were near optimum. Note that the CA06_15PF and CA06_15NPF materials achieved satisfactory compaction levels despite being compacted at a considerably lower moisture content than optimum. A good explanation is the higher compactive effort in the field, compared with the standard compactive effort in the laboratory. Since most sections were compacted at moisture levels on the dry side of optimum, satisfactory compaction levels could be achieved with the higher field compactive effort.

For the dense-graded aggregate subgrade test sections, a minimum of nine LWD drops including three seating drops were carried at the two measuring points in each section after each lift was constructed, as well as on top of the capping layer. The LWD back-calculated moduli are shown in Figure 4.11. All test sections showed a significant increase in stiffness upon the addition of the capping layer. The section constructed with nonplastic CA06 in Cell 1S had significantly higher modulus before the addition of capping layer. The capping layer was compacted 10 days after the construction of the CA06_15NPF and CA06_15PF layers. All four test sections had similar moduli on top of the capping layer, with an average modulus ranging from 31.0 to 37.7 ksi (214 to 260 MPa).

Table 4.3 Achieved field densities, moisture contents and relative compaction in Cell 1 sections

**Cell 1S (Construction working platforms)**

| Section | Material | Avg. field density pcf (kN/m$^3$) | MDD pcf (kN/m$^3$) | Relative compaction (%) | Achieved moisture content (%) | Optimum moisture content (%) | Difference in moisture content (%) |
|---|---|---|---|---|---|---|---|
| C1S3 | CA06_15PF | 129.9 (20.4) | 135.0 (21.2) | 96.6 | 4.4 | 6.5 | -2.1 |
| C1S4 | CA06_15NPF | 140.0 (22.0) | 138.8 (21.8) | 100.9 | 4.6 | 6.8 | -2.2 |
| C1S1 | CA06_R Capping | 135.6 (21.3) | 131.8 (20.7) | 102.7 | 4.6 | 5.4 | -0.8 |
| C1S2 | CA06_R Capping | 129.9 (20.4) | 131.8 (20.7) | 98.5 | 5.0 | 5.4 | -0.4 |
| C1S3 | CA06_R Capping | 138.1 (21.7) | 131.8 (20.7) | 104.7 | 5.4 | 5.4 | 0 |
| C1S4 | CA06_R Capping | 137.5 (21.6) | 131.8 (20.7) | 104.2 | 5.5 | 5.4 | +0.1 |

**Cell 1N (Low volume roads)**

| Section | Material | Avg. field density pcf (kN/m3) | MDD pcf (kN/m$^3$) | Relative compaction (%) | Achieved moisture content (%) | Optimum moisture content (%) | Difference in moisture content (%) |
|---|---|---|---|---|---|---|---|
| C1S3 | CA06_15PF | 125.4 (19.7) | 135.0 (21.2) | 93.1 | 4.2 | 6.5 | -2.3 |
| C1S4 | CA06_15NPF | 135.0 (21.2) | 138.8 (21.8) | 97.4 | 4.9 | 6.8 | -1.9 |
| C1S1 | CA06_R Capping | 130.5 (20.5) | 131.8 (20.7) | 99.0 | 5.6 | 5.4 | +0.2 |
| C1S2 | CA06_R Capping | 133.0 (20.9) | 131.8 (20.7) | 100.6 | 5.3 | 5.4 | -0.1 |
| C1S3 | CA06_R Capping | 141.3 (22.2) | 131.8 (20.7) | 107.0 | 5.3 | 5.4 | -0.1 |
| C1S4 | CA06_R Capping | 135.0 (21.2) | 131.8 (20.7) | 102.4 | 5.5 | 5.4 | +0.1 |

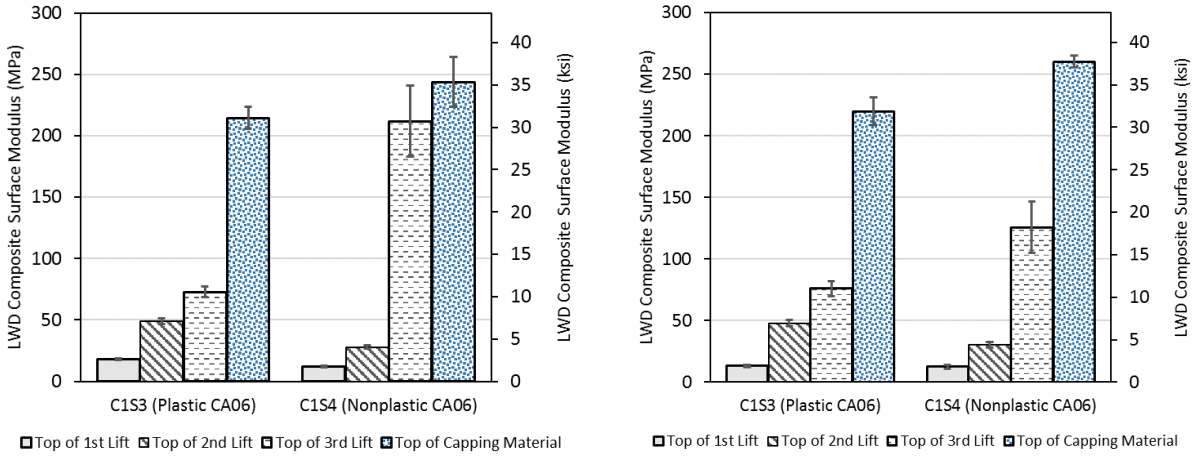


(a) (b)

Figure 4.11 Average composite surface moduli measured by LWD for C1S3 and C1S4 for (a) Cell 1S construction platform, and (b) Cell 1N low volume road sections

#### 4.3.2.3 Construction of CA06_R Layers in Cell 3

Layers of CA06_R were constructed as base layers in three sections of Cell 3. For two of these sections, namely C3S2 and C3S3, CA06_R layers were constructed as a single 6 in. (152 mm) lift on top of the chemically stabilized subbase layers. For the third section, C3S4, the CA06_R for the control section was constructed in two equal 6 in. (152 mm) lifts. The CA06_R material was constructed at the optimum moisture content by adjusting the moisture content after collecting representative samples of the materials to test for field water contents.

Initially, CA06_R construction in Cell 3 resulted in some fine pockets visible on the surface at some locations, and less than desirable densities in C3S2 (i.e. relative compaction lower than 95%). Nuclear gauge density measurements also indicated that the moisture content was on the wet side of optimum in some locations, with moisture contents exceeding 6.7%. Due to these issues, and the possibility of aggregate materials segregation, the whole construction was reworked by scraping the layer and bringing new material blended and compacted at the optimum moisture content. After reworking these sections, visual inspection and nuclear density measurements indicated that satisfactory compaction and moisture contents were achieved, with better uniformity of gradation. The results for the final achieved densities and moisture contents are given in Table 4.4 and Figure 4.12**.** Shown also on Figure 4.12 are the achieved dry densities before and after reconstructing the test sections, with measurements taken at two locations in each section.

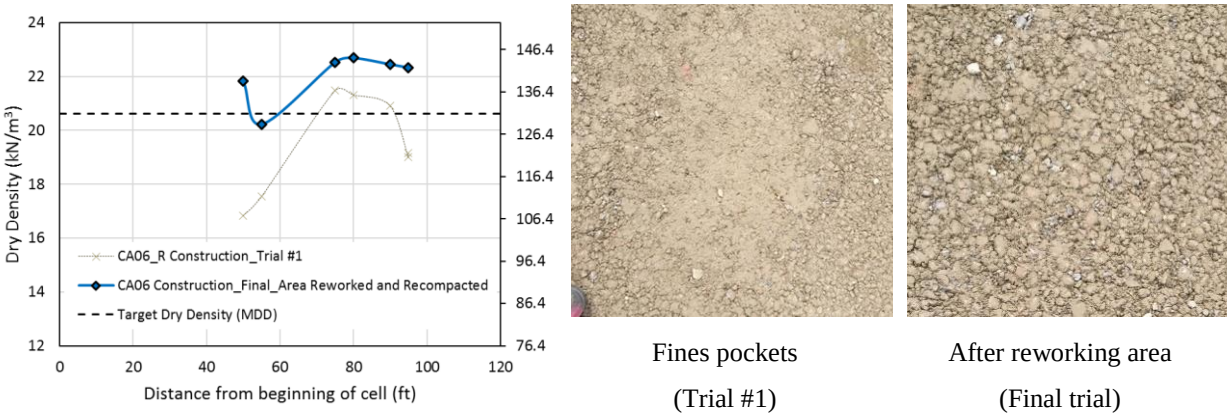


Figure 4.12 Nuclear gauge densities measured for CA06_R layer construction in Cell 3

### 4.3.3 Construction of Chemically Stabilized Test Sections in Cells 2 and 3

In total, seven chemically stabilized test sections were constructed in Cells 2 and 3 to investigate the performance of pavements with stabilized QB sublayers. The chemical stabilizers used were 3% cement or 10% class 'C' fly ash by the dry weight of the QB. QB blends with FRAP and FRCA for test sections C2S1, C2S2, and C2S3 were prepared off-site in a local asphalt plant and then delivered to the construction site.

The procedure of constructing the chemically stabilized test sections was similar for all sections as outlined in Figure 4.13. As part of the quality assurance of the construction, a maximum time of two hours between mixing with the stabilizing agent on-site and compaction was enforced. Any material not compacted after two hours was discarded. The process involved the following steps:

- Stockpiles of known volume of the QB materials or QB blends with FRAP/FRCA were dry-mixed several times (at the in situ moisture contents of the stockpiles) with the bucket of a backhoe to ensure uniformity of moisture and particle size distribution.
- Moisture samples were taken to assess the in situ moisture contents of the stockpiles and to calculate the dry weights of the stockpiles accordingly.
- The stabilizing agent (cement or fly ash) was then added in the desired quantities by weight, and mixed with the QB materials or QB blends with FRAP/FRCA for uniformity using a backhoe bucket.
- Water was added, as needed, to the mixed stockpiles from a water truck to adjust the moisture content to the OMC.
- The blends were further mixed to uniformly distribute the moisture and the stabilizing agent.
- The final mixes were transferred to the construction site, placed and tilled several times using a soil tiller to ensure uniformity.
- The test sections were constructed and compacted typically in 6 in. (152 mm) lifts. Only Section 3 in Cell 2, comprising QB blended with FRAP and fly ash was tilled and compacted in three 4-in. (102-mm) lifts; since the material was tilled with a smaller sized tiller due to access constraints of a regular-sized soil tiller.

Table 4.4 lists a summary of the achieved relative compaction and field moisture contents for all the constructed layers in Cells 2 and 3. The field densities and moisture contents were determined using a nuclear density gauge through the help of engineers from IDOT District 5. The MDD and OMC values were determined from laboratory testing using the standard compaction effort as per ASTM D698 standard (ASTM, 2012).

Except for C2S1, all other sections were compacted at moisture contents drier than optimum. However, satisfactory compaction levels exceeding 95% relative compaction were still achieved at these lower moisture contents for most test sections due to the higher compactive energy applied during construction. C2S2 had a significantly low relative compaction, while C2S4 and C3S2 (subbase layer) had lower than desired relative compaction levels of 91.9% and 92.5%, respectively. The layers with lower compaction levels were not reworked due to the difficulty of constructing these sections. However, a Dynatest Model 3031 LWD was later used to assess the quality of the constructed layers and monitor curing of these sections. There were no issues observed in satisfactory strength gain over time.


Figure 4.13 Construction steps of chemically stabilized test sections in Cells 2 and 3

To monitor the curing of the chemically stabilized test sections, LWD drops were done regularly on the surface of the constructed test sections in Cells 2 and 3 before the HMA paving. Each time a test was conducted, a minimum of nine LWD drops, including three seating drops, were carried out at the two measuring points in each section. The LWD backcalculated moduli are shown in Figure 4.14. All test sections showed a significant increase in stiffness with time. The highest LWD surface moduli and increases in stiffness were seen for the test sections in Cell 2, particularly the cement-stabilized test sections with QB2 and QB2 blended with FRAP/FRCA. The fly ash-treated sections had significantly lower backcalculated moduli and stiffness increases when compared to the cement-stabilized test sections. Note that the calculated modulus is a composite surface modulus including effects of all underlying layers, which explains the noticeably lower back-calculated moduli values in C3S2 and C3S3 before the placement of the CA06_R base layer. This is because the LWD drops were conducted on top of the 6 in. (152 mm) subbase layer with higher influence from the underlying much softer subgrade when compared to the thicker 12 in. (305-mm) stabilized base layers constructed in Cell 2 test sections.

Table 4.4 Achieved field densities, moisture contents and relative compaction in Cell 2 and Cell 3 sections

**Cell 2 Test Sections**

| Section | Material | Avg. field density pcf (kN/m$^3$) | MDD pcf (kN/m$^3$) | Relative compaction (%) | Achieved moisture content (%) | Optimum moisture content (%) | Difference in moisture content (%) |
|---|---|---|---|---|---|---|---|
| C2S1 | QB2 + FRAP + Cement | 129.2 (20.3) | 135.0 (21.2) | 95.6 | 9.1 | 8.0 | 1.1 |
| C2S2 | QB2 + FRCA + Cement | 113.9 (17.9) | 128.6 (20.2) | 88.7 | 7.8 | 9.8 | -2.0 |
| C2S3 | QB2 + FRAP + Fly ash | 135.0 (21.2) | 136.2 (21.4) | 99.4 | 5.6 | 7.5 | -1.9 |
| C2S4 | QB2 + Cement | 126.7 (19.9) | 137.5 (21.6) | 91.9 | 8.8 | 9.1 | -0.3 |

**Cell 3 Test Sections**

| Section | Material | Avg. field density pcf (kN/m$^3$) | MDD pcf (kN/m$^3$) | Relative compaction (%) | Achieved moisture content (%) | Optimum moisture content (%) | Difference in moisture content (%) |
|---|---|---|---|---|---|---|---|
| C3S1 | QB3 + Cement | 128.0 (20.1) | 129.9 (20.4) | 98.4 | 5.3 | 8.4 | -3.1 |
| C3S2 | QB2 + Cement Subbase | 127.3 (20.0) | 137.5 (21.6) | 92.5 | 8.7 | 9.1 | -0.4 |
| C3S2 | CA06_R Base | 133.7 (21.0) | 131.8 (20.7) | 101.5 | 5.0 | 5.4 | -0.4 |
| C3S3 | QB2 + Fly Ash Subbase | 131.1 (20.6) | 135.6 (21.3) | 96.6 | 6.5 | 8.0 | -1.5 |
| C3S3 | CA06_R Base | 143.9 (22.6) | 131.8 (20.7) | 109.2 | 4.2 | 5.4 | -1.2 |
| C3S4 | CA06_R Base | 142.6 (22.4) | 131.8 (20.7) | 108.1 | 4.1 | 5.4 | -1.3 |

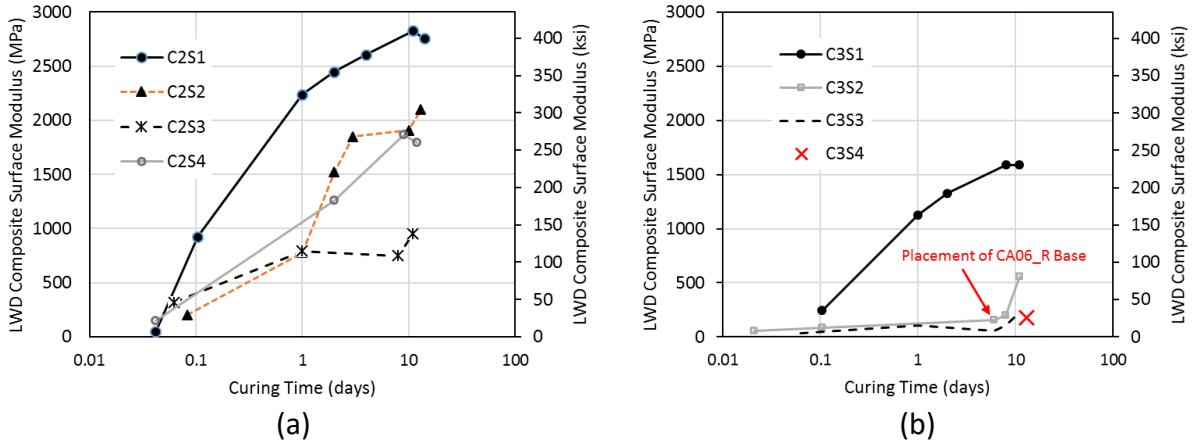


Figure 4.14 Average composite surface moduli measured by LWD for (a) Cell 2 test sections, and (b) Cell 3 test sections

### 4.3.4 Hot Mix Asphalt Placement and Compaction

The HMA layer was constructed in two equal 2-in. (51-mm) lifts. The HMA used for both lifts had an asphalt binder with a Superpave performance grade of PG 64-22. Both surface course lifts had the same mix design with a 0.375 in. (9.5 mm) nominal maximum aggregate size. Note that there was no binder course with larger size aggregates (i.e. the same HMA mix design and material was used for both lifts). Therefore, 2 in (51 mm) thickness was selected for both lifts in order to meet the 4 in. (102 mm) total HMA thickness. Loose mixes were sampled in the asphalt plant and from the paver during construction. The two HMA lifts were compacted using the same vibratory roller compactor, and density measurements were taken with a nuclear density gauge on top of the final surface. Figure 4.15 shows three photos covering the sampling and paving activities. All test section HMA surfaces were paved on the same day. Paving was started from the west end of Cell 1, moving east towards Cell 2, and finally, Cell 3 was paved last.

Figure 4.15 Hot mix asphalt sampling and paving

The achieved HMA centerline field densities and air voids are presented in Figure 4.16. In total, two density measurements were taken for each constructed test section, one at each measuring point. Cell 1 test sections had considerably higher densities/lower air voids compared to Cell 2 and Cell 3 sections. Specifically, C3S4 (control section) had the highest air voids of 11.9%. These air voids are based on a theoretical maximum specific gravity ($G_{mm}$) of 2.486 reported by the contractor. The field cores obtained directly after construction from the wheel path at the transition zones of Cells 1, 2, and 3, and tested at ATREL had air void contents of 8.5%, 9.0%, and 10.1%, respectively. The air void contents from the tested cores were in good agreement with the trends and values calculated from the field nuclear density measurements.

Additionally, the air void contents and relative compaction reported by the contractor, through the contractor's own nuclear density gauge measurements for the constructed test sections, ranged between 7%–10% for air voids, and 90%–93% for relative compaction for Cells 1-3. The contractor's reported air void values were consistently ~2% lower than the values measured by IDOT and reported in Figure 4.16.

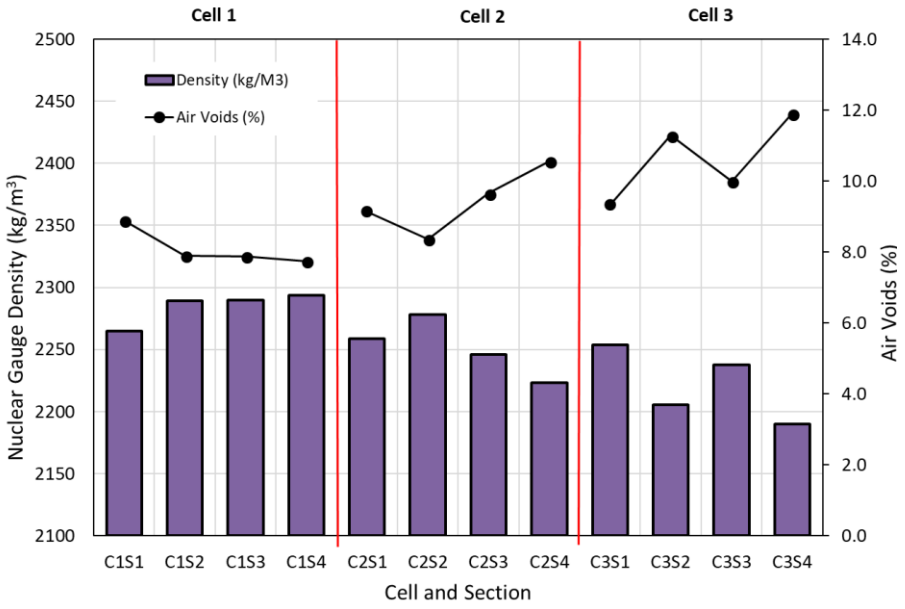


Figure 4.16 Achieved HMA densities and air void contents (%). [1000 kg/m$^3$ = 62.4 pcf]

## 4.4 INSTRUMENTATION OF FULL-SCALE TEST SECTIONS

Soil pressure cells were installed on top of the subgrade in four of the test sections constructed in Cells 2 and 3; specifically under sections C2S1, C2S4, C3S2, and C3S4. The pressure cells were installed in the wheel path on each of the transverse measurement lines in the chosen test sections. To ensure that the pressure cells lied directly under the wheel path and therefore minimized loading eccentricity, total station equipment and land surveying techniques were used to identify the locations of the pressure cells and relocate those locations after the construction of the HMA layer. In total, eight Geokon model '3500' soil pressure cells, with a standard range of 58 psi (400 kPa) and a 9 in. (230 mm) diameter were installed. The locations of the installed soil pressure cells, and installation photos are highlighted in Figure 4.17. Data from soil pressure cells provided the levels of wheel load deviator stresses applied on the subgrade and helped to compare the performance trends of the instrumented test sections.

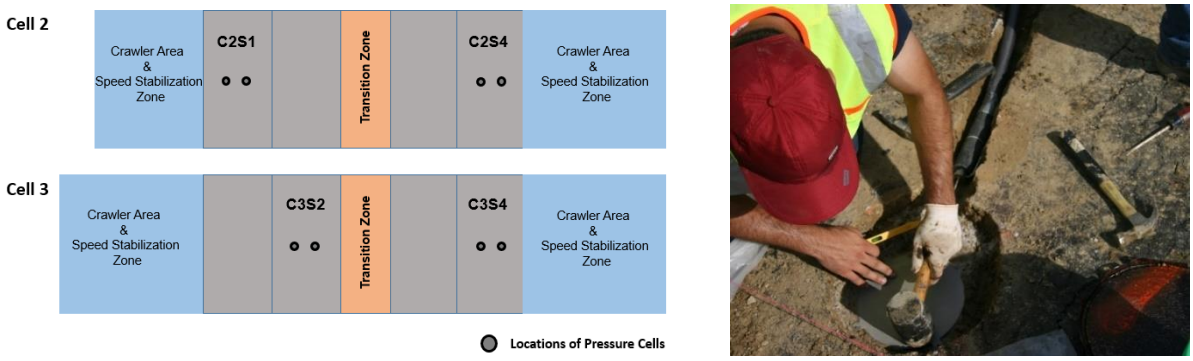


Figure 4.17 Soil pressure cell locations in Cell 2 and Cell 3 sections and installation photo

## 4.5 SUMMARY

This chapter provided a discussion of the layout of the constructed test sections, a detailed description of the evaluated QB applications, and details for the construction of the various pavement layers: engineered subgrade, unbound and chemically stabilized aggregate subgrade/subbase/base layers, and HMA pavement layers. Measures to reduce variability and ensure high quality construction and proper curing of the stabilized layers were emplyed. This included using a nuclear density gauge to ensure proper compaction of the constructed layers, using DCP to ensure proper strength of the engineered subgrade, and uing a LWD to ensure proper modulus and proper curing over time of the stabilized pavement layers utilizing QB.

The evaluation of the constructed layers through different means indicated that the subgrade was properly engineered to a CBR of 1% or less in Cell 1, and a CBR of approximately 6% for Cells 2 and 3. Density measuremnts for the engineered subgrade in Cells 2 and 3 and subbase/base layers in Cells 1, 2 and 3 indicated that proper density exceeding 95% of the laboratory maximum dry density was generally achieved except for a few sections such as C2S2. HMA compaction and air voids measured in the field generally showed good compaction for the HMA layer, except for C3S4 which had a relatively high HMA air void content of approximately 12%. Cell 1 test sections also showed better HMA compaction and lower air voids than Cell 2 and 3 test sections.

# CHAPTER 5: FULL-SCALE TESTING AND PERFORMANCE MONITORING

## 5.1 INTRODUCTION

Following the construction of the three test Cells at the University of Illinois ATREL facility in Rantoul, the constructed test sections were monitored for performance through accelerated pavement testing (APT). Heavy vehicle loads were applied using the Accelerated Transportation Loading ASsembly (ATLAS) shown in Figure 5.1. Important features of the ATLAS equipment include:

1. 124 ft. (37.8 m) long, 12 ft. (3.65 m) high, and 12 ft. (3.65 m) wide;
2. 85 ft. (25.9 m) loading length with approximately 65 ft. (19.8 m) of constant velocity loading of the wheel;
3. ATLAS weighs 175 kips (780 kN) and is mounted on four crawler tracks;
4. The ATLAS wheel carriage assembly can accommodate a single tire, dual-wheel tire, aircraft tire, or a single-axle rail bogey;
5. The load level can vary between 0 and 80 kips (355.6 kN);
6. The wheel carriage can wander up to 3 ft. (0.9 m) laterally;
7. The maximum speed of the wheel is 10 mph (16 km/h); and
8. Aluminum panels can be attached on both sides and heaters can be distributed inside the panels to control and maintain constant temperatures. Temperature control is divided into three zones with six heaters that can be controlled individually.

Accelerated Transportation Loading Assembly (ATLAS) at ICT

Super-single tire (455/55R22.5) Insulation panels Heaters- temperature control

Figure 5.1 ATLAS accelerated pavement tester at ICT, showing some features

This chapter provides a detailed discussion for the results of the performance evaluation records of the evaluated QB applications. Details are given for the setup and parameters of the APT study, and for the means and approaches utilized for measuring periodic surface ruts. A summary of the data collected for the surface rut progression in the construction platform and HMA-surfaced test sections are presented. Data for the measured deviator stress on top of the subgrade in the four test sections that were instrumented with soil pressure cells are also provided and discussed.

## 5.2 APT LOADING PARAMETERS AND DATA COLLECTION

Each Cell, comprising four test sections, marked one location for ATLAS. Accordingly, Cell 1S, Cell 1N, Cell 2 and Cell 3 were trafficked separately. The trafficking of Cell 1S with construction platform test sections was completed first, followed by Cell 1N, Cell 2, and finally Cell 3. The details of the test sections in these four cells were previously discussed in Section 4.2 (see Figure 4.2, Table 4.1, and Table 4.2).

A super-single tire (455/55R22.5), shown in Figure 5.1, was used to traffic the test sections. The first number (455) refers to the tire width from wall to wall in mm, the second number (55) corresponds to the side wall height expressed as a percentage of tire width, and the third number (22.5) is the rim diameter in inches.

For the purposes of this research, a constant unidirectional wheel load of 10 kip (44.5 kN), a tire pressure of 110 psi (760 kPa), and a constant speed of 5 mph (8 km/h) were assigned to load the constructed sections, and to evaluate their rutting potential. Channelized wheel loading was applied with no wander considered. The same loading parameters were used to test all flexible pavements and construction working platform test sections. Once the Cell 2 and Cell 3 sections were done receiving 100,000 wheel passes at the above listed standard load/pressure, the wheel load was increased to 14 kips (62.3 kN) and the tire pressure was increased to 125 psi (862 kPa), and additional 35,000 passes were applied at these increased load/pressure levels.

Performance monitoring was conducted by periodic surface profile measurements after a certain number of passes. For each measuring point, the non-trafficked profile measurement, i.e. at zero pass, was taken as the reference. Measurements of deflections at the wheel path were taken on more frequent occasions for the initial (e.g. 1, 10, 100, 250, 500, 750, and 1,000) passes, and then less frequently (e.g. every 2,000 passes for construction platforms, and every 5,000 passes for HMA-paved sections). On occasions when heavy rain occurred, especially for the construction platform sections, rut measurements were collected more frequently after each such occurrence. Trafficking was continued until a certain threshold was achieved or a sufficient number of passes were applied. The wheel path rut threshold was selected to be 3 in. (76 mm) for the construction platforms, while that for the HMA-paved sections was selected to be 0.5 in (12.5 mm).

The transverse surface rut profile measurements for the construction working platforms were taken using a customized surface rut measurement device as shown in Figure 5.2(a). The device consists of a hollow perforated channel with holes at an interval of 2 in. (50.8 mm) and calipers that measure depths to the nearest 0.4 mils (0.01 mm). Transverse rut measurements (orthogonal to the travel direction) were taken at the two measuring points in

each test section, and up to a lateral distance of 30 in. (760 mm) on each side of the centerline of the wheel path to capture any possible heaving of materials on the sides of the wheel path. The rut depth was reported as the average rutting of the centermost 11.8 in. (300 mm) of the wheel path.

The transverse surface rut profile measurements for the HMA-paved test sections were measured using an automated laser profiler as shown in Figure 5.2(b). Transverse rut measurements at the two measuring points in each test section were taken up to a distance of 16 in. (405 mm) on each side of the centerline of the wheel path. At each measuring point, a total of six 31.9 in. (810 mm) lateral scans were performed at 0.2 in. (5 mm) spacing, and the rut depth was reported as the average rutting of the centermost 11.8 in (300 mm) of the wheel path from the six measurements.

Customized rut depth measuring device

Automated laser profiler

Figure 5.2 Rut measurements for construction platforms and flexible pavement test sections

## 5.3 PERFORMANCES OF CONSTRUCTION PLATFORM TEST SECTIONS (CELL 1S)

Rutting is the primary mode of failure in constructed unbound aggregate layers and subgrade. Thus, the rutting performance was assessed through measurements of the permanent deformation accumulation in the construction working platforms. This section presents analyses and comparisons of rut accumulations in the construction platform test sections.

Figure 5.3 presents the average accumulations of permanent deformation with increasing number of passes in Cell 1S test sections, and the individual rut accumulations at each measuring point. The horizontal dashed lines indicate the 3 in. (76 mm) threshold. Additional details of the collected rut data are presented in Appendix B. At each measurement point, the wheel path deflection was calculated as the average deflection at thirteen points along the width of the wheel path. Except for section 3 in Cell 1S, constructed with CA06 having 15% plastic fines (i.e. CA06_15PF), all other sections showed good performance up to a total of 20,000-wheel loading passes. On average, section 3 showed consistently higher permanent deformation trends than the other three sections, while the similar Cell 1S section 4 with 15% nonplastic fines (i.e. CA06_15NPF) had consistently the lowest permanent deformation accumulations; clearly contrasting the drastic effect of the plasticity of fines on construction platform performance.

Additionally, Cell 1S section 1 constructed with PCR/QB1 in two equal lifts showed higher rut accumulations than Cell 1S section 2, which was constructed in a single lift. Specifically, the East measuring point in section 1 constructed in two lifts had considerably higher rutting, which upon trenching also showed a crack

propagating the full depth of the capping layer and half the depth of the aggregate subgrade layer, i.e. the second lift (see Figure 5.4). One possible explanation for the crack is an internal shear failure in the aggregate subgrade layer, which can be attributed to the construction procedure that left excess QB on the surface between the two lifts, possibly creating a weak shear plane due to loss of contact between the large PCR aggregates. The differences in performance trends of the two sections can be considered within the acceptable tolerance of construction variability.

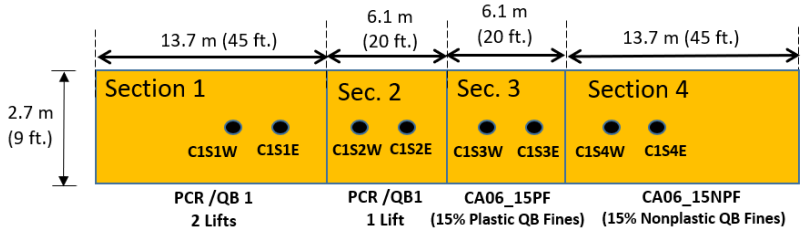


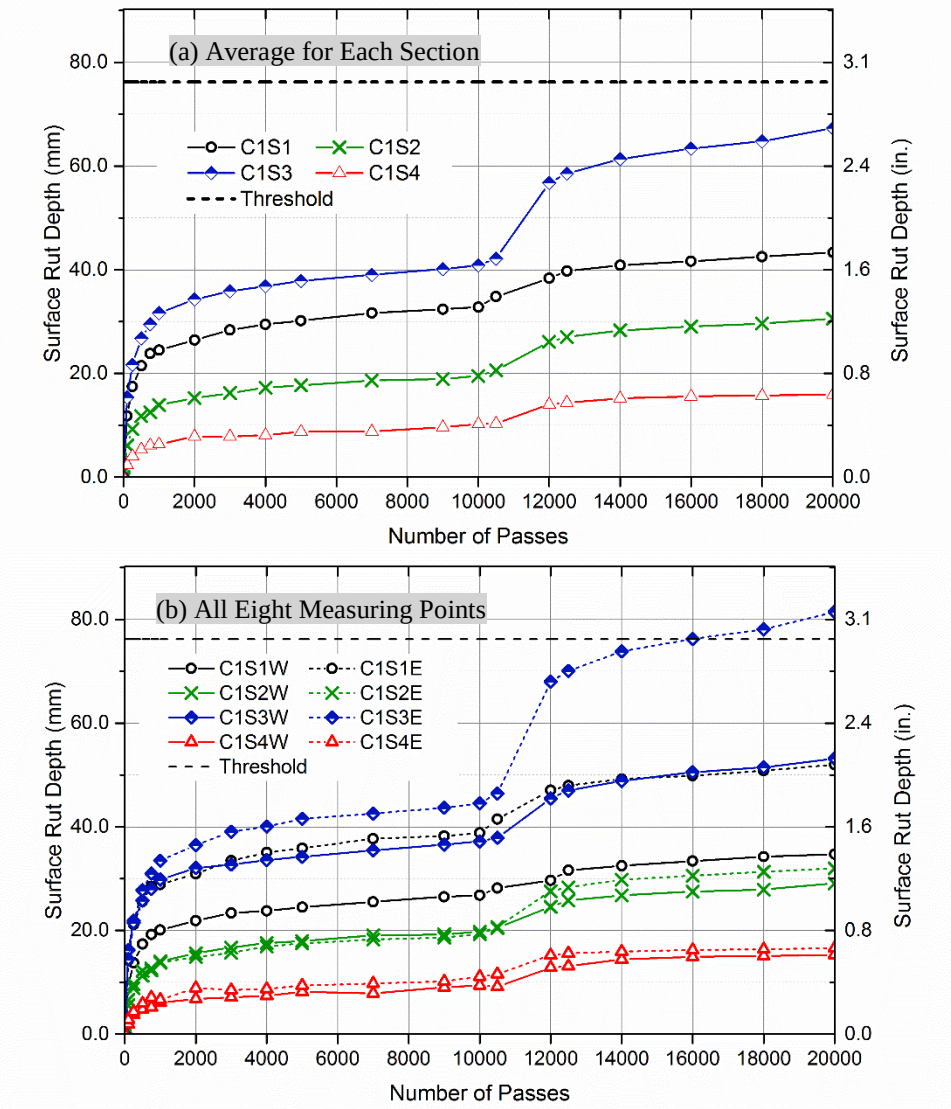


Figure 5.3 Wheel path maximum rut progression in Cell 1S test sections - construction platforms

Compared to other test sections, Cell 1S Section 3 constructed with 15% plastic fines CA06 aggregate material (i.e. CA06_15PF) showed the most severe cracking, which started to appear on the sides of the wheel path after only 100 passes, indicating possible shear failure in the aggregate subgrade material. The East measuring point in section 3 (C1S3E) had more severe cracks and accumulated significantly higher permanent deformations. Upon trenching, it was discovered that the section at this measuring point was constructed 2.5 in. (63 mm) less than the target layer thickness, which clearly affected performance. The cracks observed in Cell 1S Section 3 are shown in Figure 5.4 after 9,000-wheel passes.

Further, an incident of heavy rain was reported between passes 10,000 and 12,500, for which all test sections showed a steeper increase in the rut accumulation. This was particularly true for Cell 1S Section 3 where the plastic fines showed the steepest increase in rutting with rain, while the other three sections had comparable increases in rutting rate. Several other incidents of rain were encountered during the trafficking of Cell 1S, and heavier rain (i.e. increased moisture content in the aggregate subgrade layers) led to a more rapid progression in rut accumulation of the construction working platforms.


Cracking in C1S1E (PCR/QB1 – 2 Lifts) Plan view for cracking in C1S3 (CA06_15PF)

Figure 5.4 Visible cracks in Cell 1S - sections C1S1E and C1S3E/W

## 5.4 PERFORMANCES OF FLEXIBLE PAVEMENT TEST SECTIONS

This section discusses the performance trends of the flexible pavement test sections constructed in Cells 1N, 2 and 3. Surface rut profiles were periodically measured with the automated laser profiler in all three cells. Further, Cells 2 and 3 were instrumented with pressure cells on top of the subgrade in four of the pavement sections. The results of subgrade pressures measured are also reported and discussed in this section.

### 5.4.1 Performance of Cell 1N - Unbound Applications of QB

Cell 1N studied low volume road applications of QB as a filler material in the voids of large aggregate subgrade rocks and as a plastic/nonplastic fine material in dense-graded aggregate subgrade/CA06 layers. Flexible pavement test section performances in Cell 1N were monitored for up to 90,000 ATLAS wheel passes. Selected cross sections in Cell 1N are shown in Figure 5.5 to highlight certain construction issues (see discussion below). The wheel path rut accumulations for Cell 1N pavement sections are presented in Figure 5.6.

As shown in Figure 5.6, none of the test sections accumulated rutting greater than the 0.5 in. (12.5 mm) threshold (horizontal dashed line in the figure), which is why the decision was made to end trafficking at 90,000 wheel passes. After 90,000 wheel passes, all test sections showed, on average, comparable results and had a low rate of rut accumulation. The low rutting rate which started after 60,000 passes is highly attributed to the stiffening of the HMA layer due to the decrease in air temperatures in October/November. More details on the rutting data are presented in Appendix B.

Figure 5.6 indicates higher discrepancies in rutting trends from the two measuring points for Cell 1N Sections 1 and 4, which can both be attributed to construction variability. For section 1 (PCR/QB1 constructed in 2 lifts), trenching showed that the East point, i.e. C1S1E, which accumulated the highest rutting was short in aggregate subgrade thickness and had lower QB content packed underneath the wheel path [see Figure 5.5(a)], while the C1S1W was constructed more uniformly with the proper aggregate subgrade thickness. Additionally, C1S4W showed the second highest rut accumulation and indicated some segregation in materials, where the gradation under the wheel path was finer than anticipated (see Figure 5.5(b)), which is visible for comparison with other cross sections for section 4 in Cell 1S and with C1S4E in Cell 1N. The analyses of the full trenching data are discussed in Chapter 6. If the two measuring points with construction issues were eliminated from the comparison, the rutting accumulation trends for Cell 1N and Cell 1S would follow the same order for test sections with the same materials.

(a) C1S1E – PCR/QB1 in 2 lifts (b) C1S4W – CA06_15NPF (c) C1S4E – CA06_15NPF

Figure 5.5 Cross sections of some measuring points in Cell 1N test sections

The average rutting results for sections in Cell 1N show that section 3 with 15% plastic fines accumulated the highest rutting among all the paved test sections. This was also the case for unpaved sections in Cell 1S; which

indicate the detrimental effect of plastic fines on performance, especially when exposed to moisture. The presence of HMA cover on top of plastic fines, however, reduced the negative outcomes of plastic fines due to significantly lower load levels experienced by these aggregate layers under the HMA.

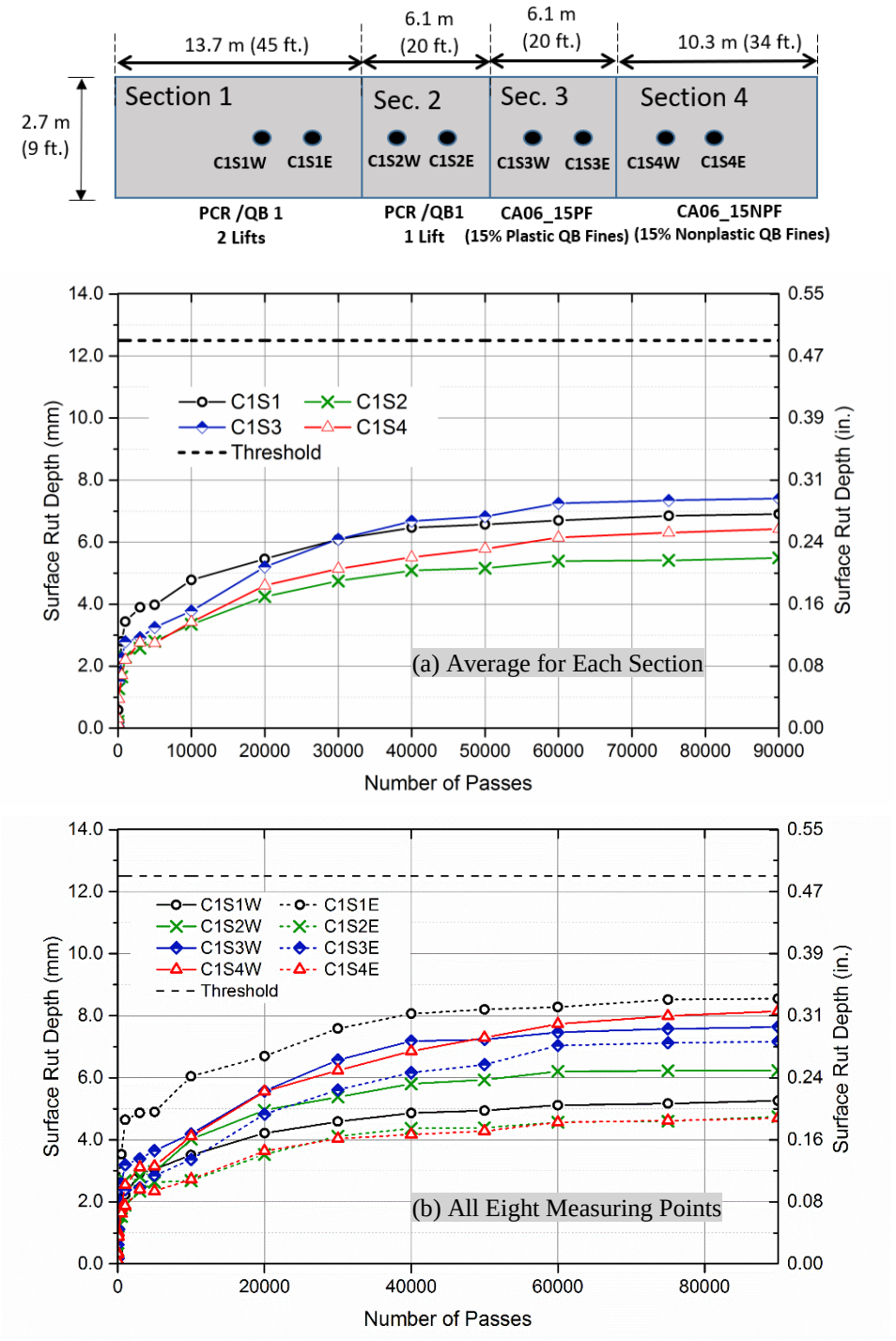


Figure 5.6 Wheel path maximum rut progression in Cell 1N test sections - flexible pavements

## 5.4.2 Performance of Cell 2 – Chemically Stabilized Base Course Applications of QB

Cell 2 test sections were constructed to study flexible pavement applications of chemically stabilized QB and QB blends with FRAP/FRCA used as base materials. The performance trends of the flexible pavement test sections in Cell 2 were monitored up to 135,000 passes. The results for the wheel path maximum rut accumulations for Cell 2 test sections are presented in Figure 5.7.

Initially, 100,000-wheel passes were applied at a load of 10 kip (44.5 kN), a tire pressure of 110 psi (760 kPa), and a constant speed of 5 mph (8 km/h). Two of the test sections (C2S1 and C2S2) studying cement-stabilized blends of 70% QB2 with 30% FRAP/FRCA had exceptionally good performance and accumulated less than 80 mils (2 mm) of rutting after 100,000 passes. Accordingly, it was decided to apply an additional 35,000 passes at the increased load level of 14 kip (62.3 kN) and an increased pressure level of 125 psi (862 kPa). The tire pressure was therefore increased to ensure that the loading mechanism did not change the pattern of stress distribution in the HMA layers due to the increased load level. The Equivalent Single-Axle Loads (ESALs) for each wheel pass at the original and increased load levels were calculated using the AASHTO equivalency factors using Equations 5.1–5.3, which are based on the results of AASHO road tests (Huang, 2004). The results are tabulated in Table 5.1. Note that these values somewhat underestimate the ESALs from one ATLAS pass, which may induce more damage since the speed of ATLAS (5 mph or 8 km/h) is significantly lower than typical highway speeds.

$$log\left(\frac{W_{tx}}{W_{t18}}\right) = 4.79\log(18+1) - 4.79\log(L_x + L_2) + 4.33\log L_2 + \frac{G_t}{B_x} - \frac{G_t}{B_{18}} \quad \text{(Equation 5.1)}$$

$$G_t = \log\left(\frac{4.2 - p_t}{4.2 - 1.5}\right) \quad \text{(Equation 5.2)}$$

$$B_x = 0.4 + \frac{0.081(L_x+L_2)^{3.23}}{(SN+1)^{5.19}(L_2)^{3.23}} \quad \text{(Equation 5.3)}$$

where

$W_{tx}$ is the number of x-axle load applications at the end at time *t;*

$W_{t18}$ is the number of 18-kip (80-kN) single-axle load applications to time *t;*

$L_x$ *is* the load in kips on one single-axle, one set of tandem axles, or one set of tridem axles;

$L_2$ is the axle code (1 for single-axle, *2* for tandem axles, and *3* for tridem axles);

SN is the structural number; and

$p_t$ is the terminal serviceability.

Table 5.1 Approximate conversions of two ATLAS load level passes to ESALs

| | **Inputs** | | | | | | **Calculations** | | |
|---|---|---|---|---|---|---|---|---|---|
| **Load Level** | **$W_{18}$** | **$L_x$** | **$L_2$** | **SN** | **$P_t$** | **$G_t$** | **$B_{18}$** | **$B_x$** | **ESALs ($W_{tx}$)** |
| **10 kip (44.5 kN) Load** | 1 | 20 | 1 | 5 | 2.5 | -0.2009 | 0.5001 | 0.5382 | **1.50** |
| **14 kip (62.3 kN) Load** | 1 | 28 | 1 | 5 | 2.5 | -0.2009 | 0.5001 | 0.7921 | **5.40** |

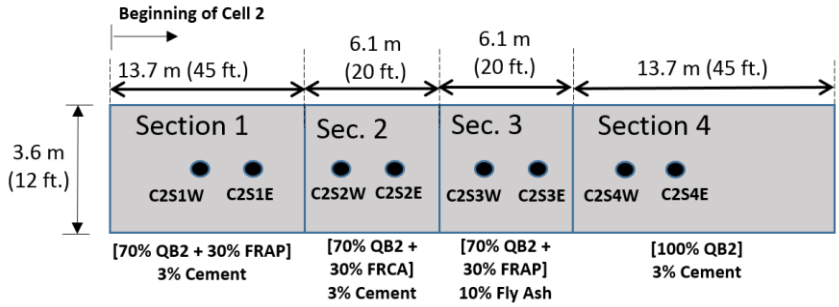


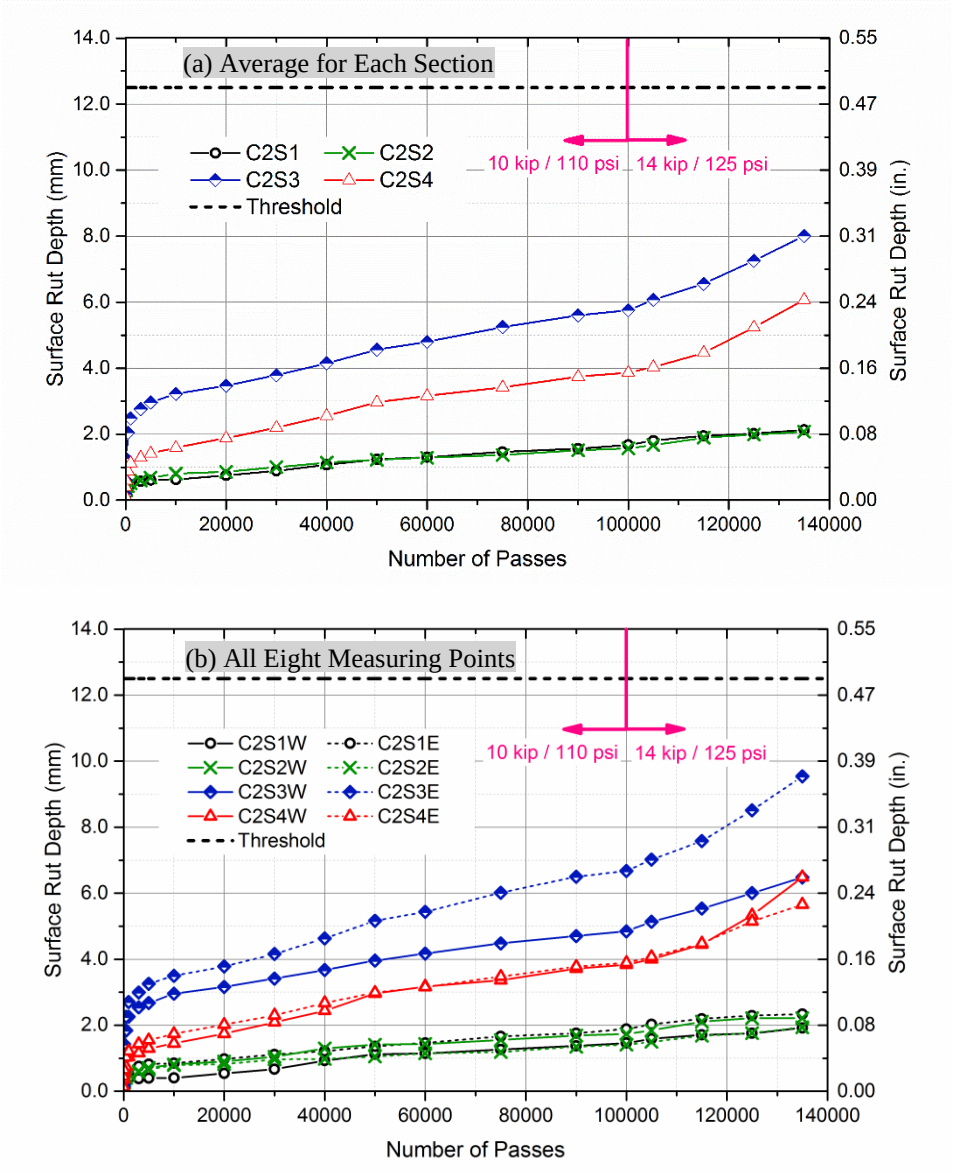


Figure 5.7 Wheel path maximum rut progression in Cell 2 test sections - flexible pavements

As shown in Figure 5.7, overall a satisfactory rutting performance was achieved for all the Cell 2 test sections utilizing QB applications, even at the increased load level. The C2S3 test section, having the blend of 70% QB2, 30% FRAP by weight, and stabilized with 10% class 'C' fly ash had significantly higher rut accumulation than the equivalent C2S1 section stabilized with 3% cement, which indicates the better performance of sections stabilized with cement. Additionally, sections with a coarse fraction of recycled FRAP/FRCA aggregates accumulated significantly lower rutting compared to C2S4 with cement-stabilized QB2 fines only. The low rutting accumulation under heavy loading by the APT in these test sections indicate the potential use of this application to sustain higher traffic levels, such as medium volume roads or county highways. Sections in Cell 2 also showed low variability in rut accumulation between the two measuring points in each section, despite the construction variability in HMA thicknesses in some sections. More details of the rutting data from Cell 2 test sections are presented in Appendix B.

Figure 5.8 shows the wheel load vertical stresses measured on top of the subgrade by the soil pressure cells in the instrumented test sections in Cell 2 (C2S1 and C2S4). Both test sections showed noticeably low subgrade pressures not exceeding 2.5 psi (17.5 kPa) for the 10-kip (44.5-kN) load level, and 5 psi (35.0 kPa) for the increased 14-kip (62.3-kN) load level. The measured pressures increased 1.5 to 2 times when the load was increased in both test sections. The pressures on top of the subgrade are also lower for C2S1 with QB/FRAP and cement blends when compared to C2S4 with QB and cement only. This observation is in agreement with the increase in moduli values and rutting trends for the two sections indicating the positive effect of having recycled coarse aggregate materials in the mix on load distribution and rutting performance. The results, shown as the average values from two pressure cells in each section, were taken after a certain number of ATLAS passes and the measurements were consistent throughout the testing period.

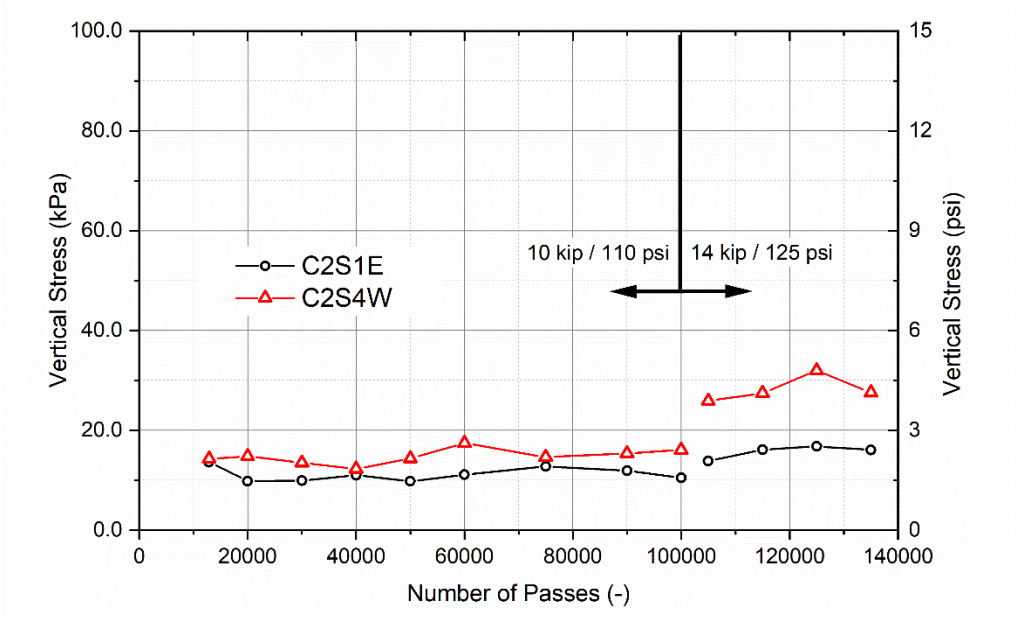


Figure 5.8 Average wheel load vertical stress on top of subgrade in the instrumented sections in Cell 2

### 5.4.3 Performance of Cell 3 – Chemically Stabilized Base/Subbase Applications of QB

Flexible pavement applications of chemically stabilized QB as base and subbase materials were investigated in Cell 3. Note that the last section in Cell 3 (C3S4) is a control section constructed with CA06_R base material without any QB or stabilization. Similar to Cell 2, the performance trends of the flexible pavement test sections in Cell 3 were monitored up to 135,000 passes, with the first 100,000-wheel passes applied at a load of 10 kip (44.5 kN), and a tire pressure of 110 psi (760 kPa). The latter 35,000 passes were applied at the increased load level of 14 kip (62.3 kN) and increased tire pressure of 125 psi (862 kPa).

Since Cells 2 and 3 have comparable applications of QB as chemically stabilized materials in base/subbase layers, it was imperative that both Cells were constructed similarly and tested at similar load levels and climatic conditions. Both Cells were constructed on top of an engineered CBR = 6% subgrade soil, and the nominal design thicknesses for subsurface and HMA layers were similar. The trafficking of Cell 3 test sections was running into winter, and temperatures during the day and night were dropping significantly. Therefore, in order to maintain similar average surface temperatures for Cells 2 and 3, it was necessary that Cell 3 test sections be covered with ATLAS panels and that heaters were set inside to maintain the HMA surface temperature at 75 °F (24 °C). This was done after 85,000 passes. This temperature was decided upon based on the average surface temperature for Cell 2 trafficking, which was calculated as 74.8 °F (23.7 °C). Due to the shading provided by ATLAS, the surface temperatures were measured to be no more than 7°F (4 °C) higher than air temperature at the wheel path. The installation of heat control panels and heaters are shown in Figure 5.9.


Panel installation | Heaters on pavement | Temperature control – 3 zones

Figure 5.9 Installation of heaters and insulation panels on Cell 3 sections for temperature control

The results of the wheel path maximum rut accumulations in Cell 3 test sections are presented in Figure 5.10. For section 4 with CA06_R base, only the west measuring point (C3S4W) was considered for the average rutting progression. The other east measuring point (C3S4E) was omitted due to the influence of the transition zone, which was paved last with less than desired HMA thickness (2.75 in. or 70 mm), and had more permeable HMA with relatively low density/high porosity. It also showed premature transverse fatigue and longitudinal wheel path cracking that is not typical for the base layers constructed with CA06 type of materials. With early cracking, the transition zone and C3S4E were exposed to higher levels of moisture that caused eventual pumping of fines from the CA06 material through the cracks and resulted in severe cracking and rutting as the loading progressed. Therefore, in order to have more representative data from this section, only C3S4W results are presented as average values and discussed herein. The individual rut progression of C3S4E is shown in Figure 5.10(b). More details of the Cell 3 test section rutting data are presented in Appendix B.

Figure 5.10 also shows additional performance data from a previous APT study labelled as "Previous Study R27-124" for comparison with the control section. The test section from the previous R27-124 study was constructed on an engineered subgrade with CBR of 3%, with an aggregate subgrade conforming to CS02 gradation and having a thickness of 9 in. (229 mm), overlain by a 3 in. (76 mm) of CA06_R material (similar to the one for C3S4) and HMA surface thickness of 4.3–4.9 in. (109–124 mm). More details about this test section can be found in the final report from the R27-124 study (Kazmee and Tutumluer, 2015).

As shown in Figure 5.10, C3S1 constructed with cement-stabilized QB2 material showed, on average, the least rutting, followed by C3S2 with a cement-stabilized QB2 subbase and a CA06_R base. The wheel path maximum rutting progression trends for C3S4 are only shown up to 40,000 passes due to the progression of fatigue to the surface, resulting in increased moisture contents in the base and overall reduction in structural capacity from that of the originally constructed cross-section. As a result, the rutting accompanied by cracking was more severe in the control section with further trafficking. It is also important to note that the structural capacity of the control section was originally weaker than the sections constructed with same base layer thickness and higher modulus stabilized QB materials.

Rutting rates increased considerably in all test sections when the load level was increased. In particular, C3S3 constructed with a fly ash-stabilized QB2 subbase and a CA06_R base showed significant increases in rutting rate at the increased load level and surpassed the threshold of 0.5 in. (12.5 mm) after 135,000-wheel passes. Comparisons of rutting progressions of C3S2 and C3S3 indicate a big discrepancy in performance trends between the fly ash and cement-stabilized QB sections, which was also clearly seen from sections in Cell 2.

Comparing the results of the stabilized test sections of C3S4 with a similar section from the R27-124 study (Kazmee and Tutumluer, 2015), these unbound aggregate sections accumulated higher rutting than the stabilized sections in Cells 2 and 3. Note that the section highlighted in Figure 5.10 from Kazmee and Tutumluer's R27-124 study (Kazmee and Tutumluer, 2015) was constructed on a weaker (CBR = 3%) subgrade soil, but had a higher HMA thickness than C3S4W, which had a constructed HMA thickness of only 2.75 in. (70 mm).

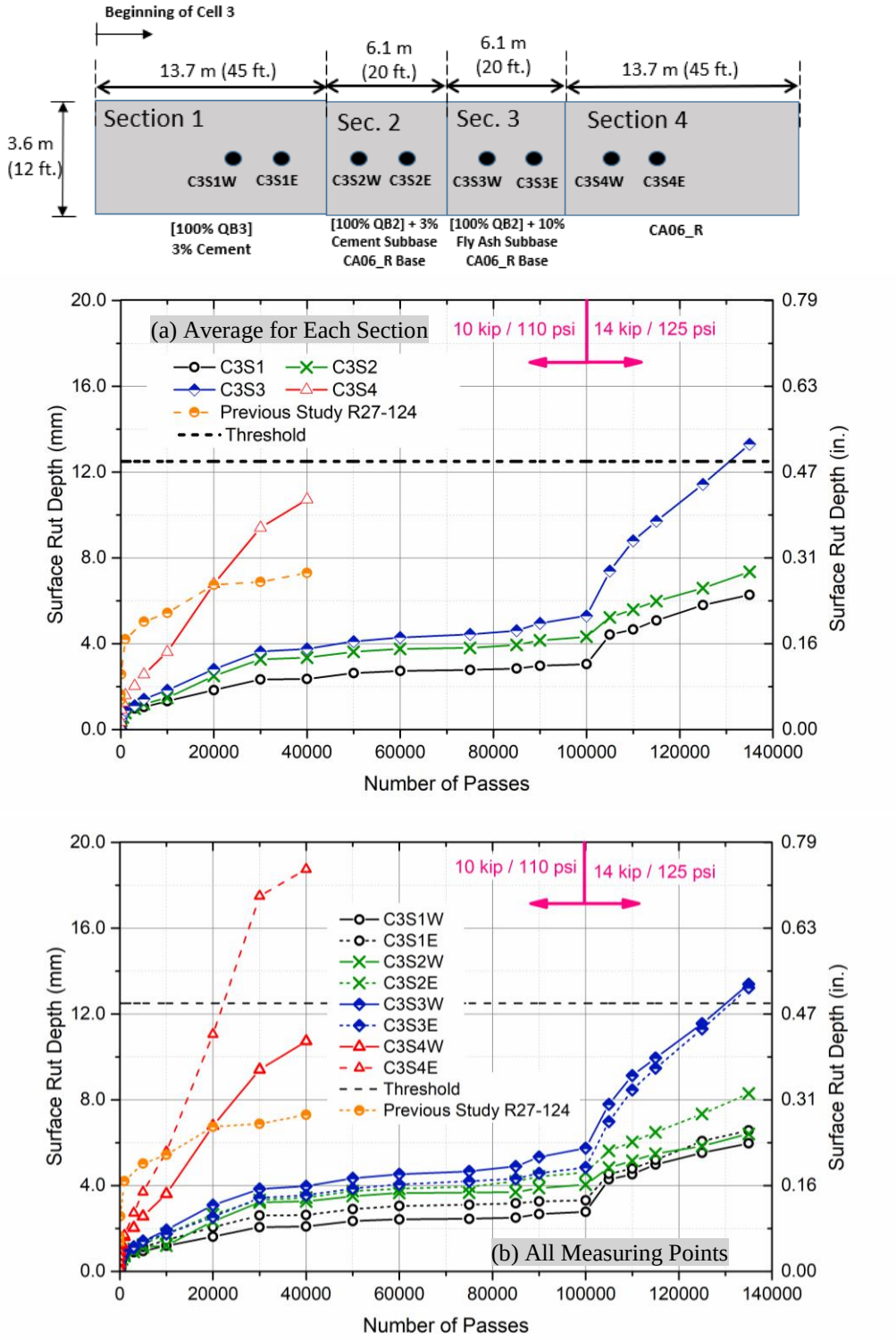


Figure 5.10 Wheel path maximum rutting progression in Cell 3 test sections - flexible pavements

Figure 5.11 shows the wheel load vertical stresses measured on top of the subgrade by soil pressure cells instrumented in two test sections in Cell 3 (C3S2 and C3S4). C3S2, which has a cement-treated QB subbase and a CA06_R unbound aggregate base, had relatively low wheel load vertical subgrade pressure not exceeding, on average, 2.5 psi (17.5 kPa) for the 10-kip (44.5-kN) load level or 5 psi (35.0 kPa) for the increased 62.3-kN (14-kip) load level. C3S4, however, had subgrade pressures that were 3–5 times higher than those measured for C3S2 and for the chemically stabilized sections in Cell 2. The measured trends for pressures on top of the subgrade are also matching with the rutting performance trends for the two sections. This finding clearly indicates that having a stiffer chemically stabilized base/subbase can significantly reduce the pressure on top of subgrade and therefore protect the subgrade by minimizing permanent deformation accumulation in this weakest pavement layer (i.e. subgrade).

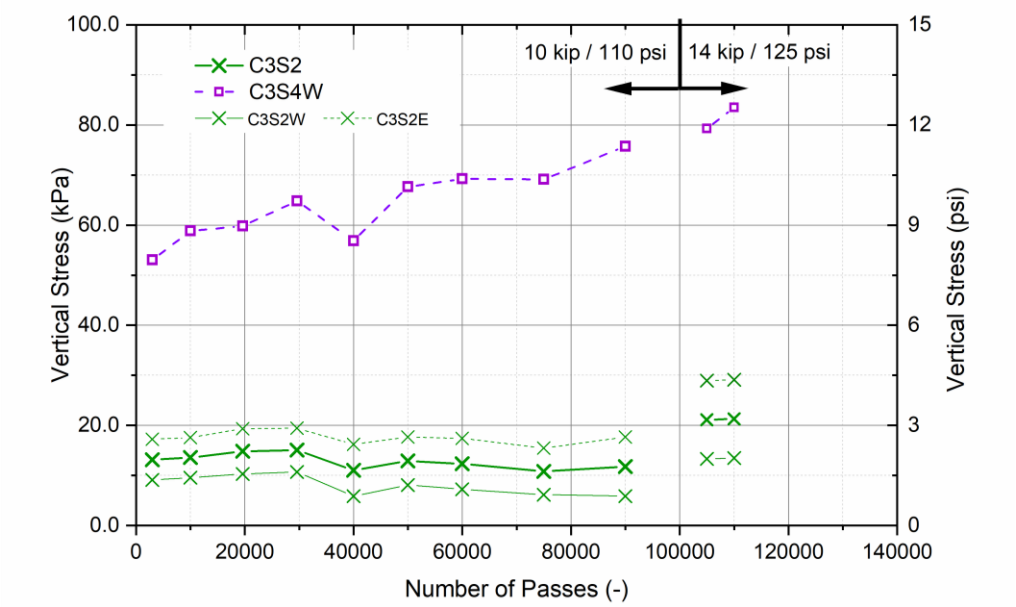


Figure 5.11 Average pressures on top of subgrade from the two instrumented sections in Cell 3

## 5.5 SUMMARY

This chapter provided a summary of the performance records of the constructed working platform and flexible pavement test sections. This includes the rutting progression in all test sections and the measured top of the subgrade vertical stresses due to wheel load for sections instrumented with soil pressure cells in Cells 2 and 3. The constructed test sections were loaded using the ATLAS accelerated pavement tester. A summary of the test Cells loading levels and the number of passes at each load level is given in Table 5.2.

Performance monitoring with accelerated pavement testing showed quite satisfactory results of QB applications for each of the construction platform and flexible pavement test sections. All construction platform sections in Cell 1S accumulated less than 3 in. (76 mm) of rutting for up to 20,000-wheel passes; while all paved

sections in Cell 1N accumulated less than 0.5 in. (12.5 mm) of rutting after 90,000 passes. Section 3 with 15% plastic fines accumulated the most rutting for both paved and unpaved sections, indicating the detrimental effect of plastic fines on pavement performance.

Chemically stabilized sections in Cells 2 and 3 accumulated relatively low rutting after 135,000 wheel passes at the two load levels. Cement-stabilized test sections outperformed those stabilized with class C fly ash. The measured vertical stresses on top of the subgrade due to the wheel load, recorded for three cement-stabilized test sections in Cells 2 and 3, indicated relatively low subgrade pressures of around 2 psi (14 kPa). These subgrade pressures were considerably lower (3–5 times lower) than those recorded for the conventional flexible pavement test section in Cell 3 (C3S4).

Table 5.2 Summary of Accelerated Pavement Testing Parameters

| **Cell** | **Number of ATLAS passes** Load: 10 kip (44.5 kN) Pressure 110 psi (760 kPa) | **Number of additional ATLAS passes** Load: 14 kip (62.3 kN) Pressure 125 psi (862 kPa) | **Total number of ATLAS passes** |
|---|---|---|---|
| Cell 1 South | 20,000 | - | 20,000 |
| Cell 1 North | 90,000 | - | 90,000 |
| Cell 2 | 100,000 | 35,000 | 135,000 |
| Cell 3 | 100,000 | 35,000 | 135,000 |

The next chapter provides a summary of tests conducted after the APT, and an interpretation of the test section performance trends in light of the different datasets collected during the stages of construction, trafficking, and forensic analysis.

# CHAPTER 6: FULL-SCALE STUDY RESULTS AND INTERPRETATIONS

## 6.1 INTRODUCTION

Chapter 5 presented the results from the accelerated pavement testing for Cells 1S, 1N, 2, and 3; constructed in full-scale to study applications of QB materials in aggregate subgrade, subbase, and base layers. This chapter presents further details from the field testing conducted before/after the APT study, and forensic analysis studies. The overall goal is to provide more detailed data in order to better evaluate the observed performance trends of the various QB applications, and to properly interpret the test results.

## 6.2 PERFORMED FORENSIC ANALYSIS TESTS

This section presents testing that was conducted after APT with the ATLAS to better understand and assess the performance trends of the test sections constructed and tested in the full-scale pavement study. The tests that were conducted are: (1) FWD testing to track changes in deflections before and after testing; (2) HMA coring at the measuring points to obtain accurate wheel path HMA thicknesses for each test section; (3) DCP testing of the aggregate subgrade/subbase/base to assess the strength profiles of the pavement foundation/substructure layers with QB applications; (4) flooded pavement tests for the aggregate subgrade/QB (i.e. PCR/QB) test sections to assess the effect of flooding on FWD deflections; and (5) trenching of the test sections to determine the as-constructed layer thicknesses and assess uniformity of the pavement test section construction. A summary overview of the constructed test sections is shown in Figure 6.1. Detailed discussions on the findings of the conducted tests are presented hereafter in Sections 6.2.1 to 6.2.5.

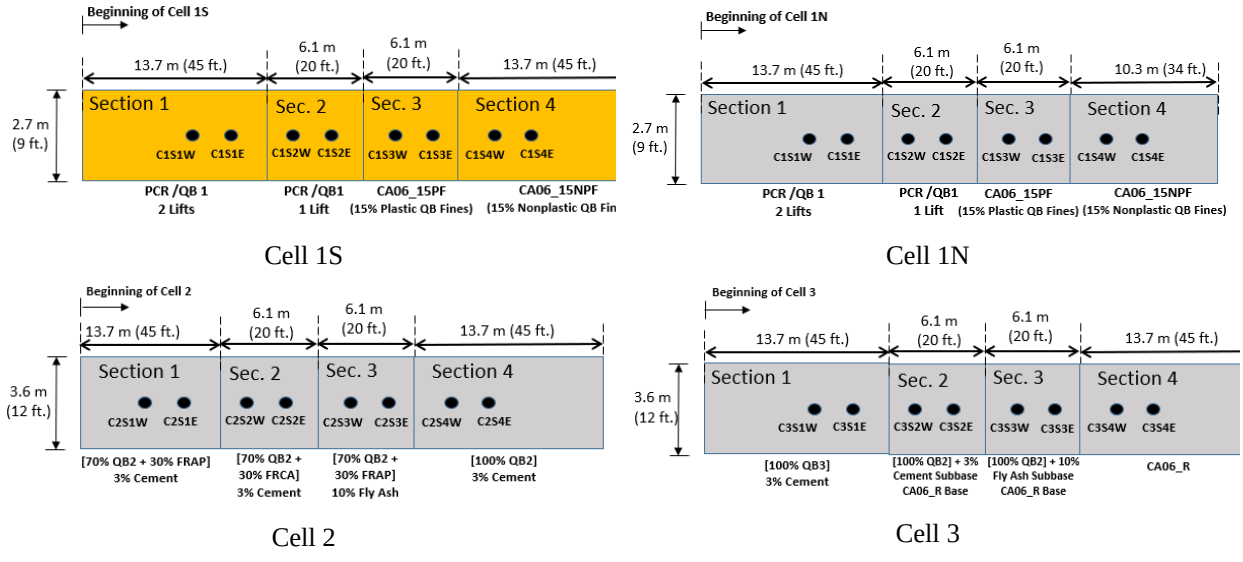


Figure 6.1 Summary overview of the constructed test sections in Cells 1S, 1N, 2, and 3

### 6.2.1 Falling Weight Deflectometer Test Results and Interpretations

Falling Weight Deflectometer (FWD) testing was carried out on all of the construction working platforms and flexible pavement test sections. For Cell 1S construction platform sections, one set of FWD tests was performed for all measuring points in September 2016, before trafficking with the ATLAS. For Cell 1N with flexible pavement test sections, FWD tests were conducted before and after trafficking to compare results. For Cells 2 and 3 studying chemically stabilized applications of QB, three sets of FWD tests were conducted for each measuring point; one after construction and two others before and after trafficking. It was imperative to monitor the curing of the test sections and detect any possible layer material property deteriorations due to freeze-thaw cycles in winter seasons.

FWD tests were conducted by dropping three different load levels at each measuring point to induce variable stress states in pavement layers, and detect the surface deflections from seven geophones that are set 12 in. (305 mm) apart; including a center geophone directly under the load drop location. The complete data covering all deflection basins from the conducted tests are presented in Appendix C, which presents the deflection basins from the three drops normalized to a standard 9-kip (40-kN) equivalent single-axle load, applying a uniform pressure of 80 psi (551 kPa) over a circular area with a radius of 6 in. (152 mm).

Figure 6.2 shows the maximum FWD deflections from the load dropped center geophone ($D_o$) for the test sections in Cell 1S, studying aggregate subgrade construction platform applications of QB. It is notable that the trend for center deflections closely follows the trend of surface rutting progression (see Figure 5.3). For each individual test section, the trends for the progression of rutting and FWD deflections at the two measuring points are matching (i.e. typically greater maximum ruts were accumulated in the wheel path at the measuring point where higher FWD deflections were recorded). Additionally, except for section 3 with the plastic fines CA06 (i.e. CA06_15PF), the trends of FWD deflection and rutting accumulation among the different pavement test sections in Cell 1S are also in agreement.

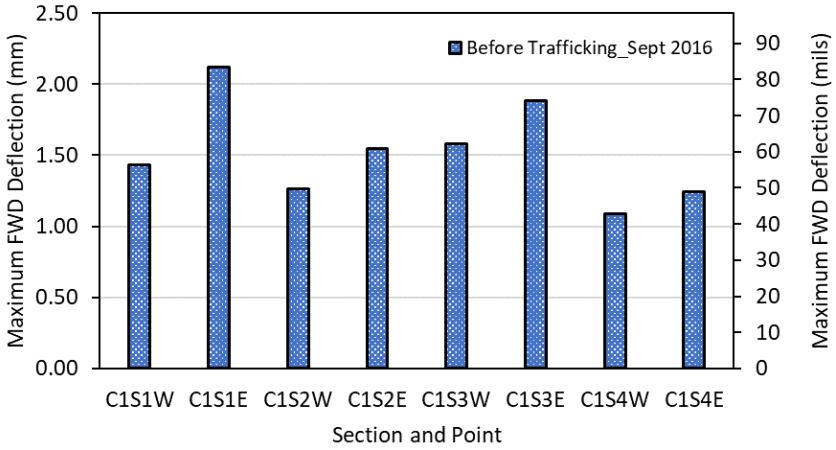


Figure 6.2 Maximum FWD deflections ($D_0$) for Cell 1S test sections (construction platforms)

Figure 6.3 presents the maximum FWD deflections from the center sensor ($D_o$) for the flexible pavement test sections in Cells 1N, 2 and 3. The temperatures indicated in the figure are average HMA surface temperatures measured during FWD testing. Similar to the construction platform test sections, the trends in FWD deflections for Cell 1N test sections closely follow the rutting progression trends for all test sections and all measuring points (see Figure 5.6). For all test sections in Cell 1N, lower FWD deflections were measured after trafficking, likely due to the densification of HMA and aggregate subgrade layers with loading, especially considering that no clear damage (e.g. fatigue cracking) was detected in these test sections.

Figure 6.3 also shows that the lowest FWD deflections measured in Cell 2 were for C2S1 and C2S2, constructed with blends of QB2 and FRAP/FRCA and stabilized with cement. These two sections had the best performance of all test sections, and also had the lowest recorded FWD deflections. The trend of FWD deflections for Cell 2 also closely follows the trend in rutting progression (see Figure 5.7). For Cell 3, the trends of rutting accumulation (see Figure 5.10) and those of FWD deflections again closely match. The highest rut amount and FWD deflections were recorded for Cell 3 Sections 4 and 3, respectively. Note that these two sections had significant changes in FWD deflections for the two sets of FWD tests conducted after construction (September 2016) and before trafficking (May 2017).

Additionally, for Cells 2 and 3, the measured FWD deflections were lower after trafficking when compared to the deflections recorded before trafficking. The exception to this general trend are points in Cell 2 Section 4 and Cell 3 Section 1 having cement-stabilized QB bases, where the FWD deflections were higher after trafficking. One possible explanation is the cracking of the base sections after construction. This is well supported by the higher FWD deflections and the higher LWD deflections that were recorded from the last measurements for these two sections before HMA paving (see Figure 4.14 for backcalculated LWD composite moduli).

### 6.2.2 Hot Mix Asphalt Coring

The HMA pavement surface layers were cored in the center of the ATLAS wheel path to obtain the most accurate HMA thicknesses at the measuring points where the rutting data and other construction quality properties were measured. Additional cores were taken from the north and south sides of the wheel path measuring points. The data for HMA cores at the center of the wheel path are summarized in Figure 6.4. Note that the target HMA thickness was 4 in. (102 mm) for all test sections. As shown in Figure 6.4, the cored HMA thicknesses varied greatly from 2.75 to 4.7 in. (70 to 120 mm) in the different pavement test sections.

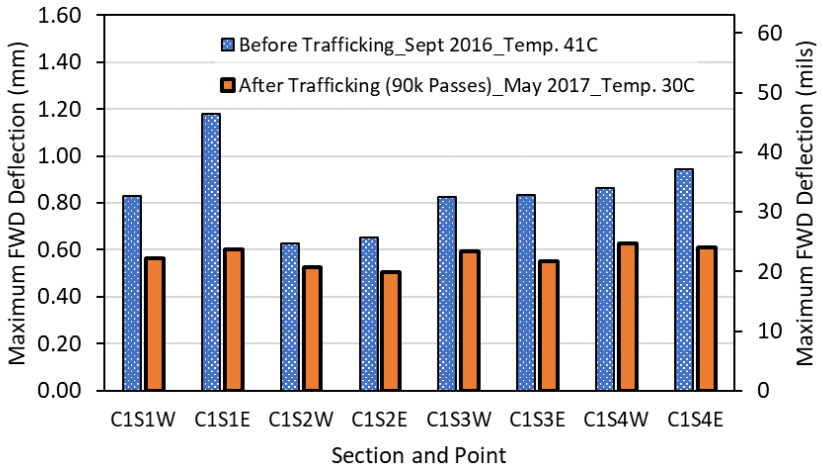


Cell 1N

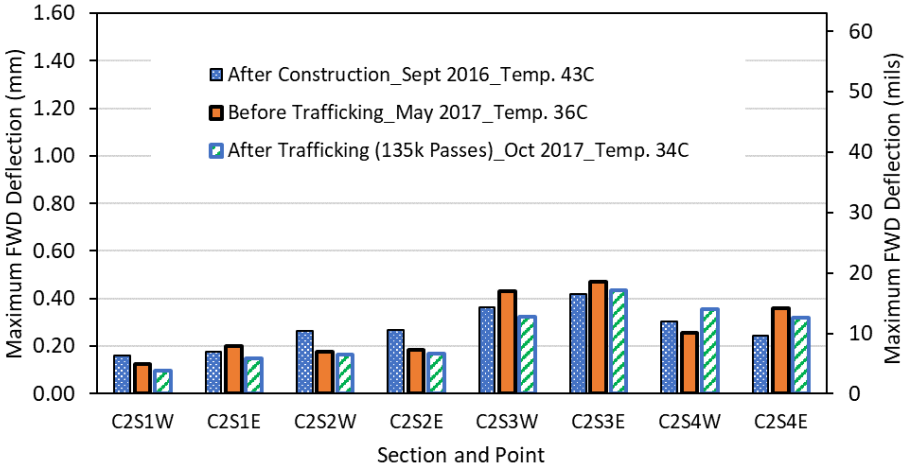


Cell 2

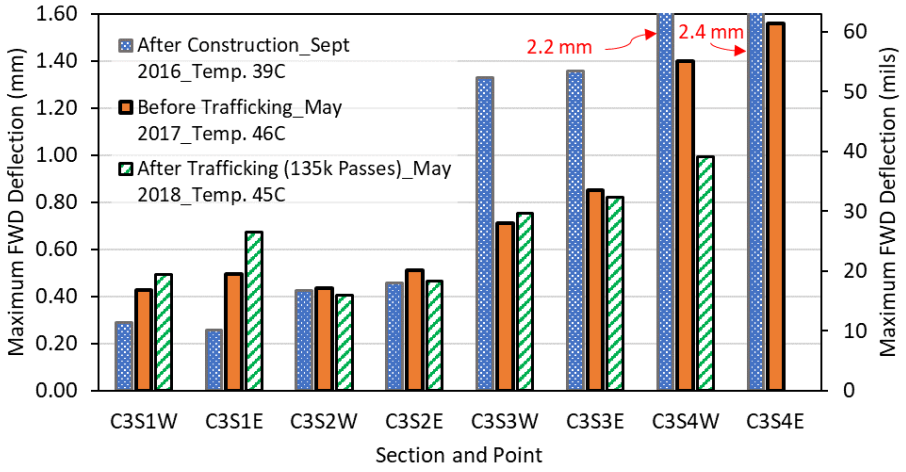


Cell 3

Figure 6.3 Maximum FWD deflections ($D_0$) for Cells 1N, 2, and 3 flexible pavement test sections

Note that the lowest HMA thickness was measured for the C3S4 section with the conventional unbound aggregate CA06_R base course, and the second lowest was measured for the C2S1E with cement-stabilized QB/FRAP, which was the best performing section. The poor performance of the control section (C3S4) can thus be highly attributed to the low HMA thickness and density (see Figure 4.16). The relatively low density allowed high amount of water penetration through the HMA and higher water table; while the low HMA thickness led to premature cracking, thus pumping fines under the ATLAS wheel loading and rapidly increasing damage potential. On the other hand, for sections with chemically stabilized base/subbase applications of QB, particularly the ones stabilized with cement, the sections generally showed good performance despite the variability in HMA thicknesses (in the same section and in different sections). This can be partly attributed to the significantly higher stiffness of the stabilized base materials which better distributes the applied wheel load to protect pavement foundation.

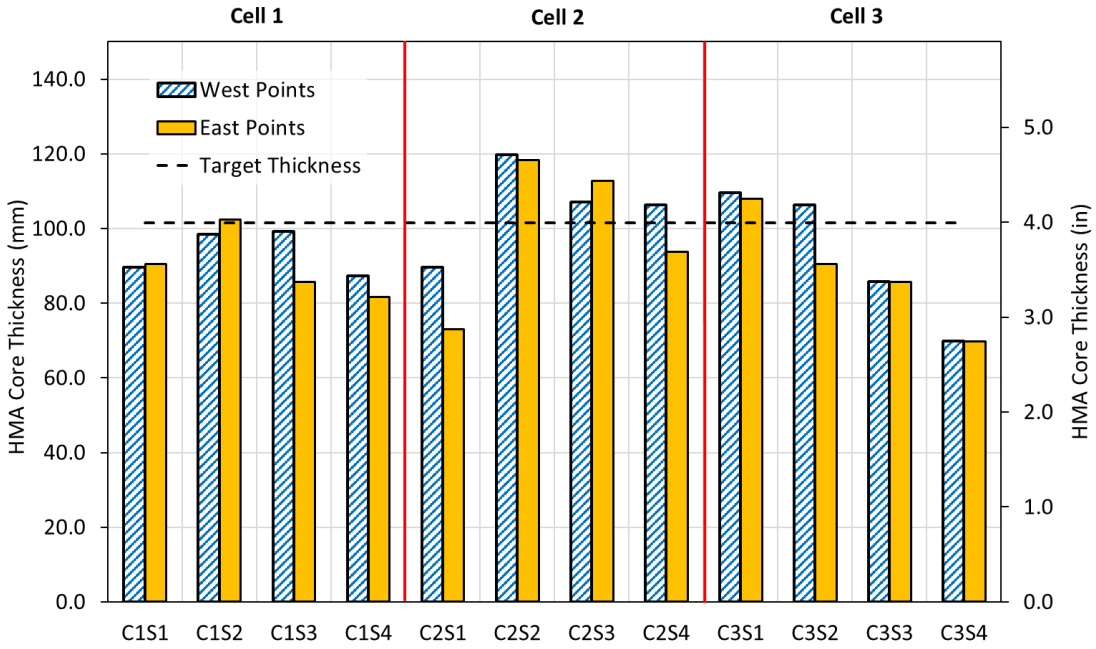


Figure 6.4 HMA core thicknesses of flexible pavement test sections in Cells 1N, 2 and 3

## 6.2.3 Subsurface Layer DCP Profiling

Following HMA coring, DCP testing was conducted into the underlying base and subbase layers of all test sections in Cells 1N, 2, and 3. The DCP tests were conducted directly in the center of the wheel path at the measuring points through the holes of the cored HMA. Note that only one test was conducted in each section at one of the measuring points due to the difficulty and time required for these tests, especially for the stabilized sections where the number of drops to penetrate the full depth was noticeably high [e.g. it took 852 DCP hammer drops for penetrating 12.25 in. (311 mm) into the C2S1 cement-stabilized QB/FRAP blend, i.e. 70 DCP drops per 1 in. (25 mm) of penetration].

All DCP tests were conducted in dry weather conditions after several days/few weeks of no rain. The results for all test sections are summarized in Figure 6.5, which shows the number of DCP drops normalized for 1 in. (25 mm) of penetration. Higher numbers correlate with higher shear strength characteristics of the stiffer subsurface layers since DCP results produce shear strength profiles.

Figure 6.5 also shows the surface rut accumulations after 40,000 ATLAS passes at the measuring points tested with DCP. For Cells 2 and 3 in particular, the strength profiles of the subsurface pavement base/subbase layers were found to correlate well with performance trends, where sections accumulating the least rutting had the highest number of DCP drops per 1 in. (25 mm). In particular, C2S1 and C2S2 with blends of QB with FRAP/FRCA accumulated the least rutting, and had the strongest DCP profiles. The rutting performance trends and DCP profile correlations were less clear for the unbound sections in Cell 1N, which might indicate that the thickness of HMA layers and the relatively weaker aggregate subgrade had greater control on performance, when compared to chemically stabilized test sections.

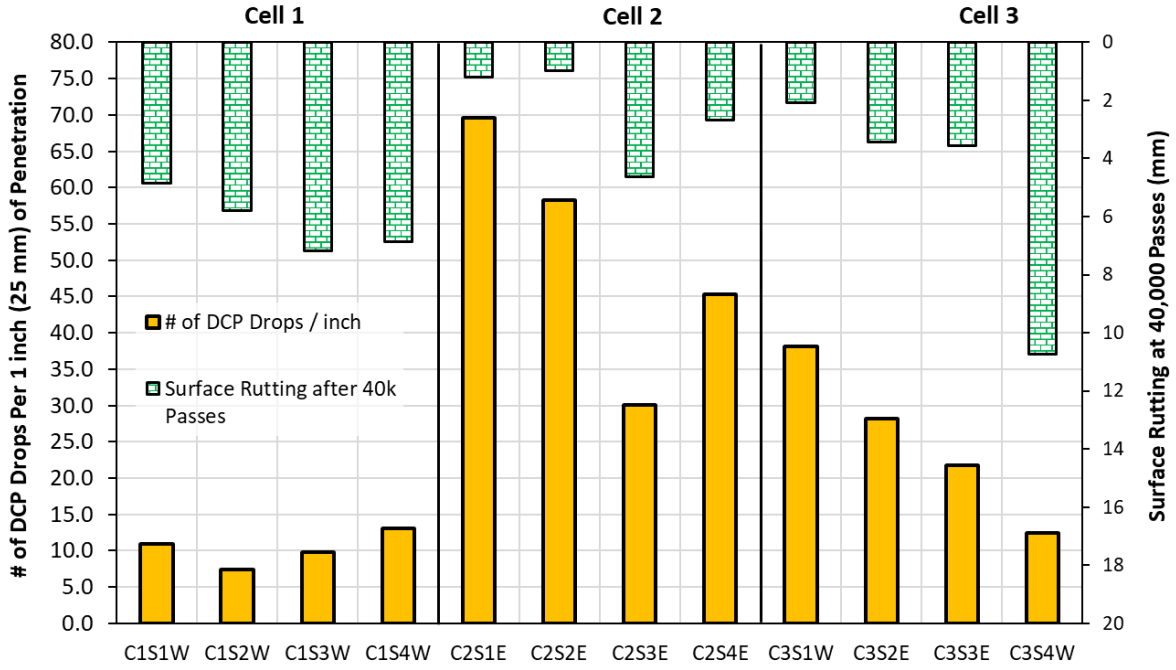


Figure 6.5 DCP penetrations into base, subbase, and subgrade layers in Cells 1N, 2, and 3

## 6.2.4 Flooded Tests for Aggregate Subgrade/QB Test Sections

For the QB applications in Cell 1 that involved using QB as a filler material in the voids of large aggregate subgrade materials (C1S1 and C1S2), an investigation of the effect of moisture on performance was pursued by attempting to flood the aggregate subgrade layers, and study the influence of flooding/saturation on the measured FWD deflections at the same locations before and after flooding. The goal of the flooding study was to evaluate the

saturated worst case scenarios on the retention of QB fines in the voids, and how to achieve stability in the large rock skeleton for the structural carrying ability of the PCR/QB designs.

Raising the water table level was achieved in the flooded test sections of PCR/QB constructed in one lift and two lifts by using hoses to apply water from the surface of the pavements. Simple calculations of the volumes of the constructed test sections and the known flow rate from the hoses indicated that the sections needed one day to flood. The sump pump that was used to store and divert the water from the test sections (see Figure 4.2) was shut off to increase water retention in the sections. The water was applied for ten continuous days, and the highest recorded water elevation was 17.5 in. (445 mm) from the surface, indicating partial flooding of the aggregate subgrade layers in both sections. The water level was monitored by drilling holes in the pavement and monitoring the water level. At the end of the experiment, these holes were used to obtain samples of the subgrade and test them for moisture content, which ranged between 14.4% and 16.8% for the different samples.

The results of FWD deflections before and after this 'partial' flooding of the PCR/QB aggregate subgrade layers in Cell 1N are shown in Figure 6.6, which shows that the center FWD deflections increased only slightly in three of the four locations, particularly for the two locations in section 2 that was constructed in one lift (possibly due to little downward QB migration). Note that the FWD tests before and after flooding were conducted at a similar air and pavement surface temperatures. The little change in the FWD deflections before and after flooding and the inspection of the pavement cross sections after digging trenches in these test sections indicated that a good QB retention in the voids of the large rocks was maintained and the PCR/QB construction technique was successful.

Note that the results shown here are preliminary results since only FWD tests were conducted, and since the test sections were partially flooded. In order to better investigate the effect of flooding on performance, it is recommended to expose these sections to real dynamic loading from heavy moving wheel loads. However, the preliminary results indicate promising results and that the construction method for these test sections was deemed adequate.

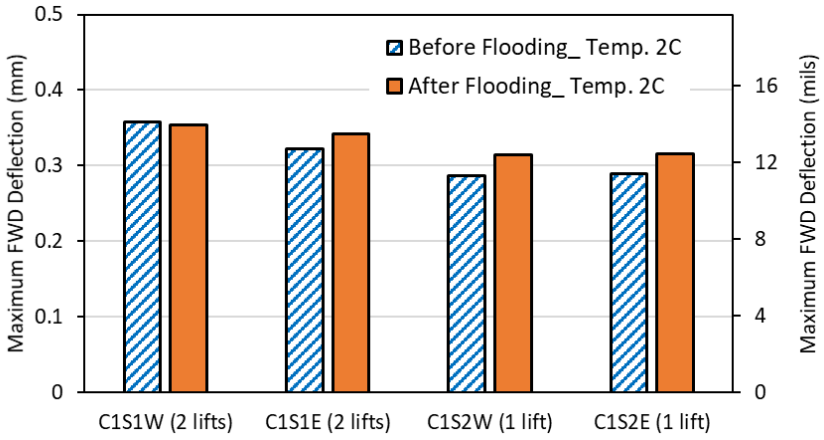


Figure 6.6 Maximum FWD deflections (D0) for Cell 1S aggregate subgrade/QB sections before and after flooding

### 6.2.5 Trenching

After the completion of the field experiment, 5 ft. (1.5 m) wide trenches were excavated along the width of the cross-section for the visual examination of the rutting patterns in all of the construction platform and flexible pavement test sections. The trenches were necessary to measure the actual layer thicknesses for each test section after ATLAS trafficking. The trenches were dug in a manner that the two faces of the trench exposed the cross sections of the West and East measuring points in each test section. The trenches were dug with the backward bucket of a backhoe loader. The chemically stabilized test sections were significantly more difficult to excavate, and it took 6–8 times more time to dig a trench in a stabilized test section.

The photos taken for the cross sections of the full-scale test sections in Cell 1S and Cell 1N are shown in Figure 6.7 and Figure 6.8, respectively. In these figures, the red lines indicate the interface between the engineered in situ subgrade and the constructed aggregate layers. A summary of the constructed thicknesses of all layers is given in Figure 6.9 and Figure 6.10 for Cell 1S and Cell 1N, respectively. For Cell 1 test sections, no subgrade failure was visible in any section. For Cell 1S test sections, which were intended to study construction platform applications of QB, the accumulated surface rut was mostly due to the permanent deformations in the capping layer and the underlying aggregate subgrade materials. For Cell 1N test sections, on the other hand, only little surface rutting was accumulated in general. These little surface ruts appeared to come mostly from the HMA layer with little or no contribution from the underlying capping and aggregate subgrade layers.

The photos taken for the cross sections of full-scale test sections in Cell 2 and Cell 3 are shown in Figure 6.11 and Figure 6.12, respectively. In these figures, the circled materials are large chunks of stabilized layer materials recovered from the trenches. A summary of the constructed thicknesses of all layers is given in Figure 6.13 and Figure 6.14 for Cell 2 and Cell 3, respectively. For both Cells, no subgrade failure was visible in any test section. For the chemically stabilized base course sections in Cell 2, and the first section in Cell 3 (C3S1), the little accumulated rutting was mostly coming from the HMA layer. For the other three sections in Cell 3 having a CA06_R base, the accumulated surface rutting appeared to be due to permanent deformations in both HMA and CA06_R layers.

From the trenching and coring results of Cell 1 test sections, the following observations can be made (see Figure 6.7 through Figure 6.10):

- For sections intended to study applications of QB for filling the voids of large aggregate subgrade materials, a uniform mixing between the PCR and QB was generally observed. QB percolated the full depth of the aggregate subgrade layer in both the one-lift and two-lift construction experiences in this research study. The QB that occupied the voids apparently survived APT loading, flooding and trenching. In particular, trenching photos for C1S1E in Cell 1S showed a crack starting from the surface and extending into mid-depth of the aggregate subgrade layer, possibly indicating an internal shear failure in the aggregate subgrade layer. Additionally, C1S1E in Cell 1N had little QB fines in the voids of the large

aggregate subgrade rocks, and was constructed short on thickness, which justifies the relatively poor performance at this measuring point compared to the other point, C1S1W, in the same section (see Figure 6.8 and Figure 6.10).

- A visual inspection of the trench photos for section C1S4W in Cell 1N, constructed with CA06_15NPF aggregates, indicates that this measuring point possibly had a higher fines content than the desired 15% fines due to materials segregation. This observation possibly explains the higher rutting accumulation at this measuring point despite the proper thicknesses and densities. The higher fines content could be detected by comparing trenching photos with those taken for measuring points C1S4E and C1S4W from Cell 1S, and with C1S4E from Cell 1N, constructed with the same materials.
- Inspection of the trench photos did not indicate a major subgrade failure in any of the test sections. The surface rut accumulations were mostly coming from the HMA layer, and/or the aggregate subgrade and capping layers. Note that no surface cracking was observed at any of Cell 1N test sections.

From the trenching and coring results of Cell 2 and Cell 3 test sections, the following observations can be made (see Figure 6.11 through Figure 6.14):

- Inspection of the trench photos did not indicate a major subgrade failure in any of the test sections, including the control section in Cell 3. The surface rut accumulations were mostly coming from the HMA layer in the chemically stabilized test sections, and the HMA/CA06_R layers in sections C3S2, C3S3, and C3S4 in Cell 3 with a CA06_R unbound conventional aggregate base. The stabilized QB layers had very little rutting. No HMA cracking was observed at any of the chemically stabilized test sections in Cells 2 and 3.

- The constructed layer thicknesses of the stabilized base layers in Cell 2 ranged from 11.3–14 in. (287–356 mm) when compared to the target 12 in. (305 mm). In particular, C2S1E was constructed with the largest base course thickness of 14 in. (356 mm), which counterbalanced the low HMA thickness at this point of 2.9 in. (73 mm). The constructed thicknesses of base or (base + subbase) layers in Cell 3 ranged from 12–13.3 in. (305–337 mm).

- For the cement-stabilized test sections, large blocks of stabilized layers were excavated and recovered during trenching. Some of these are highlighted in Figure 6.11 and Figure 6.12**.**

C1S1W – PCR/QB1 in 2 Lifts

C1S1E – PCR/QB1 in 2 Lifts

C1S2W – PCR/QB1 in 1 Lift

C1S2E – PCR/QB1 in 1 Lift

C1S3W – CA06_15PF

C1S3E – CA06_15PF

C1S4W – CA06_15NPF

C1S4E – CA06_15NPF

Figure 6.7 Trenches exposing the cross sections of test sections in Cell 1S

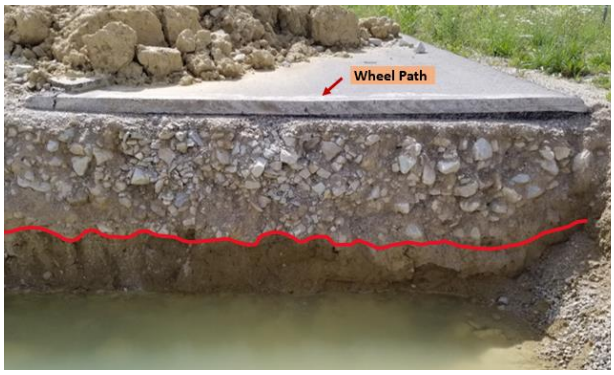


C1S1W – PCR/QB1 in 2 Lifts


C1S1E – PCR/QB1 in 2 Lifts


C1S2W – PCR/QB1 in 1 Lift

C1S2E – PCR/QB1 in 1 Lift

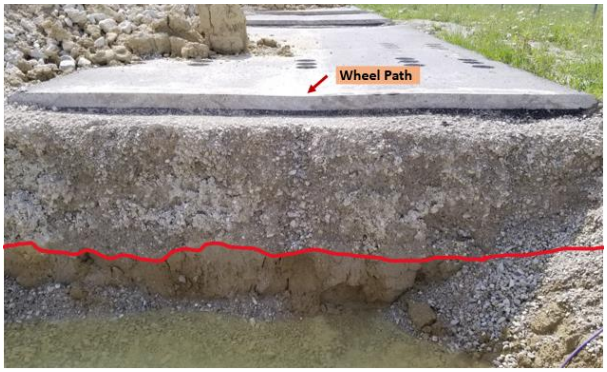


C1S3W – CA06_15PF


C1S3E – CA06_15PF


C1S4W – CA06_15NPF


C1S4E – CA06_15NPF

Figure 6.8 Trenches exposing the cross sections of test sections in Cell 1N

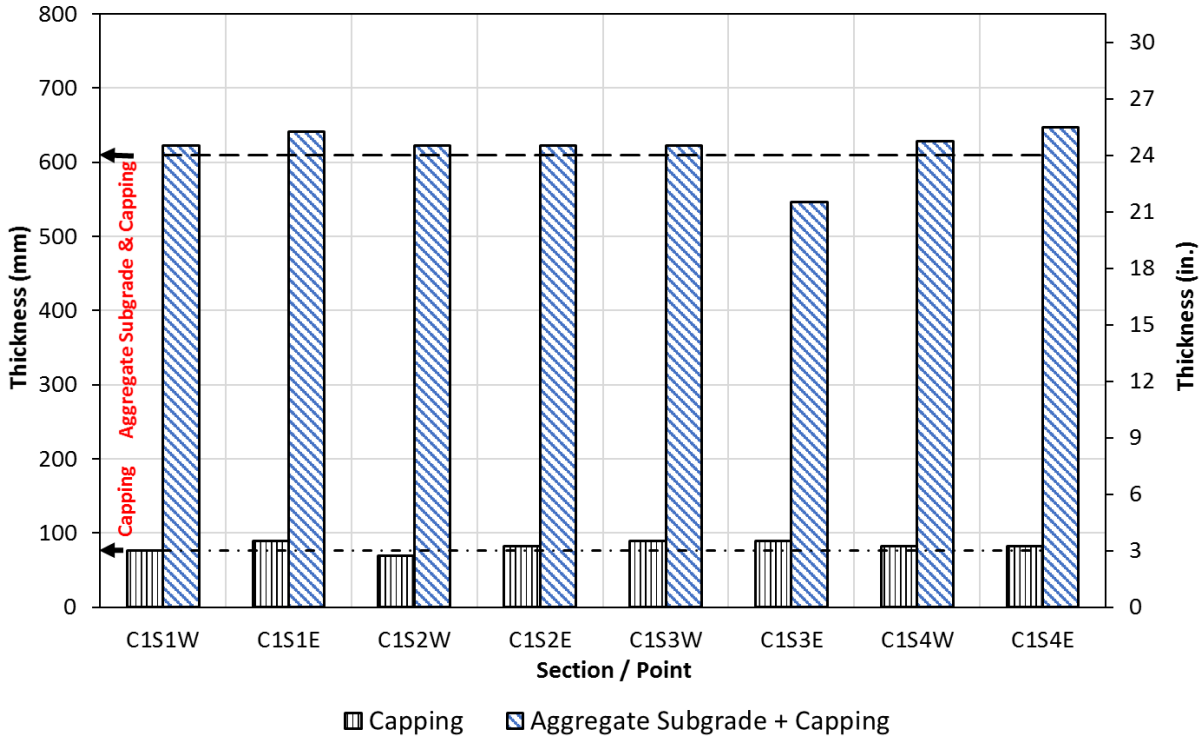


Figure 6.9 Constructed layer thicknesses of Cell 1S test sections

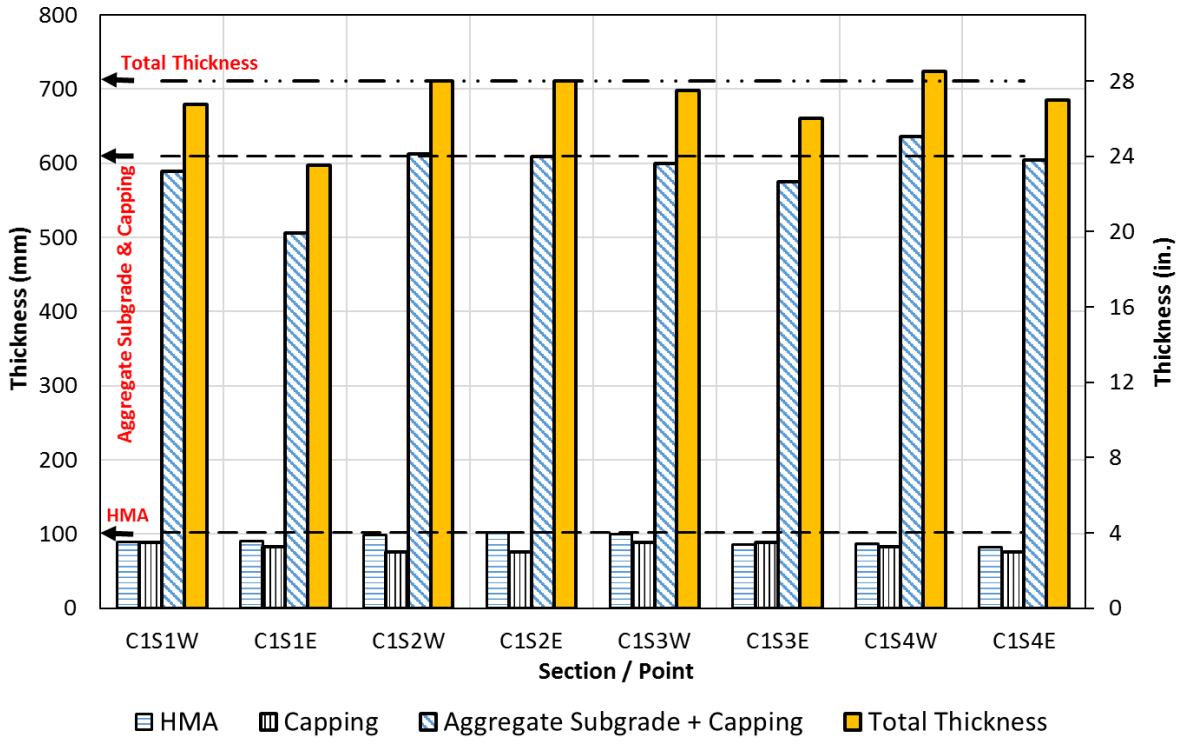


Figure 6.10 Constructed layer thicknesses of Cell 1N test sections


C2S1W – QB2 + FRAP + Cement


C2S1E – QB2 + FRAP + Cement

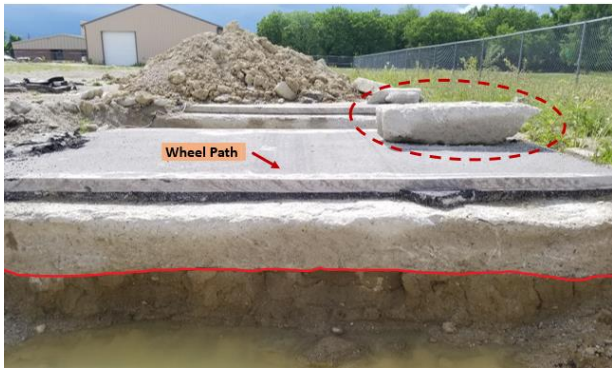


C2S2W – QB2 + FRCA + Cement


C2S2E – QB2 + FRCA + Cement


C2S3W – QB2 + FRAP + Fly Ash


C223E – QB2 + FRAP + Fly Ash


C2S4W – QB2 + Cement


C2S4E – QB2 + Cement

Figure 6.11 Trenches exposing the cross sections of test sections in Cell 2


C3S1W – QB3 + Cement


C3S1E – QB3 + Cement


C3S2W – QB2 + Cement Subbase & CA06_R Base

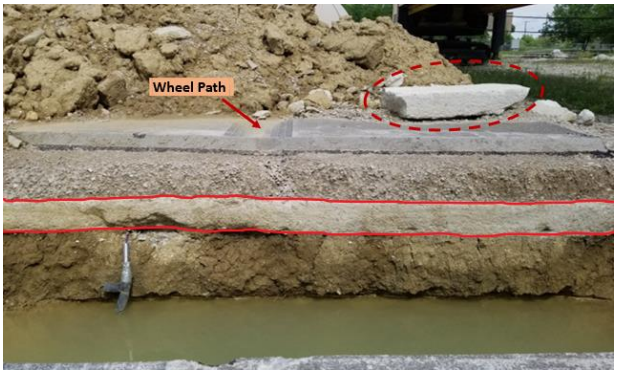


C3S2E – QB2 + Cement Subbase & CA06_R Base


C3S3W – QB2 + Fly Ash Subbase & CA06_R Base

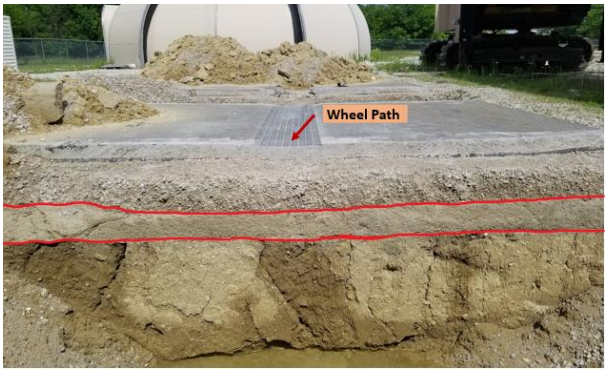


C323E – QB2 + Fly Ash Subbase & CA06_R Base


C3S4W – CA06_R

C3S4E – CA06_R

Figure 6.12 Trenches exposing the cross sections of test sections in Cell 3

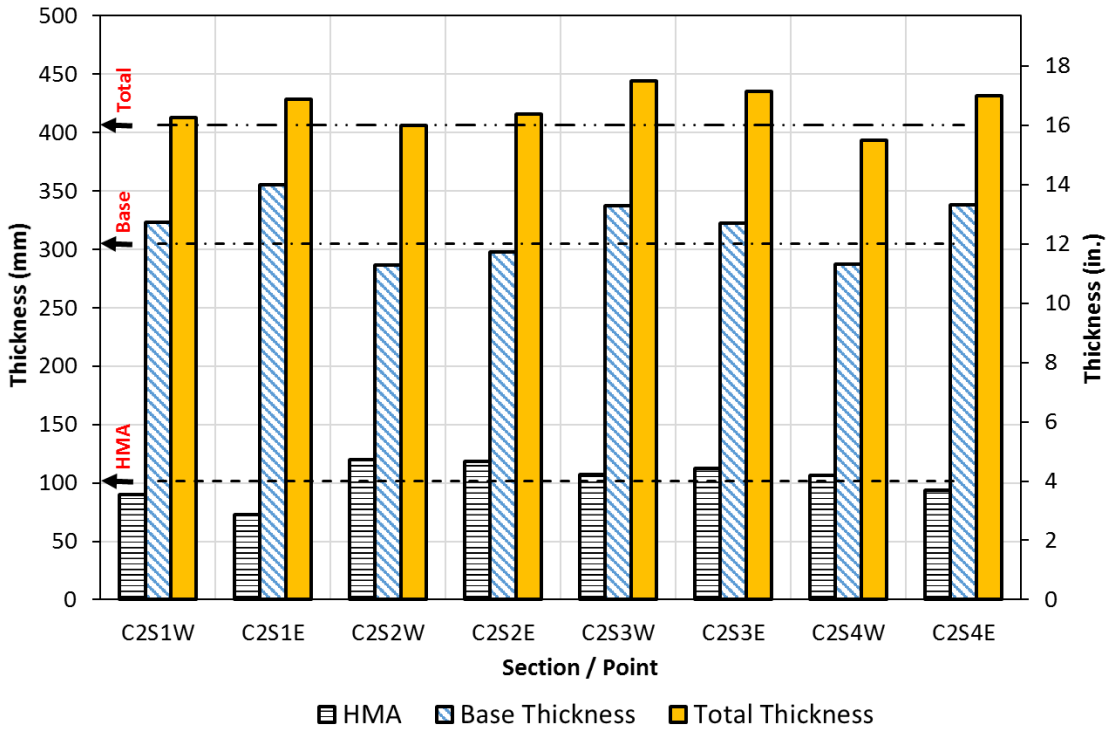


Figure 6.13 As-constructed layer thicknesses of Cell 2 test sections

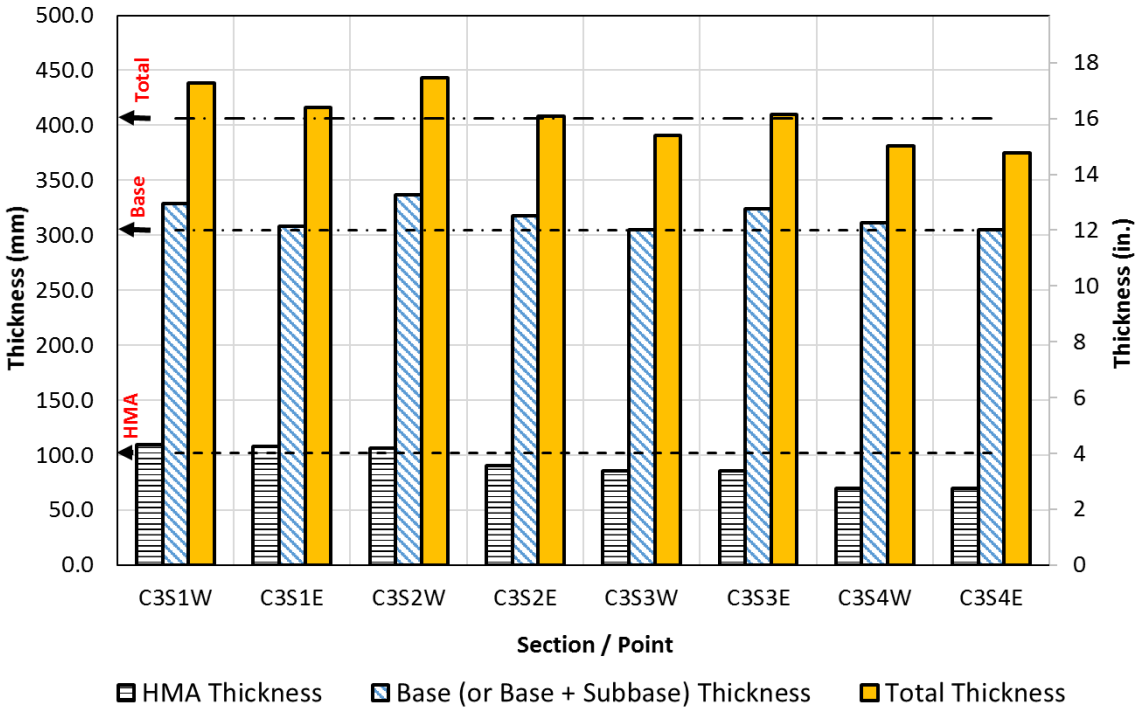


Figure 6.14 As-constructed layer thicknesses of Cell 3 test sections

### 6.2.6 Cube Unconfined Strength Tests for Stabilized Test Sections

Following trenching of the test sections, some of the stabilized materials were recovered in intact pieces that were large enough to extract laboratory samples for Unconfined Compressive Strength (UCS) testing. Earlier on, attempts to extract and test cores of the stabilized base/subbase layers from the wheel path were not successful as the materials eroded with the presence of water from the coring process. In another attempt, a dry coring technique was employed to extract cylinders from the stabilized base and subbase layers for UCS testing. However, the lightly cemented layers eroded under the drilling action, producing fine fragments that clogged the coring bit; creating high friction and preventing the recovery of fully intact cores.

Test cubes, 3 in. (76 mm) in size, were successfully saw-cut in the laboratory from the recovered intact blocks cut using a dry-sawing process. The size of the test cubes were 4 times the nominal maximum aggregate size (NMAS) for the FRAP course aggregate particles used in C2S1 and C2S3 test sections (NMAS of FRAP was 0.75 in. or 19 mm), thus conforming with ASTM recommendations for sample size. For C2S2 with QB/FRCA blends, 95% of the material blend was smaller than ¾ in. (19 mm) in accordance with the combined QB/FRCA gradation.

Three test cubes were prepared and tested for each stabilized test section in Cell 2, as well as for stabilized QB3 base in C3S1 and the stabilized subbase layers in C3S2 and C3S3. Prior to testing, the cubes were capped using a sulfuric compound to ensure more uniform loading distribution, and then tested for unconfined compressive strength at a rate of 0.04 in./minute (1 mm/minute). Figure 6.15 illustrates the procedure for cutting and testing the test cubes, while Figure 6.16 summarizes the UCS results for the different mechanically stabilized QB combinations.

Figure 6.16 compares the achieved field UCS of the tested cubes. Since only three cubes were tested for each test section, which is insufficient for conducting statistical analyses, the minimum, average, and maximum cube strengths are shown. Also shown in Figure 6.16 are the UCS for the laboratory test cylinders, which were previously presented in Figure 3.4. Note that for concrete specimens, it is generally agreed that cube strengths are 18-30% higher than cylinders with a 2:1 aspect ratio of height: diameter (Townsend et al., 1977; Kumavat and Patel, 2014).

On average, the highest UCS was achieved for the QB2 with 3% cement combination (C2S4 and C3S2), which was significantly higher than the USCS for laboratory cylinders, followed by cement-stabilized QB/FRCA and QB/FRAP (C2S2 and C2S1), respectively. The lowest strength was achieved for the fly ash-stabilized QB2/FRAP combination, which was the only combination that achieved a lower average UCS than the laboratory cylinders. Note that the reported strength values for the field cubes can be considered to represent the UCS for the recovered intact blocks. The cubes were visually inspected to ensure no cracks or fractures were visible prior to testing, but the presence of internal cracks resulting from trenching and handling might have contributed to lower strength. Generally, the strength values of these cubes are expected to be on the higher end since they were extracted

from the intact blocks recovered after trenching, while the weaker parts of the stabilized pavement layers would not be found intact.

Saw-cutting cubes for strength testing

Saw-cut cubes from different sections

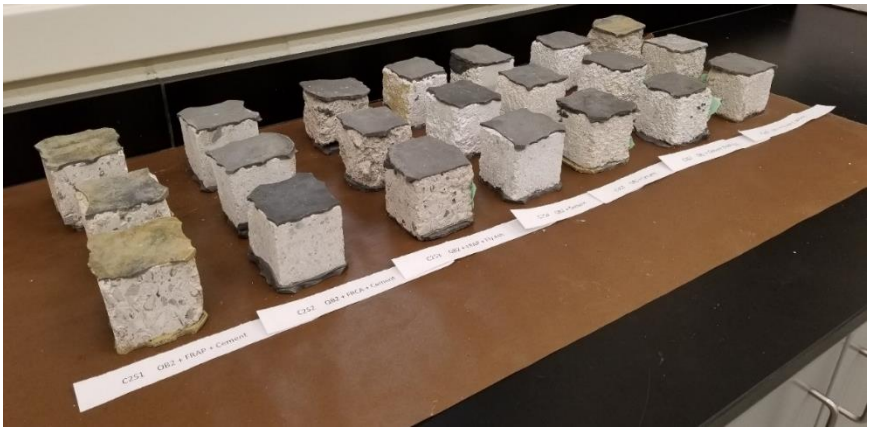

Capped cubes prepared for UCS testing

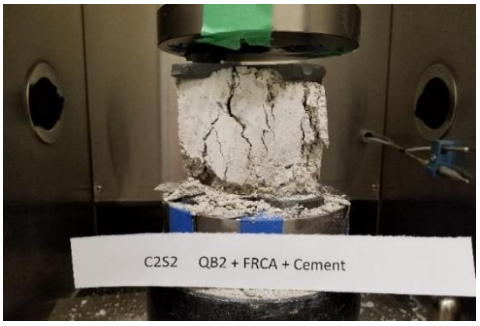


UCS testing of a cube

Strength cubes after UCS testing

Figure 6.15 Preparation and testing of the field cubes

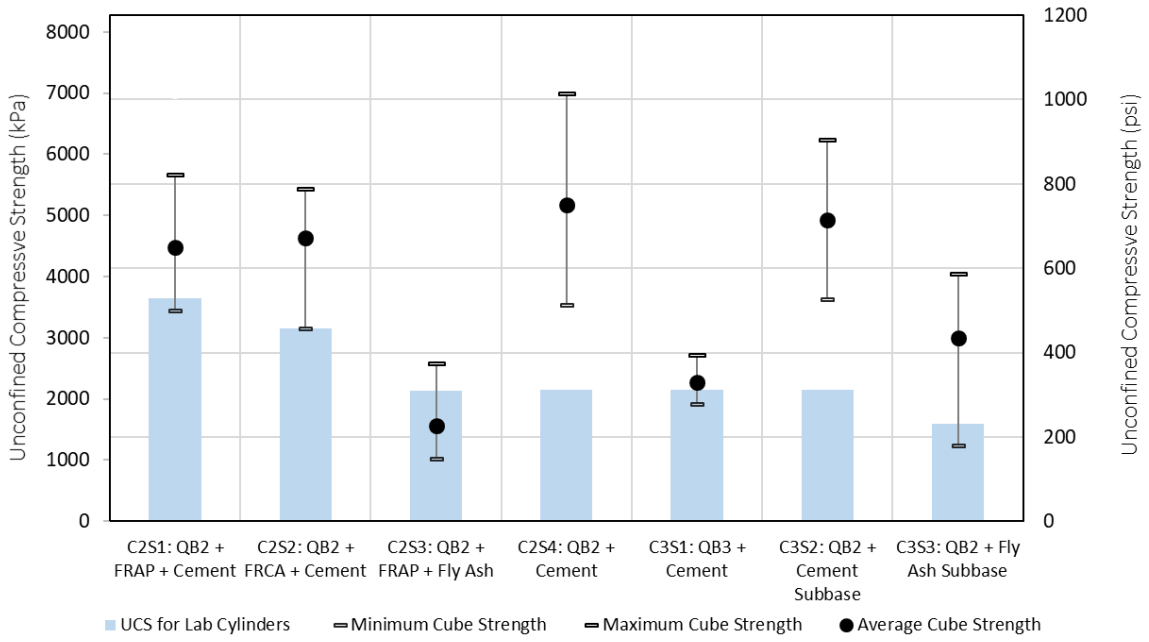


Figure 6.16 Unconfined compressive strength (UCS) values of the cement ad fly ash stabilized QB and aggregate material combinations retrieved from the field test sections

## 6.3 SUMMARY AND INTERPRETATION OF TEST RESULTS

The complete sets of detailed rutting progression results for Cells 1S, 1N, 2, and 3 were presented in Chapter 5 and Appendix B. Comparisons of maximum wheel path rutting progressions of test sections in Cell 2 and Cell 3, intended to study chemically stabilized layer applications of QB, are made in Figure 6.17. Overall, for the stabilized sections, the two sections chemically stabilized with 10% class 'C' fly ash (C2S3 and C3S3) consistently accumulated higher rut amounts and also showed higher rates of rutting progression at the increased load level when compared to the other test sections chemically stabilized with 3% Portland cement. For the two sections, intended to study the effect of QB source, i.e. C2S4 with cement-stabilized QB2 base and C3S1 with cement-stabilized QB3 base, the trends of rutting progression were similar, indicating little effect of the source of QB on performance. Further, satisfactory rut performance was achieved for C3S2 inverted test section with a cement-stabilized QB subbase. The best performances with the lowest rut amounts were obtained for C2S1 and C2S2 having stabilized base courses of the QB blends with FRAP/FRCA, and the highest rutting accumulation was observed for C3S4 with a conventional unbound aggregate (i.e. CA06_R) base.

A comparison of the measured wheel load deviator stresses on top of the subgrade for all the test sections instrumented with soil pressure cells in Cells 2 and 3 is presented in Figure 6.18**.** It shows that the stiffer chemically stabilized test sections (C2S1, C2S4, and C3S2) consistently recorded lower pressure on top of the subgrade when

compared to the C3S4 control section, both at the original and increased ATLAS load levels. Clearly, the stiffer stabilized base materials are changing the mechanism of stress distribution in the pavement structure, allocating a higher share of the load to the stiffer base/subbase layers, and thus reducing subgrade pressures and subgrade rutting potential.

Figure 6.19 compares the wheel path average rutting progressions for C1S1 and C1S2 construction platform test sections built with QB filling the voids of large aggregate subgrade rocks (in 2-lifts and 1-lift, respectively) to the average rutting of a previous study in which a test section was constructed and tested with the same large rocks, same capping materials, same layer thicknesses, as well as a similar subgrade strength of CBR = 1% in the previous R27-124 study (Kazmee and Tutumluer, 2015). This test section was loaded with 4,000 load passes with the same wheel type and load levels as the current study. It can be seen that up to 4,000 passes, the construction platform with 'PCR aggregates only' (i.e. with no QB filling the voids) had accumulated significantly higher rutting levels; indicating that the packing of QB in the voids has indeed increased the stability of the rockfill layers in the current study and reduced their wide variations in rutting performance as reported in the aforementioned study (Kazmee and Tutumluer, 2015).

Measurements of groundwater height were also taken after trenching by inspecting the water table levels in the excavated trenches. The measurements, reported in Figure 6.20, are for water table depths measured from the surface of the HMA after one week of trenching and with no rain event encountered. Note that the highest water table level was measured for the C3S4 control section (43 in. or 1.09 m from the surface of HMA), and the lowest water table level was reported for C1S4 (57.5 in. or 1.46 m). For all pavement test sections, wheel path rutting performance trends and rutting progression with number of passes correlated with the heights of water table levels in the different sections. Note that the water table levels were relatively high in the subgrade, but this level could have been higher during/after rain events when the test sections were trafficked. Additionally, the nature of the silty subgrade soil at the test site could have allowed for significant capillary action of water movement towards the top of the subgrade, which could have resulted in higher moisture content conditions than the constructed near optimum moisture levels in the sections during testing. Therefore, the height of the water table could have influenced performance.

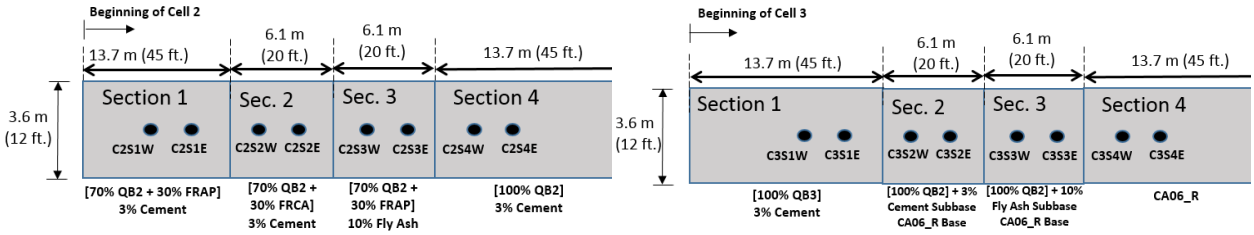


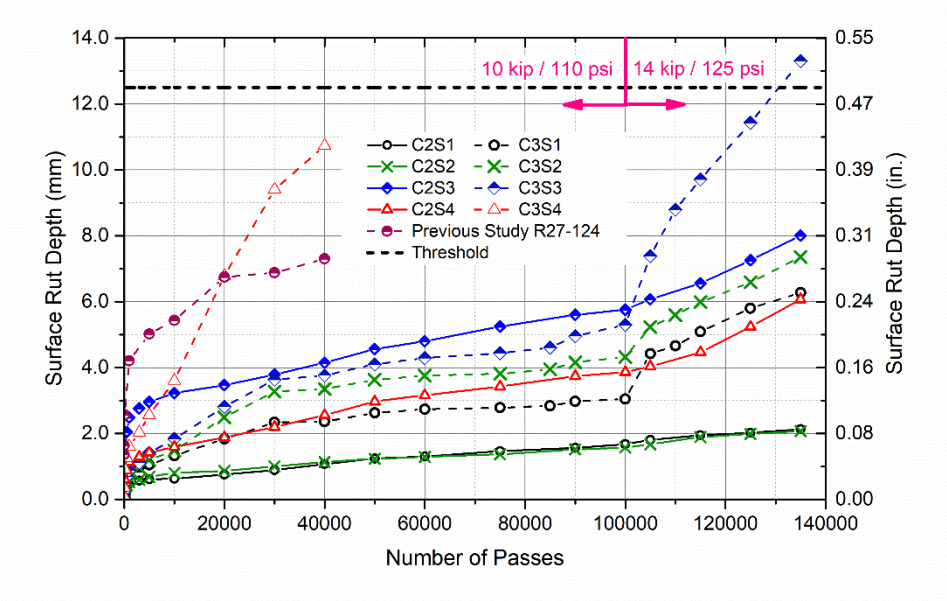


Figure 6.17 Comparisons of maximum wheel path rutting progressions in Cell 2 and Cell 3 test sections

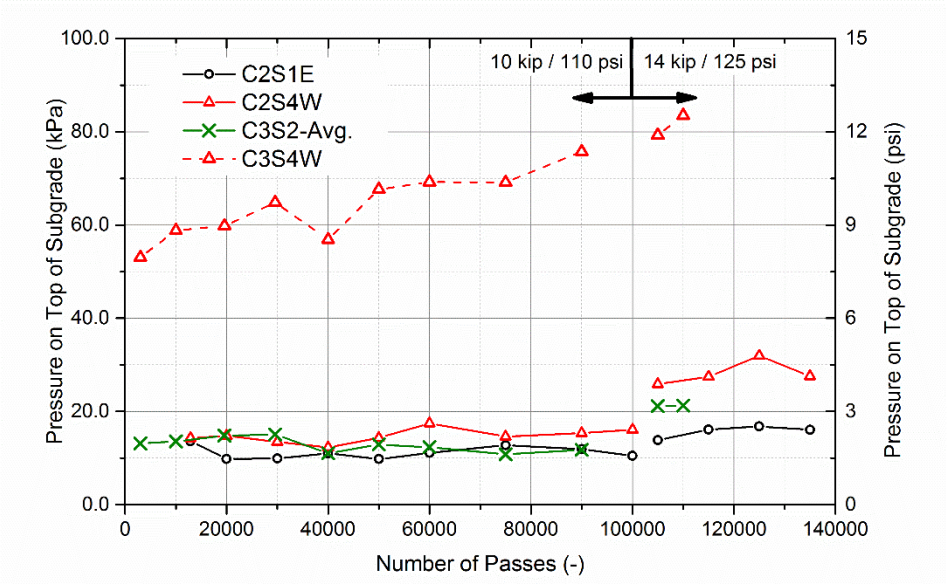


Figure 6.18 Comparisons of measured subgrade pressures in Cell 2 and Cell 3 test sections

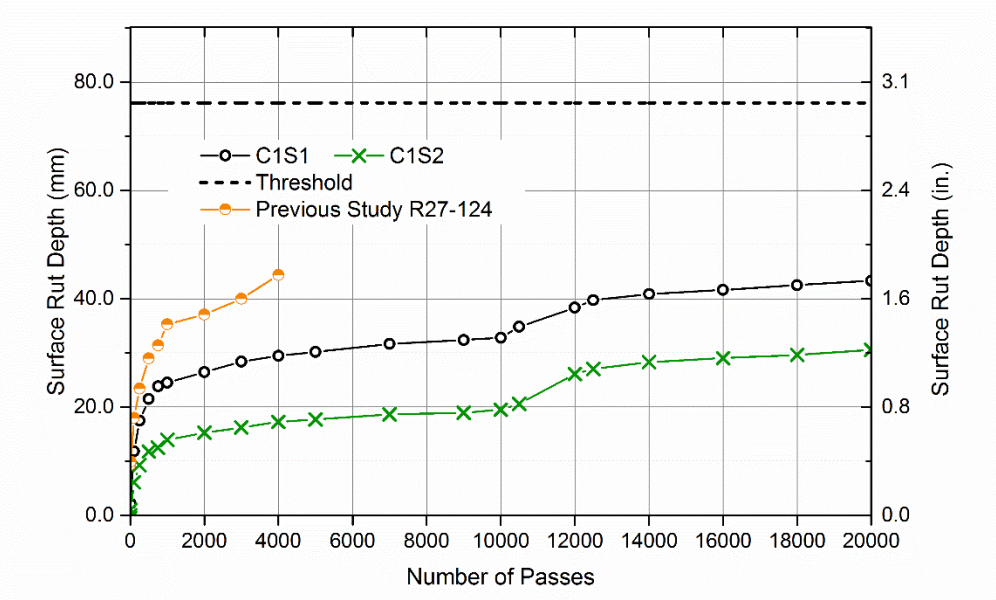


Figure 6.19 Comparisons of wheel path average rutting progressions for aggregate subgrade with and without QB

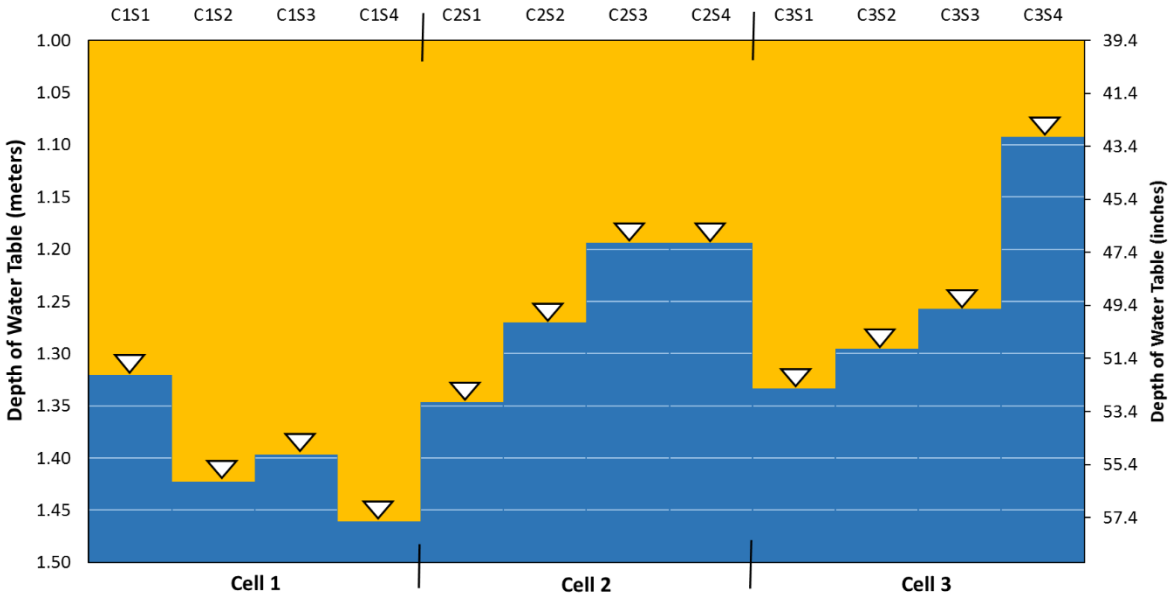


Figure 6.20 Depth of water table levels from the surface for all full-scale pavement test sections

# CHAPTER 7: MECHANISTIC ANALYSES OF PAVEMENT TEST SECTIONS

## 7.1 INTRODUCTION

This chapter presents a modeling study based on Finite Element (FE) analysis to mechanistically evaluate the constructed pavements studying the QB applications discussed in the previous chapters. First, FWD Deflection Basin Parameters (DBPs) are calculated and compared to critical pavement responses to draw conclusions about the structural adequacies of the QB pavement test sections. Then, the moduli of the constructed pavement layers are backcalculated from the FWD deflections using a mechanistic forward calculation analysis approach. The analyses of FWD deflections are achieved by modeling the pavement sections with the QB applications using GT-PAVE axisymmetric FE analysis program. The modulus properties are changed systematically by a trial and error approach to match the surface deflections computed from the model with the measured FWD deflections. For stabilized QB applications, the layer properties calculated from this analysis for the base/subbase layers were further used to calculate the critical pavement responses and the resilient surface deflections for the as-designed and newly proposed pavement structures. Response benefit, defined as the ratio of maximum resilient surface deflection in a conventional pavement section with dense-graded aggregate base to the maximum surface deflection for the section in consideration, was reported for each case as a performance indicator.

In chapter 6, the maximum center deflections were presented for the full suite of FWD tests that were conducted on the pavement test sections at multiple occasions: after construction, and before and after trafficking (see Figure 6.2 and Figure 6.3). For the purposes of the analyses conducted in this chapter, the FWD deflections were collected in September 2016, right after the construction of the pavement test sections and before any trafficking was conducted with ATLAS. Flexible pavement test sections in Cells 1N, 2 and 3 are analyzed in this chapter using a mechanistic analysis approach. The FWD data were collected from all test sections with tests conducted at three load levels: 6000, 9000, and 12,000 lbs. (27, 40 and 53 kN). The pavement surface temperatures ranged from 90 to 113 ºF (32 and 45 ºC) among the different test sections. The FWD data collected at the three load levels were normalized to a 9,000-lb. (40-kN) load level. The full FWD deflection basins are presented in Appendix C - Figure C.2, Figure C.4, and Figure C.7.

## 7.2 FWD DEFLECTION BASIN PARAMETERS

Initially, before the FWD deflections were thoroughly analyzed using a finite element approach, seven of the commonly known and used deflection basin parameters were calculated from the measured FWD deflections for all the studied pavement test sections with different QB applications. The deflection basin parameters were used to assess/compare the overall structural adequacies of the different test sections and draw conclusions about the effects of layer thicknesses and stiffness on pavement responses. For the purpose of these analyses, the innermost geophone

of the FWD equipment located under the load drop location is referred to as $D_0$ (also known as the maximum center deflection), while the other six geophones spaced 12 in. (305 mm) apart are referred to as $D_1$ to $D_6$. This section provides a discussion of the seven deflection basin parameters and a discussion of the measured deflection basins in light of the calculated deflection basin parameters.

The FWD deflections measured for each section from sensors $D_0$ to $D_3$ are plotted in Figure 7.1. These deflection values were averaged for the two measuring points in each section, except for sections C1S1 and C3S4. For these two sections, C1S1W and C3S4W data points only were used due to significant discrepancies in the measured FWD deflections between the two measuring points. For the other sections, the FWD deflections were fairly consistent and similar in magnitudes for the two measuring points, and were thus averaged to be more representative of the test section. Deflections from sensors $D_0$ to $D_3$ are essentially needed for the calculation of the deflection basin parameters and for the forward calculation FE approach used to backcalculate the layer moduli. Deflections measured for sensors $D_4$ to $D_6$ are presented in Appendix C.

From Figure 7.1, the FWD deflections can be sub-grouped into three categories in the order they are presented: Cell 1N test sections, C2S1 to C3S2, and C3S3 and C3S4. For test sections in Cell 1, the measured FWD deflections were in the same order of magnitude, particularly for sensors $D_1$-$D_3$, indicating similarities in the expected modulus values for the aggregate subgrade and engineered subgrade layers. For sections C2S1 - C3S2, the measured FWD deflections were significantly lower than those in the other test sections, largely due to a higher stiffness of the pavement structure due to the chemically stabilized QB subsurface layers. The engineered subgrade stiffness was also likely similar in these sections according to the similar shapes of the deflection basins. For sections C3S3 and C3S4, significantly higher deflections were measured indicating a weaker pavement structure. The higher sensor deflections measured for sensors $D_2$ and $D_3$ were also an indication of a weaker engineered subgrade for these two sections, likely due to the excessive wetting of the subsurface layers due to a more porous HMA layer in C3S4, leading to higher moisture intrusion.

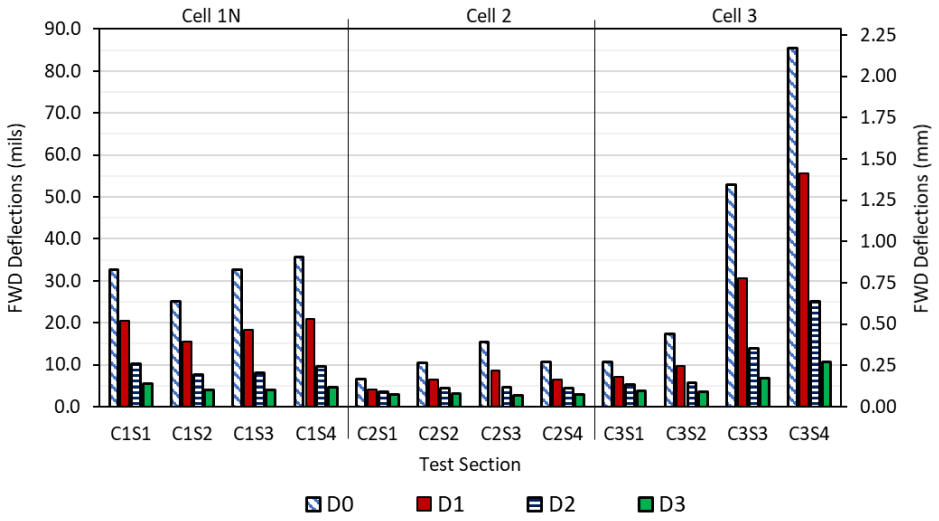


Figure 7.1 Recorded FWD deflections for sensors $D_0$ – $D_3$

Deflection basin parameters are introduced and calculated next. First, parameters that indicate strength properties of individual pavement layers were investigated. These parameters are Surface Curvature Index (SCI), Base Damage Index (BDI), and Base Curvature Index (BCI). The calculated parameters from the averaged and normalized FWD deflections in each test section are shown in Figure 7.2. The definition of each parameter and its unit of measurement are explained in Equations 7.1 to 7.3. SCI is an indication of the stiffness of the upper portion of the pavement structure, particularly the HMA layer. BDI, on the other hand, indicates the strength of the intermediate base/subbase layers, while the BCI is an indication of the stiffness of the lowermost subgrade conditions (Horak, 1987; Hoffman, 1981; Hossain and Zaniewski, 1991; Talvik and Aavik, 2009).

- Surface Curvature Index (SCI), measured in units of mils ($\mu m$), is calculated as the difference between maximum center deflection ($D_0$) and the deflection at 12 in. (305 mm) from the center deflection using the following equation:

$$SCI = D_0 - D_1 \quad \text{(Equation 7.1)}$$

- Base Damage Index (BDI), measured in units of mils ($\mu m$), is calculated as the difference between second deflection sensor ($D_1$) and the third deflection sensor ($D_2$) using the following equation:

$$BDI = D_1 - D_2 \quad \text{(Equation 7.2)}$$

- Base Curvature Index (BCI), measured in units of mils ($\mu m$), is calculated as the difference between the third deflection sensor ($D_2$) and the fourth deflection sensor ($D_3$) using the following equation:

$$BDI = D_2 - D_3 \quad \text{(Equation 7.3)}$$

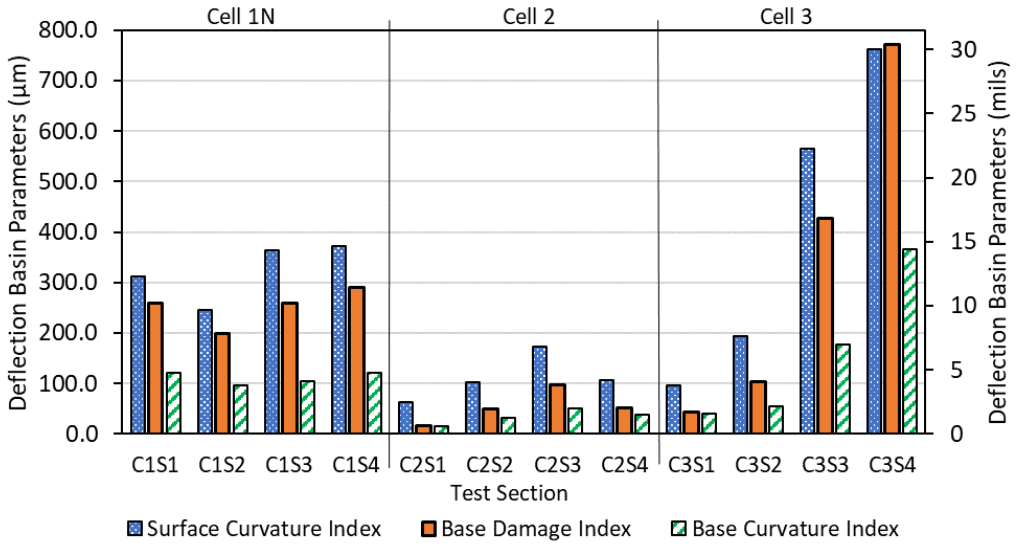


Figure 7.2 FWD deflection basin parameters: SCI, BDI, and BCI

Based on Figure 7.2, the test sections constructed in Cell 1 for investigating unbound QB applications have comparable FWD deflection basin parameters and are thus expected to have similar structural capacities. This was also evident from the field rutting data collected and presented in the previous chapters. For Cell 2 and Cell 3 test sections, it is evident that C3S3 and C3S4 have significantly higher deflection basin parameters and were also the poorest performers. The moisture intrusion from the more porous HMA in C3S4 is evident from the weaker subgrade and base, indicated by the high values of the calculated BDI and BCI. Overall, the trends in calculated FWD deflection basin parameters and backcalculated layer moduli are reasonably correlated and will be given later in this chapter.

Next, the shape factor parameters F1 and F2 were calculated and are shown in Figure 7.3. These parameters identify the relative differences among pavement layer properties (Hoffman, 1980, Hoffman and Thompson, 1981; Hossain and Zaniewski, 1991). The definition of these unitless parameters are given in Equations 7.4 and 7.5. Generally, given similar thicknesses of the pavement structure, a higher value of shape factor F1 is an indication of a lower $E_1/E_2$ ratio; i.e. the ratio of the modulus of the top HMA layer and the underlying layer. Shape factor F2 on the other hand is more sensitive to the thickness of the top layer(s), and its value increases as the thickness decreases.

- The dimensionless shape factor F1 calculates the relative difference between the first and third sensor deflections ($D_0$ and $D_2$, respectively) normalized to the deflection of the second sensor ($D_1$) using the following equation:

$$F1 = \frac{D_0 - D_2}{D_1} \qquad \text{(Equation 7.4)}$$

- The dimensionless shape factor F2 calculates the relative difference between the second and fourth sensor deflections ($D_1$ and $D_3$, respectively) normalized to the deflection of the third sensor ($D_2$) using the following equation:

$$F2 = \frac{D_1 - D_3}{D_2} \qquad \text{(Equation 7.5)}$$

Based on the calculated shape factors shown in Figure 7.3, the following observations can be made. For Cell 1 test sections, the calculated F1 and F2 shape factors were relatively similar for the different test sections. No clear correlations were found between the measured layer thicknesses and the calculated F2 factors. For Cell 2 and Cell 3 test sections having similar design thicknesses, it is evident that sections C3S3 and C3S4 with lower constructed HMA thickness have significantly higher F2 shape factors than the other pavement sections in these Cells. These two sections have a granular unbound base underneath the HMA layer. The lower HMA thickness in C2S1 with a cement-stabilized QB/FRAP blend is not reflected in the low value calculated for the F2 factor, likely due to the underlying stiff base material. Overall, for Cells 2 and 3, the trend in F2 shape factors follow the trend for rut accumulations measured in the field, and lower F2 factors were calculated for sections with lower surface rut

accumulations. The same trend is observed for shape factor F1, but is less evident when different sections are compared.

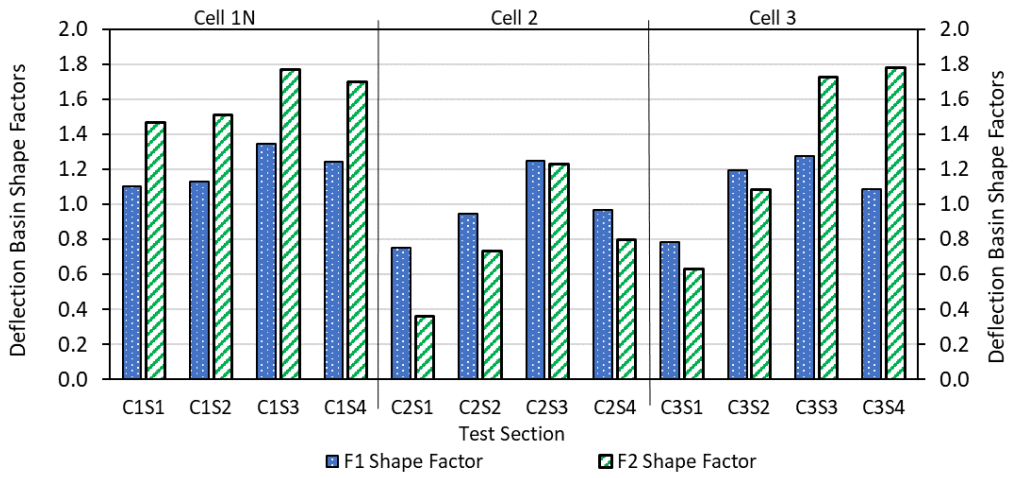


Figure 7.3 FWD deflection basin parameters: shape factors F1 and F2

Finally, the AREA parameter and the Area Under Pavement Profile (AUPP) were calculated according to Equations 7.6 and 7.7:

- AREA parameter, measured in units of inches (mm), calculates the area of deflection basin over a radial distance of 36 in. (914 mm) from the center of the load plate, normalized with respect to $D_0$ sensor deflection. It is calculated using the following equation:

$$AREA = \frac{6[D_0+2D_1+2D_2+D_3]}{D_0} \quad \text{(Equation 7.6)}$$

- Area Under Pavement Profile (AUPP), measured in units of mils ($\mu m$), calculates the area beneath the deflection basin over a radial distance of 36 in. (914 mm) from the center of the load plate.

$$AUPP = \frac{5D_0-2D_1-2D_2-D_3}{2} \quad \text{(Equation 7.7)}$$

The calculated parameters are shown in Figure 7.4. The AREA parameter combines multiple measured deflections into one value and thus minimizes the contribution of malfunctioning sensors, if any (Hoffman, 1980). Higher AREA values generally indicate better structural integrity. From the results shown Figure 7.4, the constructed pavement test sections in all three Cells had similar calculated AREA values. For Cell 2 test sections in particular, the calculated AREA values and the measured surface ruts from field evaluation follow the same trends for all four sections, where sections with higher AREA values accumulated the least rut depths. Note that FWD deflections are resilient, and they relate to pavement responses directly, but do not directly relate to performance trends. In most cases, however, FWD deflections and performance follow similar trends.

The AUPP deflection basin parameter is complementary in definition to the AREA profile, and a lower AUPP is typically indicative of a higher pavement stiffness and better integrity. Based on extensive ILLI-PAVE FE analysis database, the AUPP was correlated to the magnitude of the horizontal tensile strain at the bottom of the AC layer ($\varepsilon_{AC}$), and good correlations were achieved for conventional and full-depth asphalt pavements (Hill and Thompson, 1988; Gopalakrishnan et al., 2010). From Figure 7.4, it can be concluded that the computed AUPP values follow the trends of surface rut accumulations, particularly for the chemically stabilized pavement sections in Cells 2 and 3. Out of all deflection basin parameters considered in this section, AUPP is in fact the deflection basin parameter that correlated the most with the field measured data.

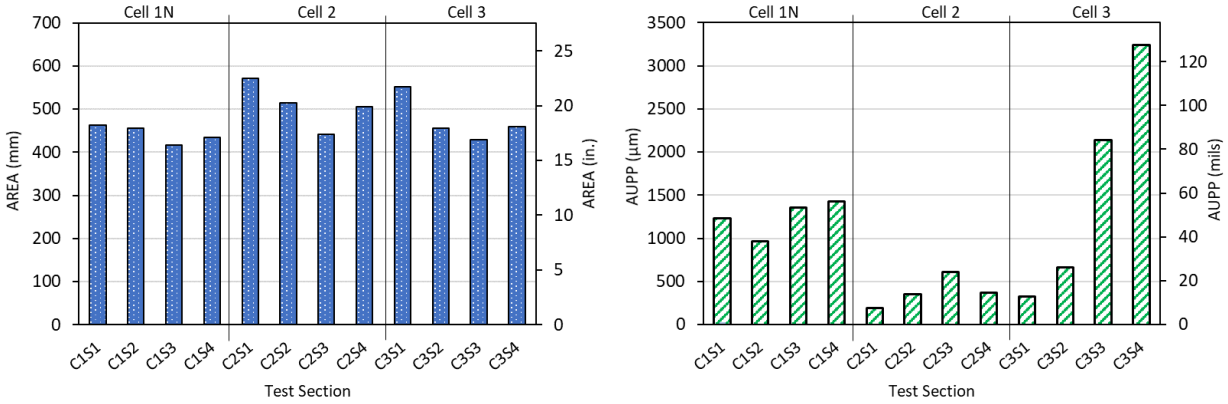


Figure 7.4 FWD deflection basin parameters: AREA parameter and AUPP

## 7.3 MECHANISTIC ANALYSES OF FWD RESPONSES

This section presents a mechanistic forward calculation approach that was adopted to analyze the FWD deflections collected for the QB field applications. First, a discussion about the available methods for the analyses of FWD results is presented. Advantages and limitations of each method are highlighted. Next, the mechanistic approach used to analyze FWD results is introduced. Background information about GT-PAVE program capabilities and limitations are first discussed, followed by the framework used to model the field pavement structures, including the assignment of material properties, selection of domain size and mesh configuration, analysis scheme, and other specific model details. Finally, the results of the forward calculations of layer moduli from collected FWD data are presented.

### 7.3.1 Existing Analysis Techniques for FWD Data

The analyses and interpretations of FWD data can be divided into two broad approaches: (1) Forward analysis methods, which are methods that calculate pavement responses, and (2) backcalculation methods, which are methods that predict pavement responses (Smith et al., 2017). This subsection presents a discussion of the available static and dynamic backcalculation and forward analysis techniques for FWD data, along with some of the most commonly used analysis programs and their features.

#### 7.3.1.1 Backcalculation techniques for FWD data

Tutumluer and Sarker (2015) presented a classification of backcalculation analysis approaches into three categories: (1) simplified methods, (2) direct interpolation methods, and (3) gradient-relaxation methods. Both simplified and direct interpolation methods can be tricky and are thus less commonly used since numerous local minimum solutions might require a global optimization to be conducted. Gradient-relaxation methods are among the most common backcalculation methods adopted by many FWD backcalculation software programs. With this method, mathematical models and nonlinear algorithms are employed to describe the pavement condition. Seed moduli values are assigned to the different pavement layers to start the backcalculation algorithm and finally predict the layer moduli that closely match the experimental data from FWD testing. This method produces accurate results given the algorithm is well designed and the right assumptions are made about the layer thicknesses, materials homogeneity and other pavement properties (Tutumluer and Sarker, 2015).

The most commonly used FWD backcalculation software programs and the features of these programs are presented in Table 7.1. MODULUS, EVERCALC, and ELMOD are among the most commonly used FWD backcalculation software. Note that the majority of these programs use linear elastic approaches for solutions, and do not account for the nonlinearity and stress-dependency of granular materials and fine-grained subgrade soils. Other advanced (and nontraditional) backcalculation techniques for the analyses of FWD results also exist. Such methods include linear regression methods, Artificial Neural Networks (ANN), and Generic Algorithms (GAs). These methods provide quick and stochastic method for analyzing FWD results (Ceylan et al., 2005; Pekcan et al., 2006; Tutumluer and Sarker, 2015). Other methods include dynamic backcalculation methods that use forward solutions based on dynamic, damped elastic finite element methods. Such methods calculate steady state deflection basins at multiple frequencies and match them to the experimental data. They include time and frequency domain methods, and are computationally more expensive (Uzan, 1994; Smith et al., 2017; Kazmee, 2018).

#### 7.3.1.2 Forward calculation techniques for FWD data

Forward calculation methods for FWD are methods that calculate pavement responses. Such methods include: (1) closed-form solutions based on Boussinesq's original half-space solution, (2) multi-layered elastic solutions based on Burmister's original two- and three-layer solutions, and (3) finite element solutions (Smith et al.,

2017). Other forward analysis methods include probabilistic analysis methods and discrete element models (Kazmee, 2018). Some of the commonly used forward analysis computer programs for flexible pavement analysis along with their features are presented in Table 7.2.

Layered elastic methods are the most commonly used, and the solutions are deemed accurate as long as the materials remain in the linear elastic range. Some of the limitations of layered elastic analysis include considering layers as homogeneous, isotropic, and linear elastic as well as using a circular area to distribute the load uniformly. Some layered elastic programs such as NELAPAV allow nonlinear responses, while others such as KENPAVE allow viscoelastic responses (Smith et al., 2017). Closed form solutions, on the other hand, are simple, fast, and reliable. The most useful closed form solution is the Method of Equivalent Thickness (MET) solution, which transfers the layered system into an equivalent single layer that satisfies Odemark transformation equation (Ullidtz, 1987; Smith et al., 2017).

Finite element solutions have an advantage over the linear elastic and closed-form solutions in their ability to consider nonlinearity, cross-anisotropy, stress dependency, and more sophisticated constitutive models. These solutions can be computationally more expensive depending on the number of elements and input parameters. Many FEM programs have been developed for pavement-specific purposes. Forward analysis finite element programs include two-dimensional axisymmetric programs such ILLIPAVE, MICHPAVE, GT-PAVE (Elliott and Thompson, 1985; Tutumluer, 1995; Smith et al., 2017), and three-dimensional programs such as CAPA-3D (Smith et al., 2017). Other general purpose finite element programs such as SAP®, ABAQUS®, and ANSYS® have been also employed for the forward analysis of pavement structures (Kim, 2007; Smith et al., 2017). For the purpose of this dissertation, a finite element-based forward analysis method will be employed to analyze FWD results using GT-PAVE FEM program, developed at Georgia Institute of Technology by Tutumluer (1995).

Table 7.1 Features of the most commonly used FWD backcalculation programs (Tutumluer and Sarker, 2015)

| **Software Program** | **Forward Calculation Routine** | **Convergence Rule** | **Backcalculation Approach** |
|---|---|---|---|
| MODULUS (Scullion et al. 1990) | Linear elastic approach, WESLEA | Root mean squared (RMS) error | Minimize the difference between the predicted and the measured basin by adjusting the modulus of the various layers through searching a database |
| MICHBACK (Harichandran et al. 1993) | Linear elastic approach, CHEVRON | Root mean squared (RMS) error | Minimize the difference between the predicted and the measured basin by adjusting the modulus of the various layers through a number of iterations |
| MODCOMP (Irwin 2001) | Linear elastic approach, CHEVRON | | |
| ELMOD | Odemark equivalent thickness approach | | |
| EVERCALC (Sivaneswaran et al. 1991) | Linear elastic approach, WESLEA | | |
| WESDEF (Van Cauwelaert et al.1989) | Linear elastic approach, WESLEA | | |

Table 7.2 Features of the most commonly used FWD forward analysis programs (Smith et al., 2017)

| **Software Name** | **Method Used in Response Model** | Type* | Nonlinearity | Rheology | Anisotropy | Interface | Climate Effects | Dynamic Loading | Axle Spectrum | Tire Characteristics | Stochastic | Crack Propagation | Thermal Effects | Cumulated Damage | Fatigue | Permanent Deformation |
|---|---|---|---|---|---|---|---|---|---|---|---|---|---|---|---|---|
| APAS-WIN | Multilayer | 3 | — | — | — | — | Y | — | Y | Y | — | — | Y | — | Y | — |
| AXYDIN | Axi-symmetric FEM | 1 | — | — | — | — | — | Y | — | — | — | — | — | — | — | — |
| BISAR/SPDM | Multilayer | 3 | — | — | — | Y | Y | — | Y | — | — | — | — | — | Y | Y |
| CIRCLY | Multilayer | 3 | — | — | Y | Y | — | — | Y | Y | — | — | — | Y | Y | — |
| CAPA-3D | 3D-FEM | 3 | Y | Y | Y | Y | — | Y | — | Y | — | Y | Y | Y | Y | Y |
| CESAR | 3D-FEM | 3 | Y | Y | Y | Y | Y | Y | — | Y | Y | Y | — | Y | Y | Y |
| ECOROUTE | Multilayer | 1 | — | — | — | Y | — | — | — | Y | — | — | — | Y | — | — |
| ELSYM 5 | Multilayer | 1 | — | — | — | — | — | — | — | — | — | — | — | — | — | — |
| KENLAYER | Multilayer | 2 | Y | Y | — | Y | — | Y | — | Y | — | — | — | Y | Y | Y |
| MICHPAVE | Axi-symmetric FEM | 1 | Y | — | — | — | — | — | — | — | — | — | — | — | Y | — |
| MMOPP | Multilayer | 2 | Y | — | — | — | Y | Y | Y | Y | Y | Y | — | Y | Y | Y |
| NOAH | Multilayer | 3 | — | — | Y | Y | Y | Y | Y | — | — | — | Y | Y | | |
| ROADENT/ WESLEA | Multilayer | 2 | — | — | — | Y | Y | — | Y | Y | — | — | — | — | — | — |
| SYSTUS | 3D-FEM | 2 | Y | Y | Y | Y | — | Y | — | Y | — | Y | — | — | — | — |
| VAGDIM 95 | Multilayer | 3 | — | — | — | — | Y | — | — | — | — | — | Y | Y | Y | Y |
| VEROAD | Multilayer | 1 | — | Y | — | — | — | — | Y | Y | Y | — | — | — | — | — |
| VESYS | Multilayer | 3 | — | — | — | — | Y | — | Y | Y | Y | — | — | Y | Y | Y |

* Type: 1 = Response only, 2 = Response + Partial Performance, and 3 = Full Design Procedure

### 7.3.2 Background: GT-PAVE Program

GT-PAVE is a nonlinear axisymmetric Finite Element (FE) program that was developed by Tutumluer (1995) at Georgia Institute of Technology. The program uses axisymmetric, isoparametric eight node quadrilateral elements for the continuum representation of flexible pavement structures and unsurfaced roads. The GT-PAVE was developed for an accurate modeling of the nonlinearity and cross-anisotropic behavior of pavement geomaterials, i.e. unbound aggregate layers and subgrade soils. Essential features of GT-PAVE include considerations for nonlinear analysis, residual compaction stresses, pre- and post-processing, incremental loading, and horizontal tension corrections in the unbound aggregate base (Tutumluer, 1995). The program is capable of eliminating horizontal tension in unbound granular base layers through the use of a stress transfer approach.

Wheel loading is applied in GT-PAVE as a uniformly distributed line load in global coordinates. Both material properties and boundary conditions are independent of the rotation angle. The software is capable of considering several types of loads including gravity forces, initial residual stresses, nodal concentrated loads, temperature loads, and uniformly distributed edge loads. The nonlinear analysis procedure used in GT-PAVE accommodate a direct secant stiffness approach using a damping factor to calculate a new resilient modulus from the calculated stress states for each load increment by an iterative procedure (Tutumluer, 1995). Further, GT-PAVE was verified by solving several pavement problems involving linear and nonlinear analysis, and comparing the solutions to closed form solutions and laboratory results. Over the past two decades, the GT-PAVE program has been validated in several research studies that measured pavement responses from full-scale pavement sections and also compared solutions with three-dimensional finite element analysis results using commercially available software (Tutumluer and Thompson 1997; Kim et al. 2009; Kwon et al. 2009; Kazmee, 2018).

### 7.3.3 Domain Size Selection

The GT-PAVE axisymmetric FE program was first used to investigate an appropriate size of the FE model to minimize the influence of boundary effects. The domain size must be several multiples of the radius of the loaded area (R) in order to calculate accurate responses and eliminate boundary effects. The main studies found in literature, particularly those that utilized GT-PAVE analysis program, are discussed here:

- A study by Duncan et al. (1968) advised that the fixed boundaries at the bottom of the FE model had to be at least 50 times the radius of the loaded area (R), while the roller boundaries at the sides of the model required to be at least 12 times the radius of the loaded area, measured from the center of the load.
- Kazmee (2018) modeled full-scale flexible pavement test sections using the GT-PAVE program, and used a domain size of 12R (Horizontal) by 54R (vertical) to analyze FWD results. The domain size was chosen considering the dimensions of the full-scale test sections, which were 15 ft. (4.6 m) long and 9 ft. (2.7 m) wide.
- Mishra (2012) used the GT-PAVE FE program with a 33R by 66R domain size to design the thicknesses of unpaved construction working platform test sections using cross-anisotropic unbound aggregate material properties. The size and configuration of the mesh were deemed appropriate for considering boundary conditions and minimizing the effects of boundary truncation.
- Xiao and Tutumluer (2012) modeled flexible pavement test sections using the GT-PAVE program to characterize unbound aggregate base and granular subbase layers as nonlinear and stress dependent with the Uzan (1985) resilient modulus model. Their mesh consisted of 780 isoparametric eight-node quadrilateral elements and had a domain size of 27R in the horizontal direction. The domain size in the vertical direction varied based on the thicknesses of the engineered subgrade, subbase, base, and HMA layers. A domain size larger than 140R in the vertical direction was used for all 2,592 analyses.

- Kim (2007) and Kim et al. (2009) reported that the effects of boundary truncation became negligible when a domain size greater than 150R was utilized in the vertical direction. Kim et al. (2009) also compared results from analytical solutions using KENLAYER linear elastic layered program and finite element solutions using GT-PAVE axisymmetric software, and concluded that accurate responses could be measured when a domain size of 20 R in the horizontal direction and 140 R in the vertical direction was used. Eight-node isoparametric quadrilateral elements were used in the FE analyses. The effect of the domain size in the horizontal direction on the calculated surface deflections is shown in Figure 7.5, which shows that stable results were obtained for a domain size exceeding 20R.

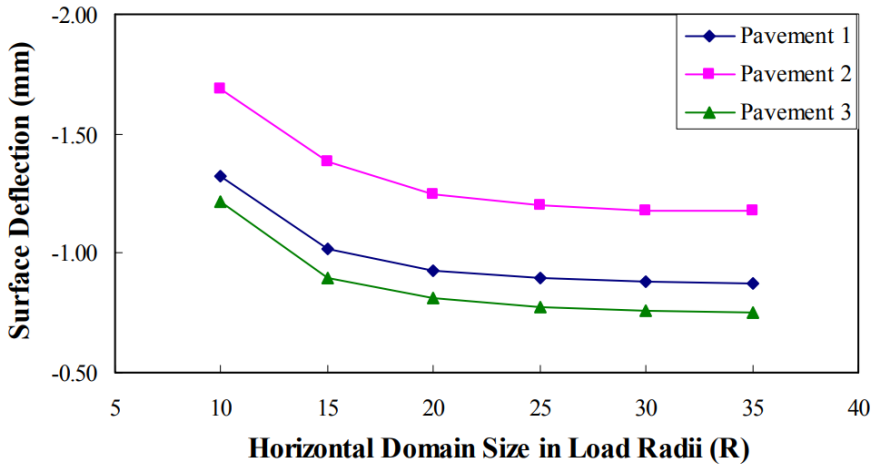


| | Pavement Case 1 | | Pavement Case 2 | | Pavement Case 3 | |
|---|---|---|---|---|---|---|
| Sections | Thickness (mm) | Modulus (MPa) | Thickness (mm) | Modulus (MPa) | Thickness (mm) | Modulus (MPa) |
| AC | 76 | 2,759 | 102 | 2,069 | 76 | 2,759 |
| Base | 305 | 207 | 254 | 124 | 457 | 207 |
| Subgrade | 20,955 | 41 | 20,980 | 28 | 20,803 | 41 |

Figure 7.5 Effect of horizontal domain size on predicted responses. 1 in. = 25.4 mm, 1 ksi = 6.89 MPa. (Adapted from Kim, 2007)

For the analyses of FWD results in this study, eight node quadrilateral and isoparametric finite elements were used. The mesh created in GT-PAVE, shown in Figure 7.6, consisted of 744 elements. A domain size of 20R by 54R was utilized. Based on the analysis conducted by Duncan (1968), Kim (2007), and Kazmee (2018), the utilized 20R by 54R domain size is deemed sufficient for the analyses of FWD results. Further, the adopted mesh had 24 columns and 31 rows, and the sizes of the elements were increased gradually away from the load in the horizontal and vertical directions. The elements were numbered in an increasing order from bottom to top. Column widths (in inches) from left to right are: [1.97, 1.97, 1.97, 2.09, 2, 2, 2, 2, 2, 2, 2, 2, 3, 3, 3, 3, 6, 6, 12, 12, 12, 12, 12,

and 12]. Nominal row heights (in inches) from top to bottom are: [1, 1, 1, 1, 1, 1, 1, 1, 1, 1, 1.5, 1.5, 1.5, 1.5, 2, 2, 3, 3, 3, 4, 4, 8, 12, 18, 24, 30, 32, 36, 38, 40, and 44]. The FWD load was modeled as a uniformly distributed load over the three elements at the top-left corner of the model, as shown in Figure 7.6. The mesh size for these elements was chosen to simulate a 9,000-lb. (40-kN) FWD load uniformly distributed over 5.9 in. (150 mm), which is equal to the radius of the FWD plate.

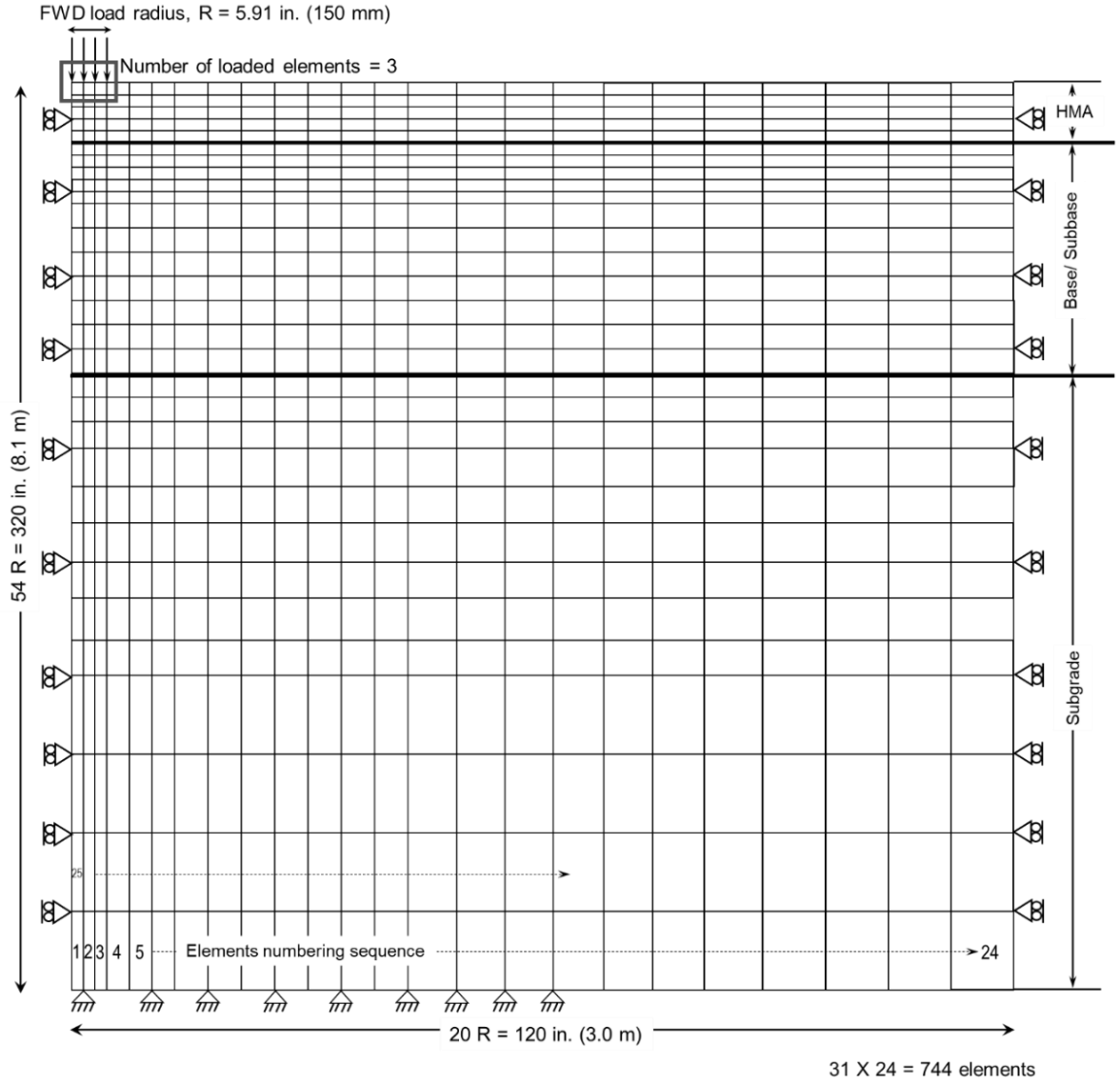


Figure 7.6 GT-PAVE FE mesh for analyzing FWD data

### 7.3.4 Selection of Material Properties for FEM Analysis

The main advantage of using the GT-PAVE program for the mechanistic analyses of FWD results stem from the ability to consider stress-dependent and cross-anisotropic characterizations of unbound granular materials. This is necessary for the analyses of Cell 1 test sections, in particular those sections with nontraditional large rock and QB mixes. The GT-PAVE can also accommodate nonlinearity and stress dependency for fine-grained subgrade soils, but assumes the HMA layer to be linear elastic. This assumption was adopted for the purposes of the mechanistic analyses; that is, the assigned value for the HMA modulus corresponds to the modulus value at the peak load when the FWD data were acquired. Further, a linear elastic subgrade soil assumption was also adopted in the mechanistic analysis.

To ensure that the backcalculated HMA moduli reasonably represent the expected range of modulus values in the field under FWD loading conditions, an estimate of the modulus based on the loading frequency, temperature and other specific mix design inputs was calculated using the HMA modulus equation by the Asphalt Institute (Huang and Witczak, 1979; Huang, 2004). The values assigned to the variables in the equation were calculated for the HMA mix design that was used to construct the field test sections.

$$|E^*| = 100{,}000\ x\ 10^{\beta_1} \quad \text{(Equation 7.8)}$$

$$\beta_1 = \beta_3 + 0.000005\ \beta_2 - 0.00189\ \beta_2\ f^{-1.1} \quad \text{(Equation 7.9)}$$

$$\beta_2 = {\beta_4}^{0.5}\ T^{\beta_5} \quad \text{(Equation 7.10)}$$

$$\beta_3 = 0.553833 + 0.028829 P_{200} f^{-0.1703} - 0.03476 V_a + 0.070377\lambda + 0.931757 f^{0.02774} \quad \text{(Equation 7.11)}$$

$$\beta_4 = 0.483\ V_b \quad \text{(Equation 7.12)}$$

$$\beta_4 = 1.3 + 0.49825 \log f \quad \text{(Equation 7.13)}$$

where

$P_{200}$ = Percentage by weight of aggregates passing No. 200 (0.076 mm) = 4.8%;

$V_b$ = volume of binder in the mix = 11.1%;

$V_a$ = air voids (%) = 7% for the freshly constructed mix;

$f$ = frequency of the loading (Hz);

T = Temperature of the loading (°F); and

$\lambda$ = Binder viscosity at 70 °F ($10^6$ poise).

Note that the original Witczak equation was modified by Andrei et al. (1999) with data from 205 mixtures with 2,750 data points. This modified Witczak equation is one of available options for level 3 analysis using AASHTOWare Mechanistic-Empirical design software (Kim et al., 2011). The modified equation is as follows:

$$log_{10}|E^*| = -1.2499337 + 0.02923P_{200} - 0.001767(P_{200})^2 - 0.002841P_4 - 0.05809V_c - 0.082208\frac{V_{beff}}{V_{beff}+V_a} + \frac{3.871977-0.0021P_4+0.003958P_{\frac{3}{8}}-0.000017\left(P_{\frac{3}{8}}\right)^2+0.00547P_{\frac{3}{4}}}{1+\exp(-0.603313-0.313351\log f-0.393532\log \eta}$$ (Equation 7.14)

where

$E^*$ = dynamic modulus;

$\eta$ = binder viscosity ($10^6$ Poise);

f = loading frequency (Hz);

$V_a$ = air void content (%);

$P_{3/4}$ = cumulative percentage retained on the 3/4 in. (19 mm) sieve; and

$P_{3/8}$ = cumulative % retained on 3/8 in. (9.5 mm) sieve

$P_4$ = cumulative % retained on No. 4 sieve (4.75 mm); and

P200 = % passing the No. 200 (0.076 mm) sieve.

For FWD loading, Loulizi et al. (2002) argue that an FWD load drop induces a stress pulse that can be estimated with a haversine wave having a duration of 0.03 seconds. Given this assumption, a loading frequency of 16 Hz can be assumed for FWD loading ($[2*0.03]^{-1}$ to account for rest period). Further, the concept of viscosity graded asphalt binders was outdated with the introduction of the Superpave performance grading system. IDOT published a pavement technology advisory in 2005 with a grade translation chart to transfer viscosity grades to performance grades. According to this advisory, a PG 64-22 asphalt binder is equivalent to a viscosity grading asphalt concrete of 20, or AC 20, having a viscosity of 2 x $10^6$ poise (IDOT, 2005b). Using these two assumptions and the mix design information for the mix that was used to construct the field test sections, the range of AC modulus for FWD drops was calculated by the original Witczak equation as 97-340 ksi (670-2350 MPa), for HMA surface temperatures between 90 and 113 ºF (32 and 45 ºC). Based on this estimate, the value of the HMA modulus assigned to the HMA layer was constrained between 100 and 400 ksi (690 and 2750 MPa).

For the modulus values of the chemically stabilized pavement layers utilizing QB applications, linear elastic modulus characteristics were assumed. This assumption was reasonably accurate considering that low variations in the normalized FWD deflection basins were measured for the three different FWD load levels in the field. This was not the case for pavement sections with unbound granular layers, where the effects of stress-

dependency were clearly seen in the normalized FWD deflection basins. Thus, a stress-dependent cross-anisotropic modulus assignment was adopted for all granular layers in the GT-PAVE analyses. The full suite of FWD results showing these trends are presented in Appendix C. An example to support these statements is shown in Figure 7.7. Note that in Figure 7.7, stress-dependency is clearly seen for the normalized FWD deflections in C1S3 and C2S3 encompassing unbound granular layers, while it is much less foreseen in C2S2 and C3S1 with chemically stabilized QB bases. These trends were thus adopted in the modulus assignments for the base and subbase layers when analyzing FWD responses.

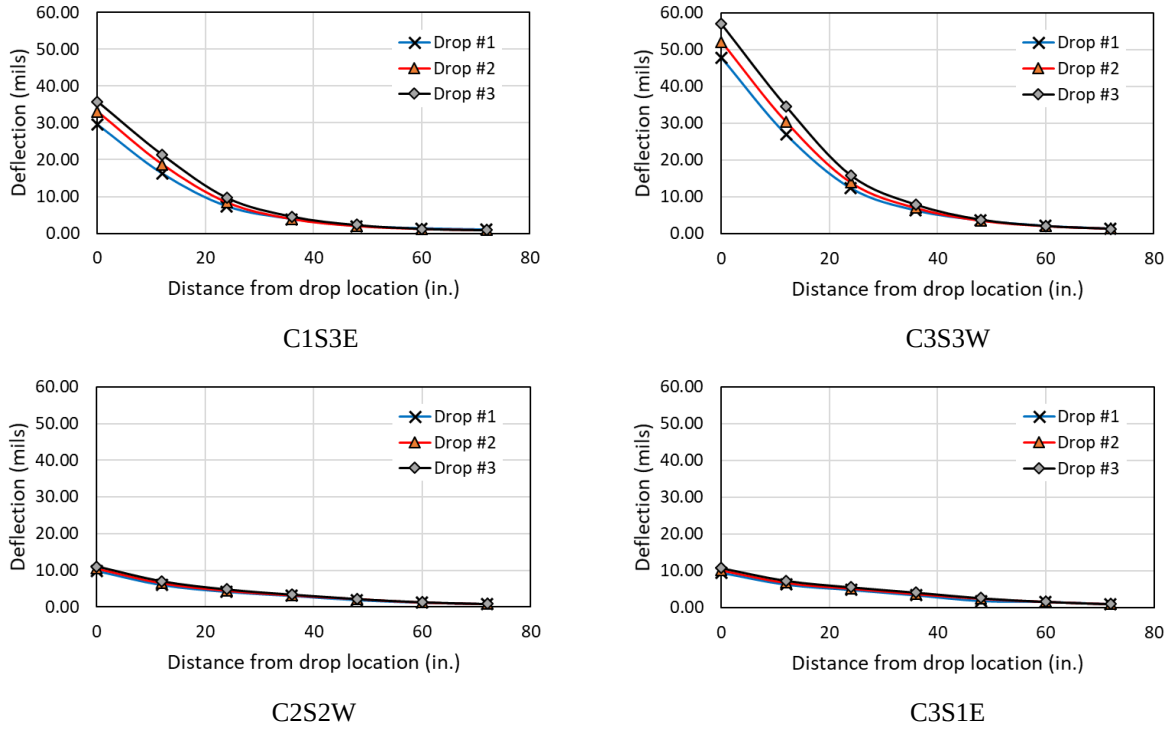


Figure 7.7 Selected FWD Deflection Basins

For the purpose of modulus assignment for the stress-dependent granular layers, the widely used bulk stress model, also known as the K-θ model was utilized (Hicks and Monismith, 1971). Cross-anisotropy was considered by assigning fixed ratios of the vertical modulus ($M_{Rv}$) to the horizontal ($M_{Rh}$) and shear (G) moduli. The horizontal to vertical modulus ($M_{Rh}/M_{Rv}$) and shear to vertical modulus ($G/M_{Rv}$) ratios for the granular layers in Cell 1 and C3S2-C3S4 were assumed to be 0.15 and 0.35, respectively. This assumption was consistent with the findings of Kazmee (2018) who reported both these ratios and other commonly used ratios from the literature. Based on the research of Karasahin and Dawson (2000), who studied the ranges of these ratios for blends of sand and gravel, the anisotropic ratios could vary from 0.1 for low cyclic pressures (7.2 psi or 50 kPa) to 0.7 for high cyclic pressures (36.2 psi or 250 kPa).

Rada and Witczak (1981) developed a predictive equation for the relation between the regression parameters in the K-θ model by compiling a database of 271 resilient modulus tests. Similarly, Mishra and Tutumluer (2012) proposed a relation between the regression parameters in the K-θ model applicable to the unbound aggregates typically used in the state of Illinois. The two relations are shown below. Note that the relations proposed by Rada and Witczak (1981) utilized imperial units (i.e. psi), while the relation developed by Mishra and Tutumluer (2012) utilized SI units (i.e. kPa).

Rada and Witczak (1981): $\log_{10}(K) = 4.657 - 1.807n$ (Equation 7.15)

Mishra and Tutumluer (2012): $K = 868.29n^{-3.78}$ (Equation 7.16)

where

$M_R$ = resilient modulus = $K\theta^n$;

θ = bulk stress; and

K, n = regression coefficients.

### 7.3.5 Results of FWD Forward Calculations Using GT-PAVE Analyses

Initially for the first iteration, the seed HMA modulus was assigned according to the range calculated using the Asphalt Institute HMA modulus equation, taking into consideration the pavement surface temperature measured for the field tests. For the unbound aggregate layers, the K-θ modulus parameters (K and n) were assigned based on the predictive equation by Mishra and Tutumluer (2012). The Rada and Witczak (1981) correlation was used to set the upper bound for the calculated modulus for unbound materials. The modulus values backcalculated for the chemically-stabilized layers from Light Weight Deflectometer (LWD) tests were assigned as the seed values for the stabilized layers. For the subgrade soil, the seed modulus value assigned was 1500 times the design CBR (Engineered subgrade strength).

Following this initial assignment, the layer moduli values were changed systematically on a trial and error basis. After each trial, the surface deflections calculated from the FE model at locations corresponding to FWD sensor locations $D_0$ - $D_3$ were compared to the field-measured FWD deflections. For each trial, the measured and calculated deflections were plotted, and the percentage error in deflections at each FWD sensor location was calculated with respect to the measured FWD deflections. The modulus values were increased or decreased (one at a time for each layer) based on whether the calculated deflections were higher or lower than the measured ones, and this step was repeated for the different layers to minimize the difference. The exhaustive trial and error matching was repeated to minimize the differences between the measured and calculated deflections. The values of the sensors distant from FWD drop location were more sensitive to the modulus of the subgrade and subsurface layers. Thus,

the error of the farthest sensor, and the moduli of the bottom layers were minimized/ backcalculated first, followed by innermost sensors and upper pavement layers. The final layer moduli values were selected when the best match between the measured and calculated deflections was furnished. For most of the test sections, the average errors were reduced to lower than 5% for individual sensors, and lower than 3% average combined error for all four sensors.

The measured surface deflections and the predicted deflections from GT-PAVE analyses for the test sections in Cells 1N, 2, and 3 are shown in Figure 7.8, Figure 7.9, and Figure 7.10, respectively. The results indicate that the modulus assignments and assumptions predicted deflections reasonably in the close proximity of actual measured FWD deflections. Generally, the targets of maintaining the error between measured and calculated deflections for individual FWD sensors below 5%, and the average error for the first four sensors below 3% were met for all 12 analyzed test sections encompassing chemically stabilized and unbound QB applications. After matching the predicted and measured FWD deflection basins, the modulus properties obtained are summarized in Table 7.3, which details the forward calculated modulus properties for the HMA, base, subbase, and subgrade layers.

Note that for some test sections in Cells 2 and 3, two modulus values were reported for HMA in Table 7.3. For six of the test sections with stiff chemically stabilized QB materials, significantly low modulus values were predicted for HMA; most likely due to the high stiffness of the base resulting in significantly low FWD deflections, and thus a prediction error of 1 to 2 mils (25 to 51 µm) for the $D_0$ sensor under drop location can lead to high variability/errors in the backcalculated HMA modulus. The two moduli shown for HMA for these sections represent the modulus that produces the best fit prediction of FWD deflection, as well as a more reasonable constant HMA modulus of 300 ksi (2070 MPa). The predicted FWD deflection basins with the higher HMA modulus, i.e. 300 ksi or 2070 MPa, are presented in Figure 7.11. The difference between the measured and predicted FWD deflections with the 300 ksi (2070 MPa) ranged between 0.8 and 4 mils (20 to 102 µm) for all test sections.

Cell 1N studied unbound applications for QB materials. These applications included using QB as a filler material in the voids of large aggregate subgrade rocks, and using QB in dense graded aggregate subgrade layers with higher fines content (i.e. up to 15% fines passing sieve No. 200 or finer than 0.076 mm). For the purposes of the analyses of these sections, nonlinear stress-dependent and cross-anisotropic modulus assignments were used for the unbound aggregate subgrade layer. Both aggregate subgrade and capping layer were combined for one modulus assignment due to the relatively low thickness of the capping layer. From the backcalculation study findings, it can be seen that the subgrade modulus ranged between 9 and 13 ksi (62-90 MPa), which is significantly higher than the engineered subgrade strength corresponding to a CBR of 1%. The higher subgrade strength can be attributed to the penetration of the large rocks into the weak subgrade soil, thus increasing the strength and stiffness. For the test sections with dense-graded aggregate materials, the relatively high values of the calculated subgrade modulus are likely due to the compaction and consolidation of the subgrade when constructing the lowermost aggregate subgrade lifts in proximity of the subgrade. On the other hand, reasonable HMA and unbound layer modulus values were

calculated for all QB applications in Cell 1N. For the resilient moduli of the unbound layers, the K parameter ranged between 4800 and 6560 psi (33 and 45 MPa), while the 'n' parameter values were similar for all sections, and ranged between 0.44 and 0.49.

Cells 2 and 3 investigated the chemically stabilized QB applications for a base course or for a subbase course in inverted pavements. From the results shown in Table 7.3 for Cell 2 test sections, C3S1 and C3S2, the backcalculated subgrade moduli ranged between 12 and 16.2 ksi (83 – 112 MPa). This is also higher than the engineered subgrade strength, likely due to the compaction and consolidation of the soil during construction. Note that subgrade stress dependency was not considered in this analysis due to the low stress states in the subgrade. The backcalculated layer moduli for the chemically stabilized bases accurately followed the trends for surface rut measurements from the field study. These modulus values were also compared to those obtained from LWD backcalculated moduli. The modulus values obtained from both backcalculations closely matched each other in three of the five test sections. For C3S2 having an inverted pavement test section, relatively high modulus values were obtained for the stabilized subbase layer and the unbound aggregate base. Good compaction was achieved for the aggregate base on top of the stiff subbase, which is one of the main advantages of constructing inverted pavements.

For the last two sections in Cell 3, i.e. C3S3 inverted pavement with a fly ash-stabilized subbase and C3S4 conventional flexible pavement, the backcalculated subgrade moduli were lower than the remaining sections in Cells 2 and 3, and corresponded to lower modulus values than expected from the engineered subgrade strength. Additionally, the backcalculated modulus properties for the granular aggregate layers were significantly low. These low backcalculated modulus properties were expected since high FWD deflections were measured for these sections, and the results for FWD analyses are in good agreement with the conclusions presented in the previous chapters regarding the poor performance trends of these sections, particularly C3S4. In conclusion, the higher porosity of HMA layer, moisture intrusion, and shallower water table all led to weaker subgrade and pavement layers, which is reflected in the backcalculated layer moduli for these two pavement sections.

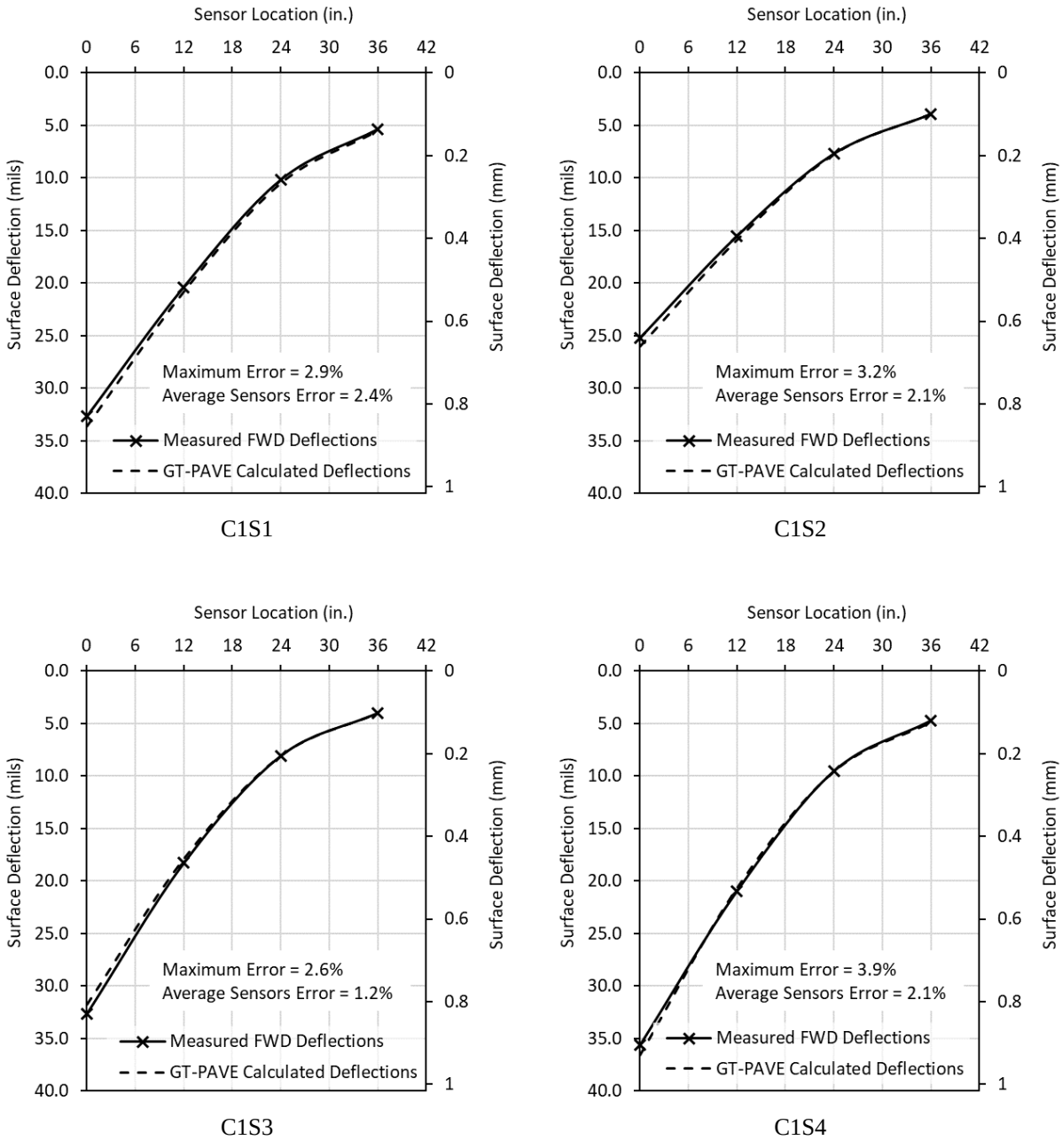


Figure 7.8 Measured and predicted FWD deflections for test sections in Cell 1N

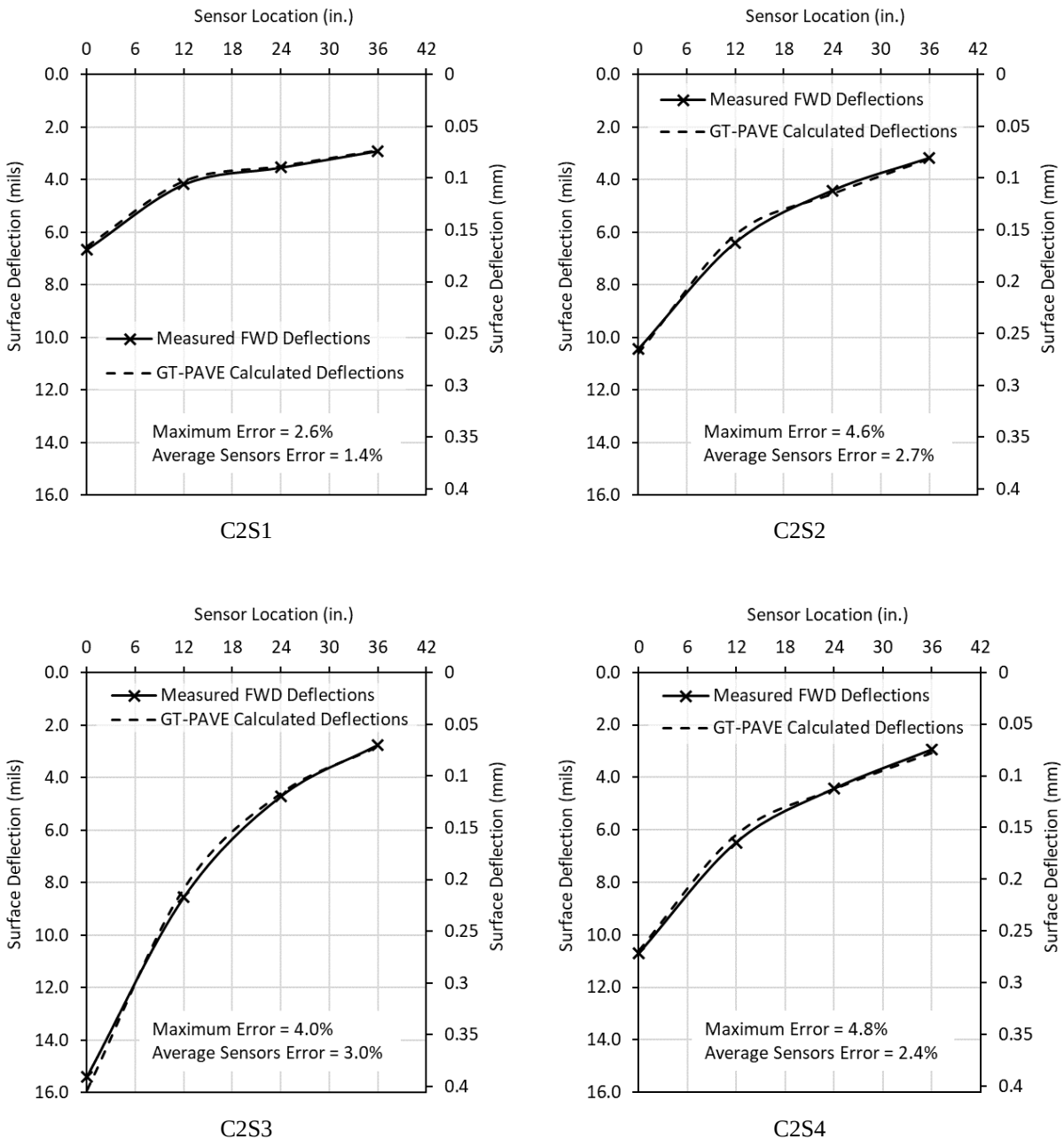


Figure 7.9 Measured and predicted FWD deflections for test sections in Cell 2

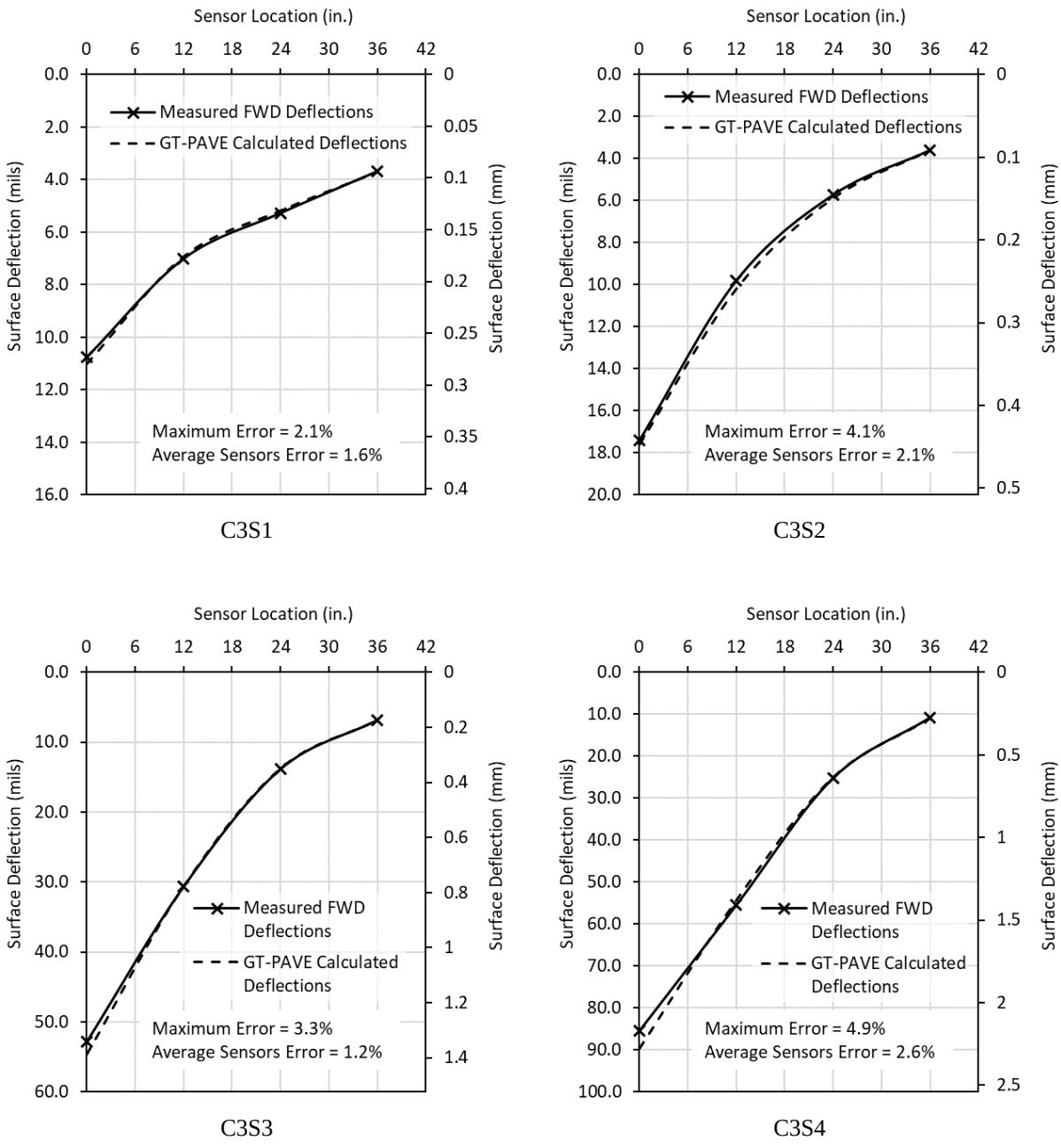


Figure 7.10 Measured and predicted FWD deflections for test sections in Cell 3

Note different y-axis scales for FWD deflection plots for sections in Cell 3

Table 7.3 FWD backcalculated layer moduli obtained using GT-PAVE by matching deflection basin

| Section | Description of base/subbase materials | HMA ksi (MPa) | Base / Subbase psi (MPa) | Subgrade ksi (MPa) |
|---|---|---|---|---|
| C1S1 | Primary Crusher Run (PCR) rocks with 25% QB1, constructed in two lifts | 450 (3100) | K = 5,098 psi (35 MPa); n = 0.48 | 9.0 (62) |
| C1S2 | PCR with 16.7% QB1 by weight, constructed in one single lift | 450 (3100) | K = 6,557 psi (45MPa); n = 0.44 | 13.0 (90) |
| C1S3 | Dense-graded CA06 aggregates with 15% plastic fines | 300 (2070) | K = 5,415 psi (37 MPa); $n$ = 0.47 | 12.5 (86) |
| C1S4 | Dense-graded CA06 aggregates with 15% nonplastic fines | 300 (2070) | K = 4,808 psi (33 MPa); n = 0.49 | 10.0 (69) |
| C2S1 | A blend of 70% QB2 and 30% FRAP mixed with 3% Type I cement | 300 (2070) + 100 (690) * | 1,250,000 (8,620) | 12.0 (83) |
| C2S2 | A blend of 70% QB2 and 30% FRCA mixed with 3% Type I cement | 300 (2070) + 100 (690) * | 350,000 (2,410) | 14.0 (97) |
| C2S3 | A blend of 70% QB2 and 30% FRAP mixed with 10% Class 'C' fly ash | 300 (2070) + 200 (1380) * | 46,000 (320) | 16.2 (112) |
| C2S4 | A Blend of QB2 and 3% Type I cement | 300 (2070) + 110 (760) * | 250,000 (1,720) | 15.0 (103) |
| C3S1 | A Blend of QB3 and 3% Type I cement | 300 (2070) + 135 (930) * | 250,000 (1,720) | 11.7 (81) |
| C3S2 | Subbase layer: A Blend of QB2 and 3% cement<br>Base layer: CA06_R; a dense-graded unbound aggregate | 300 (2070) | Base layer: K = 7,800 psi (54 MPa); $n$ = 0.5 $M_{Rh}$ = 0.15 $M_{Rv}$; G = 0.35 $M_{Rv}$<br>Subbase layer: 280,000 (1,930) | 12.6 (87) |
| C3S3 | Subbase layer: A Blend of QB2 and 10% Class 'C' fly ash<br>Base layer: CA06_R | 300 (2070) + 225 (1550) * | Base layer: K = 1,750 psi (12.1 MPa); n = 0.55 $M_{Rh}$ = 0.15 $M_{Rv}$; G = 0.35 $M_{Rv}$<br>Subbase layer: 45,000 (310) | 6.5 (45) |
| C3S4 | CA06_R | 350 (2410) | $M_{Rv}$: K = 1,350 psi (9.3 MPa); n = 0.51 $M_{Rh}$ = 0.15 $M_{Rv}$; G = 0.35 $M_{Rv}$ | 4.6 (32) |

+ HMA Modulus Fixed to 300 psi (2070 MPa) * Backcalculated HMA modulus that produces best fit predicted deflection basin

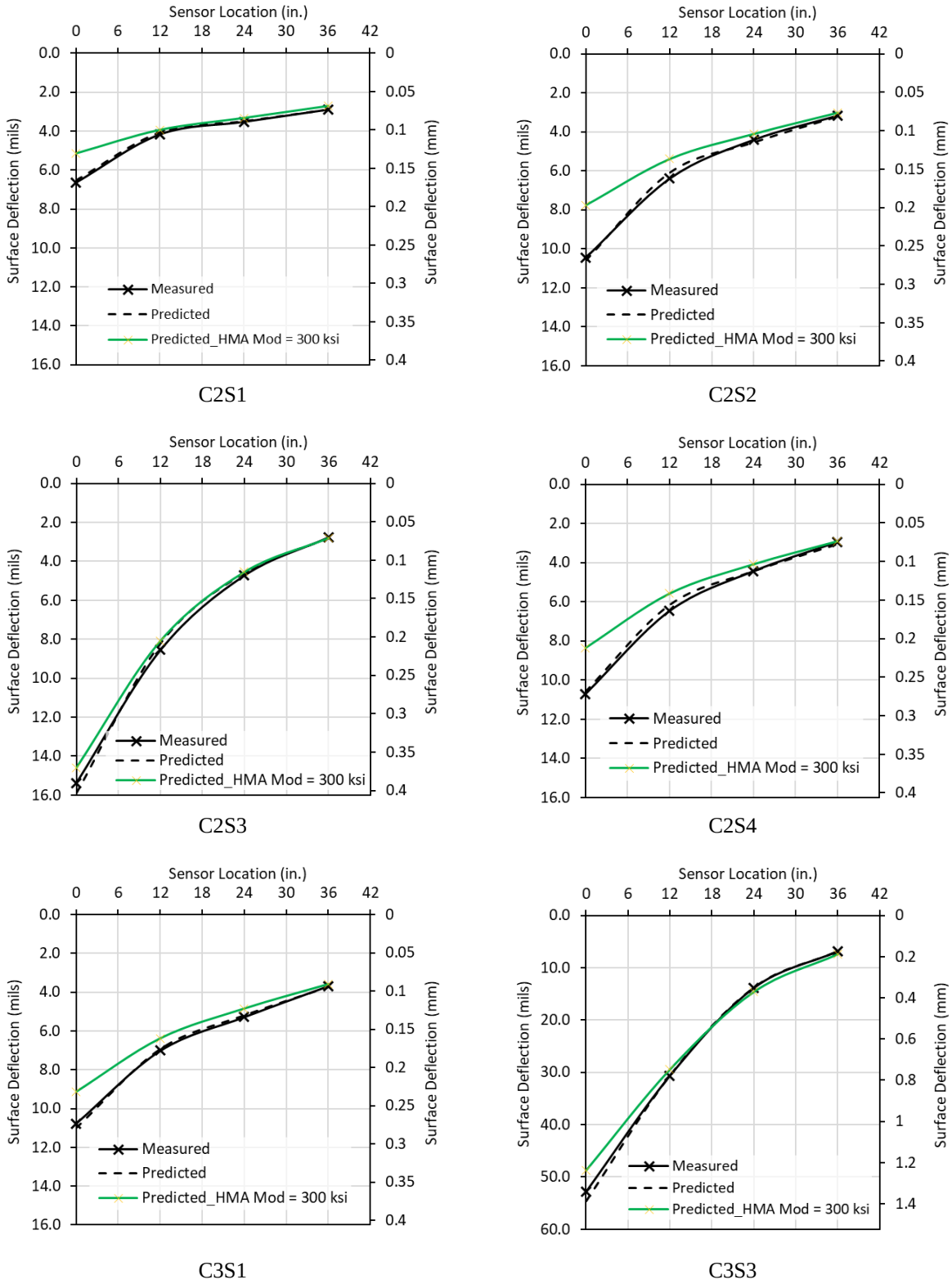


Figure 7.11 Measured and predicted FWD deflections for test sections assuming 300 ksi (2070) HMA modulus

### 7.3.6 Validation of FWD Backcalculation Analyses

In the previous sections, an approach to use GT-PAVE FE program to backcalculate layer modulus properties by matching FWD resilient surface deflections was presented. In this section, a validation study for the backcalculated layer moduli is presented. Data from pressure cells installed on top of the subgrade in four of the test sections in Cells 2 and 3 were collected and presented in Chapters 5 and 6. A comparison is presented here between the field measured vertical stresses on top of the subgrade and the GT-PAVE predicted top of subgrade stresses considering the as-constructed layer thicknesses and the layer modulus properties obtained from FWD backcalculation. Further, the subgrade modulus values backcalculated by GT-PAVE were compared to those obtained from regression equations based on ILLI-PAVE nondestructive testing and analysis procedures (Thompson, 1989).

The results of predicted and measured subgrade stresses on top of subgrade are presented in Table 7.4. All field measured top of subgrade pressures from the installed pressure cells were for the 10 kip (44 kN) load level. Further, note that the values shown in Table 7.4 for the predicted and measured vertical stresses on top of subgrade indicate pressures due to wheel load only, excluding any overburden pressure. For the predicted values, these values were obtained by subtracting the total pressure due to the weight of the pavement structure from the stress predicted on top of the subgrade, thus reporting the vertical stress due to wheel load only. From the results shown, it can be realized that the predicted pressures on top of subgrade are generally larger than those measured in the field, except for C2S1 constructed from cement-stabilized QB mixed with FRAP, which had a lower predicted vertical stress than that measured from pressure cells. This is often explained due to a possible lack of restraining support under the installed pressure cells and the pressure cells not fully registering wheel load pressures especially if there is permanent deformation recorded in soft subgrades. Two of the test sections instrumented with soil pressure cells (C2S1 and C3S4) had a good agreement between predicted and measured pressures on top of subgrade. For the other two sections (C2S4 and C3S2), the predicted subgrade vertical pressures due to the wheel load were approximately 2-4 psi (14-28 kPa) higher than those of the measured ones.

Another approach to validate FWD backcalculated layer modulus for the subgrade layer in each constructed pavement section was to use established correlations to predict the modulus of subgrade using the FWD $D_3$ sensor deflections, located at 36 in. (914 mm) from the FWD load drop location. For this goal, correlations provided by Thompson (1989) were utilized. These correlations were developed for different pavement structures such as full depth asphalt, conventional flexible pavements, and flexible pavements with High Strength Stabilized Base (HSSB). ILLI-PAVE finite element program was used to develop these procedures and algorithms used in their backcalculation of subgrade moduli from the FWD $D_3$ sensor deflection. The following correlations were reported by Thompson (1989):

For a flexible pavement with granular base, $ER_i = 24.1 - 5.08\ D_3 + 0.28\ D_3^2$ (Equation 7.17)

For a flexible pavement with HSSB, $ER_i = 25.75 - 7.28\ D_3 + 0.53\ D_3^2$ (Equation 7.18)

where

$ER_i$ is the subgrade soil breakpoint resilient modulus (ksi); and

$D_3$ is the deflection 36 in. (914 mm) from center of loading plate (mils).

Based on these correlations, the breakpoint subgrade resilient modulus was calculated and compared to the subgrade moduli values obtained from the GT-PAVE FWD backcalculation analysis. Equation 7.17 was used for Cell 1 test sections, while Equation 7.18 was used for Cell 2 and Cell 3 test sections with stabilized QB applications. The correlations could not be used to predict the subgrade modulus for C3S3 and C3S4 since the FWD deflections measured for these two test sections at the $D_3$ location were higher than the range supported by the equations, and thus gave unreasonable modulus values. Based on the results presented in Table 7.4, subgrade modulus predicted by GT-PAVE was consistently higher than those predicted by the correlations from ILLI-PAVE. The difference in subgrade modulus for all test sections ranged between 2,900 and 6,500 psi (20 and 45 MPa).

Table 7.4 Predicted subgrade vertical stress and subgrade modulus

| Section | GT-PAVE predicted subgrade vertical stress * psi (kPa) | Measured subgrade vertical stress * psi (kPa) | FWD $D_3$ Deflection mils (mm) | Subgrade Modulus ksi (MPa) | |
|---|---|---|---|---|---|
| | | | | GT-PAVE | Correlations |
| C1S1 | - | - | 5.41 (137.5) | 9.0 (62) | 4.8 (33) |
| C1S2 | - | - | 3.91 (99.4) | 13.0 (90) | 8.5 (59) |
| C1S3 | - | - | 4.01 (101.8) | 12.5 (86) | 8.2 (57) |
| C1S4 | - | - | 4.74 (120.3) | 10.0 (69) | 6.3 (44) |
| C2S1 | 1.06 (7.3) | 1.42 - 1.98 (9.8 - 13.7) | 2.91 (73.8) | 12.0 (83) | 9.1 (63) |
| C2S2 | - | - | 3.17 (80.6) | 14.0 (97) | 8.0 (55) |
| C2S3 | - | - | 2.75 (67.0) | 16.2 (112) | 9.7 (67) |
| C2S4 | 4.86 (33.5) | 1.78 - 2.53 (12.3 - 17.4) | 2.95 (74.9) | 15.0 (103) | 8.9 (61) |
| C3S1 | - | - | 3.68 (93.6) | 11.7 (81) | 6.1 (42) |
| C3S2 | 6.69 (46.1) | 2.24 - 2.82 (15.4 - 19.4) | 3.60 (91.5) | 12.6 (87) | 6.4 (44) |
| C3S3 | - | - | 6.82 (173.1) | 6.5 (45) | - |
| C3S4 | 11.95 (82.4) | 7.69 - 10.99 (53.0 - 75.8) | 10.75 (273.0) | 4.6 (32) | - |

* Positive values indicate compressive stresses; measured stresses from installed pressure cells

## 7.4 RESPONSE PREDICTIONS OF PAVEMENT SECTIONS WITH QB APPLICATIONS

This section presents the GT-PAVE predicted critical pavement responses for the chemically stabilized applications of QB studied in Cells 2 and 3. In addition, the critical pavement responses predicted for two additional scenarios using the studied QB applications are considered. These additional scenarios are for as-designed pavement sections, assigned the design layer thicknesses and the same modulus properties for subgrade and HMA layer, as well as a proposed scenario of thinner pavement structures having 3-in. (76-mm) thick HMA and 8-in. (203-mm) thick base or combined base and subbase of equal thicknesses, i.e. 4 in. (102 mm) each. The predicted critical pavement responses reported herein include the tensile strain at the bottom of the HMA layer and both the tensile strain and stress at the bottom of the base/subbase for sections utilizing stabilized QB applications. Further, the resilient surface deflections at FWD sensors $D_0$ – $D_3$ locations, i.e. the load drop location, 12 in. (305 mm), 24 in. (610 mm), and 36 in. (914 mm), respectively from load drop location are reported; considering an FWD load of 9 kips (40 kN) and a 11.8-in. (300-mm) FWD plate diameter.

The reasoning behind reporting the resilient surface deflections at the FWD sensor locations for the various studied QB applications is to provide a framework to assess pavement performance and structural capacity based on FWD nondestructive testing, which is a common practice by many state DOTs and transportation agencies. Further, a 'response benefit' term is introduced for any pavement based on the maximum surface deflection at the FWD test location in comparison to that for a standard conventional pavement section with the same layer thicknesses and a dense-graded aggregate base material. The response benefit was introduced in order to meaningfully interpret the structural adequacies and advantages of constructing pavement sections utilizing QB applications in terms of environmental impacts and cost. The response benefit term therefore enables a quantifiable assessment of the structural capacity, which may or may not be linked to an anticipated number of load repetitions to failure depending on damage models adopted of different pavements and the demonstrated/anticipated performance trends. Note that Cell 1 test sections were not included in the response benefit analyses since similar good performance was observed for the four flexible pavement sections from the field study. Whereas, Cells 2 and 3 had notably varying performance trends depending on the characteristics and layer materials of the base/subbase and whether cement or class C fly ash were used as the stabilizing agent. The response benefit is calculated using the following equation, where higher response benefits indicate a stronger section:

$$Response\ Benefit = \left(\frac{D_{0\,(i)}}{D_{0\,(conv.)}}\right)^{-1} \quad \text{(Equation 7.19)}$$

where

$D_{0\,(i)}$ = maximum FWD center deflection for a test section 'i' utilizing QB application; and

$D_{0\,(conv.)}$ = maximum FWD center deflection for a conventional pavement section with comparable thicknesses.

The test sections evaluated in Cells 2 and 3 had equal design thicknesses, i.e. 4 in. (102 mm) HMA and 12 in. (305 mm) of combined base and subbase, but different stiffness, strength, and performance characteristics. To meaningfully quantify the sustainability and life cycle costs of the test sections, two approaches can be considered. The first approach is performing sustainability and cost evaluation for a 20- or 30-year analysis period and including materials procurement, construction, use, maintenance and rehabilitation, and end of life. The second approach is to report the response benefit of each test section as a direct indication of structural capacity comparison, and based on that comparison of expected performance trends, as well as the minimum expected cost and environmental benefits from constructing pavement sections utilizing QB applications.

The first option provides a more comprehensive life cycle assessment approach for the evaluated QB applications. However, since most of these applications were newly proposed and tested with accelerated pavement testing, very little information is readily available to predict the durability and long term performance of the different test sections, including long term damage accumulation, and the progression of International Roughness Index (IRI) during the use phase and after each rehabilitation activity. Since this critical information is lacking, underlying assumptions and simplifications that might not be realistic can be of major concern. Accordingly, it was decided to utilize the second approach for the purposes of this dissertation: reporting the response benefits as the direct indication of structural capacity comparison.

First, the critical pavement responses and the response benefits for the as-constructed test sections are calculated and presented in Table 7.5. These pavement responses and response benefits were calculated by considering the constructed pavement thicknesses in Cells 2 and 3 and the FWD backcalculated layer modulus properties presented in the previous sections. Note that the HMA moduli values that produced the best fit predicted FWD deflection basins were used for the purposes of these analyses. Also, note that the reported FWD deflections, and consequently, the reported response benefits are based on the predicted resilient deflections from GT-PAVE FE analyses. These FWD deflections are quite similar to the measured deflections from the constructed test sections given the very accurate GT-PAVE predictions that were presented in the previous section.

As presented in Table 7.5, the fly ash-stabilized test sections had higher tensile strains at the bottom of the stabilized base, generally higher FWD surface deflections, and the lowest response benefits. On the other hand, compared to the fly ash stabilized sections, the test sections with cement-stabilized QB bases had lower tensile stresses at the bottom of the base, lower FWD deflections, and in turn higher response benefits; particularly C2S1 with cement-stabilized QB and FRAP, accumulated the least surface rut and had the lowest measured FWD deflections. Note that the response benefits reported for this analysis considered C3S4 as the reference, which had a poor performance due to the low HMA thickness, high HMA porosity, and moisture intrusion. These effects are eliminated in the two other scenarios considered next by assuming proper layer thicknesses and modulus properties for the conventional pavement sections.

For analysis purposes discussed hereafter, and to differentiate the analyzed pavement sections from the test sections that were constructed in the field evaluation study, the as-designed and the newly proposed pavement

sections are referred to as sections 1-8 in Table 7.6, which presents a description for the materials used to construct the base and subbase layers utilizing QB materials. The analyses for these test sections were conducted using GT-PAVE axisymmetric FE program, which was also used earlier to analyze the FWD deflections measured for the constructed test sections.

Table 7.5 Critical pavement responses and response benefits for the constructed pavement sections with QB

| Section | Tensile strain (microstrain) | | Tensile stress at bottom of stabilized layer psi (kPa) | FDW Deflections mil (micrometer) | | | | Response benefit |
|---|---|---|---|---|---|---|---|---|
| | Bottom of HMA* | Bottom of stabilized layer | | $D_0$ | $D_1$ | $D_2$ | $D_3$ | |
| C2S1 | - 24.9 | 33.1 | 51.42 (355) | 6.61 (168) | 4.16 (106) | 3.51 (89) | 2.83 (72) | 13.3 |
| C2S2 | - 19.4 | 88.0 | 37.41 (258) | 10.6 (269) | 6.1 (155) | 4.55 (116) | 3.22 (82) | 8.3 |
| C2S3 | 250.6 | 173.2 | 8.00 (55) | 15.9 (404) | 8.21 (209) | 4.59 (117) | 2.81 (71) | 5.5 |
| C2S4 | 22.9 | 101.2 | 30.35 (209) | 10.6 (269) | 6.17 (157) | 4.44 (113) | 3.06 (78) | 8.3 |
| C3S1 | - 2.4 | 100.2 | 30.23 (208) | 11 (279) | 6.93 (176) | 5.19 (132) | 3.73 (95) | 8.0 |
| C3S2 | 265.8 | 124.5 | 41.95 (289) | 17.6 (447) | 10.2 (259) | 5.89 (150) | 3.61 (92) | 5.0 |
| C3S3 | 842.1 | 384.8 | 19.33 (134) | 54.6 (1387) | 30.6 (777) | 13.8 (351) | 6.91 (176) | 1.6 |
| C3S4 | 1003.3 | - | - | 87.6 (2225) | 52.9 (1344) | 24.3 (617) | 11.1 (282) | 1.0 |

* Negative values indicate compressive strain at the bottom of HMA layer

Table 7.6 Descriptions of base and subbase material types for the as-designed and the newly proposed pavement sections

| Pavement | Description of base and subbase layers composition |
|---|---|
| Section 1 | A blend of 70% QB2 and 30% FRAP by weight, stabilized with 3% Type I cement |
| Section 2 | A blend of 70% QB2 and 30% FRCA by weight, stabilized with 3% Type I cement |
| Section 3 | A blend of 70% QB2 and 30% FRAP by weight, stabilized with 10% Class 'C' fly ash |
| Section 4 | A Blend of QB2 and 3% Type I cement |
| Section 5 | A Blend of QB3 and 3% Type I cement |
| Section 6 | Subbase layer: A Blend of QB2 and 3% Type I cement<br>Base layer: dense-graded unbound dolomite aggregates |
| Section 7 | Subbase layer: A Blend of QB2 and 10% Class 'C' fly ash<br>Base layer: dense-graded unbound dolomite aggregates |
| Section 8 | Dense-graded unbound dolomite aggregates |

The modulus values that were backcalculated from the FWD tests were used as the corresponding layer moduli for calculating the critical pavement responses and the response benefits. For the dense-graded unbound aggregate layers in Sections 6-8, the K-θ model with a 'K' value of 7800 and an 'n' value of 0.5 were assumed, which correspond to the modulus properties of the unbound aggregate base layer backcalculated from C3S3 inverted pavement section and had a proper construction. The same cross-anisotropic properties assumed earlier were also utilized. To account for the effects of the stabilized QB applications only, and exclude the effects of variability in subgrade and HMA, the layer properties of subgrade and HMA were fixed for all sections. A fixed HMA modulus of 200 ksi (1,380 MPa) was chosen as a reasonable but conservative HMA modulus for all pavement sections analyzed hereafter (Masada et al., 2004; Tutumluer and Sarker, 2015; Texas DOT, 2019; Garg et al., 2017). Similarly, a subgrade soil modulus of 9 ksi (62 MPa), equivalent to a CBR of 6%, was assigned to all pavement sections since this is the lower end of modulus requirement before the need for subgrade remediation by IDOT Subgrade Stability Manual (see Figure 2.11).

Using the modulus assignments discussed above, the critical pavement responses and the response benefits for the as-designed pavement sections were calculated first (see Table 7.7). These pavement sections had the design layer thicknesses of 4 in. (102 mm) HMA layer and 12 in. (305 mm) of base or 6 in. (151 mm) of base and subbase for the cases of inverted pavements. The as-designed layer thicknesses presented herein will be referred to as 'Scenario #2' for the purposes of the life cycle assessments presented in the next chapter. As presented in Table 7.7, the calculated response benefits are significantly lower than those reported for the constructed test sections, mainly due to considering a properly designed conventional pavement section (Section 8), which led to significantly lower measured FWD deflections. Nevertheless, response benefits exceeding 2.6 were reported for all as-designed pavement sections with a cement-stabilized QB or QB blended with recycled coarse aggregate base. Similar to the Scenario #1 for the as-constructed pavement test sections, the fly ash-stabilized sections had the highest tensile strain at the bottom of the stabilized base, higher FWD surface deflections, and the lowest response benefits. The cement-stabilized sections, on the other hand, had lower predicted FWD deflections and lower HMA tensile strains.

Lastly, Scenario #3 considered proposed thinner sections consisting of a 3 in. (76 mm) HMA layer and 8 in. (203 mm) of base or 4 in. (102 mm) of base and subbase for the cases of inverted pavements. The critical pavement responses and the response benefits computed for the proposed thinner pavement sections are presented in Table 7.8. These proposed Scenario #3 pavement sections were thinner because of the superior performance observed for the stabilized QB applications in the field, particularly those with cement-stabilized QB and coarse FRAP/FRCA, which justified analyzing thinner sections than what was tested in the field experiment for the purposes of designing low volume roads with QB applications. The thicknesses were chosen based on the minimum thickness requirements for flexible pavements by IDOT's Bureau of Local Roads and Streets (BLRS) manual. As presented in Table 7.8, response benefits of around 2.0 or more were still reported for all the proposed pavement sections with a cement-stabilized QB or QB blended with recycled coarse aggregate base. Similar to the first two scenarios, the fly ash-stabilized test sections had the highest tensile strain at the bottom of the stabilized base, higher FWD surface deflections, and the lowest response benefits. The cement-stabilized sections, on the other hand, had lower predicted

FWD deflections and lower tensile strains at the bottom of the HMA layer. For all pavement sections considered in Scenario #3, the strains and FWD deflections were of course much higher than those reported for the case of the Scenario #2 due to the thinner/weaker pavement structures still adequate for low volume roads.

Table 7.7 Critical pavement responses and response benefit for the as-designed pavement sections

| Section | Tensile strain (microstrain) | | Tensile stress at bottom of stabilized layer psi (kPa) | FDW Deflections mil (micrometer) | | | | Response benefit |
|---|---|---|---|---|---|---|---|---|
| | Bottom of HMA * | Bottom of stabilized layer | | $D_0$ | $D_1$ | $D_2$ | $D_3$ | |
| Section 1 | - 20.9 | 37.4 | 55.92 (386) | 7.04 (179) | 5.22 (133) | 4.45 (113) | 3.63 (92) | 4.3 |
| Section 2 | - 11.8 | 90.0 | 38.50 (265) | 10.5 (267) | 7.6 (193) | 5.97 (152) | 4.5 (114) | 2.9 |
| Section 3 | 253.3 | 199.1 | 9.28 (64) | 16.8 (427) | 8.52 (216) | 4.69 (119) | 2.82 (72) | 1.8 |
| Section 4 | 3.4 | 111.0 | 33.80 (233) | 11.7 (297) | 8.26 (210) | 6.32 (161) | 4.66 (118) | 2.6 |
| Section 5 | 3.4 | 111.0 | 33.81 (233) | 11.7 (297) | 8.26 (210) | 6.32 (161) | 4.66 (118) | 2.6 |
| Section 6 | 293.8 | 153.7 | 52.08 (359) | 21.8 (554) | 13.1 (333) | 7.97 (202) | 5.01 (127) | 1.4 |
| Section 7 | 356.8 | 297.1 | 14.62 (101) | 25.8 (655) | 15.3 (389) | 8.56 (217) | 5.04 (1228) | 1.2 |
| Section 8 | 443.8 | - | - | 30.6 (777) | 18.0 (457) | 9.19 (233) | 4.99 (127) | 1.0 |

* Negative values indicate compressive strain at the bottom of HMA layer

Table 7.8 Critical pavement responses and response benefit for the proposed pavement sections

| Section | Tensile strain (microstrain) | | Tensile stress at bottom of stabilized layer psi (kPa) | FDW Deflections mil (micrometer) | | | | Response benefit |
|---|---|---|---|---|---|---|---|---|
| | Bottom of HMA * | Bottom of stabilized layer | | $D_0$ | $D_1$ | $D_2$ | $D_3$ | |
| Section 1 | - 49.9 | 74.7 | 116.16 (801) | 10.5 (267) | 8.41 (214) | 6.59 (167) | 4.86 (123) | 3.06 |
| Section 2 | - 56.3 | 171.9 | 73.96 (510) | 15.0 (381) | 11.2 (284) | 7.93 (201) | 5.31 (135) | 2.14 |
| Section 3 | 247.7 | 501.1 | 25.97 (179) | 27.7 (704) | 15.8 (401) | 8.82 (224) | 5.1 (130) | 1.16 |
| Section 4 | - 42.5 | 210.3 | 64.16 (442) | 16.4 (417) | 11.9 (302) | 8.17 (208) | 5.34 (136) | 1.96 |
| Section 5 | - 42.5 | 210.3 | 64.16 (442) | 16.4 (417) | 11.9 (302) | 8.17 (208) | 5.34 (136) | 1.96 |
| Section 6 | 205.1 | 259.7 | 88.50 (610) | 25.8 (655) | 15.5 (394) | 8.83 (224) | 5.06 (129) | 1.24 |
| Section 7 | 305.4 | 528.6 | 26.69 (184) | 30.7 (780) | 17.6 (447) | 9.14 (232) | 4.99 (127) | 1.05 |
| Section 8 | 470.2 | - | - | 32.1 (815) | 18.7 (475) | 9.24 (235) | 4.89 (124) | 1.00 |

* Negative values indicate compressive strain at the bottom of HMA layer

## 7.5 SUMMARY

This chapter presented a finite element-based mechanistic analysis approach for studying the field pavement test sections with the constructed QB applications to analyze the FWD deflections, backcalculate layer moduli, validate backcalculation results, and calculate critical pavement responses and response benefits for different scenarios/layer thicknesses of pavement sections utilizing QB applications in base or subbase layers. First, the FWD Deflection Basin Parameters (DBPs) were calculated and used to draw conclusions about the performance of the QB sections. The trends for Area Under Pavement Profile (AUPP) and the field measured surface ruts were in good agreement for the test sections with chemically stabilized QB applications. Secondly, the modulus properties of the constructed pavement layers were backcalculated from the FWD deflections using GT-PAVE finite element program through a mechanistic forward calculation approach. Good matches were obtained between the measured and calculated FWD deflection basins with errors not exceeding 5% for all 12 analyzed test sections. The layer properties calculated from the backcalculation analyses were further used to compute critical pavement responses and response benefits, based on FWD resilient surface deflections and predicted surface deflections, for all QB applications investigated in Cells 2 and 3 under three different scenarios. The three scenarios involved pavement sections with the as-constructed and as-designed layer thicknesses, and newly proposed thinner pavement sections more suited for low volume road applications. The calculated response benefits indicated significant advantages of using cement-stabilized QB applications over fly ash-stabilized QB applications and conventional flexible pavement sections. This was evident from the high response benefits predicted for cement-stabilized QB applications.

# CHAPTER 8: ENVIRONMENTAL AND ECONOMIC IMPACTS FOR QB USAGE

## 8.1 INTRODUCTION

The Federal Highway Administration (FHWA) defines a sustainable pavement as a pavement that "achieves its specific engineering goals" while ensuring that the basic human needs are achieved, the resources are used efficiently, and the surrounding ecosystems are maintained or improved (Harvey et al., 2014). One powerful tool to evaluate the sustainability of a pavement is Life cycle Assessment (LCA), which assesses the environmental impacts that the pavement has on the surrounding environment.

This chapter provides a Life Cycle Assessment (LCA) and Life Cycle Cost Analysis (LCCA) approach for the stabilized QB applications that were discussed in the previous chapters. The economic and environmental sustainability assessment calculations were performed for the stabilized sections in Cells 2 and 3. The conducted LCA follows ISO 14044:2006 "Environmental management - life cycle assessment - requirements and guidelines" for structure and recommendations. The data obtained during the construction and testing of the test sections were used to develop the following scenarios. Three scenarios were considered for assessing the cost and environmental impacts of QB usage in cement- and fly ash-stabilized pavement layers.

- The first scenario evaluates the cost and environmental burdens of the pavement test sections constructed in Cells 2 and 3, and considers actual constructed layer thicknesses measured from trenching and HMA cores.
- The second scenario assumes that the design thicknesses were properly constructed for all evaluated applications to eliminate the variability from constructed layer thicknesses. This pavement structure with chemically stabilized QB applications is more suited for higher volume of traffic and/or longer design life.
- The third scenario calculates the environmental and economic impacts for newly proposed pavement structures for low volume road applications. The proposed pavements comprise a 3 in. (76 mm) HMA thickness, and either 8 in. (203 mm) of base layer or 4 in. (102 mm) of base and 4 in. (102 mm) subbase layers. Given the low rut accumulation and excellent performance of the tested QB applications, this pavement structure is deemed more suitable for lower volume traffic. Note that these pavement thicknesses were reported in IDOT's Bureau of Local Roads and Streets (BLRS) manual as the minimum thicknesses for conventional flexible pavements (Illinois Department of Transportation, 2005). IDOT's Class IV low volume roads are typically designed for 64,000 or 85,000 ESALs for the 15 and 20 year design periods, respectively.

This chapter discusses the results of the LCAs and LCCAs conducted for the pavement sections utilizing chemically stabilized applications of QB or QB mixed with coarse recycled aggregates. For LCA, the goal and scope are first defined; including specific information for system boundary, functional unit, impact categories, and the

quality of collected data. Life Cycle Inventory (LCI) analysis and Life Cycle Impact Assessment (LCIA) are discussed next including normalization, weighting and limitations in LCI analysis. The results and the interpretation of results are then presented and discussed for the pavement sections considered in all three LCA scenarios. Initial construction costs were included in the LCCA. Costs were estimated from the expected costs of relevant bid items involved and quantities used in the construction of the pavement sections. The results are also presented normalized with respect to expected lifetime of each application.

## 8.2 OVERVIEW OF LCA AND LCCA SCENARIOS

Three different scenarios are considered and compared for their cost, environmental impacts and energy demands. The major discrepancies among the three scenarios are the thicknesses of the HMA, base and subbase layers. The three scenarios essentially assume the same goal and scope and LCI impacts for raw materials and fuels, including allocation criteria and data sources. The three scenarios are:

- **Scenario #1: Comparison of as-constructed pavement sections.** This scenario performs a comparative LCA for test sections constructed in Cells 2 and 3 with their actual constructed layer thicknesses. The importance of conducting an LCA for the constructed pavement sections (i.e. constructed materials and layer thicknesses) stem from the known field performance. These pavement sections utilizing stabilized QB applications have been evaluated for rutting and fatigue performance. Valuable information has been collected about their behavior under heavy wheel loading. The constructed pavement sections are not design-equivalent, since they have different critical pavement responses and different pavement life expectations. Table 8.1 provides the layer thicknesses for the different pavement sections evaluated in Scenario #1. Note that to be consistent with the other two scenarios, C2S1-C2S4 are referred to by Section 1 to Section 4, respectively, while C3S1-C3S4 are referred to by Section 5 to Section 8, respectively.
- **Scenario #2: Comparison of as-designed pavement sections.** All test sections in Cells 2 and 3 were designed to have an HMA thickness of 4 in. (102 mm), and a base thickness or combined base/subbase thickness of 12 in. (305 mm). For inverted pavement sections (C3S2 and C3S3), the design thickness of the base or stabilized QB subbase were 6 in. (152 mm). The objective of this scenario is to exclude the effects of thickness variability during construction on the sustainability impacts. The design thicknesses were therefore considered in the analysis for the eight pavement sections. These pavement sections are not design-equivalent, since they have different critical pavement responses and pavement life expectations. However, this scenario will be used to compare the sections assuming design thicknesses.
- **Scenario #3: Comparison of newly proposed pavement sections.** Scenario three was added to the comparative analysis to consider the use of stabilized QB layers in pavement applications with low to medium levels of traffic. The proposed pavement structure consists of 3 in. (76 mm) of HMA, and 8 in. (203 mm) of base layer. For inverted pavements, 4 in. (102 mm) of base and 4 in. (102 mm) subbase layers

are assumed. Similar to Scenario #2, these pavement sections are not design-equivalent, but provide a quantification of environmental and economical impacts when lower levels of traffic are expected.

Table 8.1 Summary of pavement layer thicknesses for the three LCA scenarios

| **Sections and Scenarios for LCA** | | **Scenario #1 As-constructed pavement sections thicknesses** | | | **Scenario #2 As-designed sections** | **Scenario #3 Proposed pavement sections** |
|---|---|---|---|---|---|---|
| Section | Description* | HMA in. (mm) | Base in. (mm) | Subbase in. (mm) | 4 in. (102 mm) HMA, 12 in. (305 mm) base. For inverted pavement sections 7 and 8, base and subbase thicknesses are 6 in. (152 mm) each | 3 in. (76 mm) HMA, 8 in. (203 mm) base. For inverted pavement sections 7 and 8, base and subbase thicknesses are 4 in. (102 mm) each |
| Section 1 | Cement-stabilized [QB2 and FRAP] | 3.20 (81) | 13.36 (339) | - | | |
| Section 2 | Cement-stabilized [QB2 and FRCA] | 4.69 (119) | 11.50 (292) | - | | |
| Section 3 | Fly ash-stabilized [QB2 and FRAP] | 4.33 (110) | 12.98 (330) | - | | |
| Section 4 | Cement-stabilized QB2 | 3.94 (100) | 12.31 (313) | - | | |
| Section 5 | Cement-stabilized QB3 | 4.28 (109) | 12.53 (318) | - | | |
| Section 6 | Cement-stabilized QB2 Subbase Conventional aggregate base | 3.88 (98) | 6.00 (152) | 6.88 (175) | | |
| Section 7 | Fly-ash stabilized QB2 Subbase Conventional aggregate base | 3.38 (86) | 6.50 (165) | 5.88 (149) | | |
| Section 8 | Conventional aggregate base | 2.75 (70) | 12.13 (308) | - | | |

* Cement content = 3% by weight. Fly ash content = 10% by weight. For sections constructed with QB mixed with recycled coarse aggregates, the weight ratio is 70% QB to 30% recycled aggregates (FRAP / FRCA)

## 8.3 LCA METHODOLOGY

### 8.3.1 Goal and Scope

The goal of the study is to provide a comparative LCA to evaluate the environmental impacts of constructing flexible pavements utilizing the stabilized QB base and subbase applications. The pavement sections evaluated include the seven cement and fly ash-stabilized QB or QB mixed with coarse recycled aggregates sections evaluated in Cells 2 and 3, as well as the conventional test section used as control in the accelerated testing program. The scope of the study covers three scenarios: constructed layer thicknesses, as-designed layer thicknesses, and newly proposed layer thicknesses. The as-designed and proposed layer thicknesses account for thicker/thinner pavement structures for cases where higher/lower traffic volumes are anticipated, respectively.

### 8.3.2 System Boundaries

System boundaries define the life cycle stages that are considered in the LCA analysis, and the unit processes that are included within each stage. For pavement systems, five life cycle stages (phases) are commonly considered: materials, construction, use, maintenance/rehabilitation, and end of life (Yang, 2017). In this study, the materials and construction stages are considered for all different alternatives and scenarios. This includes impact considerations for materials acquisition, materials production, plant operations, transportation, and construction activities. The system boundaries for the analyses are presented in Figure 8.1.

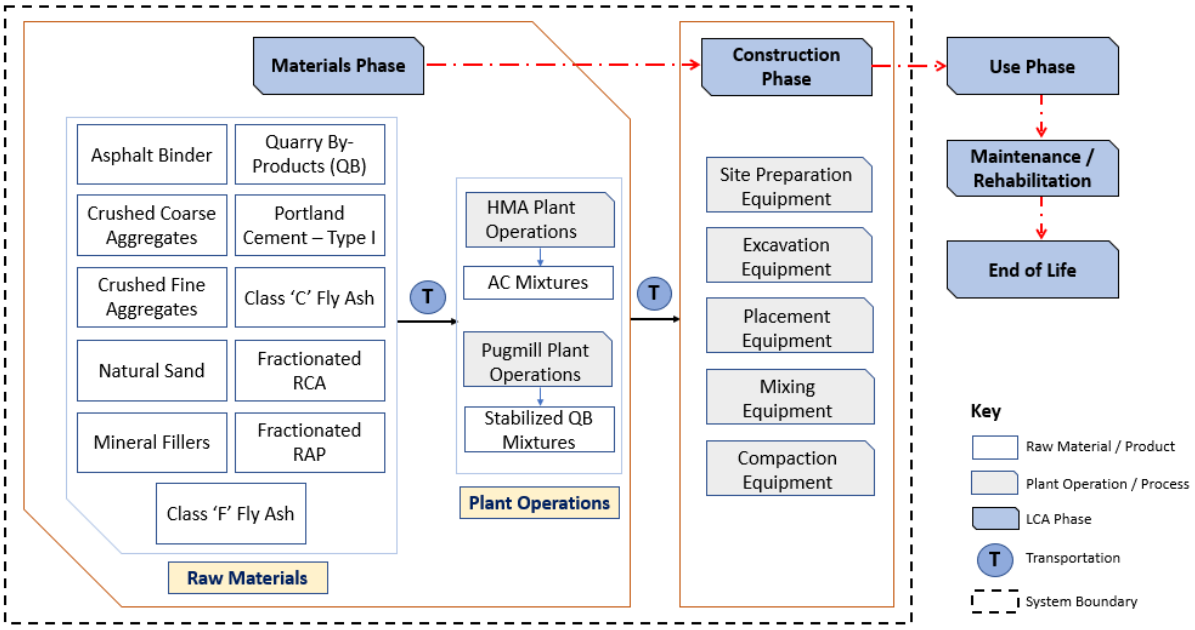


Figure 8.1 Pavement life cycle stages considered in the analysis and system boundaries

For the three scenarios considered, no sufficient historical and field data is available to assume performance in the use stage or maintenance and rehabilitation schemes. Thus, the analyses were limited to the materials and construction stages. For Scenario #1, the normalized materials and construction impacts were calculated and reported per 100,000 Equivalent Single Axle Loads (ESALs). For all three scenarios, the response benefit is reported as the ratio of the surface deflection of the conventional pavement structure (section 8) to the surface deflection of the pavement structure in consideration. The surface deflections are FWD deflections at the load drop location with the standard 9-kips (40-kN) load level. More details about the calculation of the response benefits for each pavement structure were given in Chapter 7. Note that the response benefit is an indication of the anticipated use stage performance. The impacts of the end-of-life stage, on the other hand, can be different for the pavement sections due to the differences in layer thicknesses, particularly HMA layer thickness, which can be later retrieved as RAP and reused in other construction projects.

### 8.3.3 Functional Unit

Functional unit refers to the unit used to report the normalized input and output results of conducting a LCA (Harvey et al., 2014; Harvey et al., 2016). A common functional unit used for the analyses of pavements is one-lane mile (Harvey et al., 2014). Another widely accepted functional unit is vehicle-miles travelled. The functional unit selected for this analysis is 'one-lane mile' of constructed pavement; which is deemed suitable for the LCA stages being covered by the system boundary (i.e. materials and construction stages). No analysis period was selected for this LCA since the use stage and maintenance/rehabilitation activities are not considered as part of the system boundaries. The lane width considered is 12 ft. (3.66 m) for all calculations, while the depths of the pavements vary depending on the design option being evaluated. The choice of a lane-mile functional unit allows suitable assessment of how different material types and quantities, and construction practices can affect the overall environmental impacts for each evaluated design.

### 8.3.4 LCA Data and Data Quality Requirements

All data collected for LCA are divided into primary and secondary data. Primary data refers to region- or product- specific data collected for a unit process, while secondary data covers more generic average data for the product/process being considered (Yang, 2017). ISO 14044:2006 entails that "Data quality requirements shall be specified to enable the goal and scope of the LCA to be met." Further, the data quality requirement should address the following: time-related coverage, geographical coverage, technology coverage, precision, completeness, representativeness, consistency, reproducibility, sources of the data, and uncertainty of the information.

For the purposes of this LCA, secondary data specific to the U.S. Midwest region and Illinois, when available, were collected. The data sources included: Ecoinvent Library in SimaPro (a commercial LCA software), data collected for the state of Illinois and published in public LCA reports or peer reviewed papers, nationwide statistics, as well as data from the LCI specifically collected from the previous Illinois Center of Transportation (ICT) Illinois Tollway projects and made available through research personnel at ICT (e.g. Kang, 2013; Kang et al., 2014; Ozer et al., 2014; Al-Qadi et al., 2015). Some regionalized primary data for the productivity rates of construction activities were also collected by contacting local contractors in the state of Illinois. The data quality requirements for ISO 14044 are thus met for this LCA analysis.

### 8.3.5 Allocation

According to FHWA, allocation is commonly used when Recycled, Co-product, and Waste Materials (RCWMs) are produced or used (Harvey et al., 2014). Allocation is used to distribute the environmental impacts of a product or a system. Allocation is deemed necessary in this study since many of the raw materials are by-product or recycled materials, and since many of the construction materials are produced during multi-output processes. For

example, quarry by-products and fly ash are by-products of aggregate production and coal combustion, respectively. FRAP and FRCA are recycled materials produced from the demolition of pavements and structures. Commonly used end-of-life allocation criteria used for pavement LCA include (Van Dam et al., 2015):

- Cut-off Method (recycled content method): The benefits of using a recycled or by-product material in a product/process are assigned to the product/process that utilize the recycled material.
- Substitution method: The benefits are assigned to the product/process that produced the recycled or by-product material.
- 50/50 method: Half of the benefits are allocated to the product/process that uses the recycled or by-product material, while the other half is allocated to the process that produced it.

For the purposes of this LCA, allocation was avoided when possible, and was used only for materials produced from multi-output processes (i.e. multi-output allocation) and for recycled and by-product materials. For QB, allocation was based on mass, and the impacts of producing one ton of QB was assumed similar to those of producing one ton of coarse aggregates. These impacts have been compiled from the previous ICT Tollway projects (Kang et al., 2014; Ozer et al., 2017). For the other recycled and by-product materials (i.e. FRAP, FRCA, and fly ash), a cut-off allocation criterion is assumed. Thus, the only burdens that are considered for these materials are attributed to materials processing and handling during plant operations and construction. Conducting a sensitivity analysis for considering different types of allocation is not considered in the scope of the conducted LCA study.

### 8.3.6 Impact Categories

The primary purpose of conducting this pavement LCA is to evaluate the environmental impacts resulting from decisions for materials use and construction practices. Thus, the evaluation was performed in accordance to a set of metrics that evaluate the environmental burdens. For the purpose of this comparative LCA, the Tool for the Reduction and Assessment of Chemical and other environmental Impacts (TRACI), which was developed by the Environmental Protection Agency (EPA) and used for environmental impact categories was considered as the metrics for LCA decision making (Bare, 2011; Bare, 2012). The TRACI impact assessment methods that were considered for the unit processes are:

- Emissions: primarily Global Warming Potential (GWP), in units of kg $CO_2$ equivalent. Emissions were quantified for each unit process, such as asphalt mixture production, Portland cement production, materials hauling and transportation, placing and construction operations.
- Other TRACI emissions were also calculated and tabulated for each performed LCA. These emissions are ozone depletion, smog, acidification, eutrophication (excessive enrichment of water bodies with nutrients), carcinogenics, non-carcinogenics, respiratory effects, ecotoxicity, and fossil fuel depletion.

Another metric used to compare the sustainability of the evaluated pavement sections in the different scenarios is the Total Energy Demand (TED), in units of Mega Joules (MJ). For simplicity, the performed LCAs considered reporting one value for total energy demand, which includes both renewable and nonrenewable primary and secondary energy demands. Energy used as fuel and non-fuel energy (feedstock energy) are reported as a single metric for all conducted LCAs. Feedstock energy is not commonly reported for comparative studies between flexible and rigid pavements. Since the three scenarios studied deal primarily with flexible pavements, the feedstock energy (i.e. intrinsic energy value of an organic material not used as an energy source) was reported.

### 8.3.7 Limitations and Assumptions

One of the main limitations for the conducted life cycle assessments was relying on secondary data sources to perform the comparative LCAs. Primary data from project-specific locations were not collected due to lack of access to reliable sources and time/cost limitations. Additionally, the variable thicknesses in pavement layers, particularly that of HMA layer, produces high variability and uncertainty for the end of life stage, which was not considered in the system boundaries due to the unknown demand for pavement materials at the end of life. Additionally, a sensitivity analysis that considers other allocation methods is ideally required to compare the effects of the allocation method on the environmental burdens. The cut-off allocation method was only considered to account for the use of recycled and by-product materials. These limitations shall be considered for a more thorough analysis.

## 8.4 DEVELOPMENT OF LIFE CYCLE INVENTORY DATABASE

Data collected included data for materials production, materials processing, plant operations, transportation, and construction activities. Data for unit processes and the accompanying Environmental Product Declarations (EPDs) were collected from various sources. The Life Cycle Inventory (LCI) data were mostly secondary data obtained from modeling the unit processes in SimaPro commercial LCA software, particularly using data from its ‘Ecoinvent’ library. The advantages of SimaPro are that it accounts for the impacts of all upstream processes, and it provides detailed emissions and energy usage records (Yang, 2014; Yang, 2017). \

### 8.4.1 Raw Materials and Fuels

Secondary LCI data sources were generally used to compile the TRACI impacts and energy demand for the raw materials and fuels (energy flows) required for the materials and construction stages of the conducted LCAs. The unit processes for raw materials and fuels, measurement units, and data sources are presented in Table 8.2.

Table 8.2 Summary for secondary data sources for raw materials, fuels, and hauling

| Unit Processes | Measuring Unit | LCI Data Source |
|---|---|---|
| **Raw materials** | short ton | ICT Tollway Database [(1)] |
| Coarse Crushed Aggregates | | |
| Fine Crushed Aggregates | | |
| Fine Natural Aggregates | | |
| Quarry By-Products | | |
| Portland Cement (Type I) | | |
| Fly Ash (Class F) | | |
| Fly Ash (Class C) | | |
| AC Binder, PG 64-22 | | |
| FRCA | | |
| FRAP | | |
| Water | | |
| Tack coat | | |
| Prime coat | | |
| **Fuels** | | |
| Electricity Generation | kWh | eGRID [(2)] |
| Natural Gas Combustion | $ft^3$ | U.S. LCI [(3)] |
| Diesel burned in machinery | MJ | Ecoinvent 3 [(4)] |
| **Transportation** – Truck hauling | short ton.mile | Kang et al. (2018) |

(1) Ozer et al., 2017; and Kang et al., 2014
(2) Emissions & Generation Resource Integrated Database (eGRID) 2010 [Software]
(3) U.S. Life Cycle Inventory Database. (2012)
(4) EarthShift. (2013). US-Ecoinvent database. Version 2.2. [database]

### 8.4.2 Plant Operations

Plant operations refer to the activities and processes required to transform raw materials and fuels into final pavement products. Two types of plant operations are considered for this LCA study: (1) Asphalt plant operations involved in producing HMA mixes, and (2) plant operations involved in producing stabilized QB aggregate mixes through a batch pugmill process.

8.4.2.1 Asphalt Plant Operations

The main inputs for asphalt plant operations are divided into two categories: materials and fuels. Materials include aggregates (coarse and fine, virgin and recycled, crushed and natural), asphalt binder, and mineral fillers. The energy inputs for an asphalt plant are mainly electricity from grid or from generators, burning of natural gas in the drums for heating aggregates, and diesel used in construction equipment in the plant. Emissions and environmental impacts contributing to the life cycle assessments stem from the upstream processes involved in materials and fuels production, the burning of various types of fuels during plant operations, as well as the transportation of materials and fuels to the asphalt plant prior to and during the production of the asphalt mix.

For the purpose of the conducted LCA, two asphalt mix designs were used: one surface course mix, and one binder course mix. For LCA scenario # 1 involving the constructed pavement sections, only the surface coarse mix design was used for the 4 in. (102 mm) thick HMA layer. For pavement sections in scenarios #2 and #3, the surface course included a 0.5-in. (12.5 mm) Nominal Maximum Aggregate Size (NMAS) used for the top layer, and the binder course mix had a 1.0 in. (25 mm) NMAS used for the bottom layer. The HMA thickness was divided equally between the two mixes, i.e. for each HMA mix, 2 in. (50 mm) for scenario #2 and 1.5 in. (38 mm) for scenario #3.

Note that the surface course is the most expensive mix with the finest aggregate gradations and the highest binder content, while the binder course mix has lower binder content, and a larger NMAS mix. The details for the two mix designs are given in Table 8.3 and Table 8.4. The aggregate gradations for the mixes are presented in Table 8.5. The mix design for the surface course (Table 8.3) is identical to the one that was constructed in the field evaluation study detailed in the previous chapters.

Table 8.3 HMA mix design for the surface course mix*

| **Material** | **Source city in Illinois** | **Weight in total mix (%)** | **Weight lb./US sh ton (kg/ton)** |
|---|---|---|---|
| Crushed coarse aggregates | Manteno | 50.7 | 1014.48 (507.2) |
| Crushed fine aggregates | Manteno | 11.4 | 227.55 (113.8) |
| Natural sand | Paxton | 16.1 | 322.36 (161.2) |
| Mineral filler (fly Ash class F) | Decatur | 2.4 | 47.41 (23.7) |
| RAP (5% binder content) | Rantoul | 14.2 | 284.43 (142.2) |
| Asphalt binder (PG 64-22) | Urbana | 5.2 | 103.78 (51.9) |
| | **Sum** | **100.0 %** | **2000.0 lbs. (1000 kg)** |

Total Binder Content (by Weight of aggregate) = 5.9%, and the theoretical maximum specific gravity ($G_{mm}$) = 2.484

* This mix design is used for the full HMA depth for LCA scenarios #1 and #2

Table 8.4 HMA mix design for the binder course mix

| Material | Source city in Illinois | Weight in total mix (%) | Weight lb./US sh ton (kg/ton) |
|---|---|---|---|
| Crushed coarse aggregates | Manteno | 57.3 | 1146.93 (573.5) |
| Crushed fine aggregates | Manteno | 14.3 | 286.73 (143.4) |
| Natural sand | Paxton | 13.4 | 267.62 (133.8) |
| Mineral filler | Decatur | 1.0 | 19.12 (9.6) |
| RAP (5% binder content) | Rantoul | 9.6 | 191.16 (95.6) |
| Asphalt binder (PG 64-22) | Urbana | 4.4 | 88.44 (44.2) |
| | **Sum** | **100.0 %** | **2000.0 lbs. (1000 kg)** |

Total Binder Content (by Weight of aggregate) = 4.9%, and the theoretical maximum specific gravity ($G_{mm}$) = 2.559

Table 8.5 Aggregate gradations and tolerances for the various HMA mix designs

| Sieve Sizes | | Surface Course Mix | | Binder Course Mix | |
|---|---|---|---|---|---|
| **Sieve Size (in.)** | **Sieve Size (mm)** | **Total % Passing (%)** | **Tolerance (% + or -)** | **Total % Passing (%)** | **Tolerance (% + or -)** |
| 1 ½ in. | 37.5 | 100 | 0 | - | - |
| 1 in | 25 | 96 | 2.8 | 100 | 0 |
| ¾ in. | 19 | 84 | 2.8 | 97 | 2.8 |
| ½ in. | 12.5 | - | - | 86 | 2.8 |
| 3/8 in. | 9.5 | - | - | - | - |
| #4 | 4.75 | - | - | - | - |
| #8 | 2.36 | 34 | 2.8 | 30 | 2.8 |
| #16 | 1.18 | - | - | - | - |
| #30 | 0.600 | - | - | - | - |
| #50 | 0.300 | - | - | - | - |
| #100 | 0.150 | - | - | - | - |
| #200 | 0.075 | 5.6 | 0.7 | 5.5 | 0.7 |
| **Asphalt** | **A.C.** | **4.5** | **0.21** | **4.9** | **0.21** |

Based on the raw materials utilized for producing each mix design, and the energy requirements for asphalt plant operations, the GWP and TED due to production of 1 short ton (0.91 tons) are presented in Figure 8.2 along with aggregate courses. The surface course has the highest impact per ton due to the higher asphalt binder content.

#### 8.4.2.2 Plant Operations for Producing Stabilized QB Mixes

For the purposes of constructing the chemically stabilized QB test sections for the APT study, a simple and practical on-site mixing technique was used to prepare the QB and the QB blends with the stabilizing agent and water. The mixing method involved using a front loader to proportion and prepare the mix, and a soil tiller to thoroughly mix the materials upon placement. This mixing method was deemed suitable for the small quantities of

materials prepared for the APT full-scale sections. However, for a large-scale construction project comprising miles of pavements, a faster, more reliable, automated and consistent method for preparing the chemically stabilized QB mixes is deemed necessary. The guide to cement-treated base published by the Portland Cement Association (PCA) recommends two construction methods for large-scale projects: a mixed in place method using a single shaft travelling mixing equipment, and a central plant mixing method using a twin-shaft pugmill mixing equipment (Halsted et al., 2006).

Central mixing plants can use various methods to prepare soil cement mixtures, such as continuous flow pugmills, batch-type pugmills, and rotary drum mixers (Halsted et al., 2006). The use of pugmills for soil and aggregate stabilization has been widely investigated in literature (Sugi et al., 1993; Bass, 2000; Mohammad et al., 2000; Mohammad et al., 2003). For the purpose of providing more uniform mixes and a more sustainable construction practice, a central plant mixing method was considered for all environmental impacts (LCA) and cost (LCCA) calculations. A batch pugmill operation has been selected for the preparation of chemically stabilized QB mixes. Several models of batch-type pugmills have been investigated, including a PM100-SG portable pugmill plant model that has an output of 100 tons per hour. Based on the reduced production capacity (80 tons per hour) and the horsepower of the electric motors used for the pugmill, conveyor belts, and water feeding system, a 0.27 kWh per short ton (0.3 kWh/ton) electricity consumption was estimated for each ton material produced. In addition, a front loader R/T Cat 914 is needed to transport materials to the pugmill, which has an hourly fuel consumption of 3 gallons per hour (3.79 liter per hour) (Skolnik et al., 2013). The total impacts of plant operations for the chemically stabilized QB materials considered environmental impacts from both electricity and equipment usage.

Table 8.6 presents the mix designs for the chemically stabilized QB sections including QB mixed with recycled coarse aggregates, and the conventional coarse aggregates sections. These mix designs were based on a weight mix ratio of 70% QB and 30% recycled coarse aggregates, and a stabilizer percentage of 3% or 10% for cement and class ‘C’ fly ash, respectively. The quantity of water was excluded from the percentage weight of total mix (i.e. weight of QB, FRAP/FRCA, and stabilizing agent). This quantity was calculated based on the optimum moisture contents previously presented for each material combination in Chapter 3.

Table 8.6 Mix designs for the chemically-stabilized QB sections and the conventional aggregate material

| Section | Material | Source city in Illinois | Weight in total mix (%) | Weight lb./sh ton (kg/ton) |
|---|---|---|---|---|
| **Section 1** | QB2 | Fairmount | 67.96 | 1359.22 (679.6) |
| | FRAP | Urbana | 29.13 | 582.52 (291.3) |
| | Cement | Champaign | 2.91 | 58.25 (29.1) |
| | Water | Rantoul | | 160.0 (80.0) |
| **Section 2** | QB2 | Fairmount | 67.96 | 1359.22 (679.6) |
| | FRCA | Urbana | 29.13 | 582.52 (291.3) |
| | Cement | Champaign | 2.91 | 58.25 (29.1) |
| | Water | Rantoul | | 150.0 (75.0) |
| **Section 3** | QB2 | Fairmount | 63.64 | 1272.73 (634.4) |
| | FRAP | Urbana | 27.27 | 545.45 (272.7) |
| | Fly ash | Champaign | 9.09 | 181.82 (90.9) |
| | Water | Rantoul | | 196.0 (98) |
| **Section 4** | QB2 | Fairmount | 97.09 | 1941.75 (970.9) |
| **Section 6 (subbase)** | Cement | Champaign | 2.91 | 58.25 (29.1) |
| | Water | Rantoul | | 182.0 (91.0) |
| **Section 5** | QB3 | Fairmount | 97.09 | 1941.75 (970.9) |
| | Cement | Champaign | 2.91 | 58.25 (29.1) |
| | Water | Rantoul | | 168 (84.0) |
| **Section 7 (subbase)** | QB3 | Fairmount | 90.91 | 1818.18 (909.1) |
| | Fly ash | Champaign | 9.09 | 181.82 (90.9) |
| | Water | Rantoul | | 160.0 (80.0) |
| **Section 6 (base)** | Coarse aggregates* | Fairmount | 100.0 | 2000.00 (1000.0) |
| **Section 7 (base)** | water | Rantoul | | 108.0 (54.0) |
| **Section 8** | | | | |

* Base coarse aggregates are not processed at the central plant, and are directly transported to the construction site

The total impacts of producing 1 short ton (0.91 tons) for each material combination are presented in Figure 8.2. For HMA and stabilized QB sections, the presented impacts account for raw materials acquisition and plant operations, while the impacts for conventional base course material account only for materials acquisition. The materials involved in constructing the QB test sections can be broadly divided into three categories: (1) materials with high GWP and TED, i.e. HMA layers, (2) materials with high GWP and intermediate TED, i.e. cement-stabilized QB materials, and (3) materials with low GWP and low TED, i.e. fly ash-stabilized QB materials as well as conventional base course aggregate materials.

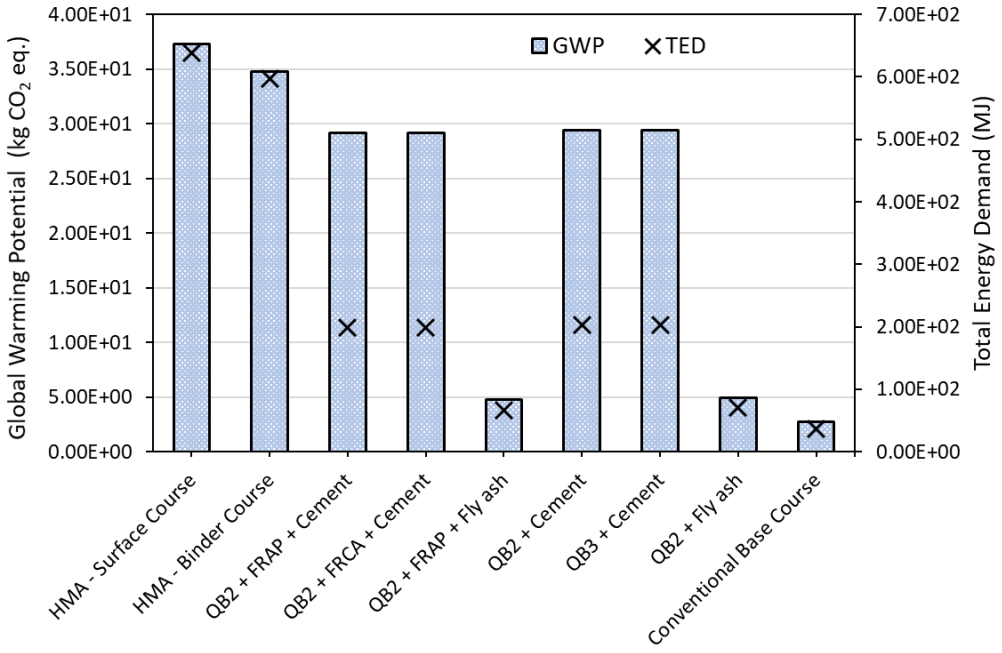


Figure 8.2 GWP and TED for producing 1 short ton (0.91 metric tons) of various material combinations

### 8.4.3 Transportation

Life cycle impacts for hauling/transportation were considered for both materials and construction stages. For raw materials production, the impacts of transportation were factored in the upstream processes and included in the unit processes modeled by SimaPro for each material individually. The impact of materials hauling was reported separately for the transportation of the raw materials to (and within) the operation plants and the construction site. Reasonable hauling distances were assumed for each material, and a Variable Impact Transportation (VIT) model was utilized to calculate the environmental impacts and energy demand for truck hauling operations (Kang et al., 2018). The model considers truck operational parameters such as the payload, roadway grade (assumed 0%), temperature (75℉ or 24 ℃), relative humidity (50%), truck speed (60 mph or 75 kmph), and the construction year (2018). The values assumed for each parameter were given above between parentheses; the impact per truck-mile is given by the following equation (Kang et al., 2018):

$$\text{Impact}_k\ (\text{per truck} \cdot \text{mi}) = \frac{\alpha_1 W + \alpha_2 G + \alpha_3 T + \alpha_4 RH + \alpha_5 v^2}{1 + e^{(\beta_1 + \beta_2 v^{\beta_3} + \beta_4 G + \beta_5 t^{\beta_6})}} \quad \text{(Equation 8.1)}$$

where

W is the truck payload (metric tons);

G is the grade (%);

T is the temperature (°F), T≥ 60°F;

RH is the relative humidity (%);

$v$ is the truck speed (mph);

t is the year of hauling, t = 1 for 2014, t = 2 for 2015, and increases by one each year; and

$\alpha_i$ , $\beta_i$ are the model coefficients, (see Kang et al., 2018)

### 8.4.4 Construction

Construction is one of the most critical activities for pavements that can govern performance and life span. High quality construction can ensure good pavement performance throughout design life, and can reduce variability due to poor construction practices. This section presents the construction activities that are considered in the LCA system boundaries, and the methodology for determining equipment types, production rates and fuel consumption per unit of construction.

The data for construction activities, equipment inventories and fuel consumption were obtained from the recent NCHRP study involved in estimating fuel usage factors for highway and bridge construction (Skolnik et al., 2013). The construction activities considered are: (1) site preparation, (2) subgrade preparation, (3) placement and compaction of conventional and chemically stabilized subbase and base layers, and (4) placement and compaction of the HMA layers. For site preparation, a new construction where trees and plant removals are needed is included. For subgrade preparation, the quantities of excavation and grading varied depending on the total pavement thickness. The construction activities involved in the construction of the conventional and the chemically-stabilized sections are assumed essentially the same, since the difference is mainly in the plant operations.

The construction activities and the inventory for equipment were compiled for the different construction activities as summarized in Table 8.7. For each construction activity, the productivity rates were compiled based on the equipment inventory. Fuel consumption rates in gallons were also compiled for each construction activity for the representative productivity units. The main source of productivity rates and fuel consumption is the NCHRP report for fuel usage factors by Skolnik et al. (2013). Note that the fuel consumption and productivity rates assume that the equipment inventory for each activity is followed closely. Further, primary data for the production rates for some of the construction activities were compiled from local sources in Illinois. The primary local data were mostly similar to the data reported by Skolnik et al. (2013), but was not completed for all construction activities, and was thus not used/reported for the purposes of this dissertation.

Table 8.7 Summary of construction activities, production rates, and fuel usage rates*

| Activities | Production Rate | Equipment | Fuel Usage |
|---|---|---|---|
| Site Preparation Clearing - Medium | 0.175 acre/hr. (708 $m^2$/hr.) | Truck ½ ton (1), Dozer D-5 (1), Excavator Cat 336 (1), Tub Grinder (1) | 171.459 Gallons/Acre (160.4 liters / Dunam) |
| Subgrade Preparation Grading - Dirt - Off Road - Short Haul | 215.32 C.Y./hr. (164.6 $m^3$/hr.) | Truck ½ ton (1), Water Truck (0.5), Dozer D-7 (1), Articulated Haul Truck- 25 Ton (2), Excavator Cat 345 (1), Motor Grader Cat 12 (0.5), Roller 815 Soil Compactor (1) | 0.263 Gallons/C.Y. (1.302 liters/$m^3$) |
| Subgrade Preparation Strip Topsoil | 120 C.Y./hr. (91.7 $m^3$/hr.) | Truck ½ ton (1), Dozer D-5 (1), Scraper 621 (1) | 0.167 Gallons/C.Y. (0.827 liters/$m^3$) |
| Base Stone Construction Stabilized QB Construction | 217 sh. ton/hr. (196.9 ton/hr.) | Truck ½ ton (1), Dump Truck - 14 CY (10), Water Truck (1), Dozer D-5 with Spreader Box (1), Motor Grader Cat 14 with GPS (1), Roller Tampo 25-35 Ton (1) | 0.406 Gallons/sh. ton (1.693 liters/ton) |
| HMA Layers Construction Hot Mix Asphalt - Structural (Binder) Course (0-5 mile haul) | 200.06 ton/hr. (181.5 ton/hr.) | Truck ½ ton (1), Truck Distributor (1), Dump Truck-14 CY (6), Water Truck (1), Asphalt Roller - Breakdown (1), Asphalt Roller - Finish (1), Asphalt Roller - Rubber Tire (1), BlawKnox PF3200 Asphalt Paver (1), RoadTec Shuttle Buggy (1), Asphalt Plant (1) | 0.58 Gallons/sh. ton (2.42 liters/ton) |
| HMA Layers Construction Hot Mix Asphalt - Surface Course (0-5 mile haul) | 150 ton/hr. (136.1 ton/hr.) | Truck ½ ton (1), Truck Distributor (1), Dump Truck-14 CY (6), Water Truck (1), Asphalt Roller - Breakdown (1), Asphalt Roller - Finish (1), Asphalt Roller - Rubber Tire (1), BlawKnox PF3200 Asphalt Paver (1), RoadTec Shuttle Buggy (1), Asphalt Plant (1) | 0.77 Gallons/sh. ton (3.214 liters/ton) |
| HMA Layers Construction Hot Mix Asphalt - Leveling Course (0-5 mile haul) | 130 ton/hr. (117.9 ton/hr.) | Truck ½ ton (1), Truck Distributor (1), Dump Truck-14 CY (6), Water Truck (1), Asphalt Roller - Breakdown (1), Asphalt Roller - Finish (1), Asphalt Roller - Rubber Tire (1), BlawKnox PF3200 Asphalt Paver (1), RoadTec Shuttle Buggy (1), Asphalt Plant (1) | 0.892 Gallons/sh. ton (3.72 liters/ton) |

* This table is reproduced after Skolnick et al. (2013), by compiling data from several tables from the original NCHRP report

## 8.5 LCA FOR SCENARIO #1: AS-CONSTRUCTED PAVEMENT SECTIONS

This section discusses the Life Cycle Impact Assessment (LCIA) for the first LCA scenario, which involves the as-constructed pavement sections. LCIA is the phase in which the results of the inventory analysis are further processed and interpreted for environmental burdens and energy demand. The Global Warming Potential and total energy demand are the two main inventory metrics being compared for the eight constructed test sections in Cells 2 and 3.

All results are reported for the construction of one, 12-ft. (3.66 m) wide lane mile of pavement structure. Note that the constructed test sections in Cells 2 and 3 were not designed to be structurally-equivalent and are thus expected to have different pavement performance and life expectancies. Different performance, i.e. variable rut accumulation and different rut rates were indeed observed during field evaluation. This section provides a comparison of the environmental impacts of the constructed pavement sections, and a normalized impact assessment based on the traffic levels (i.e. ESALs) that can be sustained by each section until failure. The failure criterion is defined as the accumulation of 0.5 in. (12.5 mm) of surface rutting. Further, the response benefit is also calculated for each pavement structure, based on resilient FWD deflections, with the conventional section (C3S4) taken as a reference. Note that the response benefit is an underestimation of the expected benefits of using the QB applications since it reports a linear ratio of deflections, while performance generally varies as a power function, i.e. exponentially, of measured/calculated responses.

The global warming potential and the total energy demand for the compared pavement sections are presented in Figure 8.3 and Figure 8.4. For both GWP and TED, the pavement section with the conventional aggregate base (i.e. C3S1) had the lowest environmental impacts, followed by the sections constructed with fly ash-stabilized QB subbase (C3S3) and base (C2S3), respectively. The major difference in GWP impact among the eight test sections is stemming from the contribution of base and subbase materials since thicknesses of HMA layers in each section was similar. Specifically, the test sections comprising a cement-stabilized QB base/subbase had significantly higher impacts than those having conventional or fly-ash stabilized base materials. This was largely due to the high $CO_2$ emissions associated with the production of cement. The same trends and observations can also be made for the total energy demand.

The differences in the GWP and TED for HMA materials are mainly due to the variation of the average HMA thickness in the constructed test sections. The sections constructed with thicker HMA have higher impacts. Additionally, it is noted that the transportation and construction activities have relatively similar impacts for GWP and TED for the different test sections, the main discrepancies in impacts between the different test sections are largely attributed to materials production and plant operations. The GWP impacts of pavements constructed with a cement-stabilized QB base (i.e. C2S1, C2S2, C2S4, and C3S1) are about two to two and a half times higher than those of the pavements constructed with conventional aggregates, while the TED are about one and a half to two times higher for the same test sections. The impacts are only provided for the materials production and construction stages excluding use-stage, maintenance and rehabilitation and end-of-life stages. When a complete system

boundary is considered for each section with varying design traffic or performance period; some of these higher impacts may be subsidized or eliminated by lower excess fuel consumption in the use stage and less demanding maintenance and rehabilitation schedules. The reported response benefits are an indication for such subsidization/elimination of the initial impacts due to materials and construction (see Figure 8.3 and Figure 8.4). Another option to incorporate the expected performance of the as-constructed sections is to normalize impacts by design traffic over the service life.

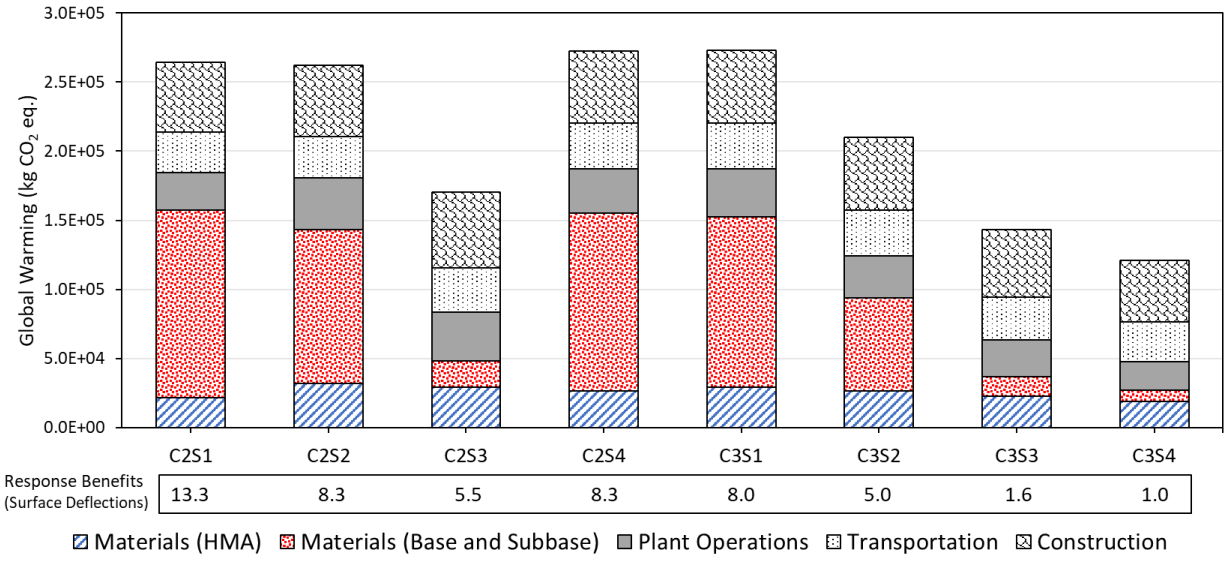


Figure 8.3 Comparisons of the global warming potential for the eight alternative designs – Scenario #1

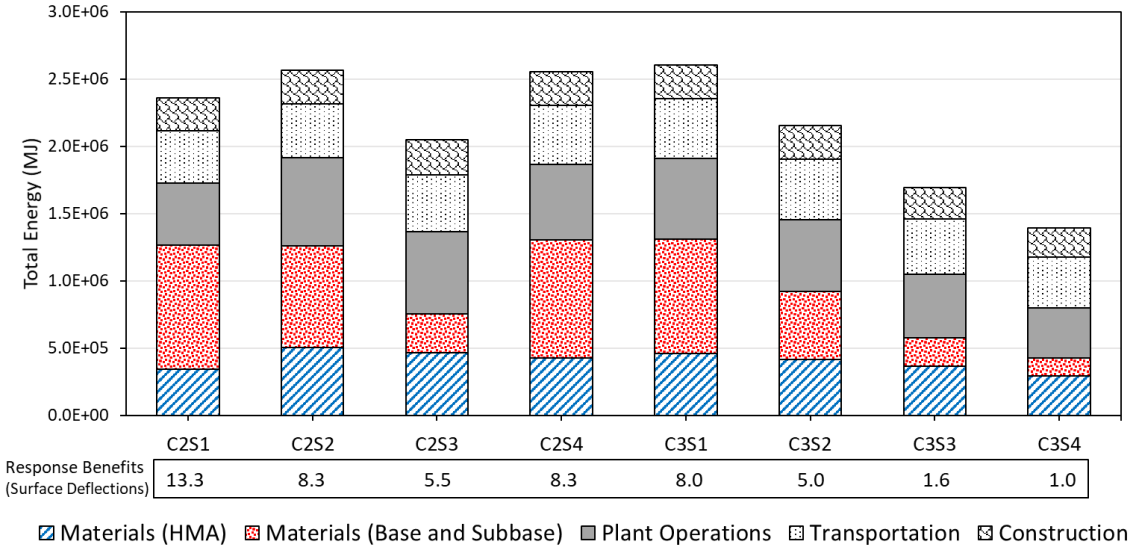


Figure 8.4 Comparisons of the total energy demand for the eight alternative designs – Scenario #1

Following the determination of the environmental impacts associated with the construction of each test section, an analysis was performed to determine the normalized impacts of each constructed test section based on performance. Since data on rutting accumulation was established as the data collected from accelerated pavement testing, the number of ATLAS wheel passes required to accumulate a 0.5-in. (12.5-mm) rutting was extrapolated for this analysis. The extrapolation was based on a piecewise regression to fit each portion of the rutting curve for each pavement section with a best fit regression equation. For all stabilized QB test section, a linear fit of the rutting data between 30,000 and 100,000 passes was adequate (see coefficient of determination values in Table 8.8, which ranged between 0.946 and 0.986). The equations of the linear fit were then used determine the number of passes required for a 0.5-in. (12.5-mm) failure criterion. The results are presented in Table 8.8, which also lists the equivalent number of ESALs associated with the failure surface rut depth. ESALs calculations were presented previously in Chapter 5 (see Table 5.1). For C3S4, the field rutting data were collected, and the number of ATLAS load repetition to accumulate 0.5 in. (12.5 mm) of rutting was estimated as 56,219 passes. The GWP and TED results can thus be normalized to determine the GWP and TD impacts of the materials and construction stages per 100,000 ESALs trafficked.

Table 8.8 Number of ATLAS load repetitions and ESALs for 0.5 in (12.5 mm) surface rut depth

| Section | Rutting Equation* | Coef. Of Determination ($R^2$) | No. of ATLAS Passes for 0.5 in (12.5 mm) rutting | Equivalent No. of ESALs |
|---|---|---|---|---|
| C2S1 | 1.051E-5 P + 0.647 | 0.984 | 1,127,772 | 1,702,935 |
| C2S2 | 7.712E-6 P + 0.812 | 0.972 | 1,515,486 | 2,288,386 |
| C2S3 | 2.819E-5 P + 3.051 | 0.986 | 335,179 | 506,120 |
| C2S4 | 2.307E-5 P + 1.664 | 0.965 | 469,694 | 709,238 |
| C3S1 | 1.005E-5 P + 2.045 | 0.946 | 1,040,277 | 1,570,819 |
| C3S2 | 1.416E-5 P + 2.842 | 0.959 | 682,032 | 1,029,868 |
| C3S3 | 2.201E-5 P + 2.928 | 0.956 | 434,896 | 656,693 |
| C3S4 | APT rutting data available | | 56,219 | 84,891 |

* 'P' stands for the number of ATLAS load repetitions

The normalized GWP and TED impacts for each test section, calculated for each 100,000 ESALs, are shown in Figure 8.5. The TED is presented on a logarithmic scale. The total environmental impacts are shown to include impacts from materials acquisition, plant operations, transportation and construction. Based on the total impacts calculated for constructing each test section and the performance data collected for each test section, the lowest impacts were calculated for C2S1 and C2S2 constructed with cement-stabilized QB mixed with FRAP and FRCA. Significantly higher GWP and TED impacts were calculated for C3S4, largely due to the low number of passes to failure for that section, which might have resulted from the poor performance of as-constructed control section with lower thickness of HMA layer than its intended design and its high porosity. Additionally, the two sections constructed with fly ash-stabilized QB bases/subbases (i.e. C2S3 and C3S3) accumulated higher GWP and

TED impacts when compared to the cement-stabilized QB section (excluding section C2S4). The normalized impacts imply that the high environmental impacts associated with cement to stabilize QB layers can be balanced or eliminated when pavement performance and expected pavement life are taken into considerations. According to the normalized results with actual performance during the APT, the sections with cement stabilization can be considered as the most environmentally and economically effective.

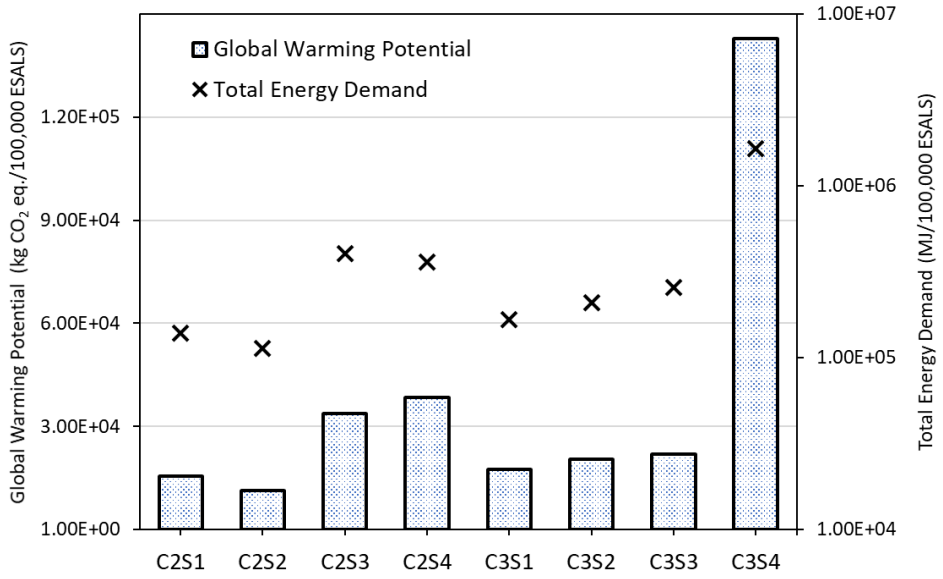


Figure 8.5 Normalized GWP and TED for each 100,000 ESALs trafficking each pavement section – Scenario # 1

The contributions of each life cycle stage/activity to the GWP and TED for each of the constructed pavement test sections in Cell 2 and Cell 3 are presented in Figure 8.6 and Figure 8.7, respectively. The life cycle stage contributing to the highest impacts varies depending on the pavement section and materials used. For global warming potential, the activity with the highest weighted impact for sections constructed with cement-stabilized QB or QB mixed with coarse recycles aggregates is the stabilized base material; totaling between 44% and 50% for sections C2S1, C2S2, C2S4, and C3S1. On the other hand, for sections with conventional aggregates or fly ash-stabilized base/subbase, the highest impacts are attributed to the construction stage; ranging between 33% and 37% for sections C2S3, C3S3, and C3S4. On the other hand, the highest TED contribution to the environmental impacts can be attributed to the base/subbase materials or the plant operation stages for all eight test sections.

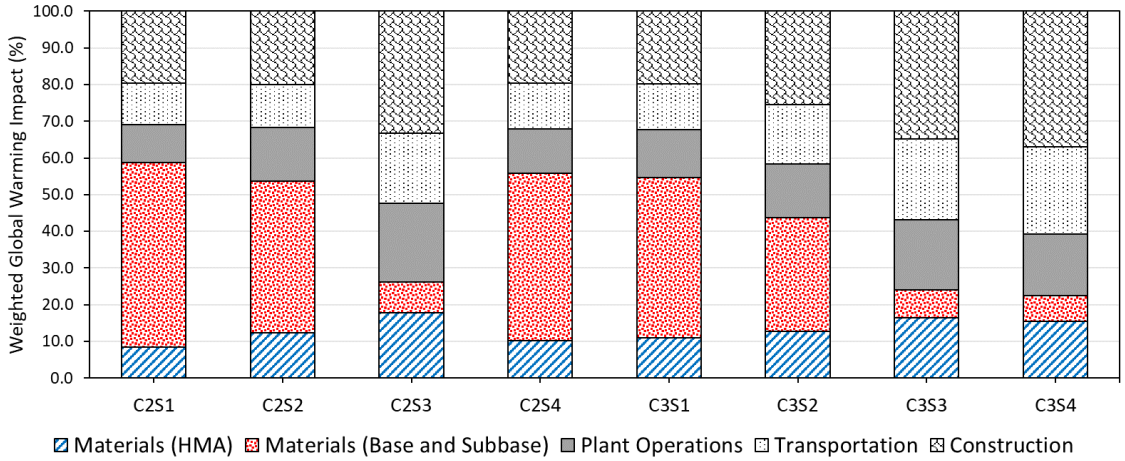


Figure 8.6 Breakdown contribution of each life cycle stage to the GWP – Scenario # 1

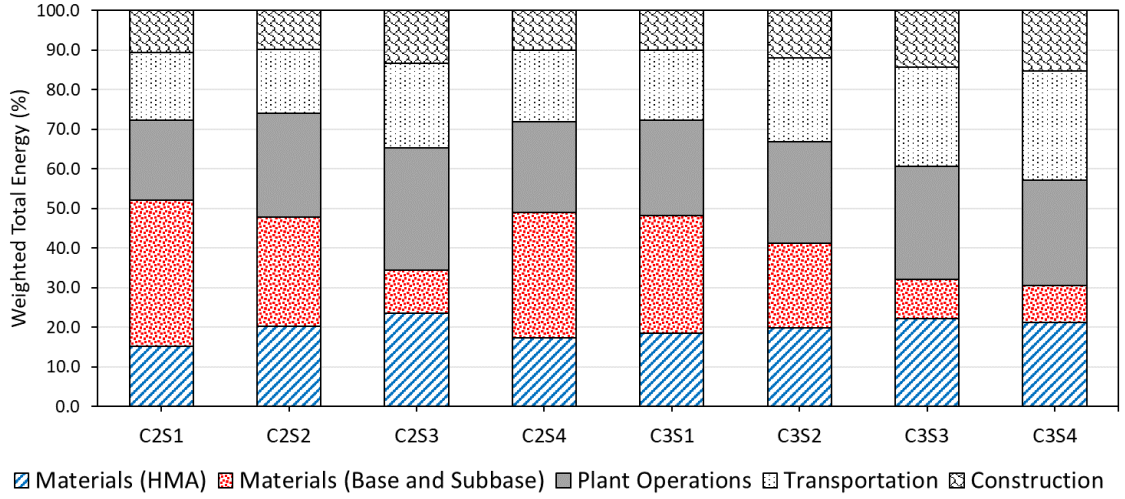


Figure 8.7 Breakdown contribution of each life cycle stage to the TED – Scenario # 1

The remaining nine TRACI impact categories are summarized below in Table 8.9 for all pavement sections. Note that these impacts are the total impacts for constructing each test section, and are not the normalized impacts. These impact categories are: ozone depletion, smog, acidification, eutrophication, carcinogenics, non-carcinogenics, respiratory effects, ecotoxicity, and fossil fuel depletion. The trends for these TRACI impact categories follow, for the most part, the trends that were discussed for GWP and TED. The impact categories are shown color-coded for comparison purposes; where green color indicates the lowest impacts and red indicates the highest values in each impact category.

Table 8.9 Summary of the remaining impact categories for all test sections – Scenario #1

| Section | Ozone depletion kg CFC-11 eq | Smog kg O3 eq | Acidification kg SO2 eq | Eutrophication kg N eq | Carcinogenics CTUh | Non-carcinogenics CTUh | Respiratory effects kg PM2.5 eq | Ecotoxicity CTUe | Fossil fuel depletion MJ surplus |
|---|---|---|---|---|---|---|---|---|---|
| **C2S1** | 2.71E-02 | 3.29E+04 | 1.64E+03 | 1.64E+02 | 4.89E-03 | 3.83E-02 | 2.08E+02 | 6.27E+05 | 6.67E+05 |
| **C2S2** | 2.90E-02 | 3.22E+04 | 1.71E+03 | 1.65E+02 | 6.00E-03 | 4.99E-02 | 2.11E+02 | 8.74E+05 | 8.71E+05 |
| **C2S3** | 2.90E-02 | 3.03E+04 | 1.46E+03 | 1.48E+02 | 5.34E-03 | 4.15E-02 | 2.19E+02 | 8.21E+05 | 8.26E+05 |
| **C2S4** | 2.90E-02 | 3.42E+04 | 1.75E+03 | 1.72E+02 | 5.50E-03 | 4.44E-02 | 2.39E+02 | 7.52E+05 | 7.79E+05 |
| **C3S1** | 2.96E-02 | 3.43E+04 | 1.77E+03 | 1.73E+02 | 5.77E-03 | 4.71E-02 | 2.40E+02 | 8.10E+05 | 8.27E+05 |
| **C3S2** | 2.74E-02 | 3.06E+04 | 1.52E+03 | 1.50E+02 | 5.09E-03 | 4.03E-02 | 2.33E+02 | 7.35E+05 | 7.55E+05 |
| **C3S3** | 2.47E-02 | 2.64E+04 | 1.25E+03 | 1.25E+02 | 4.28E-03 | 3.26E-02 | 2.12E+02 | 6.44E+05 | 6.65E+05 |
| **C3S4** | 2.12E-02 | 2.28E+04 | 1.06E+03 | 1.06E+02 | 3.58E-03 | 2.67E-02 | 1.92E+02 | 5.28E+05 | 5.53E+05 |

## 8.6 LCA FOR SCENARIO #2: AS-DESIGNED PAVEMENT SECTIONS

This section presents the results of the LCIA evaluation conducted for the as-designed pavement test sections. The performance of the pavement sections considered in this analysis has not been evaluated, but is not expected to vary greatly from the pavement sections evaluated in scenario #1; except for the last pavement section with the conventional aggregate base, which had lower constructed HMA thickness and the moisture penetration to the aggregate base had a significant adverse effect on its field performance. Similar to the LCIA evaluation conducted for Scenario #1, the comparison for environmental impacts for the eight pavement sections in Scenario #2 is not one-to-one due to different pavement responses and expected field performance and pavement life expectations.

The GWP and TED for the compared pavement sections are presented in Figure 8.8 and Figure 8.9. For both GWP and TED, all pavement sections essentially have the same impacts for HMA production and transportation, since the same mix design, HMA thicknesses, and quantities are assumed for all the pavement sections. The impacts of the base/subbase materials are significantly higher for the cement-stabilized bases with QB or QB blended with recycled coarse aggregates (sections 1, 2, 4 and 5) when compared to the conventional section. These impacts are 12-13 times higher for GWP and 4.5-4.9 times higher for TED, mostly due to the high impacts of producing cement. This difference is seen to a lower extent in section 6 with a cement-stabilized QB subbase inverted pavement due to the lower thickness of the cemented layer. When compared to the conventional aggregate base section, the impacts of the fly ash-stabilized QB pavements are only 19-54% higher for both TED and GWP. These higher impacts could be alleviated if the pavement performance and pavement life spans were considered.

The response benefits calculated for each pavement structure, based on predicted resilient FWD deflections relative to the FWD deflections predicted for the conventional section (section 8) are reported in Figure 8.8 and

Figure 8.9. Note that the response benefits are significantly lower than those reported in Scenario #1, largely due to proper modulus assignments for the conventional pavement section and the underlying subgrade, and due to considering an adequate thickness of the overlying HMA layer. With the constructed pavement sections (Scenario #1), the constructed conventional sections had low HMA thickness, and weaker base and subgrade modulus properties due to moisture intrusion. These issues were eliminated from the conventional section comparison in Scenario #2 by assuming a properly constructed conventional section with proper modulus assignments of the pavement layers. Nevertheless, the benefits of constructing pavement sections with stabilized QB applications are evident from higher response benefits of the QB sections, particularly those where cement is used as the chemical stabilizer. Note that the benefits reported are an underestimation of the expected benefits of using the QB applications since performance generally varies exponentially with the measured/calculated responses.

For plant operations, sections 1-5 have 10% higher GWP impacts and 5% higher TED, when compared to the section with the conventional aggregate base. The impacts of plant operations are 5% and 2.3% higher for GWP and TED, respectively, for the inverted pavement sections 6 and 7. These higher impacts are attributed to the plant mixing operations for the stabilized QB materials (using a batch pugmill). Transportation and construction impacts were relatively similar for all eight sections, and the slight differences were due to the differences in the compacted densities of the materials, which directly affects the weights of the materials hauled, placed, and compacted.

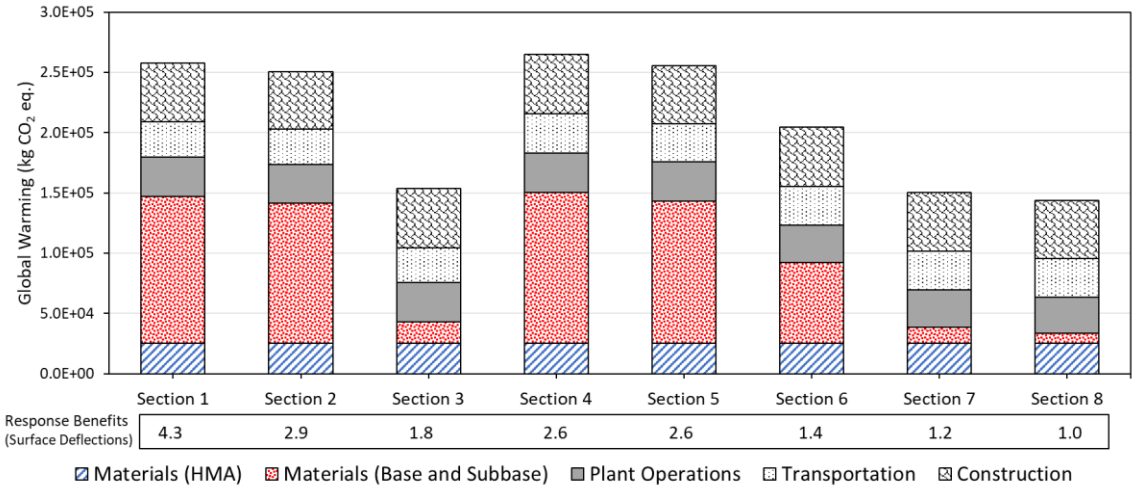


Figure 8.8 Comparisons of the global warming potential for the eight alternative designs – Scenario #2

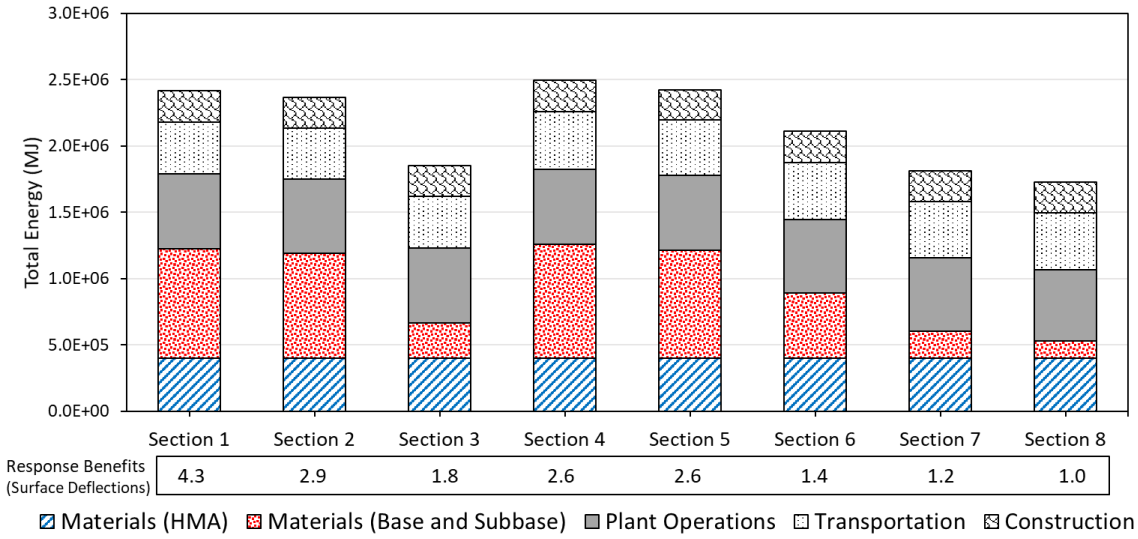


Figure 8.9 Comparisons of the total energy demand for the eight alternative designs – Scenario #2

The weighted contribution of each life cycle stage/activity to GWP and TED for the pavement sections are presented in Figure 8.10 and Figure 8.11, respectively. Similar to the results of Scenario #1, the life cycle stage contributing to the highest GWP and TED impacts is the stabilized base material for sections 1, 2, 4 and 5, having a cement-stabilized QB base. The GWP impacts totaled between 44% and 46% for these sections, while the TED ranged between 27% and 37%. For sections with conventional aggregates base or fly ash-stabilized base/subbase (i.e. Sections 3, 7, and 8), the highest impacts are due to the construction stage and ranged between 33% and 34% for GWP. For TED, on the other hand, plant operations had the highest contribution to the energy demand, totaling between 33% and 34% for sections 3, 7, and 8. The remaining nine TRACI impact categories are summarized in Table 8.10 for all pavement sections. The trends for these TRACI impact categories are similar to those previously reported for Scenario #1.

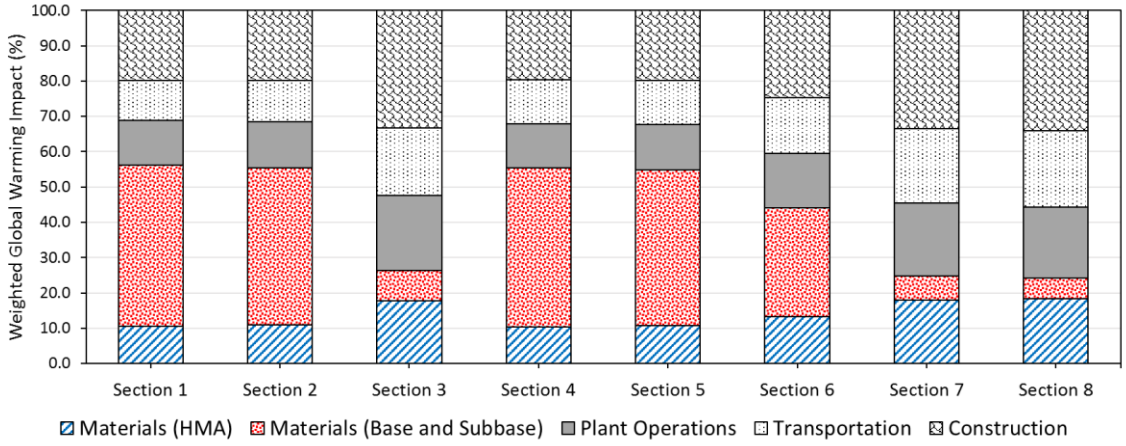


Figure 8.10 Breakdown contributions of each life cycle stage to the GWP – Scenario #2

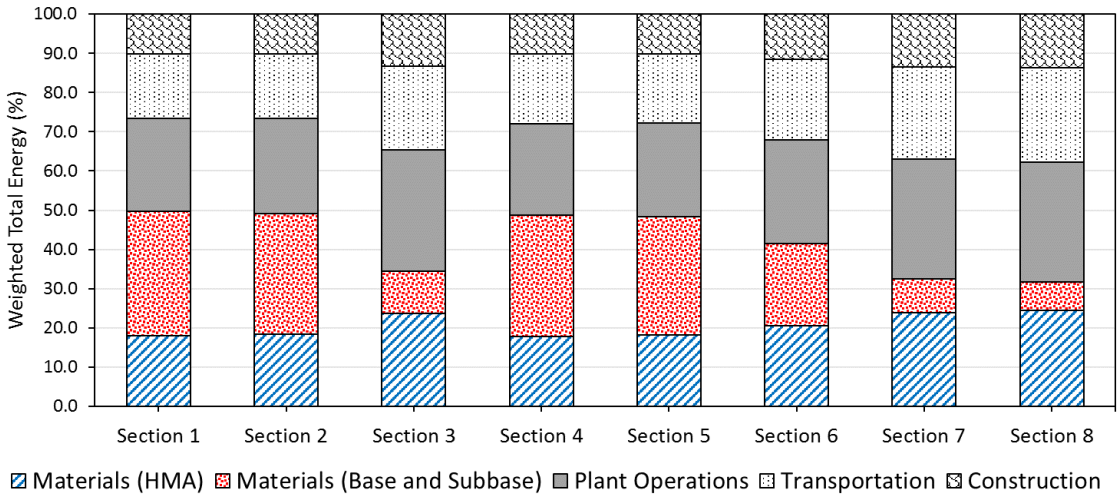


Figure 8.11 Breakdown contributions of each life cycle stage to the TED – Scenario #2

Table 8.10 Summary of the remaining impact categories for all test sections – Scenario #2

| Section | Ozone depletion kg CFC-11 eq | Smog kg O3 eq | Acidification kg SO2 eq | Eutrophication kg N eq | Carcinogenics CTUh | Non-carcinogenics CTUh | Respiratory effects kg PM2.5 eq | Ecotoxicity CTUe | Fossil fuel depletion MJ surplus |
|---|---|---|---|---|---|---|---|---|---|
| **Section 1** | 2.70E-02 | 3.16E+04 | 1.63E+03 | 1.60E+02 | 5.18E-03 | 4.19E-02 | 2.06E+02 | 7.10E+05 | 7.34E+05 |
| **Section 2** | 2.65E-02 | 3.08E+04 | 1.60E+03 | 1.56E+02 | 5.12E-03 | 4.15E-02 | 2.01E+02 | 7.07E+05 | 7.29E+05 |
| **Section 3** | 2.59E-02 | 2.73E+04 | 1.32E+03 | 1.33E+02 | 4.64E-03 | 3.58E-02 | 2.00E+02 | 7.09E+05 | 7.22E+05 |
| **Section 4** | 2.79E-02 | 3.31E+04 | 1.70E+03 | 1.66E+02 | 5.22E-03 | 4.22E-02 | 2.34E+02 | 7.12E+05 | 7.43E+05 |
| **Section 5** | 2.71E-02 | 3.19E+04 | 1.65E+03 | 1.61E+02 | 5.14E-03 | 4.17E-02 | 2.25E+02 | 7.08E+05 | 7.35E+05 |
| **Section 6** | 2.60E-02 | 2.90E+04 | 1.47E+03 | 1.43E+02 | 4.85E-03 | 3.87E-02 | 2.23E+02 | 7.04E+05 | 7.24E+05 |
| **Section 7** | 2.53E-02 | 2.66E+04 | 1.30E+03 | 1.28E+02 | 4.55E-03 | 3.55E-02 | 2.17E+02 | 7.02E+05 | 7.17E+05 |
| **Section 8** | 2.42E-02 | 2.50E+04 | 1.24E+03 | 1.20E+02 | 4.48E-03 | 3.53E-02 | 2.12E+02 | 6.96E+05 | 7.05E+05 |

## 8.7 LCA FOR SCENARIO #3: PROPOSED PAVEMENT SECTIONS

This section presents LCA results for the third scenario of proposed thinner pavement sections, having an HMA thickness of 3 in. (76 mm), and a base thickness of 8 in. (203 mm). These proposed pavement sections are more suited for low volume roads, where lower structural capacity is needed for the same design period. The global warming potential and the total energy demand for the compared pavement sections are presented in Figure 8.12 and Figure 8.13, respectively. Overall, these sections had lower impacts than those in the first two scenarios due to the lower pavement thicknesses. Additionally, the trends for GWP and TED for these sections are in good agreement with those previously reported for Scenario #2.

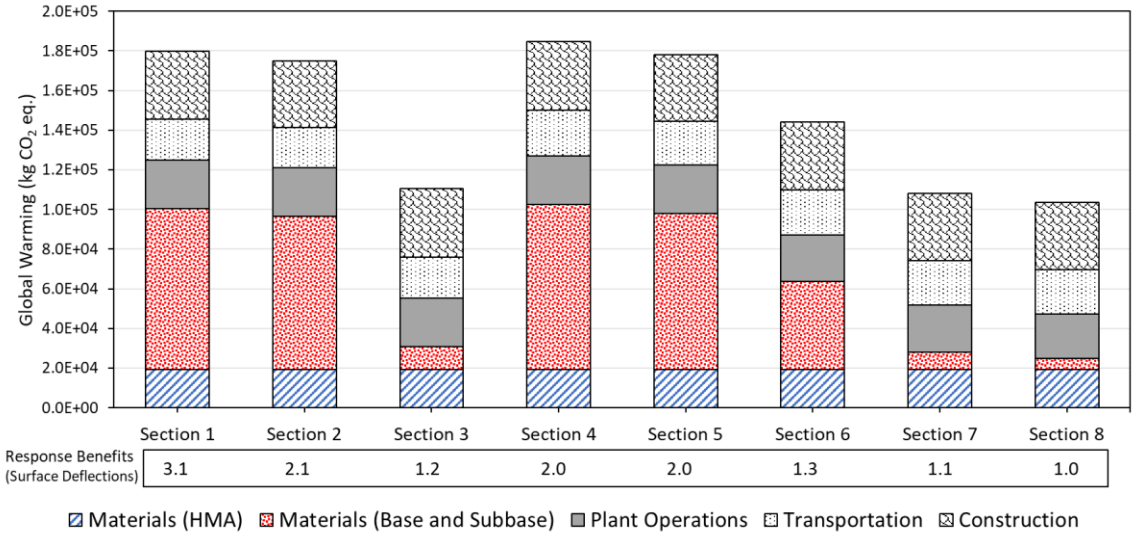


Figure 8.12 Comparisons of the global warming potential for the eight alternative designs – Scenario #3

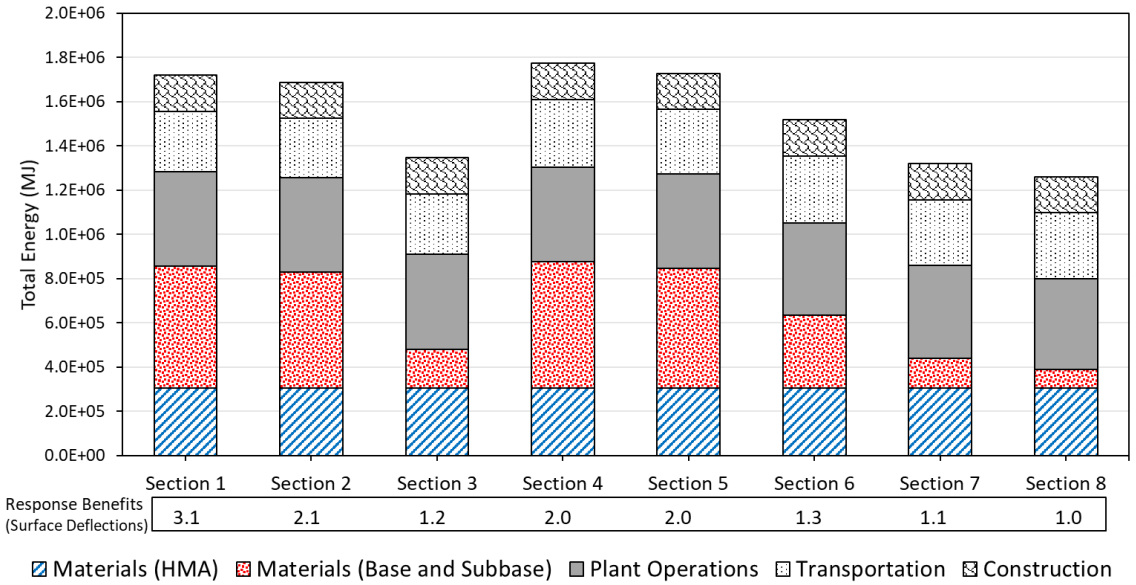


Figure 8.13 Comparisons of the total energy demand for the eight alternative designs – Scenario #3

The weighted contributions of each life cycle stage/activity to GWP and TED for the proposed pavement sections are presented in Figure 8.14 and Figure 8.15, respectively. Similar to the results of the other two scenarios, the life cycle stage contributing to the highest GWP and TED impacts is the stabilized base material for sections 1, 2, 4, 5 and 6, having a cement-stabilized QB base/subbase. The GWP impacts were 45% and 44% for sections 1 and 2, respectively and 45%, 44% and 31% for sections 4, 5, and 6, respectively. For sections with conventional aggregate base or fly ash-stabilized base/subbase (i.e. sections 3, 7, and 8), the highest GWP impacts are due to the construction stage and range between 24% and 33%. For sections 3, 7, and 8, the contribution of base/subbase

materials is minimal and ranged between 5%-11%. The total energy demand contribution is the highest for the base/subbase materials stage in sections 1,2,4, and 5 with a cement stabilized base; ranging between 31% and 33%. For sections 3 and 6-8, on the other hand, the contribution of plant operations stage is the highest for TED and ranged between 27% and 33%.

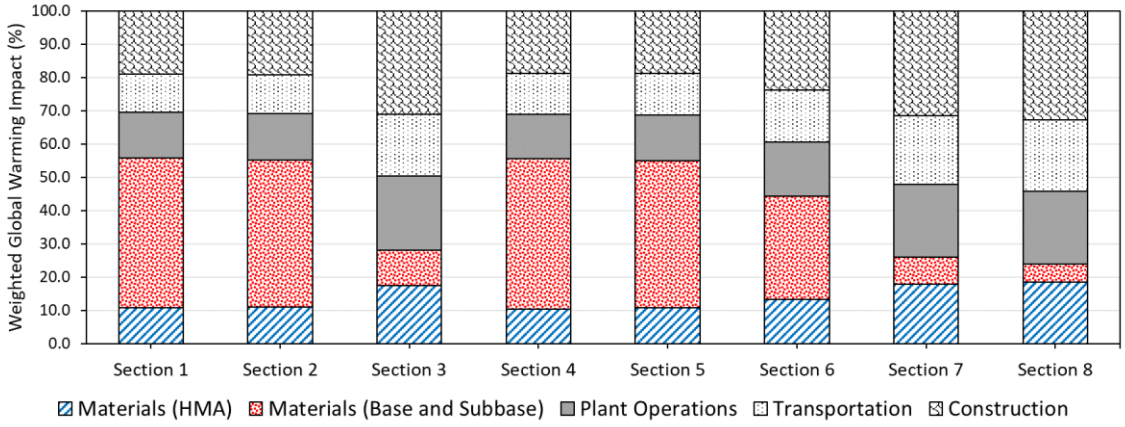


Figure 8.14 Breakdown contributions of each life cycle stage to the GWP – Scenario #3

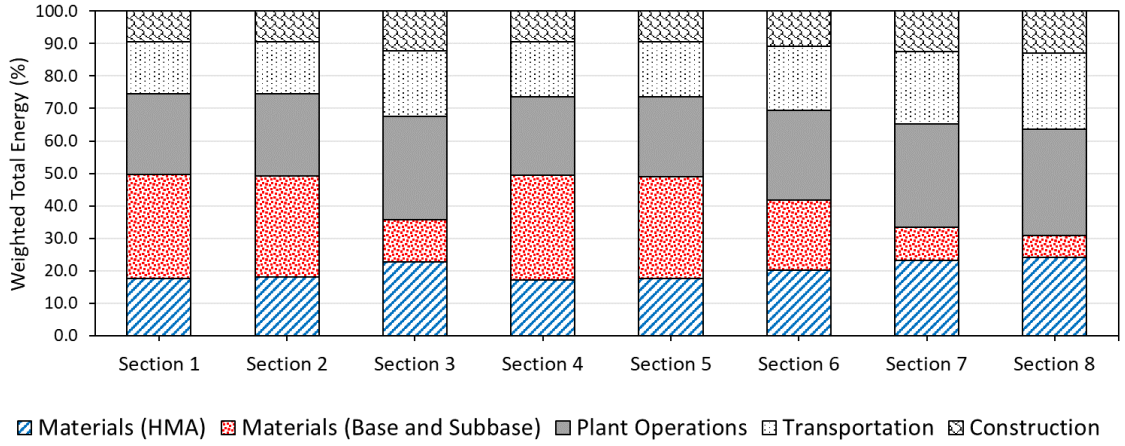


Figure 8.15 Breakdown contributions of each life cycle stage to the TED – Scenario #3

The remaining nine TRACI impact categories are summarized below in Table 8.11 for all pavement sections considered in Senario #3. The trends for these impact categories follow, for the most part, the same trends as GWP and TED, and the trends for other TRACI impacts reported for Scenario #2. The impact categories are shown color-coded for comparison purposes; where green color indicates the lowest impacts and red indicates the highest values in each impact category.

Table 8.11 Summary of the remaining impact categories for all test sections – Scenario #3

| Section | Ozone depletion kg CFC-11 eq | Smog kg O3 eq | Acidification kg SO2 eq | Eutrophication kg N eq | Carcinogenics CTUh | Non carcinogenics CTUh | Respiratory effects kg PM2.5 eq | Ecotoxicity CTUe | Fossil fuel depletion MJ surplus |
|---|---|---|---|---|---|---|---|---|---|
| **Section 1** | 1.92E-02 | 2.20E+04 | 1.15E+03 | 1.12E+02 | 3.79E-03 | 3.11E-02 | 1.45E+02 | 5.34E+05 | 5.44E+05 |
| **Section 2** | 1.88E-02 | 2.14E+04 | 1.13E+03 | 1.09E+02 | 3.75E-03 | 3.08E-02 | 1.41E+02 | 5.32E+05 | 5.41E+05 |
| **Section 3** | 1.84E-02 | 1.91E+04 | 9.43E+02 | 9.37E+01 | 3.43E-03 | 2.70E-02 | 1.41E+02 | 5.34E+05 | 5.37E+05 |
| **Section 4** | 1.97E-02 | 2.30E+04 | 1.20E+03 | 1.16E+02 | 3.82E-03 | 3.12E-02 | 1.63E+02 | 5.36E+05 | 5.51E+05 |
| **Section 5** | 1.92E-02 | 2.22E+04 | 1.16E+03 | 1.12E+02 | 3.76E-03 | 3.09E-02 | 1.57E+02 | 5.33E+05 | 5.45E+05 |
| **Section 6** | 1.85E-02 | 2.03E+04 | 1.04E+03 | 1.01E+02 | 3.57E-03 | 2.89E-02 | 1.56E+02 | 5.30E+05 | 5.38E+05 |
| **Section 7** | 1.80E-02 | 1.87E+04 | 9.31E+02 | 9.05E+01 | 3.37E-03 | 2.68E-02 | 1.52E+02 | 5.29E+05 | 5.33E+05 |
| **Section 8** | 1.72E-02 | 1.76E+04 | 8.91E+02 | 8.49E+01 | 3.32E-03 | 2.66E-02 | 1.48E+02 | 5.25E+05 | 5.25E+05 |

## 8.8 Life CYCLE COST ANALYSIS

The environmental burdens associated with the construction of pavements with chemically stabilized QB bases and subbases were presented in the previous sections. In this section, the comparative costs of constructing those pavement sections are discussed. This evaluation is deemed necessary for agencies to decide on the most feasible option to consider, based both on costs and environmental impacts. Similar to the LCA analysis, Life Cycle Cost Analyses (LCCA) were conducted for all pavement sections considered in the three scenarios. The cost estimates are limited to the capital investment required for the construction of each scenario, and do not consider the costs of maintenance, rehabilitation, or demolition activities at the end of life stage. Additionally, any indirect costs such as the costs for design, equipment mobilization, etc. have been excluded from the comparison to reflect directly on the contribution of using stabilized QB layers in pavement construction on the total cost.

Cost data, specific to the State of Illinois, were compiled and used to estimate the construction cost of each pavement section. Two sources were utilized to obtain reliable cost data. The first source was IDOT's online database for "Pay item report with awarded prices," which provides a list of the most recent awarded unit prices for specific pay items in highway projects awarded to contractors. The most recent listing available for download was released on August 3rd, 2018 (IDOT, 2018). The second source for cost data was contractor pricing in the state of Illinois and included inquiries to contractors about how they would price bid items related to the construction of chemically-stabilized QB sections. This was deemed necessary since the QB applications proposed in this study are new, and no historical cost data were available for use in Illinois. The unit prices provided by contractors were compared with data released by IDOT for the construction of cement-stabilized base materials in flexible pavements.

For simplicity, the pay items involved in the construction of the various pavement alternatives utilizing QB as a base or subbase material were divided into four broad categories: (1) subgrade preparation, (2) construction of conventional aggregate layers, (3) construction of chemically stabilized QB layers, and (4) construction of HMA

layers. For each category, more specific cost items are listed based on the materials being considered. Activities of site preparation (e.g. tree removals) were excluded from the comparison since these are site-specific and their cost is usually estimated based on the number of occurrences instead of an area or a volume. The list of bid items and the unit prices are presented in Table 8.12. The unit prices for the construction of stabilized QB layers were obtained through consultation with local contractors for materials pricing. The quantities of stabilizing agent, QB, and recycled aggregates were factored into the unit cost determined for each combination.

Table 8.12 Unit prices for construction pay items

| **Bid Item** | **IDOT's Code for Pay Item** | **Description** | **Unit** | **Unit Price ($)** |
|---|---|---|---|---|
| Subgrade Preparation | 20200100 | Earth excavation | Cubic Yard | 31.95 |
| | M2112500 | Topsoil excavation and placement | Cubic Yard | 30.00 |
| Conventional Aggregate Base | 35100100 | Aggregate base course, Type A | Sh ton | 26.50 |
| Stabilized QB aggregate base | | Cement-stabilized QB / FRAP | Sh ton | 41.71 |
| | | Cement stabilized QB / FRCA | Sh ton | 42.58 |
| | | Fly ash-stabilized QB / FRAP | Sh ton | 44.59 |
| | | Cement-stabilized QB | Sh ton | 40.40 |
| | | Fly ash-stabilized QB | Sh ton | 43.36 |
| HMA layers construction | | Hot-Mix Asphalt Surface Course, PG 64-22 | Sh ton | 95.00 |
| | | Hot-Mix Asphalt Binder Course PG 64-22 | Sh ton | 90.00 |

Based on the quantities estimated for each pay item, and the unit prices, the total cost for each pavement test section for each scenario were calculated. These costs are presented in Table 8.13, Table 8.14, and Table 8.15 for Scenario #1, #2, and #3, respectively. The costs are presented for the construction of one lane-mile of pavement, with a lane width of 12 ft. (3.66 m). For Scenario #1, the normalized cost is given for each 100,000 ESALs; calculated based on the measured field performance for each test section, and the expected number of load repetition to reach a rutting threshold of 0.5 in. (12.5 mm).

Results presented in Table 8.13 for 'Scenario #1: as-constructed pavement sections', shows that the highest cost was for C2S3 with fly ash-stabilized QB blended with FRAP. This section has a higher cost due to the use of 10% fly ash by weight. Despite being cheaper in price than Portland cement (delivered costs are $80/ton for class 'C' fly ash vs. $150/ton for Portland cement), the use of a larger percentage of fly ash (10% vs. 3% for cement)

resulted in a higher cost for this pavement section. For the conventional section, the cost of one lane-mile is significantly lower, which is expected because the costs of plant operations required to construct the stabilized layers and the cost of using a stabilizing agent are eliminated. When the performance of the test sections is considered by accounting for the expected number of ESALs to failure, the normalized cost per 100,000 ESALs was calculated. As seen in Table 8.13, the normalized cost for the pavement sections utilizing QB as a chemically stabilized base or subbase material was significantly lower than that of the conventional section (C3S8). The two pavement sections, C2S1 and C2S2, with cement-stabilized QB blended with FRAP and FRCA, respectively, had the lowest normalized cost per 100,000 ESALs due to their superior performance when compared with the other sections.

The results for 'Scenario #2: as-designed pavement sections' are presented in Table 8.14, which lists the pavement sections with chemically stabilized QB bases, i.e. sections 1 to 5, to have comparatively similar costs. The variation in the cost of these sections is mostly due to changes in the unit costs of the pay items related to constructing the chemically stabilized QB layers, in addition to the discrepancies in the total quantities of materials used to construct these layers since different materials have different maximum dry densities. Similar to scenario #1, the cost of section 3 with fly-ash stabilized QB/FRAP blend is the highest. On the other hand, the cost of the two inverted pavement sections with cement and fly ash are lower than sections 1 to 5 due to the lower thicknesses of the stabilized layer. The cost of section 8 with a conventional aggregate base is the lowest because the cost attributed to the production and construction of the stabilized materials is eliminated. The significance of the cost comparison in Scenario #2 is that the effect of layer thickness variability during construction is eliminated, thus more accurate cost comparisons can be made for test sections constructed with the same thicknesses but having different material combinations.

The results for 'Scenario #3: proposed pavement sections' are presented in Table 8.15. The pavement test sections considered in this scenario have lower costs than those reported in the first two scenarios due to the lower layer thicknesses considered. Similar to Scenario #2, the pavement sections with chemically stabilized QB bases, i.e. sections 1 to 5, have comparatively similar costs, and the cost of section 3 with fly-ash stabilized QB/FRAP blend is the highest. Additionally, the cost of the two inverted pavement sections with cement and fly ash are lower than sections 1 to 5, due to the lower thicknesses of the stabilized layer. Also, the cost of section 8 with a conventional aggregate base is the lowest. This scenario is beneficial when lower traffic levels are anticipated, and lower pavement thicknesses can be considered to accommodate such lower traffic volumes.

Table 8.13 Total costs for pavement test sections considered in Scenario #1: Constructed test sections

| Section | Pay item | Quantity | Units | Cost ($) | Normalized Cost ($/100,000 ESALs) |
|---|---|---|---|---|---|
| C2S1 | Subgrade Preparation | 2456.7 | C.Y. | 78,490.42 | |
| | Stabilized Base [QB/FRAP/Cement) | 4761.3 | Ton | 198,587.03 | |
| | HMA Surface Course | 1219.4 | Ton | 115,842.17 | |
| | | | **Total** | **$ 392,919.62** | **$ 23,073.08** |
| C2S2 | Subgrade Preparation | 2383.3 | C.Y. | 76,147.42 | |
| | Stabilized Base [QB/FRCA/Cement) | 3904.3 | Ton | 166,254.78 | |
| | HMA Surface Course | 1784.5 | Ton | 169,525.13 | |
| | | | **Total** | **$ 411,927.33** | **$ 18,000.78** |
| C2S3 | Subgrade Preparation | 2603.3 | C.Y. | 83,176.42 | |
| | Stabilized Base [QB/FRAP/Fly ash) | 4668.8 | Ton | 208,184.51 | |
| | HMA Surface Course | 1647.7 | Ton | 156,528.20 | |
| | | | **Total** | **$ 447,889.12** | **$ 88,494.66** |
| C2S4 | Subgrade Preparation | 2395.6 | C.Y. | 76,537.92 | |
| | Stabilized Base [QB/Cement) | 4469.4 | Ton | 180,556.60 | |
| | HMA Surface Course | 1499.0 | Ton | 142,401.11 | |
| | | | **Total** | **$ 399,495.62** | **$ 56,327.48** |
| C3S1 | Subgrade Preparation | 2505.6 | C.Y. | 80,052.42 | |
| | Stabilized Base [QB/Cement) | 4297.4 | Ton | 173,607.29 | |
| | HMA Surface Course | 1629.8 | Ton | 154,832.95 | |
| | | | **Total** | **$ 408,492.66** | **$ 26,005.08** |
| C3S2 | Subgrade Preparation | 2493.3 | C.Y. | 79,661.92 | |
| | Stabilized Subbase [QB/Cement) | 2178.0 | Ton | 87,986.97 | |
| | Conventional Aggregate Base | 2392.2 | Ton | 63,392.51 | |
| | HMA Surface Course | 1475.2 | Ton | 140,140.77 | |
| | | | **Total** | **$ 371,182.17** | **$ 36,041.71** |
| C3S3 | Subgrade Preparation | 2297.8 | C.Y. | 73,413.93 | |
| | Stabilized Subbase [QB/Fly ash) | 2326.9 | Ton | 100,902.67 | |
| | Conventional Aggregate Base | 2044.2 | Ton | 54,171.78 | |
| | HMA Surface Course | 1284.8 | Ton | 122,058.09 | |
| | | | **Total** | **$ 350,546.47** | **$ 53,380.56** |
| C3S4 | Subgrade Preparation | 2126.7 | C.Y. | 67,946.93 | |
| | Conventional Aggregate Base | 4218.9 | Ton | 111,801.33 | |
| | HMA Surface Course | 1046.9 | Ton | 99,454.74 | |
| | | | **Total** | **$ 279,203.00** | **$ 328,897.08** |

Table 8.14 Total costs for pavement test sections considered in Scenario #2: As-designed test sections

| Section | Pay item | Quantity | Units | Cost |
|---|---|---|---|---|
| Section 1 | Subgrade Preparation | 2346.7 | C.Y. | 74,975.93 |
| | Stabilized Base [QB/FRAP/Cement) | 4276.8 | Ton | 178,379.93 |
| | HMA Surface Course | 1522.8 | Ton | 144,661.44 |
| | | | **Total** | **$ 398,017.30** |
| Section 2 | Subgrade Preparation | 2346.7 | C.Y. | 74,975.93 |
| | Stabilized Base [QB/FRCA/Cement) | 4074.0 | Ton | 173,483.25 |
| | HMA Surface Course | 1522.8 | Ton | 144,661.44 |
| | | | **Total** | **$ 393,120.61** |
| Section 3 | Subgrade Preparation | 2346.7 | C.Y. | 74,975.93 |
| | Stabilized Base [QB/FRAP/Fly ash) | 4314.8 | Ton | 192,401.57 |
| | HMA Surface Course | 1522.8 | Ton | 144,661.44 |
| | | | **Total** | **$ 412,038.93** |
| Section 4 | Subgrade Preparation | 2346.7 | C.Y. | 74,975.93 |
| | Stabilized Base [QB/Cement) | 4356.0 | Ton | 175,973.94 |
| | HMA Surface Course | 1522.8 | Ton | 144,661.44 |
| | | | **Total** | **$ 395,611.31** |
| Section 5 | Subgrade Preparation | 2346.7 | C.Y. | 74,975.93 |
| | Stabilized Base [QB/Cement) | 4115.2 | Ton | 166,247.38 |
| | HMA Surface Course | 1522.8 | Ton | 144,661.44 |
| | | | **Total** | **$ 385,884.75** |
| Section 6 | Subgrade Preparation | 2346.7 | C.Y. | 74,975.93 |
| | Stabilized Subbase [QB/Cement) | 2178.0 | Ton | 87,986.97 |
| | Conventional Aggregate Base | 2087.7 | Ton | 55,324.37 |
| | HMA Surface Course | 1522.8 | Ton | 144,661.44 |
| | | | **Total** | **$ 362,948.70** |
| Section 7 | Subgrade Preparation | 2346.7 | C.Y. | 74,975.93 |
| | Stabilized Subbase [QB/Fly ash) | 2147.9 | Ton | 93,140.93 |
| | Conventional Aggregate Base | 2087.7 | Ton | 55,324.37 |
| | HMA Surface Course | 1522.8 | Ton | 144,661.44 |
| | | | **Total** | **$ 368,102.66** |
| Section 8 | Subgrade Preparation | 2346.7 | C.Y. | 74,975.93 |
| | Conventional Aggregate Base | 4175.4 | Ton | 110,648.74 |
| | HMA Surface Course | 1522.8 | Ton | 144,661.44 |
| | | | **Total** | **$ 330,286.10** |

Table 8.15 Total costs for pavement test sections considered in Scenario #3: Proposed test sections

| Section | Pay item | Quantity | Units | Cost |
|---|---|---|---|---|
| Section 1 | Subgrade Preparation | 1368.9 | C.Y. | 43,735.96 |
| | Stabilized Base [QB/FRAP/Cement) | 2851.2 | Ton | 118,919.95 |
| | HMA Binder Course | 588.1 | Ton | 52,925.40 |
| | HMA Surface Course | 571.0 | Ton | 54,248.04 |
| | | | **Total** | **269,829.35** |
| Section 2 | Subgrade Preparation | 1368.9 | C.Y. | 43,735.96 |
| | Stabilized Base [QB/FRCA/Cement) | 2716.0 | Ton | 115,655.50 |
| | HMA Binder Course | 588.1 | Ton | 52,925.40 |
| | HMA Surface Course | 571.0 | Ton | 54,248.04 |
| | | | **Total** | **266,564.89** |
| Section 3 | Subgrade Preparation | 1368.9 | C.Y. | 43,735.96 |
| | Stabilized Base [QB/FRAP/Fly ash) | 2876.5 | Ton | 128,267.71 |
| | HMA Binder Course | 588.1 | Ton | 52,925.40 |
| | HMA Surface Course | 571.0 | Ton | 54,248.04 |
| | | | **Total** | **279,177.11** |
| Section 4 | Subgrade Preparation | 1368.9 | C.Y. | 43,735.96 |
| | Stabilized Base [QB/Cement) | 2904.0 | Ton | 117,315.96 |
| | HMA Binder Course | 588.1 | Ton | 52,925.40 |
| | HMA Surface Course | 571.0 | Ton | 54,248.04 |
| | | | **Total** | **268,225.36** |
| Section 5 | Subgrade Preparation | 1368.9 | C.Y. | 43,735.96 |
| | Stabilized Base [QB/Cement) | 2743.5 | Ton | 110,831.59 |
| | HMA Binder Course | 588.1 | Ton | 52,925.40 |
| | HMA Surface Course | 571.0 | Ton | 54,248.04 |
| | | | **Total** | **261,740.98** |
| Section 6 | Subgrade Preparation | 1368.9 | C.Y. | 43,735.96 |
| | Stabilized Subbase [QB/Cement) | 1452.0 | Ton | 58,657.98 |
| | Conventional Aggregate Base | 1391.8 | Ton | 36,882.91 |
| | HMA Binder Course | 588.1 | Ton | 52,925.40 |
| | HMA Surface Course | 571.0 | Ton | 54,248.04 |
| | | | **Total** | **246,450.29** |
| Section 7 | Subgrade Preparation | 1368.9 | C.Y. | 43,735.96 |
| | Stabilized Subbase [QB/Fly ash) | 1431.9 | Ton | 62,093.95 |
| | Conventional Aggregate Base | 1391.8 | Ton | 36,882.91 |
| | HMA Binder Course | 0.0 | Ton | 0.00 |
| | HMA Intermediate Course | 588.1 | Ton | 52,925.40 |
| | HMA Surface Course | 571.0 | Ton | 54,248.04 |
| | | | **Total** | **249,886.26** |
| Section 8 | Subgrade Preparation | 1368.9 | C.Y. | 43,735.96 |
| | Conventional Aggregate Base | 2783.6 | Ton | 73,765.82 |
| | HMA Binder Course | 0.0 | Ton | 0.00 |
| | HMA Intermediate Course | 588.1 | Ton | 52,925.40 |
| | HMA Surface Course | 571.0 | Ton | 54,248.04 |
| | | | **Total** | **224,675.22** |

## 8.9 COMPARISONS OF LCA AND LCCA SCENARIOS

Based on the analysis and results for the three LCA and LCCA scenarios, a summary for the total Global Warming Potential (GWP) and Total Energy Demand (TED) for the three scenarios is presented in Figure 8.16 and Figure 8.17, respectively. The normalized impacts per 100,000 ESALs trafficked for Scenario #1 are also presented in these figures. All impacts were calculated for the construction of one 12 ft. (3.66 m) lane-mile, and considered impacts from materials acquisition, plant operations, transportation, and construction activities. Results from LCA analysis showed that due to the high environmental burdens associated with the production of cement, the materials acquisition stage for the cement-stabilized sections had the highest impacts. For fly ash-stabilized QB sections and the conventional test section, plant operations or construction stages resulted in the highest impacts. When the normalized impacts in Scenario #1 and the response benefits (based on FWD resilient deflections) reported for the pavement sections in the three scenarios are considered, it can be realized that cement-stabilized test sections, particularly those with QB blended with FRAP/FRCA can have relatively lower initial GWP and TED from materials and construction stages normalized over pavement life and anticipated traffic.

The results of the life cycle assessment of the pavement sections with stabilized QB applications provide guidelines for situations where the use of cement- or fly ash-stabilized QB layers can provide affordable, and sustainable pavement designs without compromising performance. Based on LCA results, it is evident that the use of stabilized QB layers can be suited for scenarios where higher traffic loads and volumes are expected. This is the result of the higher stiffness of the stabilized layers, which can deflect less and sustain more load repetitions in the use stage; thus possibly leading to environmental and economical savings. As such, sustainable applications of stabilized QB pavement layers can be especially attractive as an option for constructing local roads or higher volume roads such as county roads or collector/arterial roads.

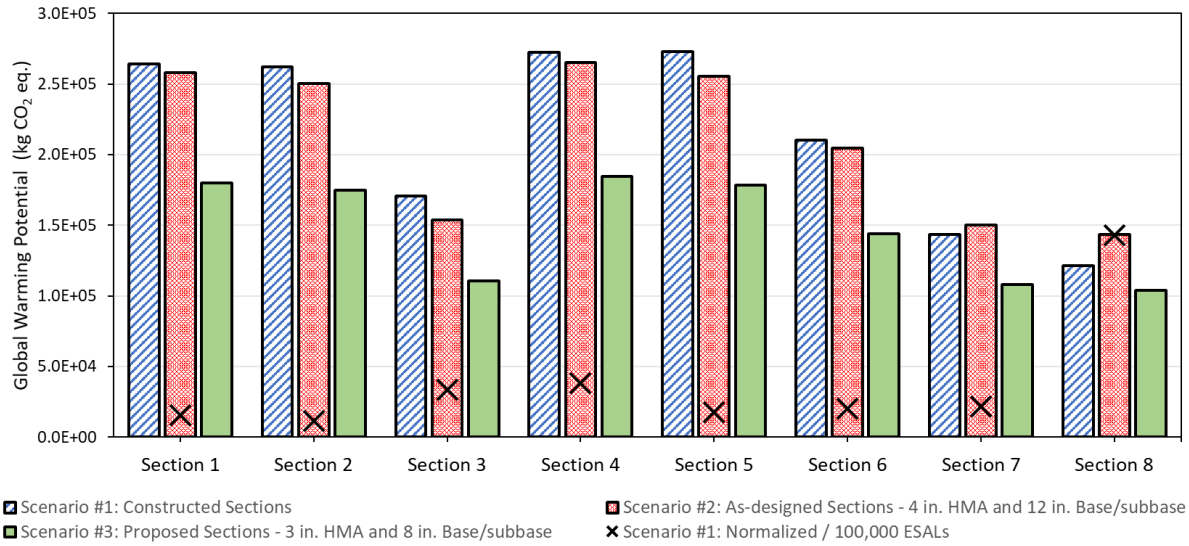


Figure 8.16 Summary of total Global Warming Potential (GWP) for all LCA scenarios [1 in. = 25.4 mm]

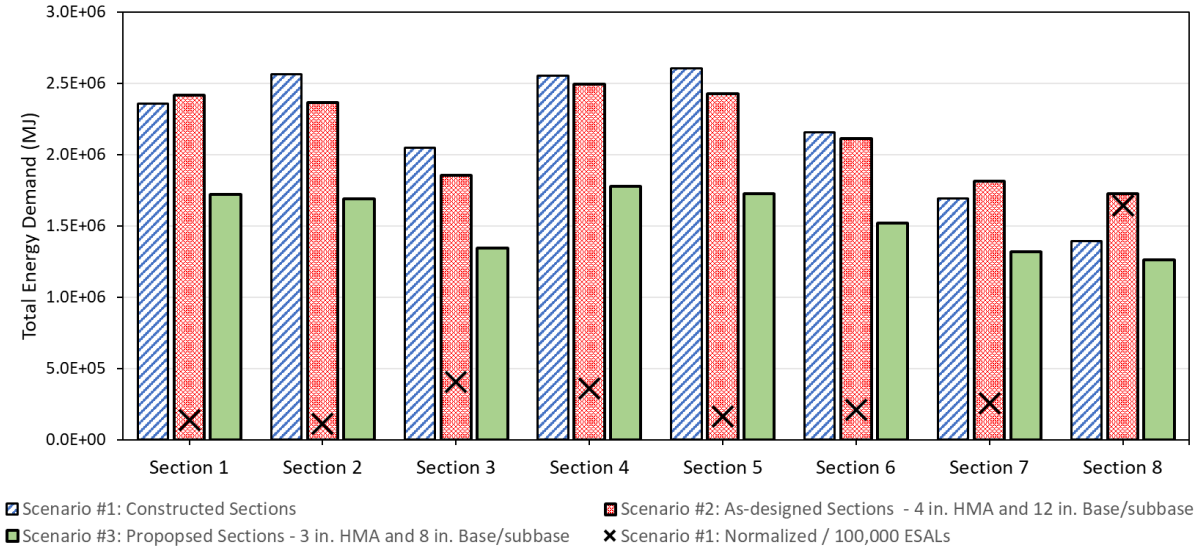


Figure 8.17 Summary of Total Energy Demand (TED) for all LCA scenarios [1 in. = 25.4 mm]

A summary of the total costs required to construct the pavement sections considered in the three scenarios are presented in Figure 8.18. For scenario #1, the cost was normalized and presented for each 100,000 ESALs trafficked. The total cost for constructing each pavement section was mostly driven by the pavement thickness, particularly the thickness of the HMA layer. The thicker the pavement structure, the higher the cost for excavation, site preparation, materials hauling, placement and compaction. When the normalized cost per traffic or the response benefits are taken into consideration, the largest savings in cost are expected when cement-stabilized base materials are constructed from QB blended with coarse recycled aggregates (FRAP or FRCA). Additionally, the cost of constructing similar thicknesses of cement-stabilized QB layers was lower than that of fly ash-stabilized layers, due to the larger percentage of fly ash used to achieve good performance (3% cement vs. 10% fly ash). Thus, considering the measured field performance of the fly ash sections, their higher cost, and the variability in fly ash composition and performance; it is recommended that cement-stabilized QB applications are considered. In addition to their proven good field performance under heavy wheel loading, these applications can be sustainable and cheaper to construct.

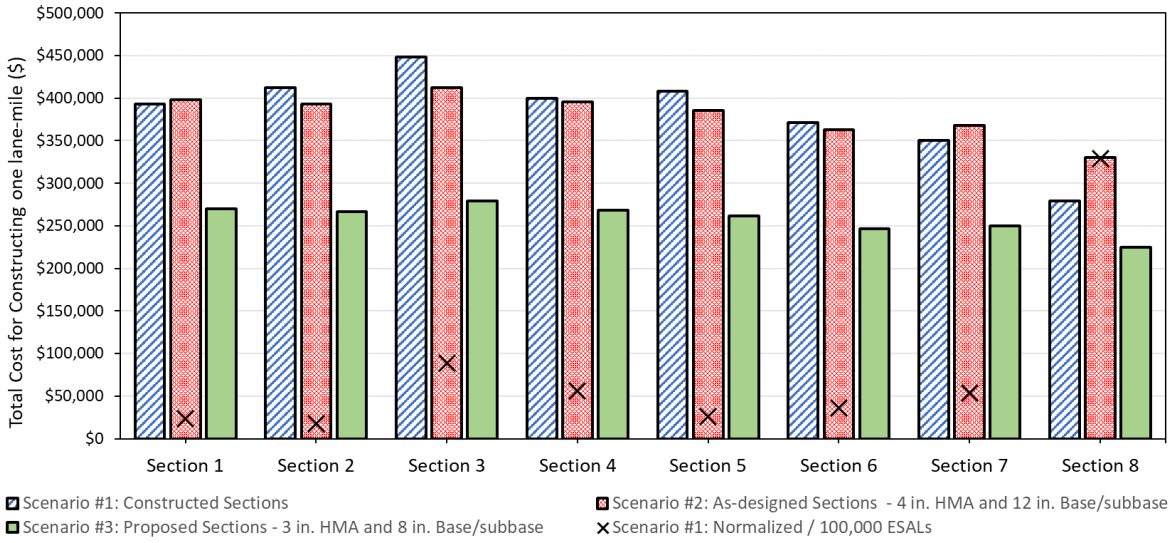


Figure 8.18 Summary of total costs for all LCCA scenarios. [1 in. = 25.4 mm]

## 8.10 SUMMARY

A comprehensive sustainability assessment of QB applications evaluated in Cell 2 and Cell 3 was conducted using Life Cycle Assessment (LCA) and a Life Cycle Cost Analysis (LCCA), and was presented in this chapter. The conducted LCA followed the structure recommended by ISO 14044:2006 and FHWA (Harvey et al., 2016). Three analysis scenarios were considered. The first scenario evaluated the cost and environmental impacts of the pavement test sections as constructed in Cells 2 and 3 by considering actual constructed layer thicknesses; measured at the end of performance monitoring from pavement test section trenching and HMA coring. The second scenario considered the as-designed thicknesses (4 in. or 102 mm of HMA and 12 in. or 305 mm of combined base and subbase) to eliminate the field variability in layer thicknesses during construction. The third scenario considered newly proposed thinner pavement structures (3 in. or 76 mm of HMA and 8 in. or 203 mm of combined base and subbase), to target applications for low volume roads.

Each of the three scenarios analyzed eight pavement sections with the QB material combinations studied in Cells 2 and 3. The first five test sections had a chemically stabilized QB or QB blended with recycled course aggregates base, the next two sections were inverted pavements, and section 8 had a conventional aggregate base. Actual field performance from the accelerated pavement testing were used to normalize sustainability impacts to present the results for each 100,000 ESALs trafficked in the first scenario. The response benefits, measured as the ratio of FWD maximum center deflection of the conventional pavement section to that of the section considered, were reported for each pavement section. The detailed results from the LCAs and LCCAs conducted for the materials and construction stages were discussed in this chapter. These results indicated that savings in costs and environmental impacts can be anticipated from constructing pavements with chemically stabilized QB base and subbase layers when the use stage benefits (i.e. higher traffic volumes and pavement lives) are accounted for.

# CHAPTER 9: SUMMARY AND CONCLUSIONS

## 9.1 INTRODUCTION

This dissertation focused on evaluating new sustainable applications of Quarry By-products (QB) or QB mixed with other nontraditional, virgin, or recycled aggregate materials in both unbound and chemically stabilized pavement layers. In total, sixteen full-scale pavement test sections were constructed to evaluate the use of QB in base, subbase, and aggregate subgrade applications. The chemically stabilized test sections utilizing QB were stabilized with 3% cement or 10 % Class 'C' fly ash, to study their effectiveness in flexible pavements. The unbound applications of QB investigated the use of QB to fill the voids between large aggregate subgrade rocks commonly used for subgrade replacement/improvement applications on top of very soft subgrade soils, as well as using dense-graded aggregate layers with high fines content up to 15% passing the No. 200 sieve, for weak subgrade remediation. These unbound test sections were constructed to investigate both construction platforms and low volume road applications.

In preparation for the field evaluations, several laboratory studies were conducted to finalize the designs of intended QB applications. All the field test sections were evaluated by Accelerated Pavement Testing (APT). Following APT, forensic tests were conducted to further evaluate the performances of the test sections. These tests included Falling Weight Deflectometer (FWD) tests before and after trafficking, hot mix asphalt coring, Dynamic Cone Penetrometer (DCP) testing for strength profiling of subsurface layers, and trenching. Results from APT and forensic analyses indicated that quite satisfactory performance results were obtained for field rutting performance trends. Pavement testing and evaluations indicated that the selected QB applications could be successfully incorporated into standard pavement construction (and rehabilitation) practices.

Using data compiled for field evaluations, mechanistic analyses were conducted using GT-PAVE axisymmetric finite-element program to analyze the FWD results and predict critical pavement responses for pavement sections with as-constructed and as-designed layer thicknesses as well as newly proposed thinner pavement structures using the backcalculated layer modulus properties. Life Cycle Assessment (LCA) and Life Cycle Cost Analysis (LCCA) studies were conducted to assess the environmental impacts and cost benefits for the studied QB applications. LCA and LCCA results indicated that chemically stabilized QB and QB blended with recycled coarse aggregates, particularly cement-stabilized QB applications, could be successfully used to construct more sustainable and low cost pavements when performance is considered through normalized traffic impacts and structural capacity is studied in pavement analysis through surface deflection response benefits.

## 9.2 SUMMARY OF FINDINGS FROM FIELD EXPERIMENT

Two categories of applications were selected and tested for field performance in Cell 1, both for construction platform and low volume flexible pavement applications with hot mix asphalt (HMA) surfacing. A

laboratory packing study suggested that the optimum quantity of QB to be mixed with the large Primary Crusher Run (PCR) aggregates by shaking them into the voids using vibratory action was 25% QB by weight of the PCR, considering more likely wet conditions of QB in the field. The study also concluded that the moisture content of the QB is one of the main factors governing the quantity of QB that can be packed in the voids.

Field construction of PCR/QB sections successfully incorporated 25% QB by weight for sections constructed in two lifts. However, for the full-scale test sections constructed in a single lift of PCR aggregate, only 16.7% QB could be packed. In-place monitoring of pavement layer responses was accomplished by dropping Lightweight Deflectometer (LWD) on top of the capping layers of all test sections and a Falling Weight Deflectometer (FWD) on top of the final surface courses. The composite surface moduli backcalculated from LWD and FWD deflections showed somewhat similar modulus values for the constructed layers.

Performance monitoring with accelerated pavement testing showed quite satisfactory results of QB applications for each of the construction platform and flexible pavement test sections. All construction platform sections in Cell 1S accumulated less than 3 in. (76 mm) of rutting for up to 20,000-wheel passes; while all paved sections in Cell 1N accumulated less than 0.5 in. or 12.5 mm of rutting after 90,000 passes. Section 3 with 15% plastic fines accumulated the most rutting for both paved and unpaved sections, indicating the detrimental effect of plastic fines on performance, especially when they were exposed to moisture. The presence of an HMA cover reduced the detrimental effect of plastic fines due to lower load levels experienced by the aggregate layers. Finally, sections with QB packed in the voids of large PCR rocks indicated a superior performing construction platform compared to PCR only, which was previously evaluated under similar loading and subgrade conditions.

Three categories of chemically stabilized QB applications were selected and tested for field performance in Cells 2 and 3 for the low volume flexible pavement applications with HMA surfacing: (1) Blending QB with coarse aggregate fractions of reclaimed asphalt pavement (FRAP) and recycled concrete aggregates (FRCA); (2) using QB as a cement or fly ash-treated base material; and (3) using QB as a cement or fly ash-treated subbase (i.e., in inverted pavements).

Satisfactory rutting performance trends were achieved for all chemically stabilized QB layer applications. No fatigue cracking was observed in any of the test sections with chemically stabilized QB applications. QB blends with FRCA or FRAP and cement had higher and statistically different unconfined compressive strengths from laboratory tests. They also proved that the most satisfactory rutting performance trends were achieved with the highest LWD moduli, lowest FWD deflections, and the highest number of drops per inch (25.4 mm) of penetration by DCP from field testing. Sections stabilized with fly ash had somewhat inferior and more variable performance trends when compared to the cement-stabilized sections. Test sections that utilized two different sources of QB for the cement-stabilized base application (i.e. QB2 and QB3) did not show any significant difference in performance, which is in agreement with the laboratory unconfined compressive strength test results showing no statistical difference for the two QB materials from two different sources in Illinois.

The performance monitoring of the stabilized test sections before and after trafficking with APT in general indicated relatively low FWD deflections for the stabilized test sections in Cells 2 and 3. Additionally, measured wheel load stresses from pressure cells installed on top of the subgrade indicated relatively low subgrade pressures of around 2 psi (14 kPa) recorded for the three cement-stabilized base/subbase test sections in Cells 2 and 3, and thus low subgrade rutting potential.

## 9.3 SUMMARY OF FINDINGS FROM MECHANISTIC ANALYSIS AND MODELING

A finite element-based mechanistic analysis approach was used for analyzing FWD deflections to backcalculate layer moduli and calculate the critical pavement responses as well as surface deflection response benefits for different scenarios/thicknesses of pavement sections utilizing QB applications in base or subbase layers. First, the FWD Deflection Basin Parameters (DBPs) were calculated to draw conclusions about the performance trends of the QB sections. The trends for Area Under Pavement Profile (AUPP) and the field measured surface ruts were in good agreement for the test sections with chemically stabilized QB applications. Then, the modulus properties of the constructed pavement layers were backcalculated from the FWD deflections using GT-PAVE finite element program through a mechanistic forward calculation approach. Stress-dependent cross-anisotropic layer moduli were assigned for all unbound base and aggregate subgrade layers. Using a systematic trial-and-error approach, the layer moduli were changed for the pavement layers until reasonable matches were achieved between measured and calculated FWD deflection basins. Good matches were achieved with low error values for all 12 analyzed test sections.

The layer properties calculated from the FWD backcalculation analysis were further used to compute critical pavement responses and response benefits, based on FWD resilient surface deflections, for all QB applications investigated in Cells 2 and 3 under three different scenarios. The three scenarios involved pavement sections with the as-constructed and as-designed layer thicknesses, and newly proposed pavement sections having thinner HMA and base and subbase layers more suited for low volume road applications of stabilized QB in pavement construction. The calculated response benefits indicated significant advantages of using cement-stabilized QB applications over fly ash-stabilized QB applications and conventional flexible pavement sections. This was evident from the high response benefits predicted for cement-stabilized QB applications.

## 9.4 SUMMARY OF FINDINGS FROM SUSTAINABILITY AND COST EVALUATIONS

Three different LCA and LCCA scenarios were considered and compared for cost, environmental impacts and energy demands. The major discrepancies among the three scenarios are the thicknesses of the HMA, base and subbase layers. The three scenarios essentially assume the same sustainability study goal and scope and LCI impacts for raw materials and fuels, including allocation criteria and data sources. Scenario #1 provided a comparison of the as-constructed pavement test sections that were evaluated in APT during field performance. Scenario #2 compared

pavement sections with the as-designed layer thicknesses to eliminate variability in pavement layer thicknesses during construction. Scenario #3 compared newly proposed pavement sections with thinner HMA, base and subbase layers that are more suited for targeting low volume roads applications of stabilized QB in pavement construction.

Both the LCA and LCCA studies included impacts and cost considerations from materials acquisition, transportation, plant operations, and construction stages. The use stage, maintenance and rehabilitation, and end-of-life stages were eliminated from the analyses. Specifically, the use stage was eliminated since it is one of the most critical stages in terms of impacts on the emissions, and it directly dictates schedules and proper measures for maintenance and rehabilitation. Since accurate data from long term performance studies needed to be collected for this stage, which was not readily available, pavement structural capacities were evaluated based on maximum surface deflections and response benefit ratios. Accordingly, the use phase was eliminated not to make many assumptions for the fuel consumption rates of the different vehicles operating on the road and related assumptions for International Roughness Index (IRI) progression and reduction factors.

Results from LCA analyses for the distribution of impacts among the considered activities showed that due to the high environmental burdens associated with the production of cement, the materials acquisition stage for the cement-stabilized sections had the highest impacts. For fly ash-stabilized QB sections and the conventional test section, plant operations or construction stages resulted in the highest impacts. QB applications generally had higher environmental impacts and cost when compared to conventional pavement sections with the same layer thicknesses, particularly when cement is used for chemical stabilization. However, when the normalized impacts in Scenario #1 and the response benefits for resilient surface deflections of the three Scenarios are compared, cement-stabilized test sections, particularly those with QB blended with FRAP/FRCA, had relatively lower normalized global warming potential and total energy demand. Similarly, the cost of constructing test sections with chemically stabilized QB applications can be lower than that of conventional pavement when performance is taken into consideration.

## 9.5 CONCLUSIONS

In light of the sustainable QB layer applications demonstrated in this PhD dissertation for satisfactory performance behavior observed in the construction platform and flexible pavement test sections, the following specific conclusions can be offered:

- Quarry By-products (QB) were successfully used as a filler material in the voids of large, unconventional, and uniformly graded ‘aggregate subgrade’ materials to improve strength and reduce potential settlement over a soft CBR=1% subgrade. Satisfactory performance results were achieved for both one-lift and two-lift construction experiences. When rutting trends were compared with previous studies (with no QB fillers), a significant improvement was observed in the stability and rutting performance of aggregate subgrade layers when QB was added to a primary crusher run aggregate filling the large voids.

- The construction platform section having Illinois DOT CA06 type dense-graded base course aggregate with 15% plastic fines accumulated the highest wheel path rut, and showed the highest rutting rate. The results from this section indicate the detrimental effect of plastic fines on performance, especially when the high fines content materials are exposed to moisture. The effect of plastic fines on performance was less apparent in flexible pavement test sections than in the construction platforms. This is because the unbound aggregate layers were exposed to lower load levels and stress states due to the presence of an HMA cover.
- Sections constructed with QB blended with FRAP/FRCA showed the best performance in terms of the least wheel path rutting progression. No significant difference in performance was observed between the FRAP and FRCA sections. The presence of coarse aggregates increased the layer stiffness and the load carrying capacity and resulted in better performance.
- The conventional flexible pavement control section (C3S4), having the standard CA06 dense-graded unbound aggregates, was in fact constructed with the lowest HMA thickness and density among all the test sections. Further, C3S4 was also exposed to the shallowest water table levels. This resulted in cracks appearing on the pavement surface even after 30,000 passes. The exposure of this control section to higher moisture levels, and the low HMA density also allowed substantial water infiltration which raised the water table and weakened the base layer as evidenced by the pumping of fines under wheel loading.
- For the chemically stabilized sections in Cells 2 and 3, the test sections stabilized with cement consistently showed better performance than those stabilized with fly ash. Despite this fact, the overall performance of the fly ash stabilized test sections is still deemed satisfactory as evidenced by below 0.5-in. wheel path rut accumulations after 135,000 passes.
- Cement-stabilized layers of two QB sources (QB2 and QB3) showed similarly good performance. Thus, preliminary results indicate no significant effect of the Illinois quarry QB source on performance.
- Inverted pavement sections constructed in Cell 3 showed good performance. In particular, C3S2 with a cement-stabilized QB subbase, established quite a satisfactory combination demonstrating the suitability of using cement-stabilized QB in inverted pavement applications.
- The thicknesses of subsurface and HMA layers had a significant effect on performance trends of the test sections. Thus, sustainable QB applications need to be brought into the mechanistic-empirical analysis and design framework for appropriate thickness design. Note that the thickness of HMA had less effect on performance for the chemically stabilized sections when compared with sections constructed with unbound materials. The variability in thickness design was addressed through the mechanistic analysis and modeling using GT-PAVE Finite Element (FE) program to draw proper conclusions about the layer moduli of the subsurface pavement layers with QB applications.
- Using GT-PAVE FE program and proper modulus assignments and assumptions, the resilient surface deflections were reasonably predicted in the close proximity of actual measured FWD deflections. The

'response benefits' were calculated for various pavement structures and QB applications using the backcalculated layer moduli. Response benefit, defined as the ratio of maximum resilient surface deflection in a conventional pavement section to the maximum surface deflection for the section in consideration, was the basis for evaluating structural pavement capacities and comparing pavement sections both constructed in Cells 2 and 3 as well as for pavement sections with as-designed layer thicknesses and newly proposed thinner HMA, base and subbase layers. Based on the favorable response benefits, the sustainability and cost benefits of QB applications could be realized when pavement structural adequacy, and expected pavement performance and pavement life were taken into consideration.

- Results of the life cycle assessment of the pavement sections proved situations where the use of cement- or fly ash-stabilized QB layers could provide affordable and sustainable pavement designs. The initial costs and environmental impacts from constructing chemically stabilized QB applications can be higher than those of constructing similar thicknesses of conventional flexible pavements. However, when performance, number of load repetitions to failure, and response benefits are accounted for, the advantages of constructing pavements with stabilized QB applications can be realized as constructing more sustainable pavements. Considerable savings linked to sustainability impacts can be realized when cement is used as the stabilizing agent.
- Based on the field performance and mechanistic modeling results, it is evident that the construction of stabilized QB layers in the thicker as-designed pavement structures can be suited for scenarios where higher traffic loads and volumes are expected. Thinner test sections with 3 in. (76 mm) HMA and 8 in. (203 mm) of base/subbase were proposed for use in low volume road applications. As such, more sustainable applications of stabilized QB pavement layers are attractive as an option for constructing local roads subjected to low or medium volume traffic.
- Cost savings and environmental benefits can be anticipated from constructing pavements with chemically stabilized QB layers. This is evident from considering normalized impacts per 100,000 ESALs or considering the response benefit comparisons for resilient surface deflections. Higher savings and improved performance are particularly anticipated when cement is used as the chemical stabilizer, and especially when QB is blended with FRAP or FRCA as coarse aggregate for high strength and stiffness properties.

## 9.6 RECOMMENDATIONS FOR FUTURE WORK

The QB applications investigated in this dissertation highlighted several potentially successful unbound and bound applications of QB in pavements. Certain aspects brought up in this study may require further investigation. The following points summarize some research needs and recommendations for further research:

- There is a need to investigate effective field construction methods for mixing QB with large sized aggregate subgrade materials for constructed layer uniformity. The practice of vibrating QB into the

inherent voids of constructed lifts of aggregate subgrade demonstrated in this study needs to be followed up by developing an automated technique to spread the QB gradually and uniformly on the surface.

- There is a likely need to further investigate the effect of QB source on chemically stabilized applications for reassurance. The effort presented in this dissertation for two sources, i.e. QB2 and QB3, should be extended to investigate the effects of particle size, particle shape, and fines composition on performance.
- There is a need to further investigate the effect of mix proportions of QB with coarse recycled aggregates. This study has investigated the performance for sections with QB mixed with coarse fractions of FRAP or FRCA at a blending ratio of 70% QB with 30% FRAP or FRCA. Different mix proportions that may provide better performance or more sustainable applications need to be studied.
- There is a need to further investigate the effect of the percentage of stabilizing agents on performance. A further investigation of these percentages, and their effect on strength and durability is required. Additionally, there is a need to better evaluate the effect of fly ash source and composition and its compatibility with the QB materials on the fly ash-stabilized mixtures.
- There is a need to study the long-term pavement performance and the durability of the evaluated QB applications, particularly the chemically stabilized applications. Durability aspects need to be thoroughly investigated to establish the performance of QB in pavement layers due to climatic effects, particularly freeze-thaw cycles during winter and wetting-drying conditions. This was partially studied in this dissertation by exposing the field test sections to realistic winter conditions in Illinois. A more controlled laboratory study is needed to confidently incorporate QB usage in standard design practices.
- Advanced modeling of the studied QB applications can be further investigated by considering viscoelastic HMA properties. Modeling can be improved by considering three-dimensional FE analyses to take into account detailed and accurate tire imprints and non-uniform tire pressures.
- LCA and LCCA analyses can further include collecting primary and site-specific data from quarries and asphalt plants, and site-specific data for construction equipment types, productivity rates, and fuel consumption. When long-term performance is better evaluated from in-service pavements exposed to realistic truck traffic and environmental conditions, cradle-to-grave LCA/LCCA studies can be conducted to investigate the effects of use stage, maintenance and rehabilitation, and end-of-life.

# REFERENCES


Abdullah, J. D., N. Ali, R. N. Mohamed, and M. M. A. Abdullahi. (2018). The effect of quarry dust with cement by-products on properties of concrete. Malaysian Journal of Civil Engineering, Vol. 30, No. 3, 2018, pp. 415 - 428

Abu-Farsakh, M. Y., K. Alshibli, M., Nazzal, and E. Seyman. Assessment of in-situ test technology for construction control of base courses and embankments. Report No. FHWA/LA 4-385, Louisiana Transportation Research Center, Baton Rouge, 2004

Ahlvin, R. G. Developing a set of CBR design curves. Instruction Report No. 4, U.S. Army Corps of Engineer Waterways Experimental Station, 1959

Ahlvin, R. G. Flexible pavement design criteria. Journal of the Aero-Space Transport Division, Proceedings of the American Society of Civil Engineers, Vol. 88, No. 1, 1962, pp.15-36

American Association of State Highway and Transportation Officials. AASHTO guide for design of pavement structures. AASHTO, 1993

Andrei, D., M. W. Witczak, and M. W. Mirza, M. W. Development of a revised predictive model for the dynamic (complex) modulus of asphalt mixtures. Inter Team Technical Report, NCHRP 1-37A Project, , University of Maryland College Park, MD, 1999

Arulrajah, A., J. Piratheepan, and M. Disfani. Reclaimed asphalt pavement and recycled concrete aggregate blends in pavement subbases: laboratory and field evaluation. Journal of Materials in Civil Engineering, Vol. 26, No. 2, 2013, pp. 349-357

Arulrajah, A., J. Piratheepan, M. Disfani, and M. W. Bo. Geotechnical and geoenvironmental properties of recycled construction and demolition materials in pavement subbase applications. Journal of Materials in Civil Engineering, Vol. 25, No. 8, 2012, pp. 1077-1088

Ashtiani, R., D. Little and E. Masad. Evaluation of the impact of fines on the performance of lightly cement-stabilized aggregate systems. Transportation Research Record: Journal of the Transportation Research Board, Vol. 2026, Washington D.C., 2007, pp. 81-88

ASTM C117-17, Standard test method for materials finer than 75-μm (No. 200) sieve in mineral aggregates by washing. ASTM International: West Conshohocken, PA, DOI: 10.1520/C0117-17, www.astm.org, 2017

ASTM C127, Standard test method for relative density (specific gravity) and absorption of coarse aggregate. ASTM International: West Conshohocken, PA, www.astm.org, 2015

ASTM C136 / C136M-14, Standard test method for sieve analysis of fine and coarse aggregates. ASTM International: West Conshohocken, PA, DOI: 10.1520/C0136-04, www.astm.org, 2014

ASTM C1435 / C1435M, Standard practice for molding roller-compacted concrete in cylinder molds using a vibrating hammer. ASTM International: West Conshohocken, PA, DOI: 10.1520/C1435_C1435M-14, www.astm.org, 2014

ASTM C29 / C29M-17, Standard test method for bulk density ("unit weight") and voids in aggregate. ASTM International: West Conshohocken, PA, DOI: 10.1520/C0029_C0029M-17A, www.astm.org, 2017a

ASTM D1632, Standard practice for making and curing soil-cement compression and flexure test specimens in the Laboratory (Withdrawn 2016). ASTM International: West Conshohocken, PA, www.astm.org, 2007

ASTM D1633, Standard test methods for compressive strength of molded soil-cement cylinders (withdrawn 2016). ASTM International: West Conshohocken, PA, DOI: 10.1520/D1633-00R07, www.astm.org, 2007a

ASTM D4643, Standard test method for determination of water (moisture) content of soil by microwave oven heating. ASTM International: West Conshohocken, PA, DOI: 10.1520/D4643-08, www.astm.org, 2008

ASTM D698, Standard test methods for laboratory compaction characteristics of soil using standard effort (12 400 ft-lbf/ft3 (600 kN-m/m3)). ASTM International: West Conshohocken, PA, DOI: 10.1520/C0698-16, www.astm.org, 2012

ASTM E2583, Standard test method for measuring deflections with a Light Weight Deflectometer (LWD). ASTM International: West Conshohocken, PA, DOI: 10.1520/E2583-15, www.astm.org, 2015a

Ayres, M. and M. Witczak, M. AYMA - A mechanistic probabilistic system to evaluate flexible pavement performance. Proceedings of Transportation Research Board, 77th Annual Meeting, Washington, DC. Paper No.980738, 1998

Bass, R. P. Quality control of soil-cement construction for water resources. Proceedings of Geo-Denver 2000: Soil-Cement and Other Construction Practices in Geotechnical Engineering, Denver, Colorado August 5-8, 2000, pp. 13-25

Bare, J. TRACI 2.0: the tool for the reduction and assessment of chemical and other environmental impacts 2.0. Clean Technologies and Environmental Policy, Vol. 13, No. 5, Springer, 2011, pp. 687-696

Bare, J. The Tool for the Reduction and Assessment of Chemical and other Environmental Impacts. TRACI 2.1: User's Manual. Pre Consultants. Document ID: S-10637-OP-1-0, U.S. Environmental Protection Agency, Washington, DC, 2012

Barksdale, R. D., Q. Robnett, J. Lai, and A. E. Zeevaert. Experimental and theoretical behavior of geotextile reinforced aggregate soil systems. In the 2nd International Conference of Geotextiles, Vol. 2, Las Vegas, 1982, pp. 375-380

Bennert, T. and A. Maher. The development of a performance specification for granular base and subbase material. Final Report No. FHWA-NJ-2005-003, 2005

Bennert, T., W. Papp Jr, A. Maher, and N. Gucunski. Utilization of construction and demolition debris under traffic-type loading in base and subbase applications. Transportation Research Record, Journal of the Transportation Research Board, Vol. 1714, 2000, pp. 33-39

Bloomquist, D., G. Diamond, M. Oden, B. Ruth, and M. Tia, M. Engineering and environmental aspects of recycled materials for highway construction. Appendix 1. Final report, September 1992-June 1993, No. PB-94-140977/XAB, Western Research Inst., Laramie, WY, 1993

Blue Group. Cone Crusher Applications. United Kingdom, accessed February 20, 2019 https://blue-group.com/en/news/cone-crusher-applications/

Brito, L. Design methods for low volume roads. Doctoral dissertation, the University of Nottingham, 2011

Broms, B. B. The Bearing capacity of pavements subjected to frost action. Highway Research Record, Vol. 39, 1963, pp. 66-180

Broms, B. B. The effect of degree of saturation on the bearing capacity of flexible pavements. Highway Research Record, Vol. 71, 1964, pp. 1-14

Brown, S. F. and J. W. Pappin. Analysis of pavements with granular bases. National Research Council, Washington, D.C., Transportation Research Board, 1981, pp. 17-23

Ceylan, H., A. Guclu, E. Tutumluer, and M. R. Thompson. Backcalculation of full-depth asphalt pavement layer moduli considering nonlinear stress-dependent subgrade behavior. International Journal of Pavement Engineering, Vol. 6, No. 3, 2005, pp. 171-182

Chang, G., Q. Xu, J. Rutledge, and S. Garber. A study on intelligent compaction and in-place asphalt density. Final report No. FHWA-HIF-14-017, Federal Highway Administration, 2014

Chen, M., J. Lin, and S. Wu. Potential of recycled fine aggregates powder as filler in asphalt mixture. Construction and Building Materials, Vol. 25, No. 10, 2011, pp. 3909-3914

Chesner, W. H., R.J. Collins, and M. MacKay. User guidelines for waste and by-product materials in pavement construction. Publication FHWA-RD-97-148. FHWA, U.S. Department of Transportation, 1998

Crockford, W. W. Modeling stress and strain states in pavement structures incorporating thick granular layers. Final Report, the Texas Transportation Institute, 1990

Cunningham, C. N., T. M. Evans, and A. A. Tayebali. Gradation effects on the mechanical response of crushed stone aggregate. International Journal of Pavement Engineering, Vol. 14, No. 3, 2013, pp. 231-241

Dehlen, G. L. The effect of nonlinear material response on the behavior of pavements subjected to traffic loads, 1969

De Rezende, L. and C. De Carvalho. The use of quarry waste in pavement construction. Resources, Conservation and Recycling, Vol. 39, No. 1, 2003, pp. 91-105

Desai, C. S. and C. W. Schwartz, C. W. Selection of finite element program for flexible pavement response model, 2000

Dumitru, I., T. Zdrilic, and G. Johnson. Further investigation of soil remineralization using quarry fines in Australia. In International Center for Aggregates Research (ICAR) 9th Annual Symposium, 2001

Duncan, J. M., C. L. Monismith, and E. L. Wilson. Finite element analysis of pavements. Highway Research Record, Washington D.C., Vol. 228, 1968, pp. 18-33

EarthShift. US-Ecoinvent database. Version 2.2. [database]. Swiss center for life-cycle inventories, St-Gallen, Switzerland, 2013

Elliott, R. P., and M. R. Thompson, M. R. Mechanistic design concepts for conventional flexible pavements. Interim Report, Department of Civil Engineering, University of Illinois at Urbana-Champaign, 1985

Emissions and Generation Resource Integrated Database (eGRID) 2010 [Software]. U.S. Environmental Protection Agency, Washington, D.C, 2014

Environmental Protection Agency. Advancing sustainable materials management: 2014 fact sheet. U.S. Environmental Protection Agency, Washington, D.C, 2016

Erlingsson, S. and A. Ahmed. Fast layered elastic response program for the analysis of flexible pavement structures. Road Materials and Pavement Design, Volume 14, No. 1, 2013 pp. 196-210

Fuller, W. B., and S. E. Thompson. The laws of proportioning concrete. Transactions of the American Society of Civil Engineers, Vol. 57, No. 2, 1907, pp. 67-143

Galetakis, M., G. Alevizos, and K. Leventakis. Evaluation of fine limestone quarry by-products for the production of building elements–An experimental approach. Construction and building materials, Vol. 26, No. 1, 2012, pp. 122-130

Garg, N., H. Kazmee, and R. Knieriem. Behavior of P-401 HMA Surface in Accelerated Pavement Testing at High Temperatures and Tire Pressures. Conference proceeding, in Airfield and Highway Pavements 2017, Philadelphia, Pennsylvania, August 27–30, 2017

Ghabchi, R., M. Zaman, N. Khoury, H. Kazmee, and P. Solanki. Effect of gradation and source properties on stability and drainability of aggregate bases: a laboratory and field study. International Journal of Pavement Engineering, Vol. 14, No. 3, 2013, pp. 274-290

Giroud, J. P., and L.Noiray. Geotextile-reinforced unpaved road design. Journal of the Geotechnical Engineering Division, Vol. 107 (GT9), No. ASCE 16489, 1981, pp. 1233–1254

Goode, J. F., and L. A. Lufsey. A new graphical chart for evaluating aggregate gradation. Monograph Accession No. 00217546: 13-26, 1962

Gopalakrishnan, K., S. Kim, and H. Ceylan. Non-destructive evaluation of in-place rehabilitated concrete pavements. Journal of Civil Engineering and Management, Vol. 16, No. 4, 2010, pp. 552-560

Hall, K. D., and J. W. Bettis. Development of comprehensive low volume pavement design procedures. Report No. MBTC-1070, US Department of Transportation, 2000

Halsted, G. E., D. R. Luhr, and W. S. Adaska. Guide to Cement-Treated Base (CTB). Portland Cement Association, Skokie, Illinois, 2006, 20 pages

Hammitt, G. M., and W. Aspinall Iii. Thickness requirements for unsurfaced roads and airfields; bare base support. Report No. AEWES-TR-S-70-5, Army Engineer Waterways Experiment Station, Vicksburg, Missouri, 1970

Harichandran, R. S., M. S. Yeh, and G. Y. Baladi. MICH-PAVE: A nonlinear finite element program for analysis of pavements. National Research Council, Washington D.C., Transportation Research Record, Vol. 1286, 1990 pp. 123-131

Harichandran, R. S., T. Mahmood, A. R. Raab, and G. Y. Baladi, G. Y. Modified Newton algorithm for backcalculation of pavement layer properties. Transportation Research Record: Journal of the Transportation Research Board, Vol. 1384, No. 15, Washington D.C., 1993, pp. 15-31

Harvey, J. T., J. Meijer, H. Ozer, I. L. Al-Qadi, A. Saboori, and A. Kendall, A. Pavement life-cycle assessment framework. Final report No. FHWA-HIF-16-014. Federal Highway Administration, Washington, July 2016

Harvey, J., J. Meijer, and Kendall, A. life cycle assessment of pavements. Federal Highway Association TechBreif No. FHWA-HIF-15-001. Transportation Reseach Record, October, 2014

Hicks, R. G. Development of the 2002 guide for design of new and rehabilitated pavement structure. National Cooperative Highway Research Program Project 1-37A, Washington D.C., 2002

Hicks, R. G., and C. L. Monismith, C. L. Factors influencing the resilient response of granular materials. Highway research record, Vol. 345, Washington D.C., 1971, pp. 15-31

Hicks, R. G., and C. L. Monismith, C. L. Prediction of the resilient response of pavements containing granular layers using non-linear elastic theory. Presented at the third International Conference on the Structural Design of Asphalt Pavements, Grosvenor House, Park Lane, London, England, Sept., Vol. 1, 1972, pp. 11-15, 1972

Hill, H. J., and M. R. Thompson. Early life study of the FA409 full-depth asphalt concrete pavement sections. Research report, University of Illinois at Urbana-Champaign, Urbana, Illinois, 1998

Hoffman, M. S. Mechanistic interpretation of nondestructive pavement testing deflections, Doctoral Dissertation, University of Illinois at Urbana Champaign, 1980

Hoffman, M. S., and M. R. Thompson. Nondestructive testing of flexible pavements: field testing program summary. Report No. UILU-ENG-2003, Springfield, IL, 1981

Horak, E. Aspects of deflection basin parameters used in a mechanistic rehabilitation design procedure for flexible pavements in South Africa. Doctoral dissertation, University of Pretoria, 1987

Horvath, A. Life-cycle environmental and economic assessment of using recycled materials for asphalt pavements. Technical report, University of California Transportation Center, 2003

Hossain, A. S. M., and J. P. Zaniewski. Characterization of falling weight deflectometer deflection basin. Transportation Research Record, Journal of the Transportation Research, Washington D.C., Vol. 1293, 1991

Huang, Y.H. Pavement analysis and design. Book. Pearsons, 2004

Huang, Y. H., and M. W. Witczak. Program DAMA (Chevron). User's manual, Department of Civil Engineering, University of Maryland, 1979

Illinois Department of Transportation. Subgrade stability manual. Illinois DOT Bureau of Bridges and Structures, Springfield, IL, 1982, 65 pages

Illinois Department of Transportation. Subgrade stability manual. Illinois DOT Bureau of Bridges and Structures, Springfield, IL, 2005, 34 pages

Illinois Department of Transportation. Pavement technology advisory - performance graded binder materials for hot mix asphalt. PTA-D4, Bureau of Materials and Physical Research, Springfield, IL, 2005a

Illinois Department of Transportation. Bureau of Local Roads and Streets Manual. Illinois DOT Bureau of Local Roads and Streets, Springfield, IL, Revised December 2018, 2346 pages

Illinois Department of Transportation. Standard specifications for road and bridge construction. Illinois DOT, Springfield, IL, 2016, 1225 pages

Illinois Department of Transportation. Pay item report with awarded prices, August 03, 2018 letting 10:00am, Notice of Letting. Retrieved from: https://webapps.dot.illinois.gov/WCTB/LbLettingDetail/Search , Vol. 21, No. 26, 2018

Irwin, L. H. MODCOMP 5.0. Cornell Local Roads Program, Ithaca, NY, 2001

Isola, M., G. Betti, A. Marradi, and G. Tebaldi, G. Evaluation of cement treated mixtures with high percentage of reclaimed asphalt pavement. Construction and Building Materials, Vol. 48, 2013, pp. 238-247

ITM No. 508-12T. Field determination of deflection using light weight deflectometer. Indiana test methods, Office of Materials Management, Indiana Department of Transportation Indianapolis, IN

ITM No. 514-15T. Test section for aggregates and recycled materials. Indiana test methods, Office of Materials Management, Indiana Department of Transportation Indianapolis, IN

Kalcheff, I. and C. Machemehl Jr. Utilization of crushed stone screenings in highway construction. Presented in the 59th Annual Meeting of the Transportation Research Board, Washington, DC, 1980

Kang, S. G. The development of a regional inventory database for the material phase of the pavement life-cycle with updated vehicle emission factors using MOVES. Masters Thesis, University of Illinois at Urbana-Champaign, 2013

Kang, S., R. Yang, H. Ozer, and I. L. Al-Qadi. Life-cycle greenhouse gases and energy consumption for material and construction phases of pavement with traffic delay. Transportation Research Record, Journal of the Transportation Research Board, Vol. 2428, No. 1, 2014, pp. 27-34

Kang, S., M. Ziyadi, H. Ozer, and I. L. Al-Qadi. Variable Impact Transportation (VIT) model for energy and environmental impact of hauling truck operation. The International Journal of Life Cycle Assessment, https://doi.org/10.1007/s11367-018-1554-5, 2018, pp. 1-15

Kazmee, H. Performance evaluation of unconventional aggregates from primary and recycled sources for construction platform and low volume road applications. Doctoral dissertation, University of Illinois at Urbana-Champaign, 2018

Kazmee, H. and E. Tutumluer. Evaluation of aggregate subgrade materials used as pavement subgrade/granular subbase. Final Report. Illinois Center for Transportation/Illinois Department of Transportation, 2015

Khazanovich, L. and Q. Wang, Q. MnLayer: high-performance layered elastic analysis program. Transportation Research Record: Journal of the Transportation Research Board, Washington D.C., Vol. 2037, 2007, pp. 63-75

Khosravifar, S., C. D. Schwartz, D. Goulias. Time-dependent stiffness increase of foamed asphalt stabilized base material. Proceedings of ninth international conference on the Bearing Capacity of Roads, Railways and Airfields (BCRRA 2013), Trondheim, Norway, 2013

Kim, M. Three-dimensional finite element analysis of flexible pavements considering nonlinear pavement foundation behavior. Doctoral Dissertation, University of Illinois at Urbana Champaign, 2007

Kim, M., E. Tutumluer, and J. Kwon. Nonlinear pavement foundation modeling for three-dimensional finite-element analysis of flexible pavements. International Journal of Geomechanics, Vol. 9, No. 5, 2009, pp. 195-208

Kim, Y. R., B. Underwood, M. S. Far, N. Jackson, J. Puccinelli, and N. C. Engineers, N. C. LTPP computed parameter: dynamic modulus. Report No. FHWA-HRT-10-035, Federal Highway Administration, Washington D.C., 2011

Kleyn, E., The Use of the Dynamic Cone Penetrometer (DCP). Transvaal Provincial Administration, 1975

Koganti, S. P., and H. R. Chappidi. Effective utilization of quarry dust in flexible pavements as per IRC-37: 2012. ARPN Journal of Engineering and Applied Sciences, Vol. 13, No. 5, 2018, pp. 1545-1552

Kumar, D.S. and W. Hudson. Use of quarry fines for engineering and environmental applications. Special Report. National Stone Association, Center for Transportation Research, The University of Texas-Austin, Austin, TX, 1992

Kumavat, H. R., and V. J. Patel. Factors influencing the strength relationship of concrete cube and standard cylinder. International Journal of Innovative Technology and Exploring Engineering (IJITEE), Vol. 3, No. 8, 2014, pp. 76-79

Kwon, J., E. Tutumluer, and M. Kim, M. Development of a mechanistic model for geosynthetic-reinforced flexible pavements. Geosynthetics International, Vol. 12, No. 6, 2005, pp. 310-320

Kwon, J., E. Tutumluer, and M. Kim, M. Mechanistic analysis of geogrid base reinforcement in flexible pavements considering unbound aggregate quality. Journal of the Korean Society of Road Engineers (한국도로학회논문집), Vol. 8, No. 2, 2006, pp. 37-47

Kwon, J., E. Tutumluer, and I. L. Al-Qadi. Validated mechanistic model for geogrid base reinforced flexible pavements. Journal of Transportation Engineering, Vol. 135, No. 12, 2009, pp. 915-926

LaHucik, J., S. Schmidt, E. Tutumluer, and J. Roesler. Characterization of cement treated base course using reclaimed asphalt pavement, aggregate by-products, and macro-synthetic fibers. Proceedings of Geo-Chicago Conference, 2016, pp. 523-533

LaHucik, J., S. Schmidt, E. Tutumluer, and J. Roesler. Cement-treated bases containing reclaimed asphalt pavement, quarry by-products, and fibers. Transportation Research Record: Journal of the Transportation Research Board, Washington D.C., Vol. 2580, 2016a, pp. 10-17

Lippert, D. L., H. Ozer, I. L. Al-Qadi, A. K. El-Khatib, R. Yang, A. Z. Dahhan, and J. S. Trepanier. Illinois highway materials sustainability efforts of 2013. Final report No. FHWA-ICT-14-015, Illinois Center for Transportation and Illinois Department of Transportation, 2014

Lohani, T. Optimum utilization of quarry dust as partial replacement of sand in concrete. International Journal of Applied Science and Engineering Research, Vol. 1, No. 2, 2012, pp. 391-404

Loulizi, A., I. L. Al-Qadi, S. Lahouar, and T. Freeman. Measurement of vertical compressive stress pulse in flexible pavements: representation for dynamic loading tests. Transportation Research Record: Journal of the Transportation Research Board, Washington D.C., Vol. 1816, 2002, pp. 125-136

MacGregor, J., W. Highter, and D. DeGroot, Structural numbers for reclaimed asphalt pavement base and subbase course mixes. Transportation Research Record: Journal of the Transportation Research Board, Vol. 1687, 1999, pp. 22-28

Manning, D. Exploration and use of quarry fines. Miro Project Final Report No. 087/MIST2/DACM/01, Mineral Solution LTD, Manchester, United Kingdom, 2004

Masada, T., S. M. Sargand, B. Abdalla, and J. L. Figueroa. Material properties for implementation of mechanistic-empirical (ME) pavement design procedures. Final report No. FHWA/OH-2003/021, Washington D.C., 2014

Massazza, F. Pozzolana and pozzolanic cements. Published in Lea's chemistry of cement and concrete, Vol 4, 1998 pp. 471-631

McClellan, G., J. Eades, K. Fountain, P. Kirk, and C. Rothfuss. Research and techno-economic evaluation: Uses of limestone byproducts. Final Report No. WPI 0510798, Department of Geological Sciences, University of Florida, 2002

McLeod N. W. Some basic problems in flexible pavement design. In Highway Research Record Proceedings, Vol. 32, 1953, pp. 90-118

McLeod N. W. The ultimate strength approach to flexible pavement design. In the proceedings of The Association of Asphalt Paving Technologists, Vol. 23, 1954

Mishra, D. Aggregate characteristics affecting response and performance of unsurfaced pavements on weak subgrades. PhD Dissertation, University of Illinois at Urbana-Champaign, 2012

Mishra, D., and E. Tutumluer. Aggregate physical properties affecting modulus and deformation characteristics of unsurfaced pavements. Journal of Materials in Civil Engineering, Vol. 24, No. 9, 2012, pp. 1144-1152

Moaveni, M., E. Mahmoud, E. Ortiz, E. Tutumluer, and S. Beshears. Evaluation of aggregate resistance to breakage, abrasion, and polishing using advanced aggregate imaging systems. Transportation Research Board, Washington, D.C., 2014

Moaveni, M. Advanced image analysis and techniques for degradation characterization of aggregates. Ph.D dissertation, University of Illinois at Urbana-Champaign, 2015

Moaveni, M., Y. Qian, I. I. Qamhia, E. Tutumluer, C. Basye, and D. Li. Morphological characterization of railroad ballast degradation trends in the field and laboratory. Transportation Research Record: Journal of the Transportation Research Board. Vol. 2545, 2016, pp. 89-99

Mohammad, L., A. Raghavandra, and B. Huang. Laboratory performance evaluation of cement-stabilized soil base mixtures. Transportation Research Record: Journal of the Transportation Research Board, No. 1721, 2000, pp. 19-28

Mohammad, L. N., M. Y. Abu-Farsakh, Z. Wu, and C. Abadie. Louisiana experience with foamed recycled asphalt pavement base materials. Transportation Research Record: Journal of the Transportation Research Board, Vol. 1, No. 1832, 2003, pp. 17-24

Mohammadinia, A., A. Arulrajah, J. Sanjayan, M. Disfani, M. W. Bo, and S. Darmawan. Laboratory evaluation of the use of cement-treated construction and demolition materials in pavement base and subbase applications. Journal of Materials in Civil Engineering, Vol. 27, No. 6, 2014

Mwumvaneza, V., W. Hou, E. Tutumluer, I. Al-Qadi, and S. Beshears. Characterization and stabilization of quarry byproducts for sustainable pavement spplications. Transportation Research Record: Journal of the Transportation Research Board, No. 2509, 2015, pp. 1-9

Naik, R., N. Rudolph, Y. Chun, C. Fethullah, and W. Bruce. Use of fly ash and limestone quarry by-products for developing economical self-compacting concrete. Proceedings of the International Congress on Fly Ash Utilisation, 4th-7th December, 2005

National Crushed Stone Association (NCSA). Flexible pavement design guide for highways. National Crushed Stone Association Publications, Washington D.C., 1972.

Nazzal, M. Non-nuclear methods for compaction control of unbound materials. National Cooperative Highway Research Program (NCHRP) Synthesis 456, Project No. 20-05, Topic 44-10, Washington D.C., 2014

Nelson, J., S. Tymkowicz, and M. Callahan. An investigation of emulsion stabilized limestone screenings. Departmental Report No. HR-309, Office of Materials, Highway Division, Iowa Department of Transportation, 1994

Ozer, H., R. Yang, and I. L. Al-Qadi, I. L. Quantifying sustainable strategies for the construction of highway pavements in Illinois. Transportation Research Part D: Transport and Environment, Vol. 51, 2017, pp. 1-13

Pekcan, O., E. Tutumluer, and M. R. Thompson, M. R. Nondestructive flexible pavement evaluation using ILLI-PAVE based artificial neural network models. Proceedings of GeoCongress 2006: Geotechnical Engineering in the Information Technology Age, 2006, pp. 1-6

Petavratzi, E. and S. Wilson. Incinerated Sewage Sludge Ash in Facing Bricks. Characterization of mineral wastes, resources and processing technologies–integrated waste management for the production of construction material. Publication WRT177/WR0115, 2007

Petavratzi, E. and S. Wilson. Sustainable utilisation of quarry by-products. Minerals Industry Research Organisation, English Heritage, The Department for Environment, Food and Rural Affairs, 2008

Puppala, A., S. Saride, and R. Williammee. Sustainable reuse of limestone quarry fines and RAP in pavement base/subbase layers. Journal of Materials in Civil Engineering, Vol. 24, No. 4, 2011, pp. 418-429

Puppala, A., S. Saride, S. Sirigiripet, R. Williammee, and V. Dronamraju. Evaluation of cemented quarry fines as a pavement base material. In GeoCongress 2008: Geotechnics of waste management and remediation, 2008, pp. 312-319

Qamhia, I., J. Cheung, W. Hou, V. Mwumvaneza, H. Ozer, and E. Tutumluer. Gradation effects on the strength properties of cement and fly ash stabilized quarry by-products. Proceedings of the Geo-Chicago Conference, Procedia Engineering, 2016. 143: pp. 911-920

Qamhia, I., L. C. Chow, D. Mishra, and E. Tutumluer. Dense-graded aggregate base gradation influencing rutting model predictions. Transportation Geotechnics, Vol. 13, 2017, pp. 43-51

Qamhia, I., H. Kazmee, E. Tutumluer, and H. Ozer. Sustainable application of quarry byproducts mixed with large size unconventional aggregates for improved performance. In International Congress and Exhibition Sustainable Civil Infrastructures: Innovative Infrastructure Geotechnology". 2017a. Springer

Qamhia, I., E. Tutumluer, L. C. Chow, and D. Mishra. A framework to utilize shear strength properties for evaluating rutting potentials of unbound aggregate materials. Proceedings of the 3rd International Conference on Transportation Geotechnics (ICTG), Portugal, Procedia engineering, 2016a

Qamhia, I., E. Tutumluer, H. Ozer, and H. Kazmee. Field performance evaluation of pavement construction platforms utilizing unconventional large size aggregates packed with quarry byproducts, and higher fines aggregate subgrade layers. In Airfield and Highway Pavements, 2017b, pp. 334-347

Qamhia, I., E. Tutumluer, H. Ozer, S. Beshears, H. Shoup, and H. Kazmee. Field performance evaluation of quarry byproducts used in unbound aggregate layers constructed over soft subgrade. Presented in Transportation Research Board 97th Annual Meeting, No. 18-05170, 2018

Qamhia, I., E. Tutumluer, and H. Ozer. Field performance evaluation of sustainable aggregate byproduct applications. Final report No. FHWA-ICT-18-016, Illinois Center for Transportation/Illinois Department of Transportation, 2018a

Qamhia, I. I., E. Tutumluer, H. Ozer, H. Shoup, S. Beshears, and J. Trepanier. Evaluation of chemically stabilized quarry byproduct applications in base and subbase layers through Accelerated Pavement Testing. Transportation Research Record, 0361198118821099, Washington D.C., 2019

Raad, L. and J. L. Figueroa. Load response of transportation support systems. Journal of Transportation Engineering, American Society of Civil Engineers, Vol. 106, No. 1, 1980, pp. 111-128

Rada, G., and M. W. Witczak. Comprehensive evaluation of laboratory resilient moduli results for granular material Transportation Research Record, No. 810, 1981

Sayed, S. M., J.M. Pulsifer, and R.C. Schmitt. Construction and performance of shoulders using UNRAP base. Journal of materials in civil engineering, Vol. 5, N. 3, 1993, pp. 321-338

Schankoski, R. A., R. Pilar, L. R. Prudêncio Jr, and R. D. Ferron, R. D. Evaluation of fresh cement pastes containing quarry by-product powders. Construction and Building Materials, Vol. 133, 2017, pp. 234-242

Scullion, T., J. Uzan, and M. Paredes. MODULUS: A microcomputer-based backcalculation system. Transportation Research Record, Vol. 1260, Washington D.C., 1990, pp. 180-191

Sivaneswaran, N., S. L. Kramer, and J. P. Mahoney. Advanced backcalculation using a nonlinear least squares optimization technique. Transportation research record: Journal of the Transportation Research Board, Vol. 1293, Washington D.C., 1991, pp. 93-102

Skolnik, J., M. Brooks, and J. Oman. Fuel usage factors in highway and bridge construction. National Cooperative Highway Research Program Report No. 744. National Academy of Sciences, Washington D.C., 2013

Smith, K. D., J.E. Bruinsma, M. J. Wade, K. Chatti, J. Vandenbossche, and H. T. Yu. Using falling weight deflectometer data with Mechanistic-Empirical design and analysis, Volume I. Final report no. FHWA-HRT-16-009, Federal Highway Administration, U.S., 2017

Stedman Machine Company. HSI crusher manufacturer. Aurora, IN, accessed: February 20, 2019: https://www.stedman-machine.com/more.html.

Stokowski, S. Pond screening from aggregate plants: an industrial minerals resource. Proceedings of the 28th Forum on the Geology of Industrial Minerals. West Virginia Geological and Economic survey, Morgantown, WV, 1992

Stroup-Gardiner, M. and T. Wattenberg-Komas. Recycled materials and by-products in highway applications. Volume 4: Mineral and quarry by-products. NCHRP Synthesis of Highway Practice (Project 20-05, Topic 40-01), Transportation Research Board, 2013

Sugi, T., Y. Ando, M. Makita, and A. Ito. Cement/asphalt mixtures and processes for preparation of the same. U.S. Patent 5,223,031, Nichireki Kagaku Kogyo Co Ltd and Osaka Cement Co Ltd, 1993

Talbot, A. N., and F. E. Richart. The strength of concrete, its relation to the cement aggregates and water. University of Illinois at Urbana Champaign, College of Engineering. Engineering Experiment Station, 1923

Talvik, O., and A. Aavik. Use of FWD deflection basin parameters (SCI, BDI, BCD) for pavement condition assessment. Baltic Journal of Road and Bridge Engineering, Vol. 4, No. 4, 2009, pp. 196-202

Tarmac Ltd and Partners. New and novel streams for quarry dust and fillers feasibility review. Final project report No. MA/7/G/5/004 – WP3, United Kingdom, 2011 (March), 85 pages

Texas Department of Transportation (Texas DOT). Section 4: FPS21 modulus inputs and backcalculation methodology, accessed February 19,2019: http://onlinemanuals.txdot.gov/txdotmanuals/pdm/fps21_mod_inputs_backcal_method.htm,

Thompson, M. R., T.C. Kinney, M. L. Traylor, J. R. Bullard, J. L. and Figueroa, J. L. Subgrade stability: final report. Technical Report No. IHR-605, Illinois Cooperative Highway and Transportation Research Program, University of Illinois at Urbana-Champaign, Urbana, Illinois, 1977

Thompson, M. R. ILLI-PAVE based NDT analysis procedures. In Nondestructive testing of pavements and backcalculation of moduli. ASTM International, 1989

Thompson, M. R., and N. Garg. Wheel load interaction: critical airport pavement responses. In Proceedings of the Federal Aviation Administration Airport Technology Transfer Conference, Atlantic City, NJ, 1999 (July)

Thompson, M. R., and T. G. LaGrow. A proposed conventional flexible pavement thickness design procedure. Report No. FHWA-IL-UI-223, Springfield, IL, 2003

Townsend, J. M., W.C. Jennings, C. Haycocks, G. M. Neall III, and L.P. Johnson III. A relationship between the ultimate compressive strength of cubes and cylinders for coal specimens. The 18th US Symposium on Rock Mechanics (USRMS), American Rock Mechanics Association, January 1977

Traxler, R. N. Plasticity as a factor in the design of dense bituminous road carpets: By LW Nijboer, Senior Research Engineer, Amsterdam Laboratory of the NV De Batâafsche Petroleum Maatschappij (Royal Dutch Shell Group). 184 pp. Elsevier Pub. Co., 1949

Tseng, K. and R. Lytton. Prediction of permanent deformation in flexible pavement materials. Implication of Aggregates in the Design, Construction, and Performance of Flexible Pavements. ASTM STP 1016, ASTM, 1989, pp. 154-172

Tutumluer, E. Predicting behavior of flexible pavements with granular bases. Doctoral dissertation, Georgia Institute of Technology, 1995

Tutumluer, E., M. R. Thompson, G. Garcia, and J. Kwon. Subgrade stability and pavement foundation requirements. In proceedings of the 15th Colombian Symposium of Pavement Engineering, Melgar, Colombia, March 9-12, 2005

Tutumluer, E. Practices for unbound aggregate pavement layers. National Cooperative Highway Research Program (NCHRP) No. Project 20-05, Topic 43-03. Transportation Research Board, 2013

Tutumluer, E., M. Moaveni, and I. Qamhia. Aggregate quality requirements for pavements. National Cooperative Highway Research Program (NCHRP) No. Project 20-05, Topic 48-10. Transportation Research Board, 2018

Tutumluer, E., H. Ozer, W. Hou, and V. Mwumvaneza. Sustainable aggregates production: Green applications for aggregate by-Products. Final Report. Illinois Center for Transportation and Illinois Department of Transportation, 2015

Tutumluer, E., and P. Sarker, P. Development of improved overlay thickness design alternatives for local roads. Final report no. FHWA-ICT-15-008. Illinois Center for Transportation and Illinois Department of Transportation, 2015

Tutumluer, E., I. Qamhia, and H. Ozer. Field performance evaluations of sustainable aggregate by-product applications. Keynote Paper, Proceedings of the International Symposium on Geotechnics of Transportation Infrastructure (ISGTI), Delhi, India, 2018a

Tutumluer, E., and M. Thompson. Anisotropic modeling of granular bases in flexible pavements. Transportation Research Record: Journal of the Transportation Research Board, Vol. 1577, Washington D. C., 1997, pp. 18-26

Ullidtz, P. Pavement Analysis. Developments in Civil Engineering, No. 19, Amsterdam, Netherlands, 1987

United Kingdon Highways Agency. Design manual for roads and bridges (DMRB). UK Highways Agency, United Kingdom, 1994

United Kingdon Highways Agency. Interim advice note 73/09: Design guidance for road pavement foundations. Design manual for roads and bridges, UK Highways Agency, United Kingdom, 2009

U.S. Life Cycle Inventory Database National Renewable Energy Laboratory, 2012, accessed March 12, 2019: https://www.lcacommons.gov/nrel/search

Uzan, J. Dynamic linear back calculation of pavement material parameters. Journal of Transportation Engineering, Vol. 120, No. 1, 1994, pp. 109-126

Van Cauwelaert, F. J., D. R. Alexander, T. D. White, and W. R. Barker. Multilayer elastic program for backcalculating layer moduli in pavement evaluation. Conference Proceeding, In: Nondestructive testing of pavements and backcalculation of moduli, ASTM International, 1989

Van Dam, T.J., J. T. Harvey, S. T. Muench, K. D. Smith, M. B. Snyder, I. L. Al-Qadi, H. Ozer, J. Meijer, P. V. Ram, J. R. Roesler, and A. Kendall. Towards sustainable pavement systems: a reference document. U.S. Department of Transportation, Federal Highway Administration, 2015

Van Gurp, C. A. P. M., and A. J. Van Leest. Thin asphalt pavements on soft soil. In International Society For Asphalt Pavements, proceedings of the ninth International Conference On Asphalt Pavements, AUGUST 17-22, Vol. 1, 2002

Ververka, V. Raming van de spoordiepte bij wegen met cen bitumineuze verharding. De Wegentechniek, Vol. 24, No. 3, 1979, pp. 25-45. Dutch reference

Walker, R. , and S. A. Pavía. Physical properties and reactivity of pozzolans, and their influence on the properties of lime–pozzolan pastes. Materials and structures, Vol. 44, No. 6, 2011, pp. 1139-1150

White, D. J., P. Becker, P. K.Vennapusa, M. J. Dunn, and C. I. White. Assessing soil stiffness of stabilized pavement foundations. Transportation Research Record, Vol. 2335, No. 1, 2013, pp. 99-109

Wood, S.A. and C.R. Marek. Recovery and utilization of quarry by-products for use in highway construction. International Center for Aggregates Research (ICAR) 3rd Annual Symposium, Vol. 10, 1995

WRAP (the Waste & Resources Action Programme). The sustainable use of resources for the production of aggregates in England. Published online in 2006, accessed November 9,2018: http://www.wrap.org.uk/downloads/WRAP_AGG0059_project_report_final_20.10.06.445bdc82.pdf

Xiao, Y., and E. Tutumluer. Best value granular material for road foundations. Research report No. MN/RC 2012-01. Minnesota Department of Transportation, Saint Paul, MN, 2012

Yang, R. Development of a pavement life cycle assessment tool utilizing regional data and introducing an asphalt binder model. Masters Thesis, University of Illinois at Urbana-Champaign, 2014

Yang, R. Y. Development and implementation of comprehensive regionalized pavement life-cycle assessment. Doctoral dissertation, University of Illinois at Urbana-Champaign, 2017

Zienkiewicz, O. C., R. L. Taylor, and J. Z. Zhu. The finite element method: its basis and fundamentals. Book, Elsevier, 2005

# APPENDIX A: PACKING STUDY OF QB MIXED WITH LARGE PCR STONES

## A.1 INTRODUCTION

This Appendix provides detailed information regarding the UIUC box packing study to determine the physical parameters and engineering properties that affect the blending of Primary Crusher Runs (PCR) and QB as aggregate subgrade layers in Cell 1. This appendix provides a further discussion to the information provided in Chapter 3 regarding the UIUC box packing study, and provides detailed information of the results for varying parameters such as the quantity of QB, the moisture content of the QB, the rigidity of the foundation, and the number/thickness of the constructed lifts. The description of the test setup, procedure, and matrix were provided in Chapter 3. More details can be found elsewhere (Qamhia et al., 2017a)

## A.2 COMPACTION TESTS OF PCR STONES

Compaction tests were conducted for the large PCR aggregates in order to study the packing and assess the void ratio. Tests were conducted in 1 lift and 2 lifts. The bulk specific gravity was measured as per ASTM C127 to be 2.67. Using this value of specific gravity, and based on the arrangement of the large rocks in the box, a void ratio of 77.5% and 83.1% were calculated for the large rocks compacted in two lifts and one lift, respectively. This corresponds to a porosity of 43.6% and 45.4% for the two and one lift arrangements, respectively. Based on these calculations, and given that some of the voids will be isolated and cannot be filled with QB; the maximum possible QB quantity to be used was set to 40% of the weight of the dry large rocks. Cross sections of the compacted large rocks in the UIUC packing box are shown in Figure A.1. The average compacted densities achieved are 93.9 pcf (14.74 kN/m$^3$) and 91.0 pcf (14.29 kN/m$^3$) for the two lifts and one lift arrangements, respectively.

(a) (b)

Figure A.1 Cross section of the compacted PCR aggregates in (a) one lift and (b) two lifts

Prior to using the PCR stones in packing studies, the size and shape properties were determined through sieve analysis and aggregate imaging. Representative samples were separated on the 3 in. (76 mm) sieve, and the gradation of aggregate particles passing the 76-mm sieve was determined with conventional dry sieve analysis; while for particles retained on the 3 in. (76-mm) sieve, the field imaging technique used previously by Kazmee and Tutumluer (2015), was used to determine the particle sizes and aggregate shape morphology. Aggregate morphological indices were also estimated for particles passing the 76-mm sieve using the Enhanced University of Illinois Aggregate Image Analyzer (E-UIAIA). Details about the E-UIAIA can be found elsewhere (Moaveni et al., 2014; Moaveni, 2015; Moaveni et al., 2016). The number of particles scanned was distributed among different sieve sizes to be proportional to the aggregate gradations, in order to get more representative values of aggregate morphological properties. The results for morphological shape properties are presented in Table A.1. Out of all particle sizes, the larger sized particles have the lowest Flat & Elongated (F&E) ratio, indicating more cubical particle shapes. The Angularity Index (AI) values for the different sizes conform to that of a good quality crushed stone material.

Table A.1 Morphological shape properties of PCR aggregate subgrade materials

| **Particle Size** | | **Angularity Index** | **Flat & Elongated Ratio** | **Surface Texture** |
|---|---|---|---|---|
| **Retained on 76 mm (3 in.)** | Average | 447.84 | 1.36 | 2.37 |
| 88 total aggregates | Max | 840.00 | 2.28 | 4.03 |
| | Min | 230.00 | 1.06 | 1.38 |
| **Retained on 50.8 mm (2 in.)** | Average | 488.37 | 2.11 | 1.54 |
| 48 total aggregates | Max | 707.83 | 3.81 | 2.75 |
| | min | 318.46 | 1.30 | 0.77 |
| **Retained on 38.1 mm (1.5 in.)** | average | 452.87 | 2.01 | 1.38 |
| 26 total aggregates | max | 686.06 | 2.69 | 2.17 |
| | min | 327.33 | 1.40 | 0.84 |
| **Retained on 25.4 mm (1 in.)** | Average | 401.69 | 2.37 | 1.44 |
| 21 total aggregates | max | 619.58 | 3.92 | 3.46 |
| | min | 280.78 | 1.47 | 0.43 |
| **Retained on 12.7 mm (0.5 in)** | Average | 462.61 | 2.48 | 2.29 |
| 6 total aggregates | max | 663.09 | 2.98 | 3.59 |
| | min | 370.44 | 1.61 | 1.27 |

## A.3 THE EFFECT OF VARYING THE QUANTITY OF QB

As described in the test matrix (see Chapter 3), the quantity of the QB to be mixed with the PCR stones was varied to determine the optimum QB quantity for the field application. The quantity of the QB was varied between 20% and 40% to study the maximum practical amount that can be added and constructed in the proposed construction method. Figure A.2 shows an example of varying the quantity of QB from 20% to 30% and to 40% for

compaction in 2 lifts in the case of dry QB. By a visual assessment of the surface and the cross section, 20% and 30% are underestimating the amount of dry QB that can be packed with the CS02, while 40% leaves excessive quantity of the QB on the surface; indicating that the optimum dry quantity of QB is around 35%. In the case of wet QB however, the optimum quantity is approximately 25% as explained in the following sections.

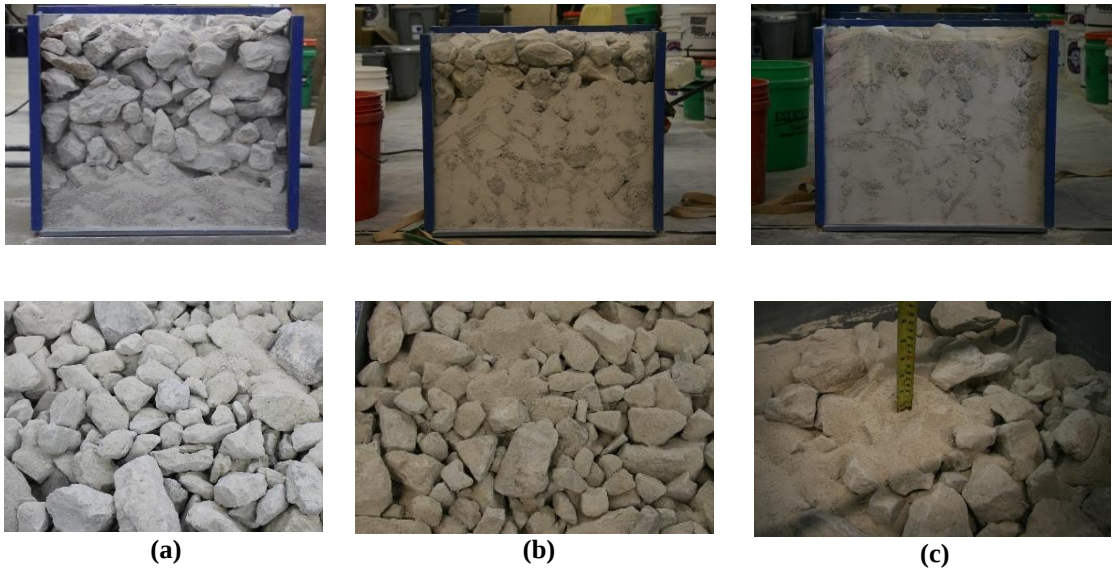

**(a)** **(b)** **(c)**

Figure A.2 Cross sections (top) and top views (bottom) of the compacted PCR aggregates with (a) 20% QB (b) 30% QB and (c) 40% dry QB by weight of PCR stones

## A.4 THE EFFECT OF VARYING THE NUMBER OF LIFTS

The main construction variable that was studied in the field is the variation of the number of lifts (i.e. layer thicknesses) for which the PCR-QB mix is constructed. In the field applications studied in Cell 1, the lift thickness was varied between one 21 in. (533 mm) lift or two approximately equal lifts, 10.5 in. (267 mm) each. Prior to the field construction, the effect of varying the construction practice was studied in the laboratory using the UIUC packing box. It was believed that constructing with two lifts could lead to a better quality control, more homogeneous mix, and would accommodate more of the QB needed for ensuring a stable improved subgrade layer. However, it was also believed that any excess QB left on the surface between the two lifts might result in loss of contact between the large aggregate particles, leading to loss of shear strength and a weaker shear plane that might jeopardize the layer performance.

Thus, the purpose of the lab study was to quantify the reasonable amount of QB to be added in both cases, as well as to qualitatively inspect the percolation of the QB with changing other variables. Initial laboratory results did not show a significant difference in densities and percolation between 1 lift and 2 lifts experiments with dry QB. However, the field application showed that only two-thirds the optimum quantity of QB that was used in a 2 lifts

construction (25%) could be used for a 1 lift arrangement before starting to accumulate fines on the surface. Figure A.3 shows images of the top surface and the cross sections with 30% QB by weight for both 1 and 2 lifts experiments.

(a) (b)

Figure A.3 Top views (top) and cross sections (bottom) of the compacted PCR aggregates with 30% dry QB by weight of PCR, constructed in (a) 1 lift and (b) 2 lifts

## A.5 THE EFFECT OF MOISTURE CONTENT OF QB

Two different moisture contents were studied in the laboratory. The first is the ideal condition of completely dry (oven dried for 24±1 hours), which is expected to maximize the amount of QB that would fill the voids between the large rocks. The other moisture content is the as-received moisture content of the QB material from the source quarry, which was measured to be around 2.5±0.2%. The second moisture content is more realistic for field construction, and was considered a typical value for the moisture content to be encountered during field construction, since several quarries reported a typical in situ moisture contents of 2-3.5% in the state of Illinois on a dry day.

Visual inspection of the cross section of the plexiglass and the top surface after compaction showed roughly similar excess amounts when 40% dry QB and 30% wet QB were used (Figure A.4). Thus, based on these results, even though 30% was found to be the optimum quantity of QB in the case of dry QB; the same quantity was

found to lead to a relatively large amount of QB left on the surface when the QB had a moisture content of 2.5%. Based on these results, a maximum quantity of 25% of the weight of the large PCR aggregates was proposed and tested, which ultimately led to good percolation, and a significantly smaller quantity left on the surface. Two final tests were performed with the 25% wet QB: the first is in two lifts on top of the rigid steel foundation, and the second is a one lift test (approximately 11.5 in. or 292 mm height). Both tests with 25% showed that this quantity was the maximum reasonable quantity to be used for increasing the stability of the PCR stones and reducing the amount of QB remaining on the surface and weakening the structure. Thus, the recommended quantity to be used for field construction was 25%.

(a) (b)

Figure A.4 Top view of the surface of the compacted PCR aggregates with (a) 40% dry QB and (b) 30% wet QB (moisture content = 2.5%), showing roughly similar quantities remaining on the surface

## A.6 THE EFFECT OF FOUNDATION RIGIDITY

Initially, the packing tests of the PCR and QB were conducted on top of a rigid steel foundation. To further simulate the field application, where the PCR-QB mix would be used for subgrade modification on top of a very soft subgrade with a California Bearing Ratio (CBR) of less than 1%, two tests were carried out in the UIUC compaction box for a PCR-QB mix compacted on top of a very soft subgrade. A representative sample (from a representative depth) of the low plasticity CL-ML subgrade on which the field test sections were constructed was obtained and used for this study. The in situ subgrade had a moisture content of 11.5% and an average CBR of 12% as estimated using the African Kleyn equation (Kleyn, 1975) using the Dynamic Cone Penetrometer (DCP). The subgrade soil was modified to a CBR of below 1% in the laboratory by raising the water content to 16% (Mishra, 2012). The achievement of the low CBR was verified with DCP tests.

For the first test, the subgrade was left loose, and the quantity of the oven-dried QB used was 35% of the weight of the PCR stones. For the second test, 25% QB was used, and the QB had a moisture content of 2.6%, which is a typical moisture content of a QB material received from the quarry on a dry day. The subgrade was compacted using a vibratory roller prior to adding the PCR stones. The 35% value for the dry test was chosen based on the

previous results with the rigid steel bottom, which concluded that 40% was excessive while 30% left room for more QB to be added. For the wet QB tests, the 25% value was chosen because 30% was found to be excessive in the case of wet QB as shown previously in Figure A.4. Figure A.5 shows the cross sections of a CS02-QB mix with 25% wet QB by the dry weight of the CS02, compacted in two lifts on top of a rigid foundation and in 1 lift on top of very soft subgrade. The 25% was found out to be the optimum value to be used in the field application, given all studied variables and conditions.

(a) (b)

Figure A.5 Cross section of the compacted PCR aggregates with 25% wet QB by weight of PCR stones, compacted on top of (a) rigid steel foundation, and (b) soft compacted subgrade soil

## A.7 SUMMARY

This Appendix presented detailed information for the use of QB to fill the gaps between large PCR rocks for increased stability during field applications, used as a subgrade improvement on top of very soft CBR of less than 1%, for pavement construction platforms and low volume roads applications. In this study, the appropriate weight mix ratio of the large-size PCR stones and the fine QB materials was studied in the laboratory using a 24 in. by 24 in. by 21 in. (610 mm by 610 mm by 533 mm) steel packing box with one transparent plexiglass side face. The optimum amount of QB was assessed visually after the QB was shaken from the surface using a vibratory action, by inspecting the surface and the cross section conditions. Several factors were found to affect the maximum quantity of QB that can be used to stabilize large PCR rocks and fill the voids between them. The moisture content of the QB was found to be one of the most important factors. Other significant factors include the gradations of both materials, the thickness of constructed lifts, and the rigidity of the foundation on top of which the QB is compacted. Based on 14 tests conducted, the recommended quantity of QB to be used for field construction was 25% by the dry weight of the large PCR stones.

# APPENDIX B: COMPILATION OF RUTTING PROGRESSION DATA

## B.1 INTRODUCTION

This Appendix provides detailed plots for the rutting progression at each measuring point. Rut measurements were conducted by periodic surface profile measurements after a certain number of passes. For each measuring point, the non-trafficked profile measurements (i.e. at 0 pass) is taken as the reference. Measurements were taken perpendicular to the wheel path, and each plot therefore shows a lateral measurement of the surface profile after a certain number of ATLAS passes. For the construction platform test sections in Cell 1S, the '0 mm' lateral distance marks the center of the wheel path, and the '-800 mm' and '800 mm' measurements mark the outermost North and South measurements, respectively. For the HMA-surfaced low volume road test sections in Cells 1N, 2, and 3, the '400 mm' lateral distance marks the center of the wheel path, while the '0 mm' and '800 mm' mark the outermost South and North measurements, respectively. A plot detailing the test sections and locations of the measuring points is shown prior to the plots of rut progression to help identify the location of each measurement.

## B.2 RUTTING PROGRESSION FOR CELL '1S' TEST SECTIONS

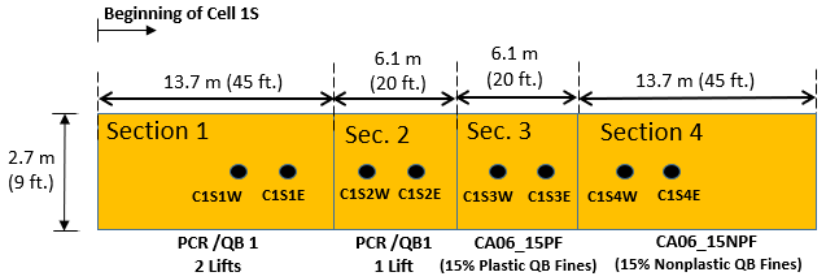


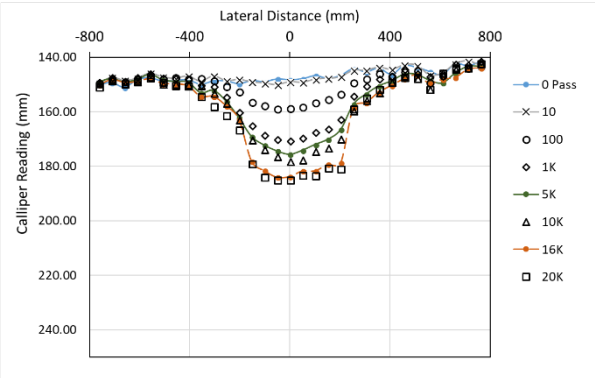


C1S1W: PCR/QB1 constructed in 2 lifts

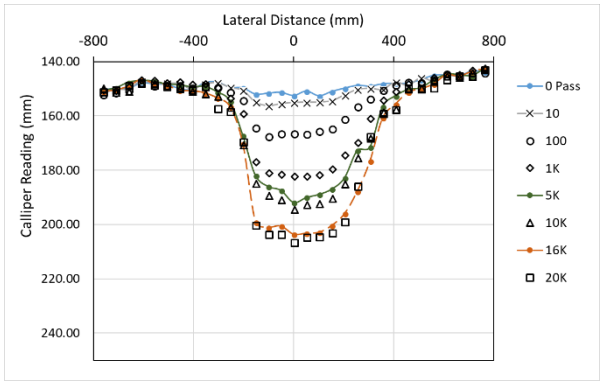


C1S1E: PCR/QB1 constructed in 2 lifts

Figure B.1 Rutting progression for Cell 1S test sections. [1 in. = 25.4 mm]

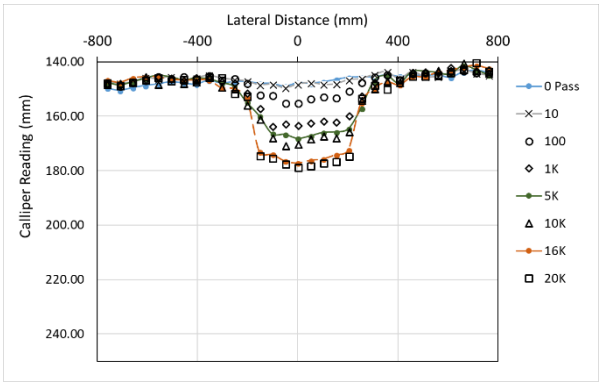


C1S2W: PCR/QB1 constructed in 1 lift

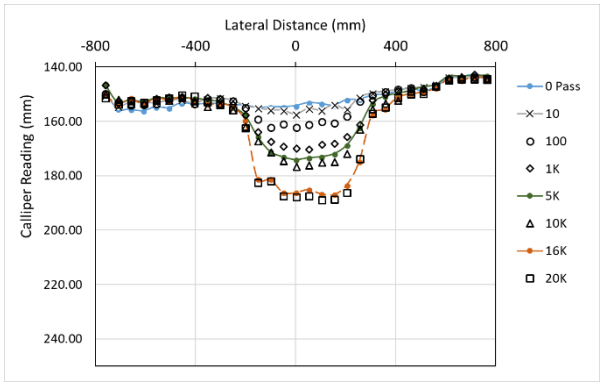


C1S2E: PCR/QB1 constructed in 1 lift

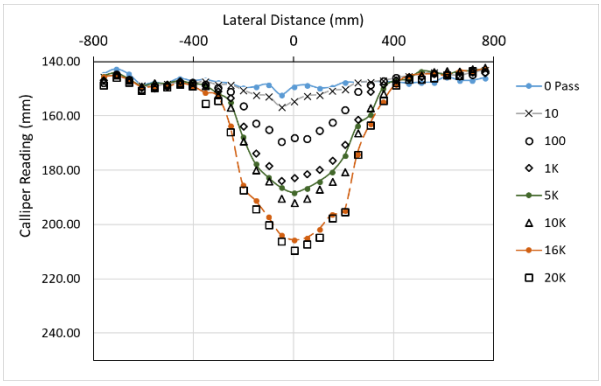


C1S3W: CA06_15PF

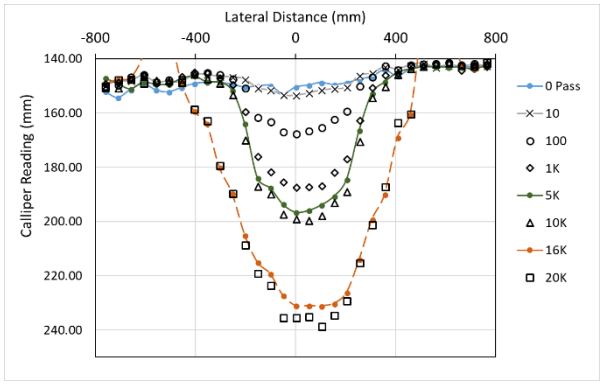


C1S3E: CA06_15PF

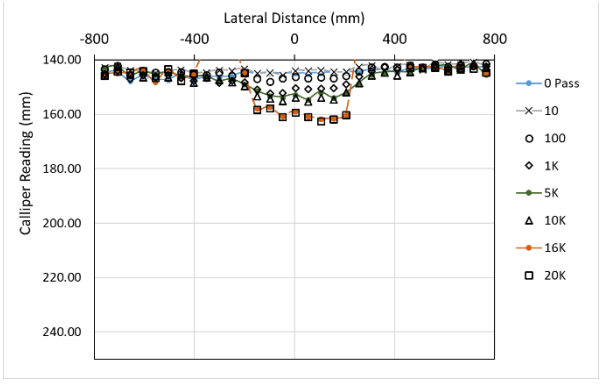


C1S4W: CA06_15NPF

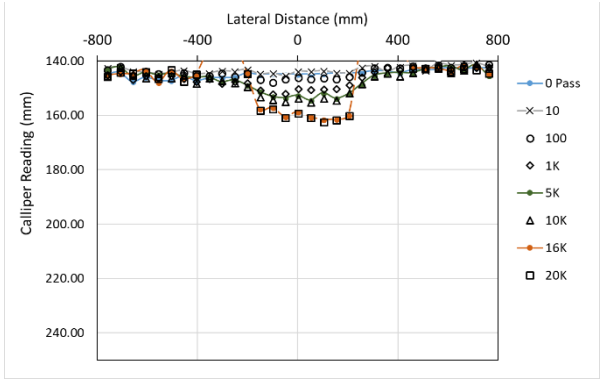


C1S4E: CA06_15NPF

Figure B.1 (cont.)

## B.3 RUTTING PROGRESSION FOR CELL '1N' TEST SECTIONS

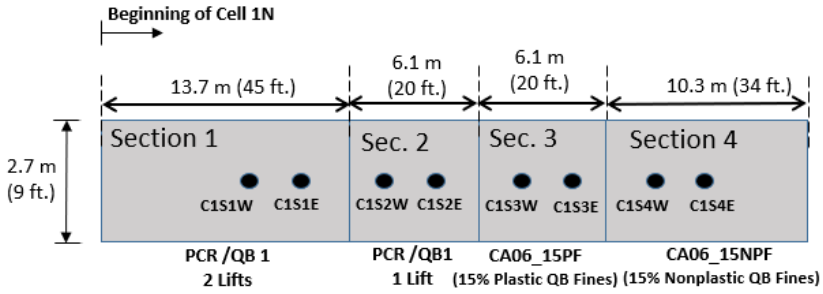


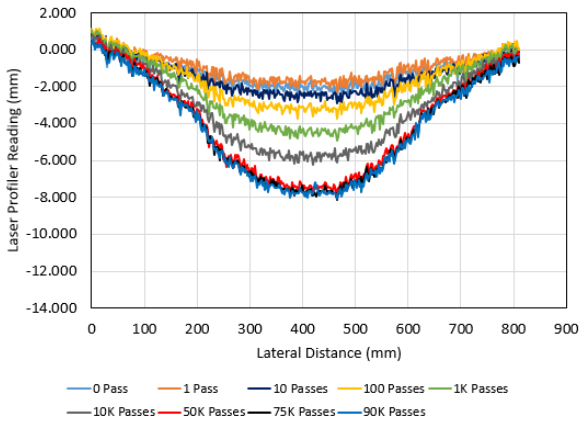


C1S1W: PCR/QB1 in 2 lifts

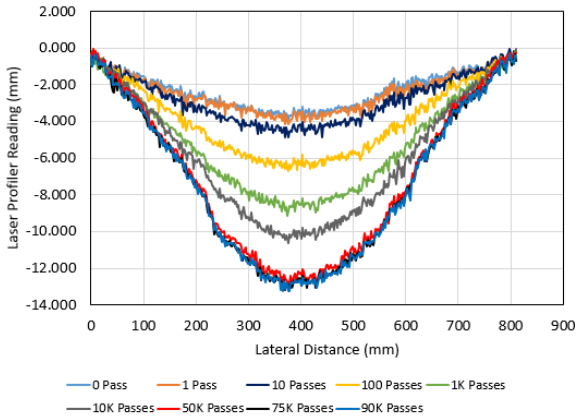


C1S1E: PCR/QB1 in 2 lifts

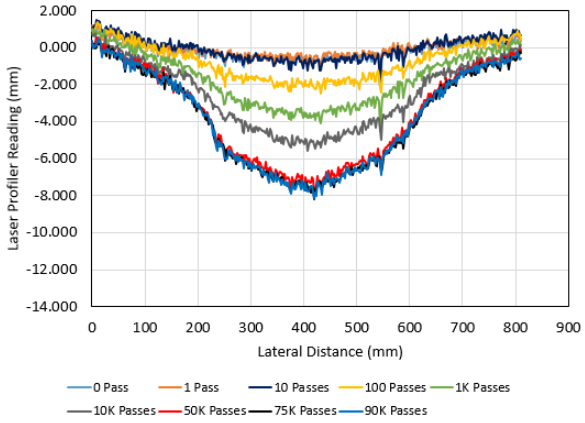


C1S2W: PCR/QB1 in 1 lift

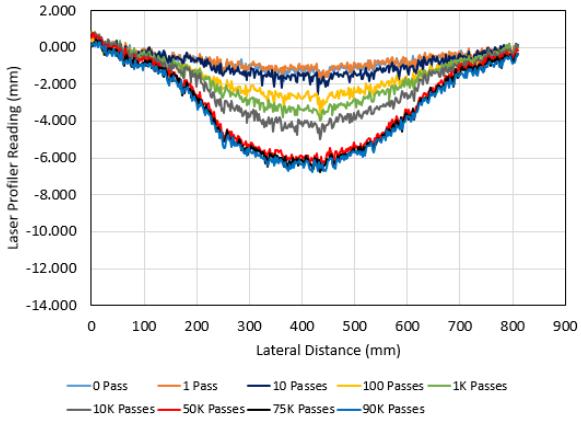


C1S2E: PCR/QB1 in 1 lift

Figure B.2 Rutting progression for Cell 1N test sections. [1 in. = 25.4 mm]

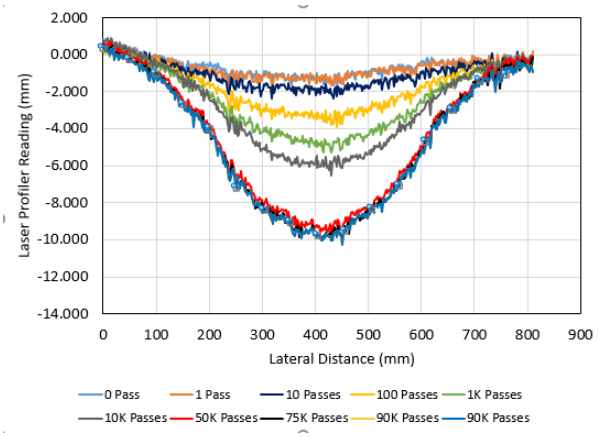


C1S3W: CA06_15PF

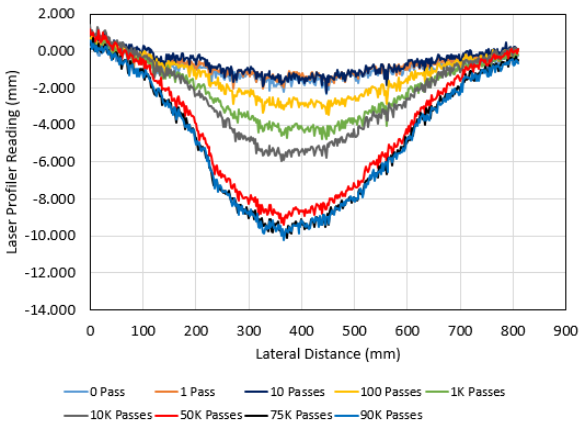


C1S3E: CA06_15PF

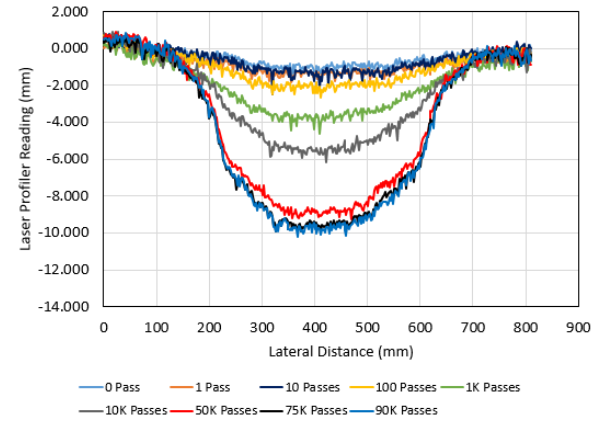


C1S4W: CA06_15NPF

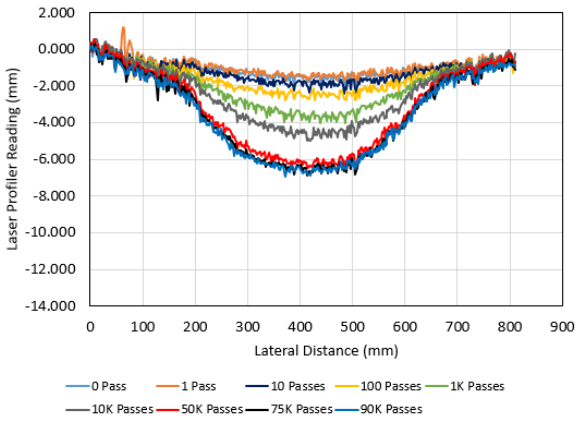


C1S4E: CA06_15NPF

Figure B.2 (cont.)

## B.4 RUTTING PROGRESSION FOR CELL '2' TEST SECTIONS

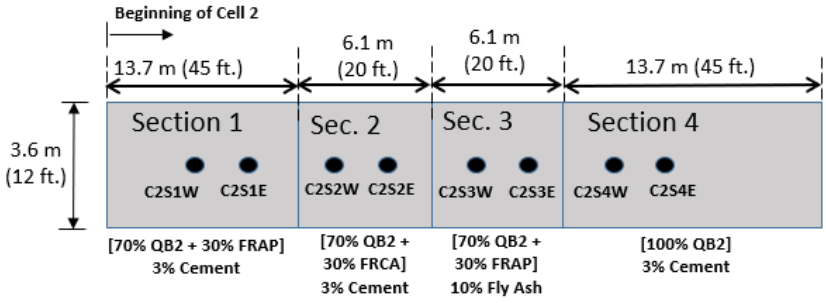


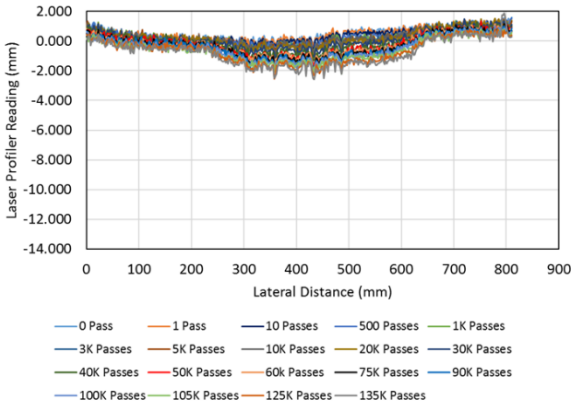


C2S1W: QB2 + FRAP + Cement Base

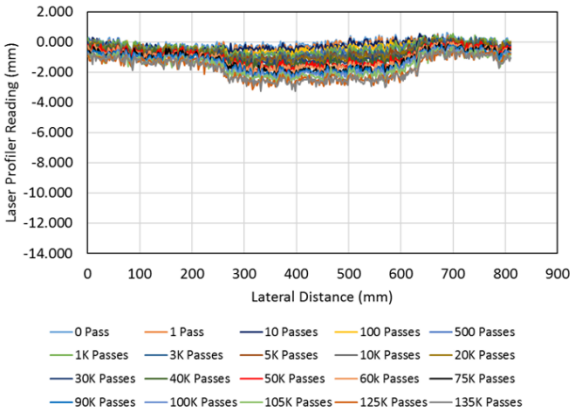


C2S1E: QB2 + FRAP + Cement Base

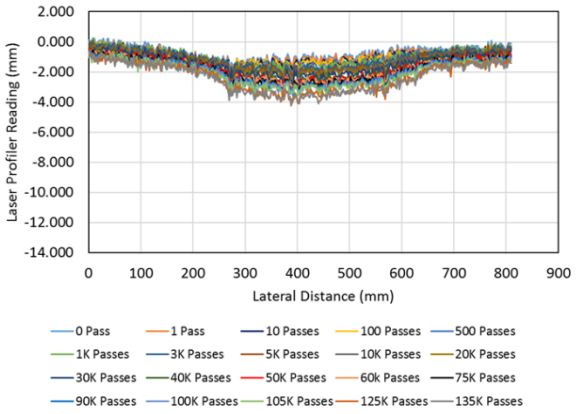


C2S2W: QB2 + FRCA + Cement Base

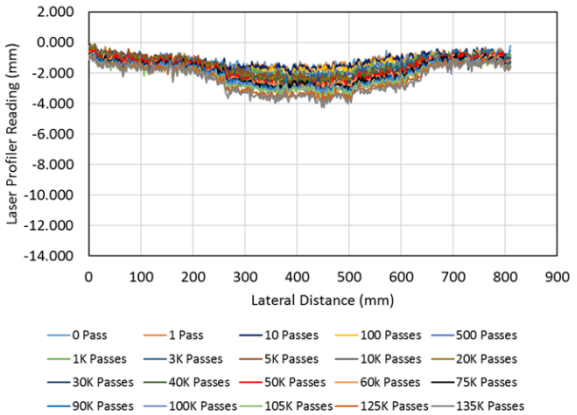


C2S2E: QB2 + FRCA + Cement Base

Figure B.3 Rutting progression for Cell 2 test sections. [1 in. = 25.4 mm]

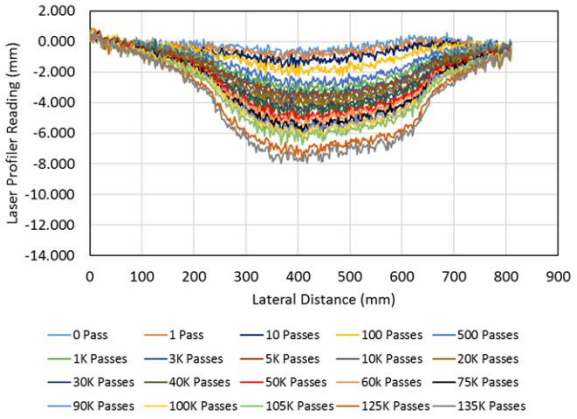


C2S3W: QB2 + FRCA + Fly Ash Base

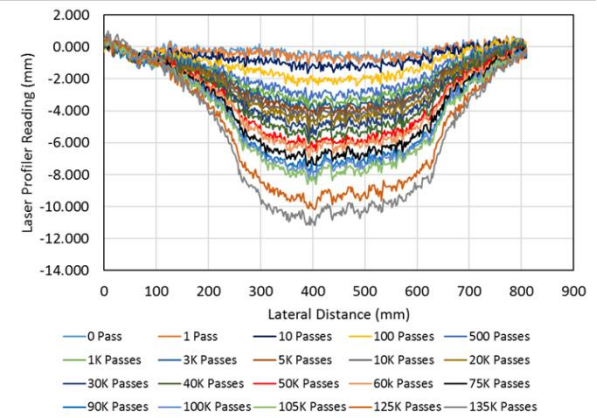


C2S3E: QB2 + FRCA + Fly Ash Base

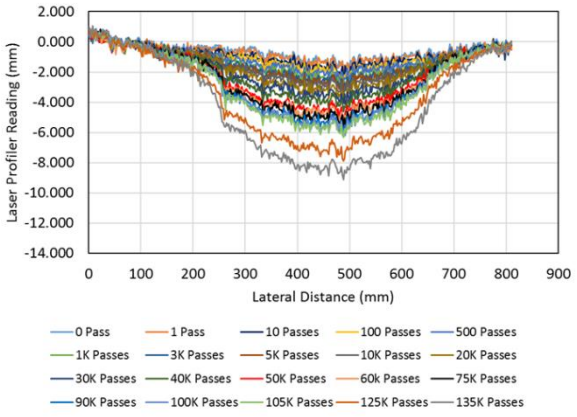


C2S4W: QB2 + Cement Base

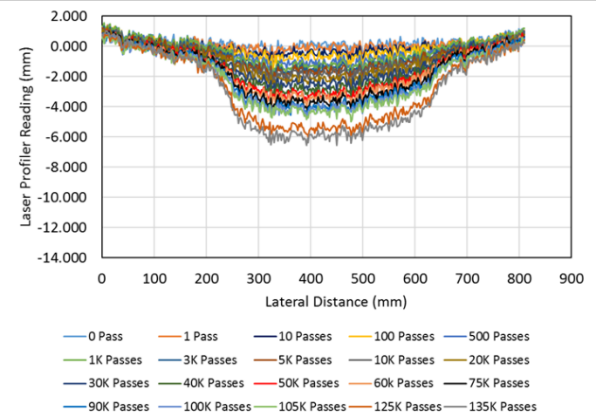


C2S4E: QB2 + Cement Base

Figure B.3 (cont.)

## B.5 RUTTING PROGRESSION FOR CELL '3' TEST SECTIONS

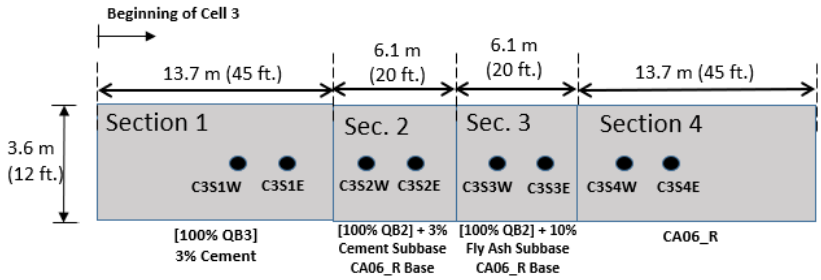


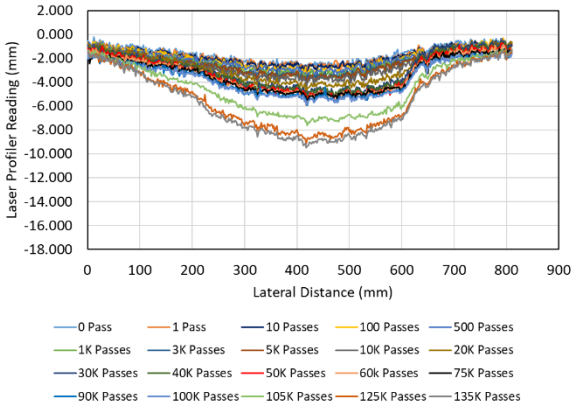


C3S1W: QB3 + Cement Base

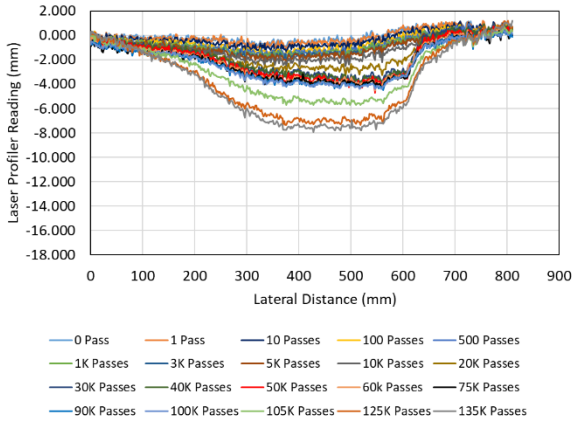


C3S1E: QB3 + Cement Base

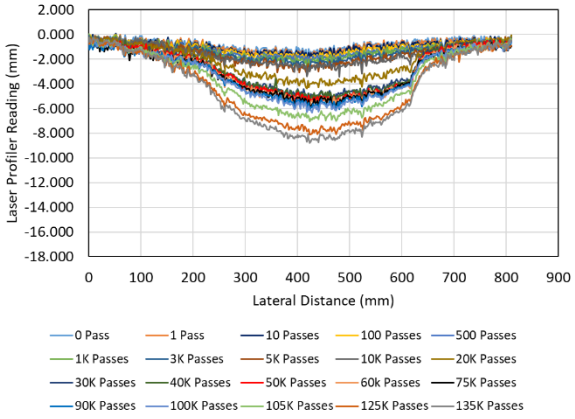


C3S2W: QB2 + Cement Subbase and CA06_R Base

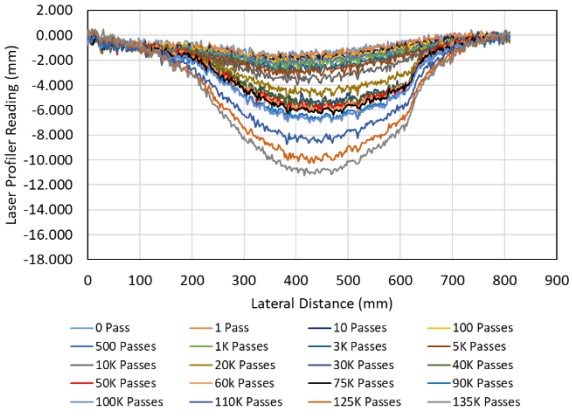


C3S2E: QB2 + Cement Subbase and CA06_R Base

Figure B.4 Rutting progression for Cell 3 test sections*. [1 in. = 25.4 mm]

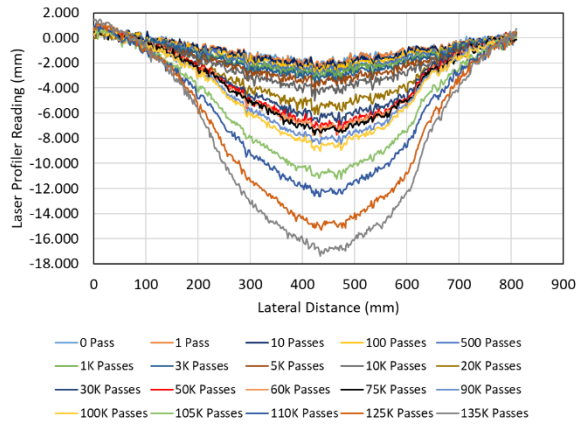


C3S3W: QB2 + Fly Ash Subbase and CA06_R Base

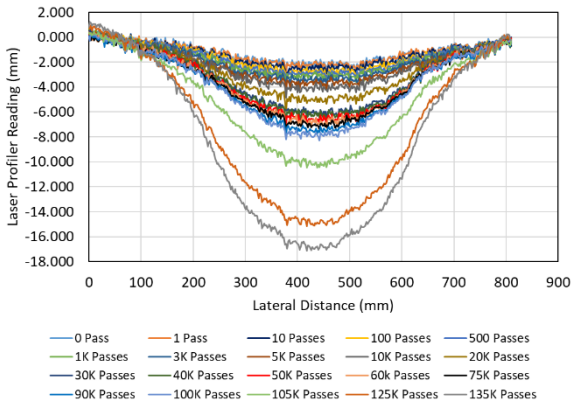


C3S3E: QB2 + Fly Ash Subbase and CA06_R Base

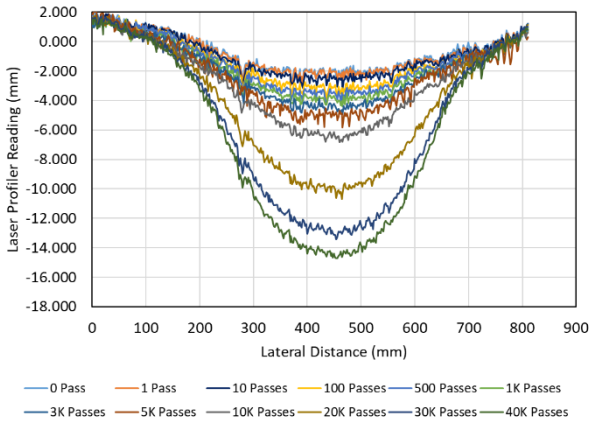


C3S4W: CA06_R Base

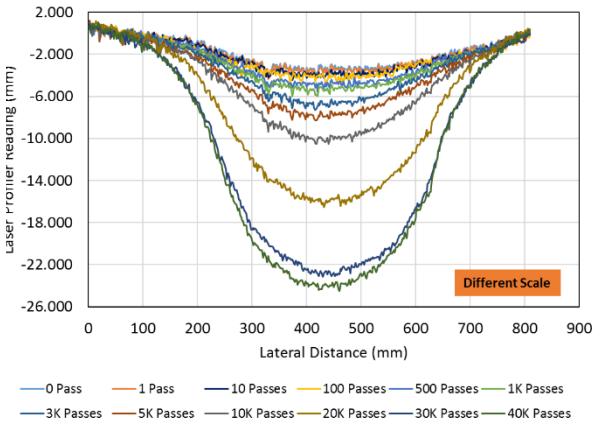


C3S4E: CA06_R Base

Figure B.4 (cont.) *

* Note difference in y-axis scale from the results of Cell 1N and Cell 2

# APPENDIX C: COMPILATION OF FWD TEST RESULTS

## C.1 INTRODUCTION

This Appendix provides detailed plots for the deflection basins measured with Falling Weight Deflectometer (FWD) testing. Tests were first carried out on all of the construction working platforms and flexible pavement test sections after the field construction was completed. Additional FWD testing was also conducted for the test sections in Cells 2 and 3 before trafficking to assess the curing of the chemically stabilized test sections. After trafficking was completed for each test Cell, additional FWD drops were carried on all flexible pavement test sections. The tests were conducted by dropping three different load levels at each measuring point to induce variable stress states. The deflection basins, shown in this Appendix, were normalized to a standard 9 kip (40 kN) equivalent single-axle load, applying a uniform pressure of 80 psi (551 kPa) over a 12 in. (305 mm) diameter circular loading area.

## C.2 FWD DEFLECTIONS FOR CELL '1S' TEST SECTIONS

The FWD deflections shown in Figure C.1 were measured after construction and before trafficking (September 2016). No other FWD deflections were measured for the construction platform sections after trafficking due to high surface deflections.

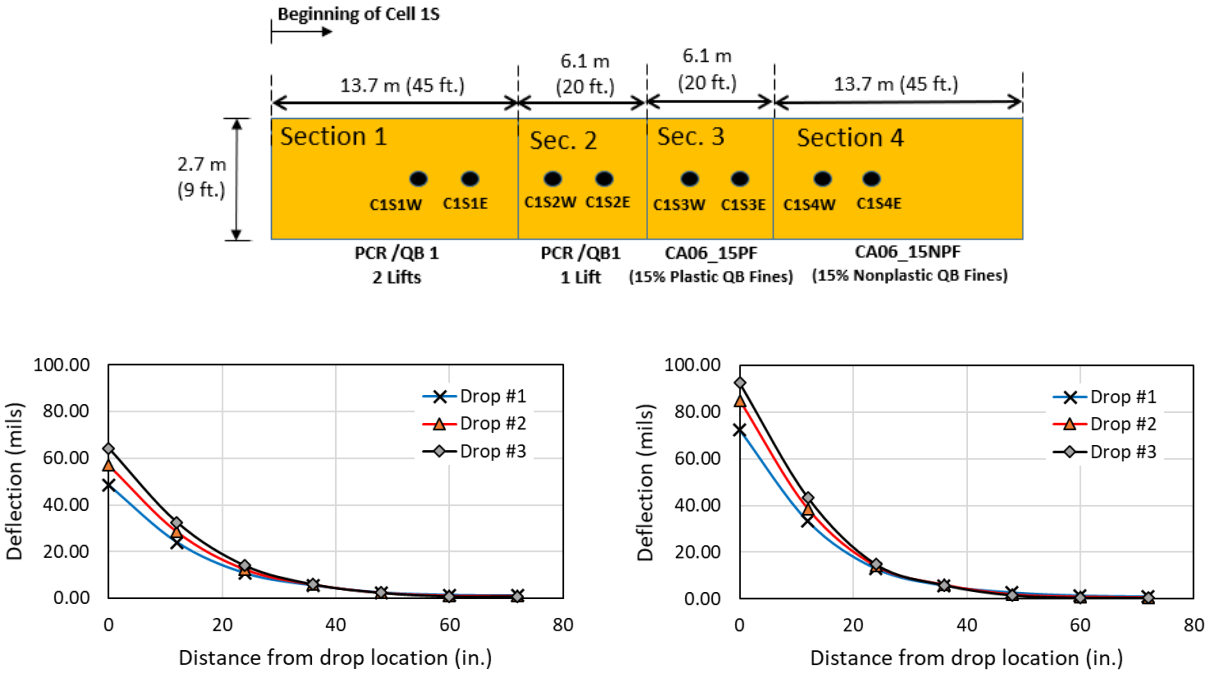


C1S1W: PCR/QB1 in 2 lifts

C1S1E: PCR/QB1 in 2 lifts

Figure C.1 FWD deflections for Cell 1S: before ATLAS trafficking

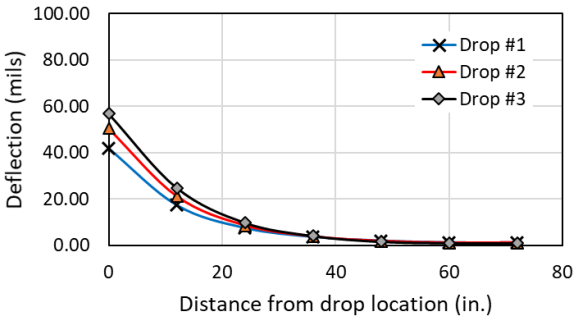


C1S2W: PCR/QB1 in 1 lift

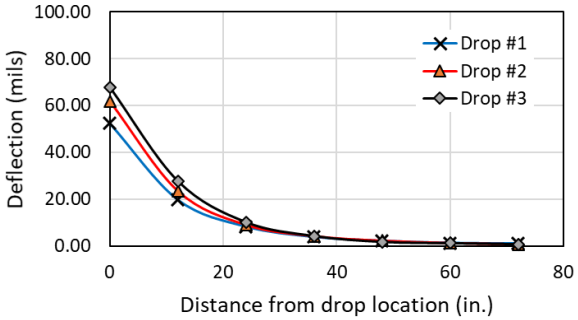


C1S2E: PCR/QB1 in 1 lift

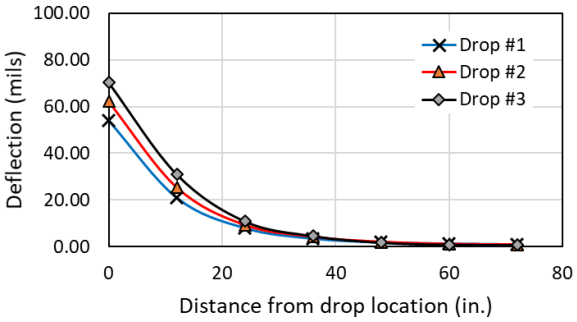


C1S3W: CA06_15PF

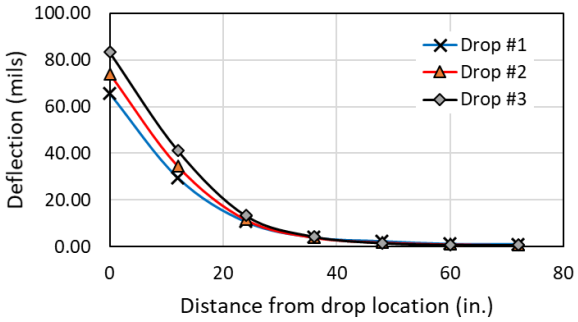


C1S3E: CA06_15PF

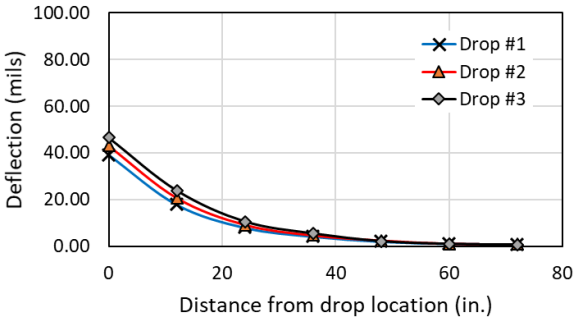


C1S4W: CA06_15NPF

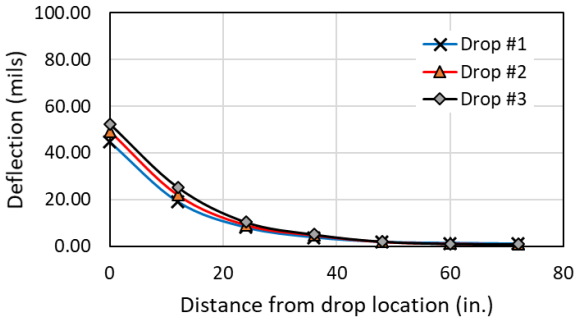


C1S4E: CA06_15NPF

Figure C.1 (cont.)

## C.3 FWD DEFLECTIONS FOR CELL '1N' TEST SECTIONS

The normalized FWD deflections shown in Figure C.2 were measured for Cell 1N after construction and before trafficking (September 2016).

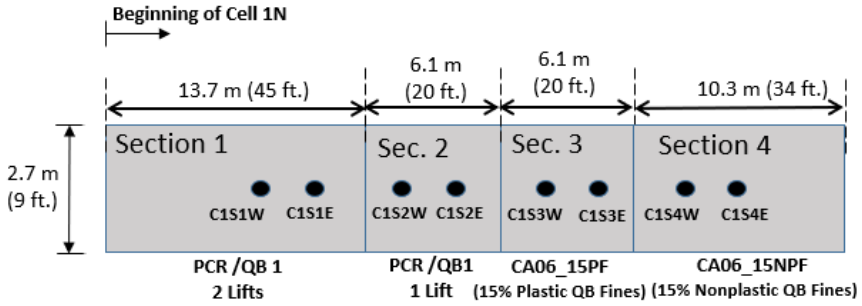


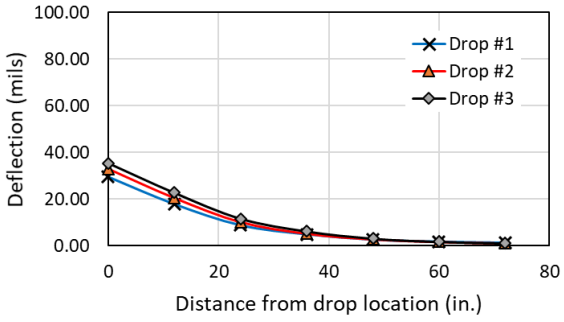


C1S1W: PCR/QB1 in 2 lifts

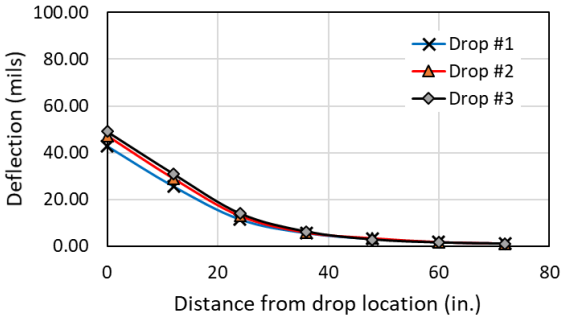


C1S1E: PCR/QB1 in 2 lifts

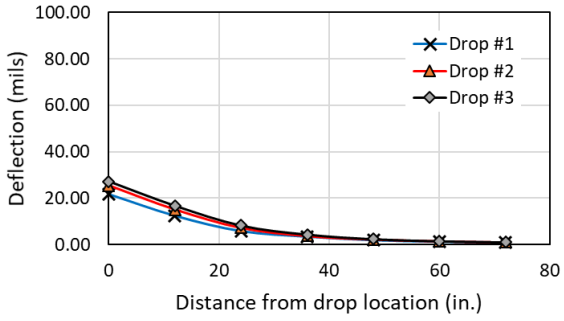


C1S2W: PCR/QB1 in 1 lift

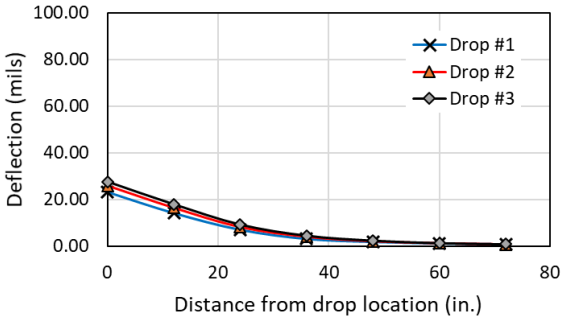


C1S2E: PCR/QB1 in 1 lift

Figure C.2 FWD deflections for Cell 1N: before ATLAS trafficking

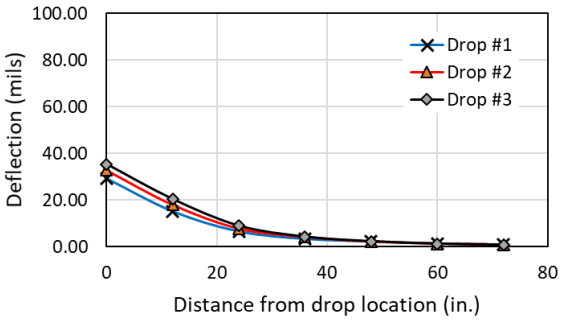


C1S3W: CA06_15PF

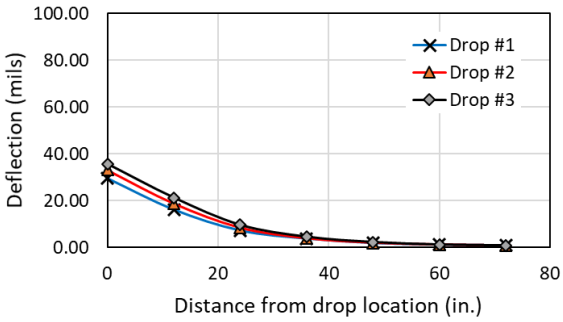


C1S3E: CA06_15PF

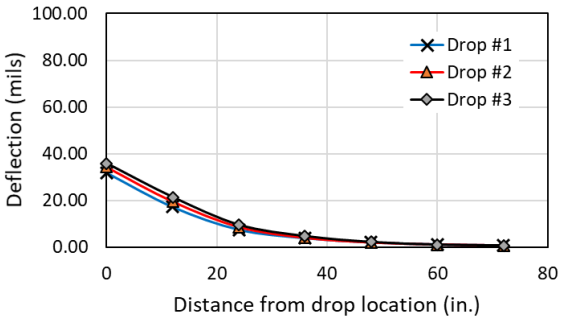


C1S4W: CA06_15NPF

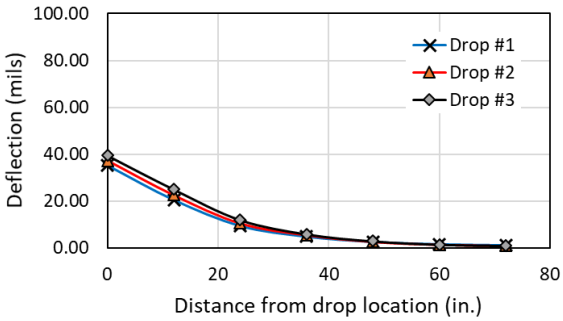


C1S4E: CA06_15NPF

Figure C.2 (cont.)

The normalized FWD deflections shown in Figure C.3 were measured for Cell 1N -flexible pavements test sections - after 90,000 wheel passes of ATLAS trafficking (May 2017).

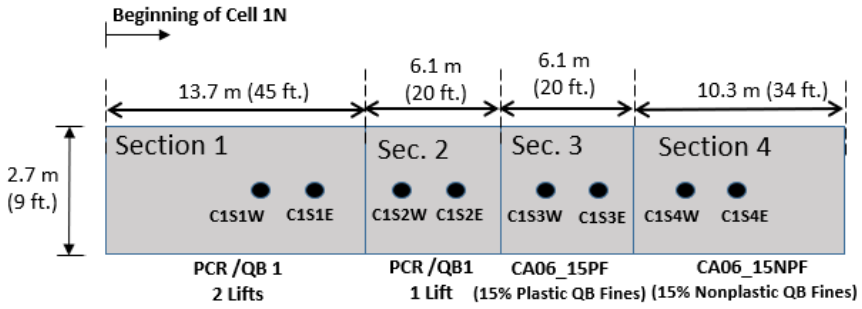


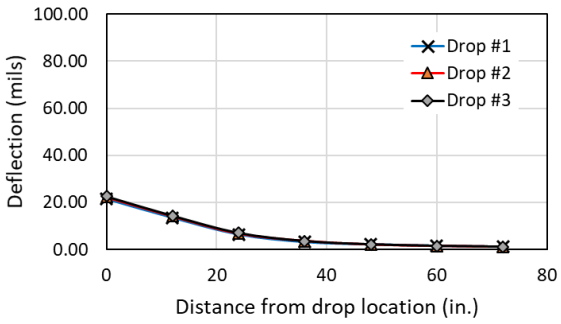


C1S1W: PCR/QB1 in 2 lifts

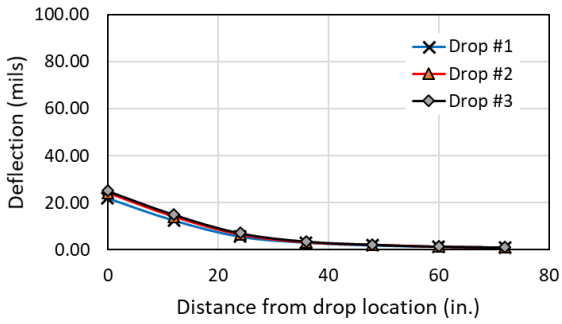


C1S1E: PCR/QB1 in 2 lifts

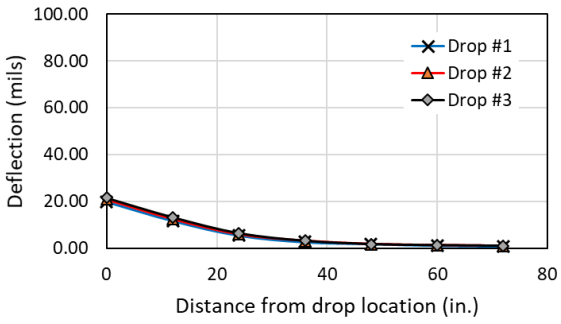


C1S2W: PCR/QB1 in 1 lift

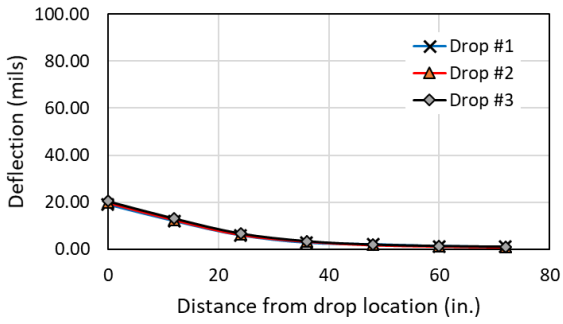


C1S2E: PCR/QB1 in 1 lift

Figure C.3 FWD deflections for Cell 1N: after ATLAS trafficking

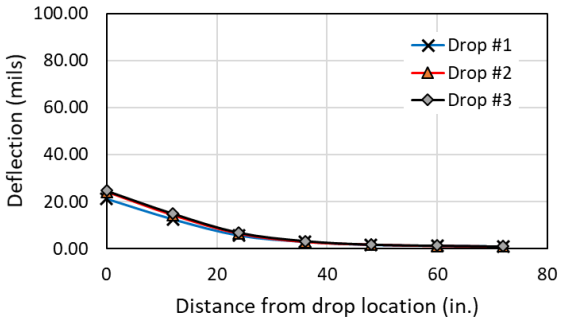


C1S3W: CA06_15PF

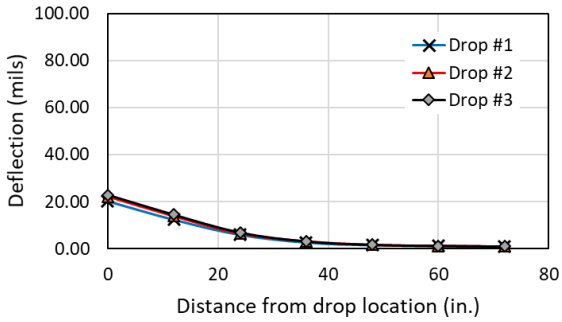


C1S3E: CA06_15PF

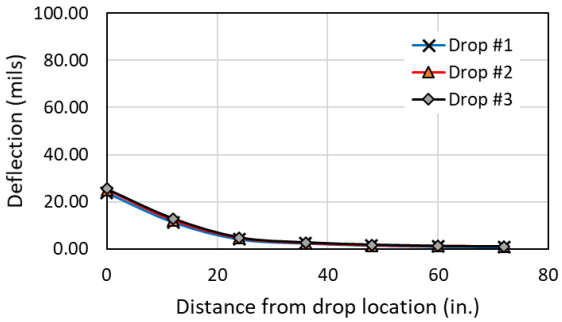


C1S4W: CA06_15NPF

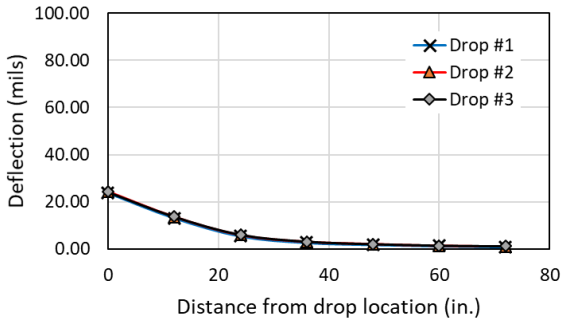


C1S4E: CA06_15NPF

Figure C.3 (cont.)

## C.4 FWD DEFLECTIONS FOR CELL '2' TEST SECTIONS

The normalized FWD deflections shown in Figure C.4 were measured for Cell 2 -flexible pavements test sections - after construction (September 2016).

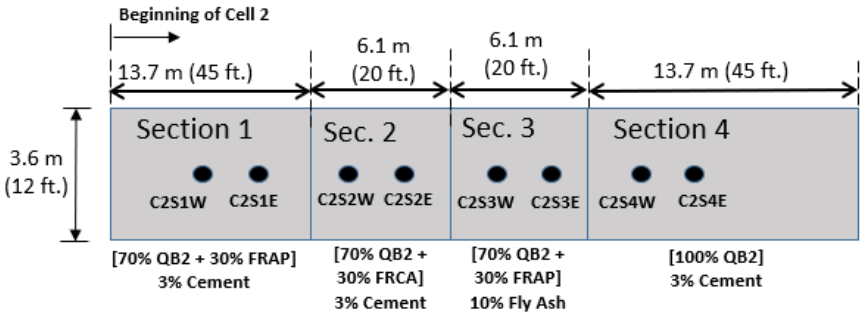


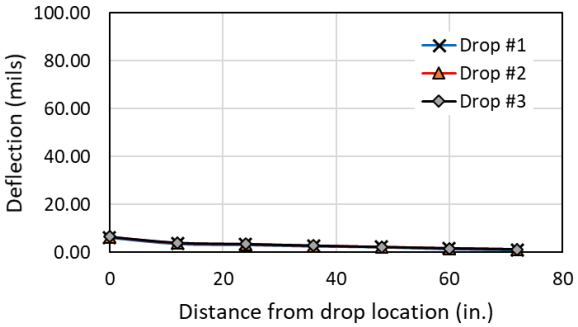


C2S1W: QB2 + FRAP + Cement Base

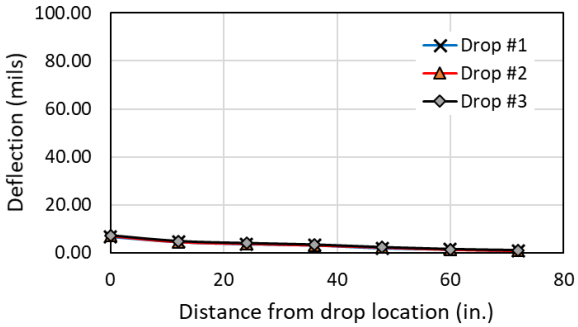


C2S1E: QB2 + FRAP + Cement Base

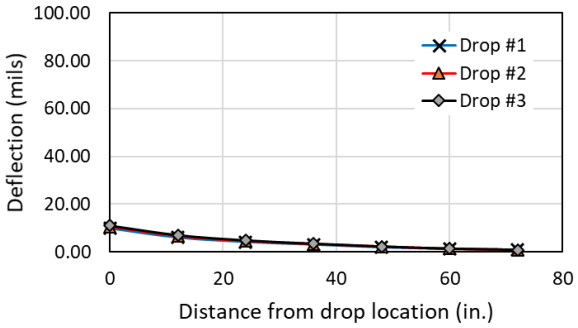


C2S2W: QB2 + FRCA + Cement Base

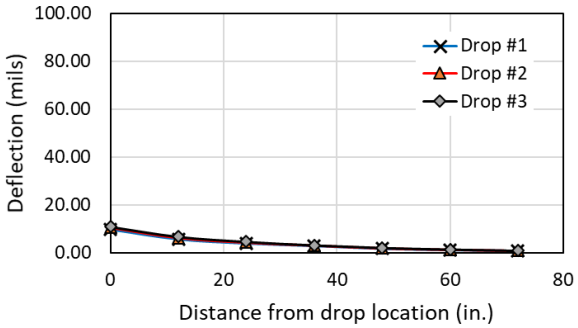


C2S2E: QB2 + FRCA + Cement Base

Figure C.4 FWD deflections for Cell 2: after construction

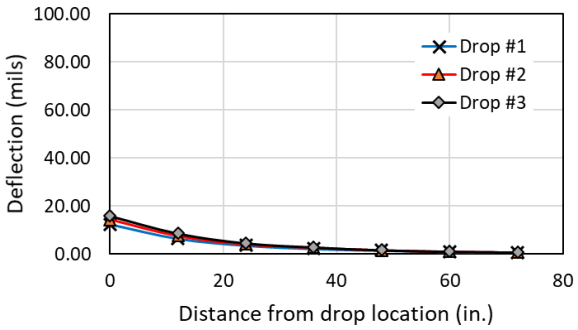


C2S3W: QB2 + FRCA + Fly Ash Base

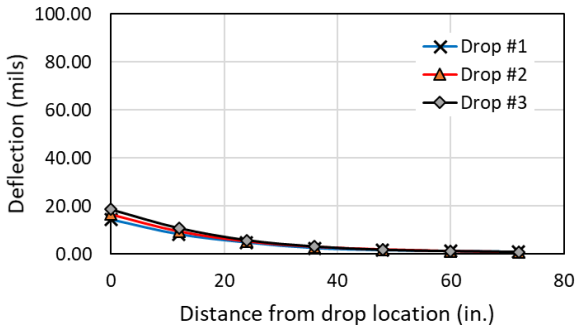


C2S3E: QB2 + FRCA + Fly Ash Base

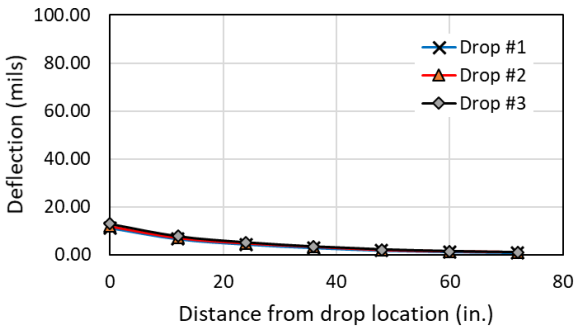


C2S4W: QB2 + Cement Base

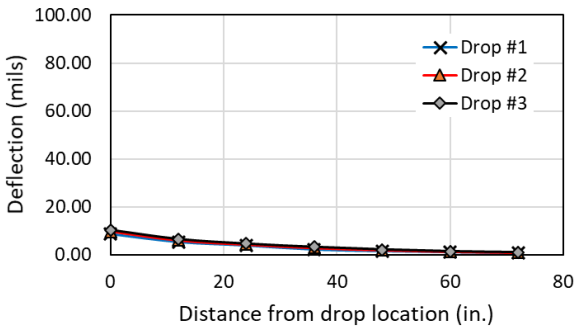


C2S4E: QB2 + Cement Base

Figure C.4 (cont.)

The normalized FWD deflections shown in Figure C.5 were measured for Cell 2 -flexible pavements test sections – before trafficking (May 2017).

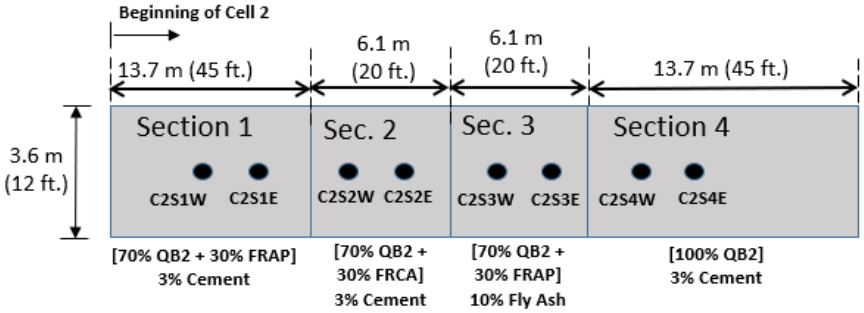


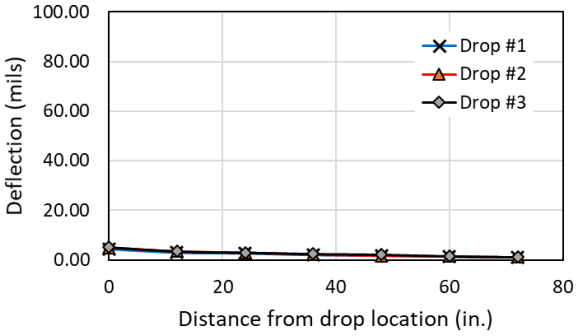


C2S1W: QB2 + FRAP + Cement Base

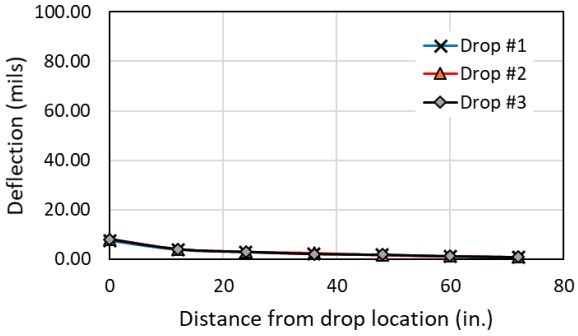


C2S1E: QB2 + FRAP + Cement Base

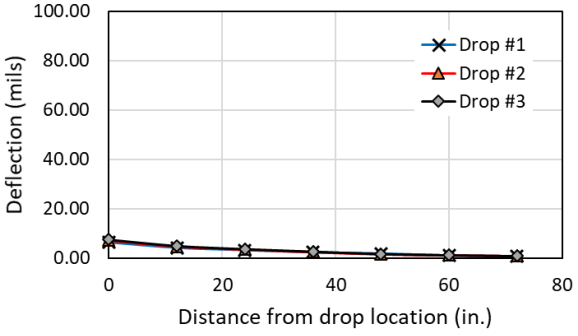


C2S2W: QB2 + FRCA + Cement Base

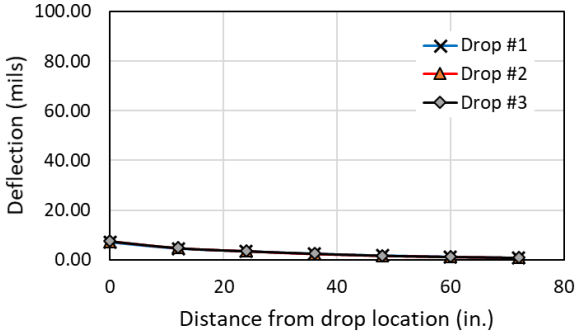


C2S2E: QB2 + FRCA + Cement Base

Figure C.5 FWD deflections for Cell 2: before ATLAS trafficking

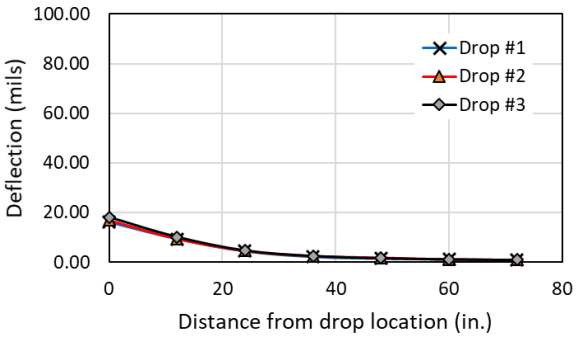


C2S3W: QB2 + FRCA + Fly Ash Base

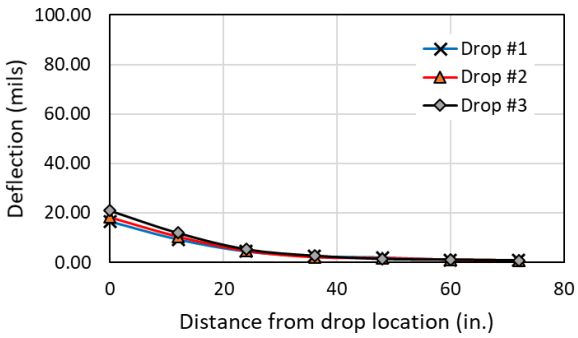


C2S3E: QB2 + FRCA + Fly Ash Base

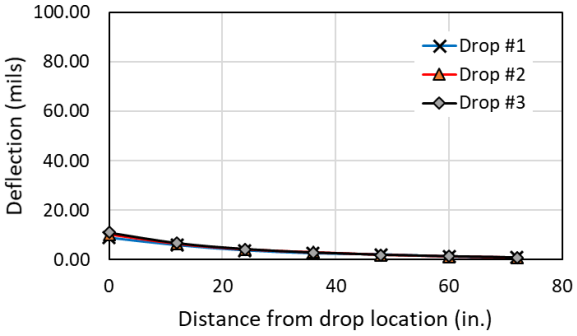


C2S4W: QB2 + Cement Base

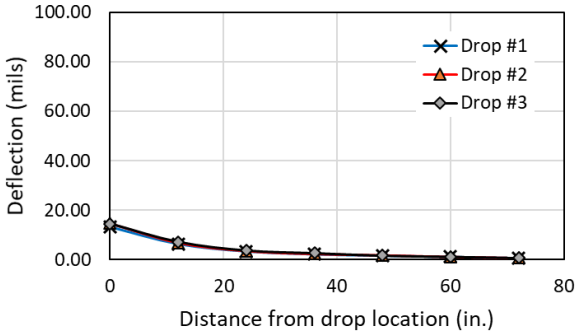


C2S4E: QB2 + Cement Base

Figure C.5 (cont.)

The normalized FWD deflections shown in Figure C.6 were measured for Cell 2 -flexible pavements test sections - after 135,000 wheel passes of ATLAS trafficking (October 2017).

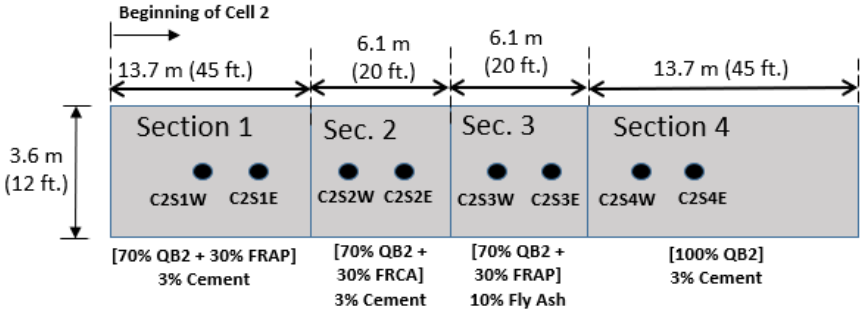


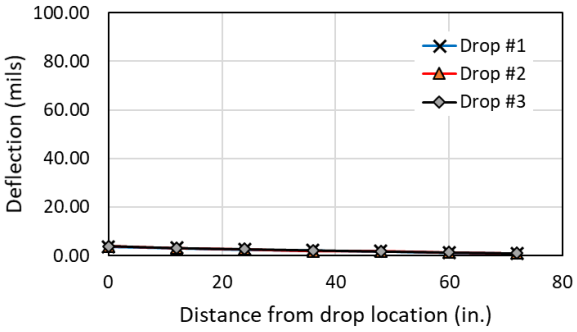


C2S1W: QB2 + FRAP + Cement Base

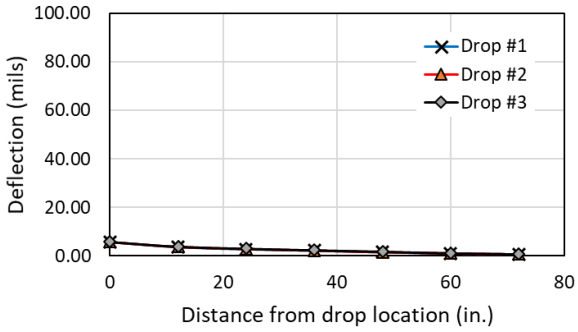


C2S1E: QB2 + FRAP + Cement Base

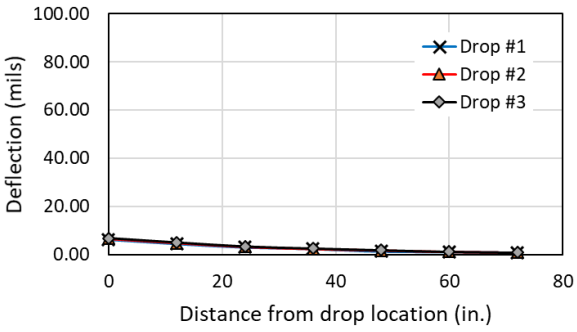


C2S2W: QB2 + FRCA + Cement Base

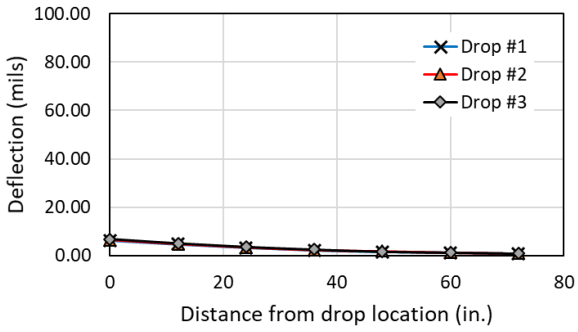


C2S2E: QB2 + FRCA + Cement Base

Figure C.6 FWD deflections for Cell 2: after ATLAS trafficking

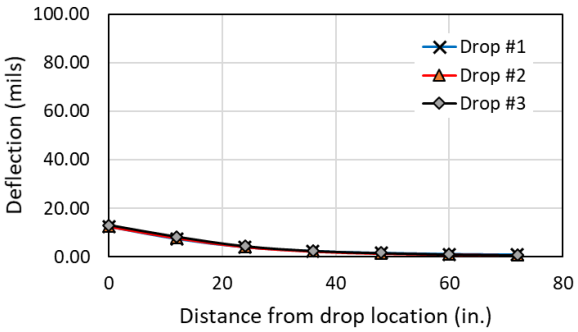


C2S3W: QB2 + FRCA + Fly Ash Base

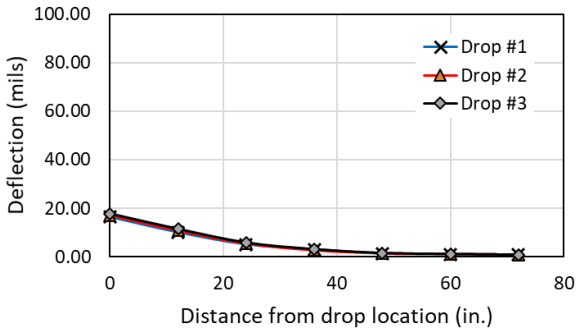


C2S3E: QB2 + FRCA + Fly Ash Base

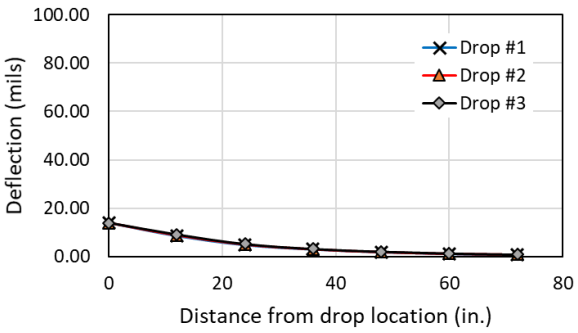


C2S4W: QB2 + Cement Base

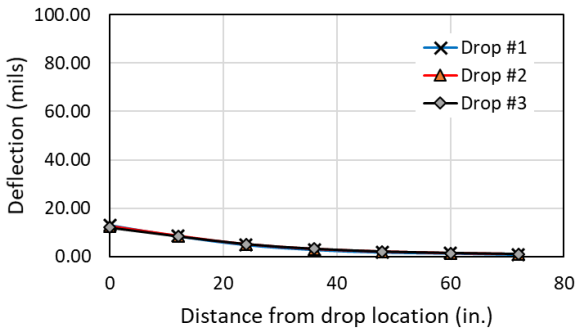


C2S4E: QB2 + Cement Base

Figure C.6 (cont.)

## C.5 FWD DEFLECTIONS FOR CELL '3' TEST SECTIONS

The normalized FWD deflections shown in Figure C.7 were measured for Cell 3 -flexible pavements test sections - after construction (September 2016).

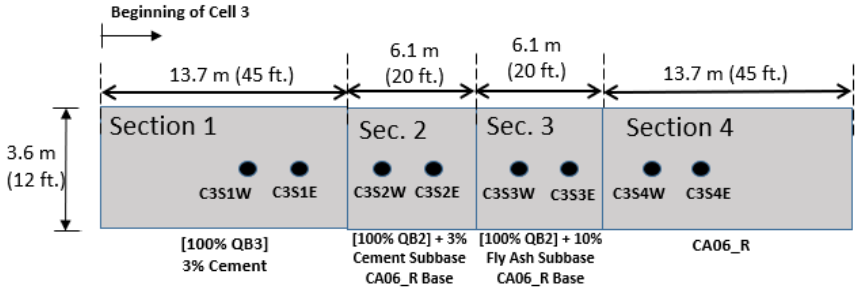


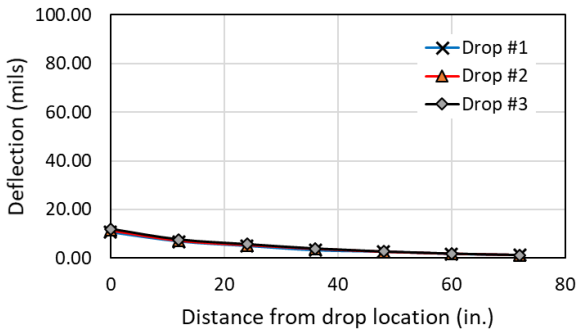


C3S1W: QB3 + Cement Base

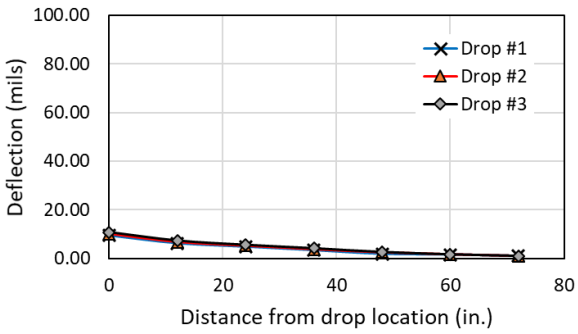


C3S1E: QB3 + Cement Base

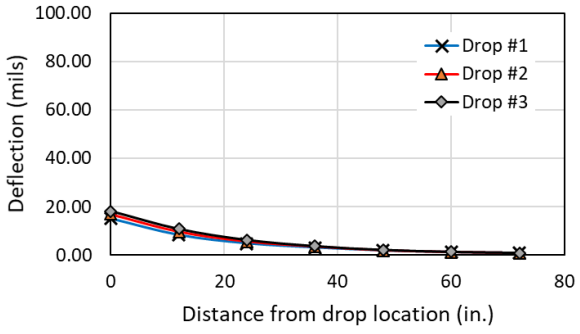


C3S2W: QB2 + Cement Subbase and CA06_R Base

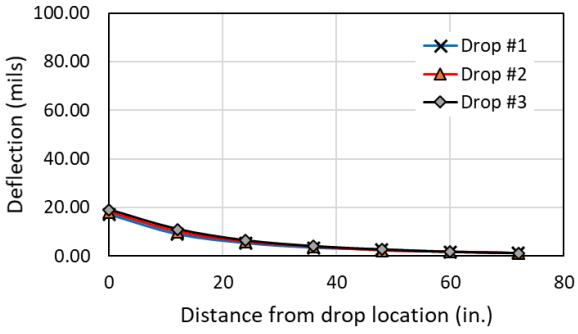


C3S2E: QB2 + Cement Subbase and CA06_R Base

Figure C.7 FWD deflections for Cell 3: after construction

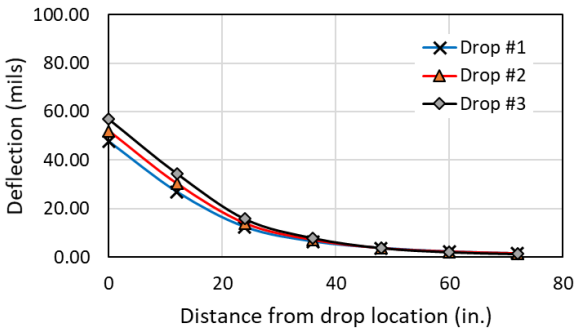


C3S3W: QB2 + Fly Ash Subbase and CA06_R Base

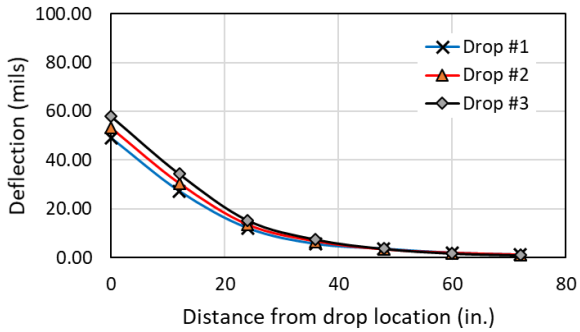


C3S3E: QB2 + Fly Ash Subbase and CA06_R Base

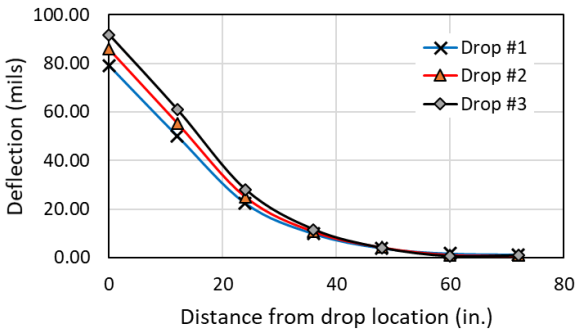


C3S4W: CA06_R Base

Figure C.7 (cont.)

The normalized FWD deflections shown in Figure C.8 were measured for Cell 3 -flexible pavements test sections – before trafficking (May 2017).

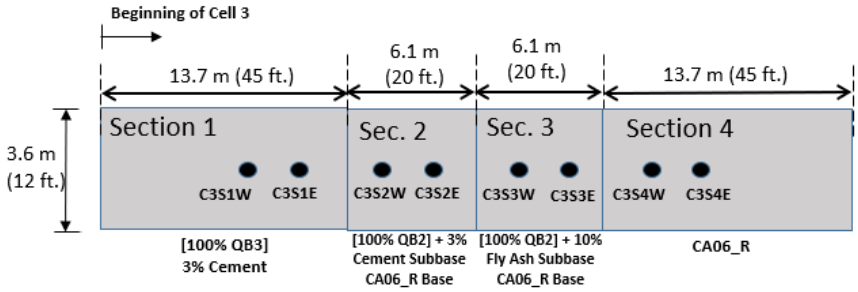


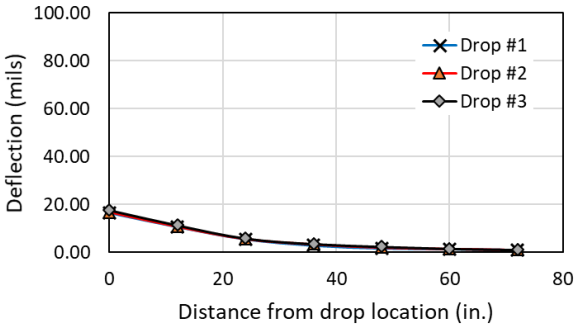


C3S1W: QB3 + Cement Base

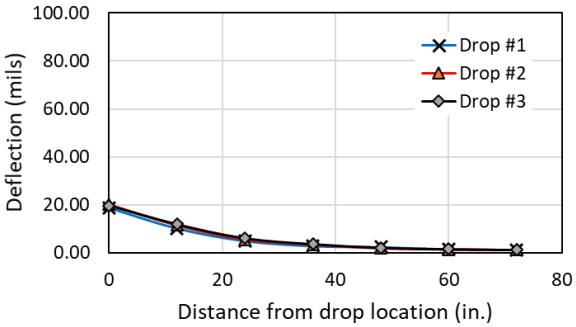


C3S1E: QB3 + Cement Base

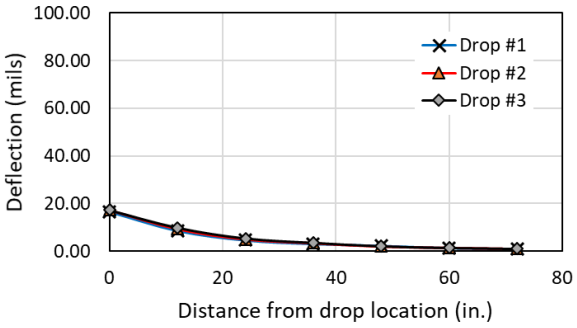


C3S2W: QB2 + Cement Subbase and CA06_R Base

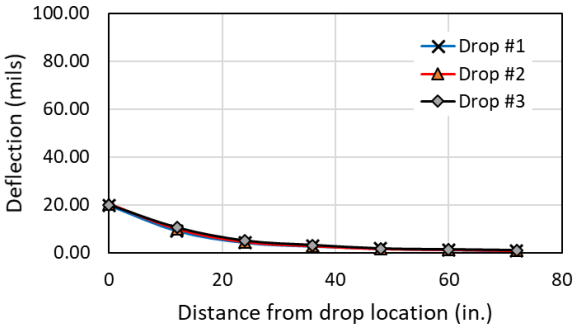


C3S2E: QB2 + Cement Subbase and CA06_R Base

Figure C.8 FWD deflections for Cell 3: before ATLAS trafficking

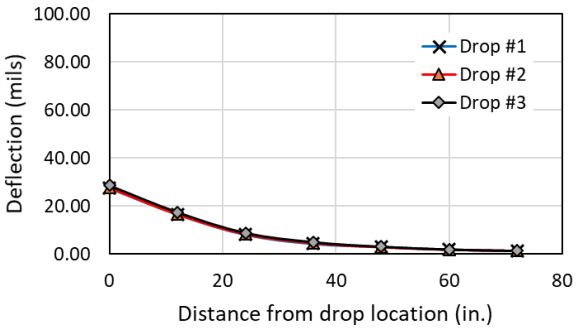


C3S3W: QB2 + Fly Ash Subbase and CA06_R Base

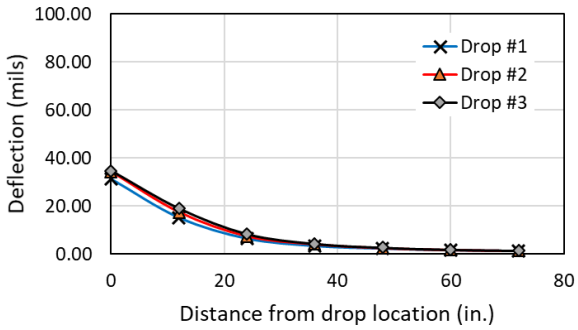


C3S3E: QB2 + Fly Ash Subbase and CA06_R Base

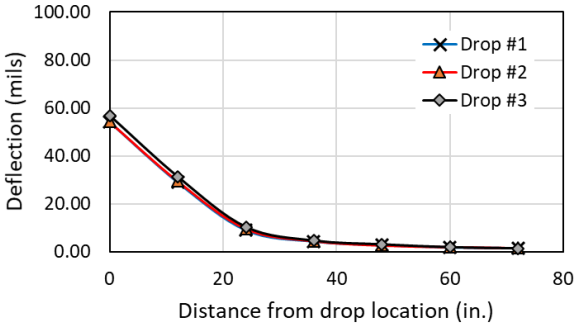


C3S4W: CA06_R Base

Figure C.8 (cont.)

The normalized FWD deflections shown in Figure C.9 were measured for Cell 3 -flexible pavements test sections - after 135,000 wheel passes of ATLAS trafficking (May 2018).

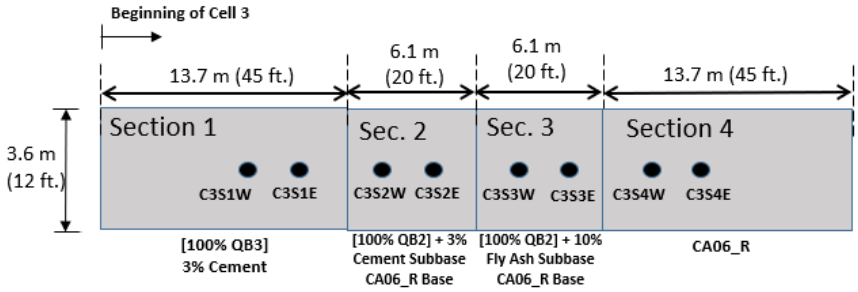


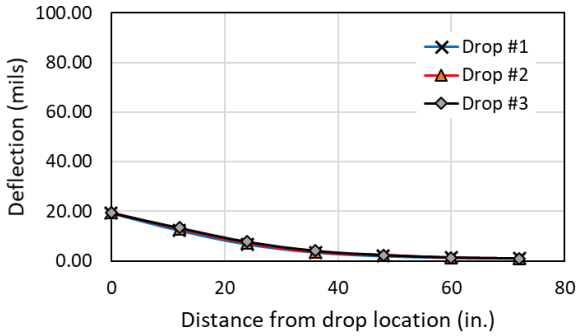


C3S1W: QB3 + Cement Base

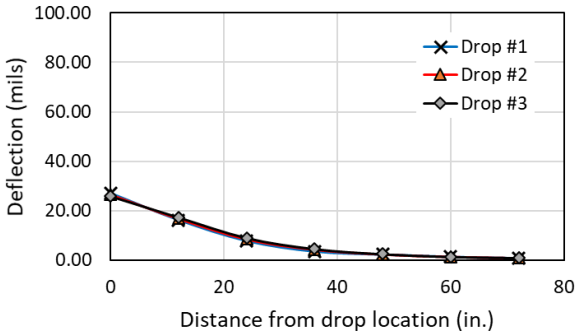


C3S1E: QB3 + Cement Base

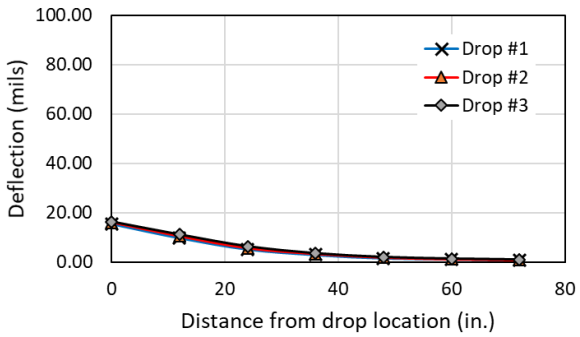


C3S2W: QB2 + Cement Subbase and CA06_R Base

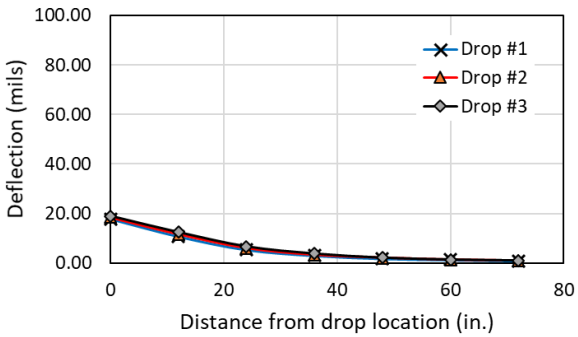


C3S2E: QB2 + Cement Subbase and CA06_R Base

Figure C.9 FWD deflections for Cell 3: after ATLAS trafficking

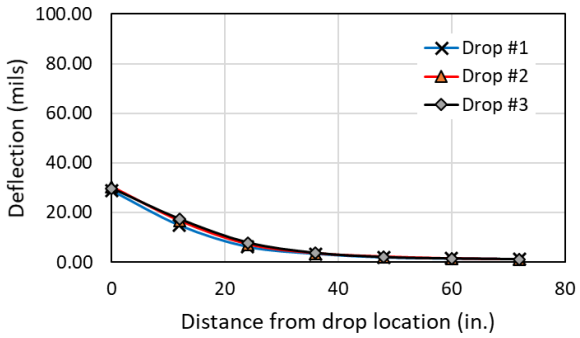


C3S3W: QB2 + Fly Ash Subbase and CA06_R Base

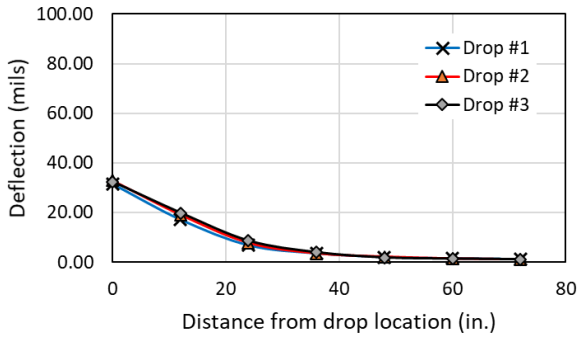


C3S3E: QB2 + Fly Ash Subbase and CA06_R Base

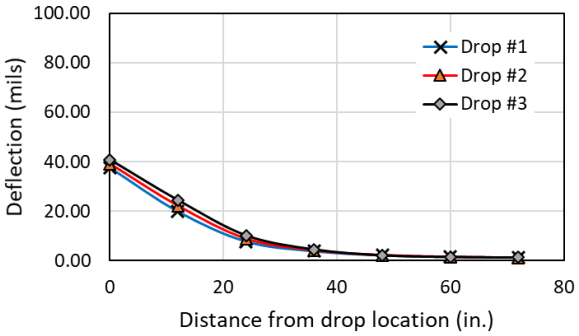


C3S4W: CA06_R Base

Figure C.9 (cont.)